Xiaoyang Gaus-Liu

High-Temperature Chlorine Corrosion during Co-Utilisation of Coal with Biomass or Waste

Cuvillier Verlag Göttingen

High-Temperature Chlorine Corrosion during Co-Utilisation of Coal with Biomass or Waste

Rauchgasseitige Hochtemperaturchlorkorrosion bei Mitverbrennung von Kohle und Biomasse/Abfall

Von der Fakultät Maschinenbau der Universität Stuttgart
zur Erlangung der Würde eines Doktors der
Ingenieurswissenschaften (Dr.-Ing.) genehmigte Abhandlung

Vorgelegt von

Xiaoyang Gaus-Liu

aus Heilongjiang, VR China

Hauptberichter:	Prof. Dr. K. Hein
Mitberichter:	Prof. Dr. E. Roos
Tag der mündlichen Prüfung:	19. November 2007

Institut für Verfahrenstechnik und Dampfkesselwesen der Universität Stuttgart

2008

Bibliografische Information der Deutschen Nationalbibliothek
Die Deutsche Nationalbibliothek verzeichnet diese Publikation in der Deutschen Nationalbibliografie; detaillierte bibliografische Daten sind im Internet über http://dnb.ddb.de abrufbar.
1. Aufl. - Göttingen : Cuvillier, 2008
Zugl.: Stuttgart, Univ., Diss., 2008

978-3-86727-568-2

D 93

Nonnenstieg 8, 37075 Göttingen
Telefon: 0551-54724-0
Telefax: 0551-54724-21
www.cuvillier.de

1. Auflage, 2008
Gedruckt auf säurefreiem Papier

978-3-86727-568-2

Preface

This dissertation is the outcome of my scientific work at the Institute of Process Engineering and Power Plant Technology at the University of Stuttgart. Prof. K.R.G. Hein and Jörg Maier are my supervisors. The work was financed by the European project: “Fireside corrosion on coal-fired utilities”.

I wish to thank Prof. K.R.G. Hein and Prof. E. Roos for the reading and the correction of my dissertation. I also wish to sincerely thank Jörg Maier for his significant technical guidance. Dr. Timm Heinzel, my former colleague, has given me support and inspiration for the experimental research. I am deeply grateful for all his support.

The laboratory team directed by Bernd Janisch has performed most of the ash analysis. Their cooperation and reliability has allowed me to develop the important results in this study. I also wish to express my thanks to the IVD-Workshop for the full support and patience during the construction and preparation of the test facilities and components. I also appreciated the support from some other colleagues, for example, the construction of the temperature-control unit for the deposition/corrosion probe by Dirk Pfeiffer, the SEM analysis by Wolfgang Scheurer and the data analysis in a combustion test by Rene Kull.

Finally, I am deeply grateful for the never failing support of my parents and my husband.

Karlsruhe, August 2007

Xiaoyang Gaus-Liu

Content

Abbreviation (Abkürzungen)

AFT	Ash fusing temperature
austen	Austenite
BE	Back-scattered electron image
Bit	Bituminous coal
CP	Compost
DTA	Differential thermoanalysis
ECN	Electrochemical current noice
EEG	Renewable energy ordinance
EPN	Electrochemical potential noise
ER	Electrical resistance
FACTsage	A thermodynamic calculation program
FBC	Fluidised bed combustion
ferr	Ferrite
g	Gas
HAZ	Heat treatment affected zone
IVD	Institut für Verfahrenstechnik und Dampfkesselwesen
l	Liquid
Lig	Lignite
Me	Metal
NOx	Nitrogen oxides
OL	Olive husk
OP	Optical microscopy
PF	Pulverized fuel

PS	Paper sludge
PWHT	Postweld heat treatment
R&D	Research and Development
RH	Reheater
REE	Reactive element effect
s	Solid
S	Straw
SAC	South Africa Coal
SH	Superheater
SE	Secondary electron imge
SEM	Scanning electron microscopy
TDS	Thermodynamic stability diagram
TEM	Transmission electron microscopy
TGA	Thermogravimetric analysis
USC	Ulter super critical
XRF	X-ray Fluorescence Analysis
ZRA	Zero-Resistance Ammetry

Symbols

symbol	unit	meaning
a	-	Activity of a species
$\Delta_r G$	$kJmol^{-1}$	Gibbs energy of reaction
$\Delta_r G^o$	$kJmol^{-1}$	Standard Gibbs energy of reaction
G^o	$kJmol^{-1}$	Standard Gibbs energy of a species
ΔG^o	$kJmol^{-1}$	Standard Gibbs energy of formation
HHV	MJ/kg	High heating value
k_l	m/s	Linear reaction rate constant
k_p	m^2/s	Parabolic rate constant
K	-	Ratio of partial pressure of reactants and products
LHV	MJ/kg	Low heating value
mol	mole	Mass unit
p	bar	Partial pressure
R-Value	-	(weight of corrosion products) / metal loss
t	second	Reaction time
T	K	Absolute temperature
T_m	K	Melting temperature
T_4	K	The temperature of a species at which its vapour pressure is equal to 10^{-4} atm
μ	-	Chemical potential
μ^o	-	Standard chemical potential
x	m	Scale thickness
λ	-	Combustion air ratio

Zusammenfassung

Forschungsschwerpunkte dieser Dissertation

Im Rahmen des dreijährigen EU-Projektes „fireside corrosion in coal-fired utility boilers“ übernahm das Institut für Verfahrenstechnik und Kampfkesselwesen (IVD), Universität Stuttgart, die Leitung für die praktischen Laborversuche, die in einer Verbrennungsversuchsanlage und im Laborofen durchgeführt wurden. In dieser auf dem EU-Projekt aufbauenden Dissertation wird die chlorinduzierte Korrosion während der Mitverbrennung von Kohle und Biomasse oder Abfallprodukten unter dem Gesichtspunkt der verschiedenen Verbrennungsparameter untersucht. Ziel der Untersuchungen war es, sowohl die unterschiedlichen Korrosionsmechanismen zu identifizieren, als auch die Wechselwirkungen zwischen Brennstoff, Rauchgas, Deposition und den Material-eigenschaften zu erklären.

Stand der Technik (Kapitel 1 und Kapitel 2)

Kohlekraftwerk

Die Erhöhung des Wirkungsgrads von Kohlekraftwerken ist eine der wesentlichen Aufgaben der Kraftwerkstechnik. Der Wirkungsgrad von Kohlekraftwerken wird maßgeblich vom Frischdampfzustand begrenzt. Der Frischdampfzustand (Dampfdruck und Dampftemperatur) ist eng mit der Entwicklung hochtemperaturfester Kesselrohrmaterialien verknüpft. Eine Grenze für die Erhöhung der Frischdampftemperatur ist das Kesselrohrmaterial für die Endüberhitzerrohre, das über einer Temperaturgrenze hinweg nicht Druck- und feuerraumseitiger Korrosion beständig ist. Obwohl erfolgreich große Anstrengungen in der Materialforschung unternommen wurden, den Frischdampfdruck in den überkritischen Grenzbereich zu steigern, werden heutzutage die meisten Kraftwerke für Dampftemperaturen unterhalb von 600°C ausgelegt.

In Kohlekraftwerken hängt die Hochtemperaturkorrosion eng mit Schwefelverbindungen im Rauchgas und in den Ascheablagerungen zusammen. In einem Temperaturfenster von 600°C bis 700°C bilden sich niedrigschmelzende Schwefelsalze an dem Wärmetauscher. Während der Bildung oder der Zersetzung solcher Schwefelsalze entstehen hochkorrosive schwefelhaltige Gase, die die Kesselmaterialien direkt angreifen. Dies führt zu einer hohen

Korrosionsrate. Oberhalb dieses Temperaturbereiches sind die Schwefelsalze nicht stabil, und als Konsequenz geht die hohe Korrosionsrate zurück.

Biomasse- und Abfallverbrennungsanlagen

Bei Biomasse- und Abfallverbrennungsanlagen wird die feuerraumseitige Korrosion überwiegend durch Chlorverbindungen hervorgerufen, wenn Chlor im obengenannten Brennstoff reichlich vorhanden ist. Diese korrosiven Prozesse unterscheiden sich grundlegend von den überwiegend durch Schwefelverbindungen verursachten Korrosionsmechanismen bei kohlegefeuerten Anlagen.

Der allgemeine Mechanismus der chlorinduzierten Korrosion war Gegenstand vieler Untersuchungen und ist als „aktive Oxidation“ beschrieben: Chlorgas in Form von Cl_2, das entweder durch die Oxidation von HCl im Rauchgas entsteht oder aus den alkali- oder erdalkalihaltigen Aschen freigesetzt wird, dringt rasch durch die Oxidschicht zur Phasengrenze Metall/Oxidschicht vor. Dort reagiert das Chlorgas mit dem Metall und bildet feste Metallchloride, welche wegen ihrer hohen Gaspartialdrücke sofort verdampfen. Die gasförmigen Metallchloride diffundieren durch die Oxidschicht in Richtung Phasengrenze Gas/Oxidschicht. Auf diesem Weg erreichen die gasförmigen Metallchloride Regionen mit höherem Sauerstoffpartialdruck und werden dort unter Freisetzung von Chlorgas oxidiert. Das Chlorgas kann zurück zur Metalloberfläche diffundieren. Diese Zirkulation des Chlorgases führt dann zu einer erhöhten Oxidation des Metalls bei einer geringen Nettobindung des Chlors.

Schwefeldioxid (SO_2) im Rauchgas spielt bei chlorinduzierter Korrosion eine wichtige Rolle. Aus eigenen Erkenntnissen kann SO_2 einen gegenläufigen Einfluss auf die chlorinduzierte Korrosion ausüben. SO_2 kann gasförmige Alkalichloride im Rauchgas zu Sulfaten umwandeln und damit die Ablagerung der Alkalichloride an den Wärmetauscheroberflächen verhindern, wodurch auch die chlorinduzierten korrosiven Vorgänge verhindert werden. Sind hingegen hohe Konzentrationen an Alkalichloriden schon in den Ablagerungen vorhanden, kann die Anwesenheit von SO_2 die Chlorkorrosion durch die Freisetzung von Chlorgas (Cl_2) oder HCl nahe der Metalloberfläche begünstigen.

Ein weiteres Kennzeichen von chlorinduzierter Korrosion ist die sogenannte „interne Korrosion“, insbesondere von austenitischen Stählen. Obwohl austenitische Stähle einen guten Schutz gegen Korrosion bei kohlegefeuerten Anlagen bieten, sind sie gegen

Chlorkorrosion den 9-12% chromhaltigen ferritischen/martensitischen Stählen nicht generell überlegen.

Hochtemperaturkorrosion in reduzierender Atmosphäre

Ein weiterer Mechanismus der feuerraumseitigen Korrosion tritt im Brennernahbereich auf und kann durch eine Fehljustierung der Brennstoff-Luftverhältnisse am Brenner oder durch den Einsatz von NOx-Minimierungstechnologien verursacht werden. In beiden Fällen entsteht eine reduzierende Atmosphäre. Der Sauerstoffmangel führt als Konsequenz zu Eisensulfid- oder pyrosulfathaltigen Ablagerungen, die in dieser Form in oxidierender Atmosphäre nicht auftreten. Hohe Korrosionsraten können durch weitere Reaktionen in diesen Ablagerungen die Folge sein.

A u f g a b e n s t e l l u n g

Obwohl die Grundtheorie der Chlorkorrosion als „aktive Oxidation“ bisher anerkannt wird, bleiben viele auf die Praxis bezogene Gesichtspunkte der Korrosionscharakteristik unbeachtet oder sie sind nicht vollständig geklärt**.** Auch spielt das Ascheablagerungsverhalten für die Korrosionsgeschwindigkeit eine wichtige Rolle, das bisher noch nicht systematisch erforscht ist.

Die Aufgabe eines großen Teiles der Arbeit war es, die folgenden Unklarheiten sowohl in Korrosionsmechanismen als auch in Ablagerungsverhalten von Chlorkorrosion zu untersuchen:

Korrosionsmechanismen

a) Morphologie und Korrosionsmechanismen der chlorinduzierten Korrosion in reduzierender und oxidierender Atmosphäre

b) Korrosionskinetik

c) Zusammenhängender Einfluss von Rauchgas und Ascheablagerung auf die Korrosionsrate

d) Korrosionsbeständigkeit der verschiedenen Kesselstähle unter dem Einfluss von Rauchgas und Ascheablagerung

Ablagerungsverhalten

e) die Einflüsse von Brennstoffmineralien auf die Ablagerung von Chlor- und Schwefelverbindungen

f) Die Verteilung von Aschekomponenten in Ablagerungsschichten und an der Rohranströmungs und –abströmungsseite

Die Arbeit hat außerdem das Ziel, mit Hilfe eines Berechnungsprogramms das Korrosionspotential von verschiedenen Brennstoffmischungen zu identifizieren, um gegen Chlorkorrosion wirksame Eigenschaften eines Brennstoffs herauszufinden, der für die Mitverbrennung von Biomasse oder Abfall geeignet ist.

Methoden und Versuchsausrüstung der Forschungsarbeit

Die im Rahmen dieser Dissertation durchgeführten Arbeiten umfassen sowohl Labor- und Verbrennungsversuche als auch thermodynamische Simulationen.

Die Laborversuche ermöglichen die Erforschung der Korrosionsmechanismen und die Bestimmung der Korrosionsraten. In einem elektrisch geheizten Ofen mit einem angeschlossenen Gasmischsystem können polierte Materialproben - entweder blank oder eingebettet in Ascheablagerungen - über eine genaue Zeitdauer unter definierten Gas- und Temperaturbedingungen ausgelagert werden. Nach der Auslagerung wurden Proben metallolographisch untersucht und ihre Gewichtänderungen und Korrosionstiefe gemessen. Die metallographische Untersuchung der Proben lieferte wertvolle Information über Korrosionsmorphologie und dahinter versteckte Korrosionsmechanismen. Über die Messungen von Probegewichtsänderung und der Eindringtiefe der Korrosionsschicht ließen sich die Korrosionsgeschwindigkeiten feststellen (Kapitel 3).

Die Verbrennungsversuche wurden in einer 500 kW Staubfeuerungsanlage mit umfangreicher Messdatenerfassung durchgeführt. Die betriebsrelevanten Verbrennungsbedingungen in der Versuchsanlage ermöglichen die Erforschung des Verbrennungs- und Ablagerungsverhaltens bei unterschiedlichen Brennstoffen und Feuerungsbedingungen. Zwei temperaturgeregelte Depositions-/Korrosionssonden wurden eingesetzt, um Ascheablagerungen bei simulierten Überhitzer- und Verdampferbedingungen zu sammeln. Zusätzlich lieferten die Rauchgaszusammensetzungen in der Brennkammer und die Analysen der Flugaschen aus der Brennkammer und den Rauchgasreinigungsaggregaten wertvolle Informationen (Kapitel 3).

Thermodynamische Berechnungen wurden mit dem kommerziellen Programm „FACTSage“ ausgeführt. Das Prinzip der Berechnungen basiert auf der Minimierung der gesamten freien Gibbs-Energie in dem System. Für einen Input einer bestimmten Brennstoffzusammensetzung kann das Programm die Verbrennungsprodukte von idealen vollständigen Reaktionen berechnen. Für die Untersuchung der Chlorkorrosion wurden in dieser Dissertation beispielweise die Mitverbrennungen von Steinkohle-Stroh und Braunkohle-Stroh untersucht, um die gasförmigen und festen Anteile der korrosionsrelevanten Verbrennungsprodukte im Temperaturbereich von 400°C bis 1400°C vorherzusagen (Kapitel 6).

Die Ergebnisse dieser Forschungsarbeit

a) Morphologie und Mechanismen der Chlorkorrosion in reduzierender und oxidierender Atmosphäre (Kapitel 4.1):

Grundsätzliche Unterschiede zwischen der Korrosionsmorphologie und den damit verbundenen Mechanismen der Chlorkorrosion in reduzierender und in oxidierender Atmosphäre wurden in dieser Forschungsarbeit festgestellt:

In sauerstoffarmer Umgebung entstehen ungeheilte Fehlstellen in der Oxidschicht, die von der Bildung und anschließender Verdampfung der festförmigen Metallchloride verursacht sind, so dass sich eine honigwabenartige Oberfläche von Metall bildet. Die Löcher in der Oxidschicht ermöglichen direkte Austauschwege zwischen dem Rauchgas und der Grenze Oxid/Metall. Als Ergebnis stellt sich kein Konzentrationsgradient von Reaktionsteilnehmern oder Reaktionsprodukten in der Korrosionsschicht ein. Deswegen können die durch Partialdruckdifferenzen verursachten Kettenreaktionen in der „aktiven Oxidation“, die als Merkmal der Chlorkorrosion in oxidierender Atmosphäre gilt, in reduzierender Atmosphäre nicht stattfinden. Die Korrosionsrate ist geringer als bei aktiver Oxidation.

In einer oxidierenden Atmosphäre wird die Diffusion von gasförmigen Metallchloriden durch die schnell nachwachsenden Metalloxide verhindert. Als Konsequenz ergibt sich eine relativ kompakte Oxidschicht. Ist eine solche Oxidschicht erst einmal gebildet, dominiert die aktive Oxidation den Prozess. Das Wachstum der Oxidschicht ist dann so groß, dass die Schicht wellig und brüchig wird.

Die Korrosionsmorphologie ist stark von der Temperatur abhängig. Bei relativ niedrigen Temperaturen (<450°C) wird die Korrosion durch das Wachstum von lokalen

„Metallchloridenblüten“ auf der Metalloberfläche charakterisiert. Bei hohen Materialtemperaturen (>600°C) tendieren feste Metallchloride in der Oxidschicht zu verdampfen und sich zu Metalloxiden umzuwandeln. Dies führt zu dem raschen Wachstum einer reinen Oxidschicht an der Metalloberfläche. Das Wachstum der Metallchloride kann nur unterhalb dieser Oxidschicht stattfinden. Dabei brechen die stabförmigen Metallchloridkristalle die bedeckende Oxidschicht oft auf.

b) Kinetik der chlorinduzierten Korrosion(Kapitel 4.1)

Ein Korrosionsprozess schließt verschiedene Transport- und Umwandlungsvorgänge ein, z.B. den An -und Abtransport der Reaktionspartner und -produkte durch die Korrosionsschicht; chemische Umwandlung wie Oxidation oder Chlorierung der Metalle; und die Verdampfung von festförmigen Korrosionsprodukten. Es ist bekannt, dass der geschwindigkeits-bestimmende Vorgang immer die langsamste Teilreaktion im Gesamtprozess ist. Bildet sich eine homogene, kompakte und anhaftende Zunderschicht an der Metalloberfläche, wie bei der Oxidation einer Eisenlegierung in Luft bei erhöhter Temperatur, wird der Antransport der Reaktionspartner und der Abtransport der Korrosionsprodukte durch die Zunderschicht behindert, so dass die Zunderschicht das Metall schützt. Dabei ist einer der Transportvorgänge der langsamste Schritt des Korrosionsprozesses. In der Fachwelt wird häufig die Korrosionsgeschwindigkeit mit der Massenänderung über der Zeit bestimmt.

Die Kinetik der chlorinduzierten Korrosion ist nur sehr schwer mit den obengenannten Wirkmechanismen zu beschreiben, da

- die Oxidschicht nicht schützend ist und der Transportvorgang nicht immer die Korrosionsgeschwindigkeit bestimmt;
- die Massezunahme durch die Metallchlorierung und die Metalloxidation mit dem Masseverlust aufgrund der Flüchtigkeit der Metallchloride gleichzeitig in Erscheinung treten.

Damit stellt sich die Frage, welche Hauptprozesse zu Beginn und im Verlauf des korrosiven Vorgangs ablaufen. Auch zur Klärung dieser Frage leisten die im Rahmen dieser Arbeit ermittelten Ergebnisse einen Beitrag.

Zuerst deutet die vorliegende Arbeit darauf hin, dass aufgrund der gleichzeitigen Gewichtszunahme und –Abnahme während der Chlorkorrosion, der Metallverlust für die

Korrosionsgeschwindigkeit ein besser beschreibender Indikator ist, als die Gewichtsänderung. Der Metallverlust ist definiert als die Masse an Metall, die an dem Korrosionsprozess teilnimmt. Anschließend wurde der Zusammenhang zwischen der Gewichtsänderung und dem Metallverlust in der Arbeit mit einem Faktor „R“ wie folgt hergestellt:

$$R = (\text{Gewichtsänderung} + \text{Metallverlust}) / \text{Metallverlust}$$

Wenn alle Korrosionsprodukte festförmig sind, hat das „R“ folgende Bedeutung:

$$R = (\text{Masse aller Korrosionsprodukte}) / \text{Metallverlust}$$

Der „R“-Wert kann sehr wichtige Information über die dominante Reaktion des gesamten Korrosionsprozesses liefern, weil der „R“-Wert aus den Einzelreaktionen in der Chlorkorrosion berechnet werden kann, z.B.:

- für die Oxidation von Fe zu Fe_2O_3 ist „R“ gleich 1,429;
- für das Chlorieren von Fe zum festförmigen $FeCl_2$ ist „R“ gleich 1,607;
- für die Bildung von dem gasförmigen $FeCl_2$, das ins Rauchgas diffundiert, ist „R gleich –1,607.

In dieser Arbeit wurden die Gewichtsänderung und der Metallverlust von unterschiedlichen Stählen nach dem Laborversuch gemessen, und dadurch die „R“-Werte bestimmt.

Der Faktor „R“ zeigte unterschiedliche Reaktionsablaufe für Stähle in der Initialphase. Z.B. bei niedrig-Cr-legierten Stählen, kann die Hauptreaktion, je nach Testmaterialien und Auslagerungszeit, von der Chlorierung, Oxidation oder der Verdampfung der Metallchloride bestimmt sein. Im Lauf der Zeit nähert sich dann das Wachstum der Oxidschicht von derartigen Stählen dem Charakter der Oxidation von Metall an. Mit Hilfe der metallographischen Untersuchung lässt sich feststellen, dass es sich um eine von Chlor induzierte aktive Oxidation handelt.

c) Einfluss von Rauchgas und Aschedeposition auf die Korrosionsrate(Kapitel 4.2)

Es ist bekannt, dass Materialien häufig verstärkt Chlorkorrosion zeigen, wenn die Ascheablagerungen mit Alkalichloriden angereichert sind. Durch die Untersuchung verschiedener Ascheablagerungen und Gasatmosphären konnte diese Arbeit die unterschiedlichen Interaktionen zwischen Rauchgas und Ascheablagerung in reduzierender

Atmosphäre und in oxidierender Atmosphäre für die Beschleunigung der Korrosionsrate feststellen:

Sowohl in reduzierender Atmosphäre als auch in oxidierender Atmosphäre ist die Korrosionsgeschwindigkeit von der Freisetzung der Chlorgasatome(Cl_2) unmittelbar an der Metalloberfläche abhängig. Jedoch ist der Mechanismus der Freisetzung von Cl_2 in reduzierender Atmosphäre und in oxidierender Atmosphäre unterschiedlich:

In reduzierender Atmosphäre ist die Freisetzung von Cl_2 wegen des Mangels von Oxidmittel O_2 und SO_2 gehemmt. Sulfate in der Ascheablagerung können verstärkt gasförmiges Cl_2 freisetzen, in dem O_2 und SO_3 durch die Zerlegung der Sulfate für die Oxidation der Alkalichloride zu Verfügung stehen. Die Korrosionsgeschwindigkeit ist von der Zerlegungsrate der Sulfate in der Ascheablagerung abhängig. Die Konzentration von Alkalichloriden in der Ascheablagerung hat keinen direkten Einfluss auf die Cl_2-Freisetzung. Im Allgemeinen ist die Geschwindigkeit der Chlorkorrosion in reduzierender Atmosphäre niedrig und die Alkalichloride in der Ascheablagerung bleiben relativ unaktiv.

In oxidierender Atmosphäre ist der Sauerstoffpartialdruck in der Umgebung hoch genug, um die Alkalichloride in der Ascheablagerung zu oxidieren. Sulfate in der Ascheablagerung sind dagegen stabil und nehmen an der Cl_2-Freisetzung wenig teil. Der Metallverlust in sauerstoffreicher Atmosphäre reagiert empfindlich auf die Chloridkonzentration in der Ascheablagerung. Die Korrosionsrate ist wesentlicher höher als in der reduzierenden Atmosphäre.

Außerdem kann SO_2 im Rauchgas die Korrosionsraten in oxidierender Atmosphäre enorm beschleunigen, wenn bereits Alkalichloride in der Ascheablagerung vorhanden sind.

d)Korrosionsbeständigkeit von verschiedenen Kesselstählen unter dem Einfluss von Rauchgas und Ascheablagerung(Kapitel 4.2)

Nach Materialzusammensetzung wurden folgende drei Gruppen von Materialen in dieser Arbeit untersucht:

- niedrig legierte ferritische Stähle mit Cr-Gehalt <2.5%
- mittlere legierte ferritische/martenitische Stähle mit Cr-Gehalt zwischen 9-12%
- austenitische Kesselstähle mit Cr-Gehalt >14%

Kohleasche und Strohasche aus Verbrennungsprozessen wurden als Ascheablagerungen für die Materialproben angewendet. Sowohl das Wachstum der Zunderschicht als auch die Eindringtiefe der inneren Korrosion wurden erforscht.

Die experimentelle Untersuchung konnte sowohl den bekannten Charakter von der Chlorkorrosion bestätigen, als auch bisher ungenau beschriebene Phänomen charakterisieren:

Bekannter Charakter der Chlorkorrosion

- Alle Stähle zeigen deutlich verstärkte Metallverluste unter chlorreicher Strohasche im Vergleich zur Kohleasche;
- Austenitische Stähle haben keine deutliche bessere Beständigkeit unter Strohasche als 9-12%-Cr ferritische/martensitische Stähle;
- SO_2 im Rauchgas beschleunigt die Chlorkorrosion bei allen Stählen zusätzlich;
- Die innere Korrosion ist nur bei 9-12%-Cr Stählen und bei austenitischen Stählen zu erkennen. Im Allgemeinen sind austenitische Stähle deutlich empfindlicher gegen innere Korrosion als 9-12%-Cr Stähle.

Bisher ungenau beschriebene Phänome

Da die Chromkarbide in der Metallmatrix zuerst von dem Chlorgas angegriffen werden, führt die unterschiedliche Mikrostruktur der Chromkarbide der Stähle zu einer unterschiedlichen Morphologie der inneren Korrosion:

- bei 9-12%-Cr Stählen entsteht eine hohe Anzahl von großen Leerstellen in Metallmatrix, Korngrenzenkorrosion ist nicht deutlich zu erkennen;
- im Gegensatz dazu sind austenitische Stähle mit 14-19% Cr durch gravierende Korngrenzenkorrosion an der Korrosionsfront gekennzeichnet;
- Austenitische Stähle mit Cr>19% haben zwar eine vergleichbare Eindringtiefe der Korrosion wie diejenige von 14-19% Cr austenitischen Stählen, aber das Leerstellenvolumen der Korrosionszone ist wesentlicher niedriger als dasjenige von den 9-12%-Cr Stählen und den 14-19% Cr austenitischen Stählen

Als Material für die Verbrennungsanlagen, die chlorreichen Brennstoff verbrennen, wird folgendes empfohlen:

- für die Wärmetauscherabschnitte, die stark von der Chlorkorrosion gefährdet sind, sollen hochwertigere Materialen als üblich eingesetzt werden:

    1. für die Materialtemperatur bis 400°C sollen, statt 15Mo3 oder 13CrMo44, 9-12%-Cr Stähle, wie T91, X20 oder HCM12A angewendet werden;

    2. für die Materialtemperatur bis 550°C sollen statt T91 oder X20, hochlegierte austenitische Stähle mit Cr > 19%, wie NF709, angewendet werden;

    3. für die Materialtemperatur bis 600°C sind Ni-Legierungen oder mit Ni-Legierung beschichtete Materialien anzuwenden.

- Der Kessel und der Wärmetauscher sind so auszulegen, dass eine spätere Revision oder ein Austausch von kritischen Wärmetauscherabschnitten möglich ist.

e) Die Einflüsse von Brennstoffmineralien auf das Depositionsverhalten von Chlor- und Schwefelverbindungen(Kapitel 5)

Durch Verbrennungsversuche wurde das Depositionsverhalten von Alkalichloriden, wie KCl, intensiv untersucht. Alkalichloride im Rauchgas sind wegen ihrer starken Ablagerungstendenz gegenüber HCl unerwünscht. Die Versuche konnten die positiven Einflüsse von SO_2 im Rauchgas und den Aluminium- und Siliziumgehalt im Brennstoff auf die Ablagerung von Alkalichloriden bestätigen:

- SO_2 kann gasförmiges KCl sulfatisieren und verringert dadurch die Deposition von KCl. Wenn allerdings genügend CaO im Rauchgas zur Verfügung steht, bildet SO_2 bei Temperaturen unter 900 °C $CaSO_4$. Dies wiederum führt zu einer bleibend hohen KCl-Konzentration im Rauchgas.

- Aluminium– und Siliziumverbindungen im Brennstoff sind im Hochtemperaturbereich in der Lage, Kaliumionen im Rauchgas aufzunehmen und in K-Al-Si Mischphase einzubinden. Wegen des Mangels an freien Kaliumionen im Rauchgas ist Chlor in Form von weniger kritischem HCl vorhanden.

Zusätzlich weist diese Arbeit darauf hin, dass die Aschemenge eines Brennstoffs eine wichtige Rolle bei der Anreicherung von Chlor und Schwefel in der Ascheablagerung spielt. Die hohe Konzentration von Chlor in einem Brennstoff kann beispielsweise für die Chlorkorrosion dennoch unkritisch sein, wenn der Brennstoff eine große Menge an

Inertmineralien enthält. Da während der Verbrennung die Cl-Konzentration in der Ablagerung von der großen Aschemenge in dem Brennstoff verdünnt werden kann.

f) Die Verteilung von Aschekomponenten in Ablagerungsschichten und an der Rohranströmungs- und Abströmungsseite (Kapitel 5)

Die Verteilung von Aschekomponenten in der Ablagerung ist für die Chlorkorrosion wichtig, weil die Anreicherung von Alkalichloriden in den inneren Ablagerungsschichten direkt zu einer hohen Korrosionsrate führt. Heterogene Ablagerungsstrukturen wurden auf der gekühlten Depositionssonde beobachtet. Aus systematischen Analysen von Ablagerungsasche an der Anströmungsseite und der Abströmungsseite wurden folgende Ergebnisse gewonnen:

- Chlorverbindungen sind überwiegend in der inneren Schicht der Ascheablagerung und im kühlen Bereich der Wärmetauscher zu finden.
- Ähnliches Verhalten zeigen auch Sulfate wie K_2SO_4 und $CaSO_4$, deren Hauptanteile sich als homogene feine Partikel unmittelbar an der Rohroberfläche sammeln. Ein Teil der K_2SO_4 in der inneren Schicht kann auch Folge der Umwandlung von KCl-Ablagerung sein. Kleinere Anteile an K_2SO_4 und $CaSO_4$ sind auch an größere Partikel gebunden, wodurch ein schnelles Wachstum der Ascheablagerung begünstigt wird.
- Al-Si-Verbindungen sind hauptsächlich in ultrafeiner Asche zu finden, die gleichmäßig um den Rohrumfang verteilt ist. Ein kleiner Teil der Aluminiumsilikate ist in großen geschmolzenen Partikel gebunden, die sich auf der Anströmungsseite sammeln.
- Kalzium- und Eisenverbindungen bilden sich hingegen als geschmolzene große Partikel, die sich bevorzugt auf der Anströmungsseite ablagern.

g.) Die geeigneten Eigenschaften eines Brennstoffs für die Mitverbrennung eines chlorreichen Sekundärbrennstoffs unter dem Gesichtspunkt der Chlorkorrosion(Kapitel 6).

Die mineralischen Bestandteile desjenigen Brennstoffs, der für die Mitverbrennung mit chlorreichen Brennstoffen (z.B. Stroh und Abfall) ausgewählt wird, sollen die Ablagerung von Alkalichloriden verhindern. In dieser Arbeit wurden Steinkohle und Braunkohle für die

Mitverbrennung von Stroh ausgewählt. Sowohl die thermodynamischen Berechnungen als auch die entsprechenden Versuchergebnisse zeigen, dass Steinkohle tendenziell für die Mitverbrennung von Stroh besser geeignet ist als Braunkohle. Der hohe Anteil an saueren Aschekomponenten, wie die Aluminiumsilikate in der Steinkohle, ist in der Lage Kalium aus dem Stroh während des Verbrennungsvorgangs zu binden. Wegen des fehlenden freien Kaliums im Rauchgas neigen Chlor und Schwefel dazu HCl und SO_2 zu bilden, die beide weniger korrosiv sind als die Verbindungen KCl und K_2SO_4.

Braunkohle enthält weniger sauere Aschekomponenten, aber deutlich höhere Anteile an Baseelementen, z.B. Calcium. Das führt zu einem hohen Bildungspotential für KCl und $CaSO_4$, die beide für eine Anreicherung von Chlor und Schwefel in der Ascheablagerung verantwortlich sind. Unter Korrosionsgesichtspunkten beträgt das Maximum des thermischen Anteils an Stroh für die Mitverbrennung mit Steinkohle ca. 25%. Dagegen ist Braunkohle nicht geeignet, mit Stroh verbrannt zu werden.

In **Kapitel 7** werden die Forschungsergebnisse aus den bearbeiteten Untersuchungs-schwerpunkten zusammengefasst und diskutiert. Darüber hinaus werden Möglichkeiten und Wege für ein weiteres Vorgehen in der rauchgasseitigen Korrosionsforschung aufgezeigt.

1. Introduction

Material failures are the leading cause of outages and availability losses in power plant boilers. According to statistics, about 50% of tube failures are related with corrosion problems. The threatened areas by corrosion could be located both on the water/steam side and on the fireside of the furnace and along the flue gas pass /1/. Whereas the material problems on the water/steam side are well understood, which are related with water quality and material strength, the fireside corrosion, which is the result of complicated interactions among fuel, flue gas, ash deposits and alloy characteristics, still requires deeper understanding. Such interactions on fireside corrosion and corresponding topics will be engaged in this research work.

1.1 Fireside corrosion limits the efficiency of coal-fired power plants

Due to unforeseeable oil and gas prices, the base-load electricity generation in Germany is based on coal –fired power plants /2/. The classic concept of pulverized-fuel (PF) combustion is still widely used due to its competitive efficiency and well-proofed technology. It is estimated that pulverized fuel will be applied in about 80% of worldwide new coal-fired power plants /3/. At present the efficiency of bituminous coal PF plants is about 45%. A further improvement of efficiency requires the application of new boiler materials /4/, which can withstand high pressure and corrosion attack. The improvement of net efficiency of PF power plants by the application of advanced materials is shown in Fig. 1.1 /5/. At present, the live steam parameters of PF plants is about 600/620°C of superheater (SH)/ reheater (RH),

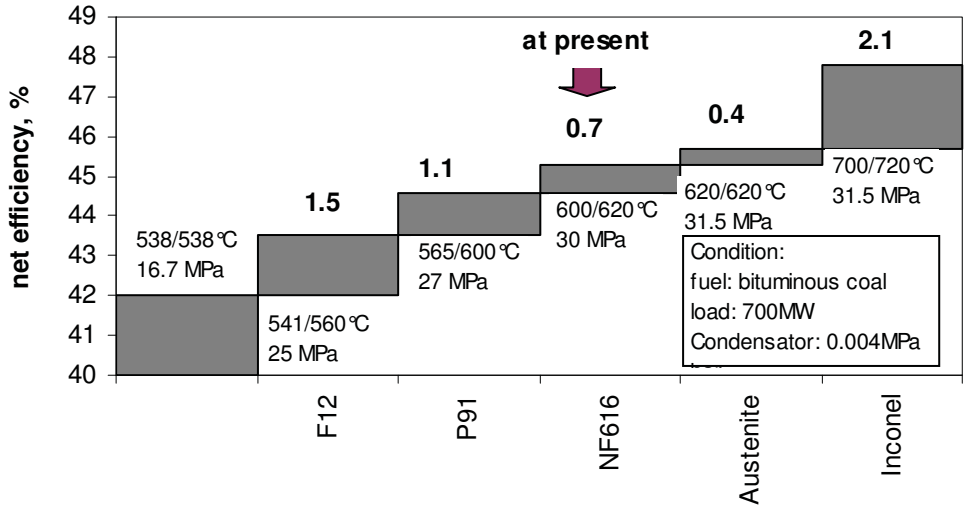

Fig. 1.1. The dependence of power plant efficiency on material development /5/

and 27MPa, corresponding to a net efficiency of 45% /6/. For such steam parameters, 9-12%Cr ferritic and martensitic steels are applied at the hottest part of superheater/reheater. For the next generation of ultra super critical (USC) plants with even higher steam temperature and pressure, austenitic and nickel-based alloys are required /7,8/.

In the last fifty years, experiences have shown that material problems are the main barrier for a further increase of steam temperature. Between 1957 and 1968, more than 30 supercritical units were put into operation in the USA /2/. Two power plants with the highest steam parameters were: Ohio Power Co. in Philo: 32Mpa, 621/565/538°C SH/RH1/RH2 and Eddystone Co.: 34.5MPa, 649/565/565°C (SH/RH1/RH2). However, such high steam parameters, especially high steam temperatures, could not be maintained due to material problems. After this period, high steam temperatures were not applied worldwide /9-11/. In the last ten years, supercritical steam parameters have gradually taken considerable share of new-built power plants. The improvement has been mainly achieved in increasing steam pressure. The increase of steam temperature, however, undergoes very cautiously. This can be shown by following examples: two 800MW units of Germany "Schwarze Pumpe" with 28.5MPa, 547/565°C SH/RH; Germany "Niederaußem" Unit K, 950MW, with 26.4MPa, 580/600°C SH/RH and China Shanghai "Waigaoqiao", two 900MW units with 25.8MPa, 542/568°C SH/RH /12/.

The obstacle to limit steam temperature exceeding 600°C comes from fireside corrosion. There is a peak value of corrosion rate between 600°C and 700°C of austenitic steels, as shown in Fig. 1.2 /13/. In this temperature range, due to interactions between flue gas and ash deposits, low-melting-point salts build up on heat transfer surfaces. During formation or decomposition of such salt melts, the product of the reaction, which can be SO_3 in oxidizing atmosphere, or SO_2/S_2 in reducing atmosphere, are transported to the scale/metal interface and

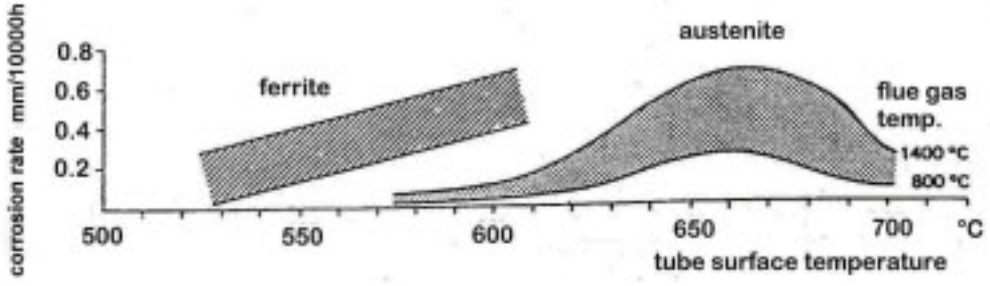

Fig. 1.2. Fireside corrosion rate as a function of material temperature /13/

lead to high corrosion rate. This kind of corrosion is so called “hot corrosion”. Over this temperature range, the salt melts are not stable, as consequence, hot corrosion is alleviated.

It is always an issue for boiler designers to balance thermal efficiency, material cost and the risk of material failures. In order to get a substantial improvement of the boiler efficiency, developing and testing new boiler tube materials are urgently required. The new materials should not only show high mechanical properties, but also show superior resistance against fireside corrosion. Moreover, a further understanding of interactions between flue gas, deposit ash and material degradation, especially for new materials, are of the same importance.

1.2 Fireside corrosion in biomass and waste combustion systems

Interests in firing biomass and waste

Biomass and waste are drawing increasing interest as renewable energy resources for power and heat supply. Firing biomass and waste is foreseeable market-near technology to reduce CO_2 emission and at the same time, to protect environment and to save valuable primary energy resources /14/. Since a gradually transition from fossil fuels to renewable energies is unavoidable on the way to reduce CO_2 emission, the European Commission demands actions to enhance the use of renewable energy that would take 12% of electrical production by year 2010. To meet this demand, the application of renewable energy should be at least doubled till the year 2010.

Germany is one of the countries which makes great efforts to encourage biomass utilization: a new renewable energy ordinance (EEG) is in power which obliges electricity distributors to buy electricity from renewable energy sources at an increased reimbursement /15/. Contaminated old wood is regarded as biomass in this ordinance. The ordinance shall make firing biomass profitable, so that the large potential of available biomass can actually be explored.

There is another reason for enhanced use of biomass in European countries: there is a great surplus of agriculture production due to intensive plantation technique. Industrial utilization of raw agriculture materials provides a new way for continuous development of agriculture, without changing land structures and cutting farming jobs.

Waste incineration becomes also an important topic of environmental protection policy. German Federal Department of Environment has made a new ordinance with high

environmental protection measures in August 1999. The ordinance ensures there will be an end of the landfill of inadequately pretreated wastes no later than 2005. Domestic waste should be either directly thermal disposed or thermal disposed after mechanical-biological pretreatments. The thermal disposal plants should meet the emission limits set by the 17th federal pollution protection ordinance (the 17th BimSchV) /16-17/.

The motivation behind the waste incineration is to reduce negative environmental impacts of waste landfill. Through thermal treatment of waste, following benefits can be achieved:

- destroying harmful or dangerous substances in wastes
- reducing amount and volume of wastes
- utilization of waste residues after thermal treatment or making it capable for deposit
- using the energy from wastes as far as possible.

Serious fireside corrosion by firing biomass and waste materials

High concentration of chlorine in biomass and waste leads to severe fireside corrosion. This becomes a new problematic for both combustion engineering and material engineering /19/. Due to the rapid material degradation, most waste incineration plants must limit their live steam temperature below 400°C /20/. In spite of this, frequent tube failures and outages can not be prevented.

High corrosion rate usually occurs when the heat transfer surface is covered with chlorine-rich deposits. In the case of biomass, the deposit is enriched in alkali chlorides; in the case of waste materials, the deposit is enriched in sodium chlorides and chlorides of some heavy metals, such as $ZnCl_2$ /21/. During oxidation of such chlorides, chlorine gas (Cl_2) is formed, which is a directly attack medium to the underlying material. Since the melting temperature of chlorine-containing ashes is usually low, fouling, slagging and sintering of the deposit occur, which in return facilitate chemical reactions among ash particles.

Another character of chlorine-induced corrosion is the structure of material degradation. Not only rapid material loss by forming a corrosion scale is reported, but also internal corrosion under the corrosion scale is detected, which results in material ability loss. Some advanced materials, such as some austenitic steels, which have good corrosion resistance against sulphate corrosion in coal-firing system, have shown deep internal corrosion zone under chlorine attack /22/.

Co-combustion of biomass with coal

The interest in co-combustion of biomass with coal in large scale plants is growing due to a number of considerations, e.g. low investment cost, well established power plant nets and existing flue gas cleaning facilities /23/.

Considered as energy resources, biomass includes a variety of low-grade fuels, characterised by high volatiles, high chlorine and high alkali content /24/. The problematic features of biomass imply a range of difficulties in operation, such as gas cleaning and residue utilization during co-combustion and fireside corrosion /25-28/. Fireside corrosion is one of the most complicated difficulties, which is strongly influenced by the selection of primary fuel (coal) and secondary fuel (biomass or waste) and operational parameters /19, 29, 30/.

1.3 Fireside corrosion on waterwall

Waterwall corrosion often appears when waterwall tube surface is impinged by particle-loaded flame or located in an oxygen-depleted zone. This kind of corrosion is usually a result of flame maladjustment or the application of low-NO_x technologies /31/. The oxide scale, which is otherwise stable in oxidizing environment, is not compact and not adherent in reducing environment. Such scale is subjected to the attack of chlorine and sulphur. Moreover, the corrosion rate in an alternative oxidizing-reducing condition is greater than only in a stable reducing atmosphere /20/.

1.4 Objectives and research methods in this study

In this study, emphases have been given on the corrosion related issues during biomass and waste combustion. Following open questions in corrosion mechanisms, deposition behaviour of chlorine compounds and fuel selection to minimize chlorine deposition were studied:

a) Corrosion mechanisms

- Morphologies and mechanisms of chlorine corrosion in reducing and oxidizing atmospheres
- Corrosion kinetics of chlorine-induced corrosion
- Combined influences of flue gas composition and ash deposits on corrosion rate
- Corrosion resistance of ferritic, ferritic/martensitic and austenitic steels under deposits from coal and biomass combustion.

The investigations of corrosion mechanisms were carried out experimentally in a laboratory furnace with well-defined gas and deposit test conditions.

b) Deposition behavior in combustion process and its influence on fireside corrosion

Since the deposition of chlorine-rich ashes on tube surface accelerates corrosion rate enormously, deposition behaviour of chlorine compounds during combustion process was the main concern in the combustion tests. The combustion tests were carried out in a well-defined test rig, in which cooled deposit probes were inserted. The influences of fuel characteristics, material temperature and flue gas temperature on the chlorine deposition were studied. Furthermore, elemental distributions in the heterogeneous deposit around a tube surface were systematically investigated.

c) Searching of suitable fuel blends to minimize chlorine corrosion

Which kind of coal is suitable to be co-fired with chlorine-enriched waste fuels, and which is the suitable share of such waste fuels? With the help of thermodynamic calculation program FACTSage, the cases of co-firing straw with bituminous coal and co-firing straw with lignite were studied. The fuel characteristics to minimize the deposition of chlorides were discussed, and the suitable mix rates of straw were predicted. The calculation results have been examined by corresponding experimental tests.

Finally, the limitation of the research work and suggestions for future research have been discussed.

2. State-of-the-Art Research of Fireside Corrosion in Coal-Fired and Biomass-Fired Boilers

2.1 Kinetics and thermodynamics of fireside corrosion

High temperature fireside corrosion involves complicated chemical and physical processes. Kinetic laws describe corrosion rate, which is determined by the slowest step in a process, whereas the stability of reactants and products depends on the thermodynamic parameters of the whole system.

2.1.1 Corrosion kinetics

The main steps of corrosion process comprise gas transport and surface reactions. Taking oxidation of metal for example, oxygen needs to be transported through oxide scale to the scale/metal interface, there, the adsorption, nucleation of oxygen on the metal surface and oxidation of metal occur. The corrosion rate remains constant as long as the transport of oxygen is faster than chemical conversions. With the buildup of a compact oxide scale, the transport of oxygen through to metal surface becomes difficult. When oxygen transport is slower than oxygen consumption at the corrosion front, the rate-determining step is transferred from surface reactions to gas transport /32/.

The surface-reaction-determined corrosion rate occurs usually in the case that there is easy contact between metal and gas environment, for example, at the initial stage of exposure or when a scale is defect /32/. The corrosion rate follows a linear growth kinetics, as described in (2.1.1) /33-34/:

$$(dx / dt) = k_l \qquad \text{or} \qquad x = k_l t \tag{2.1.1}$$

x *scale thickness*
t *reaction time*
k_l *the linear rate constant.*

When a compact scale is formed, the scale growth depends gradually on the material transport through the scale. If the material transport is a diffusion process, the corrosion rate follows parabolic law, as described in (2.1.2).

$$\frac{d(\Delta x)}{dt} = \frac{k_p}{\Delta x} \qquad \text{or} \qquad \Delta x = \sqrt{2k_p t} \tag{2.1.2}$$

k_p parabolic rate constant

It needs to note that only the growth of a compact and adhering scale can be well described by parabolic laws /36/. The growth rate of oxide scale in flue gas atmosphere is seldom perfectly parabolic /81/. The corrosion rate of heat transfer materials in chlorine-rich combustion environment is more difficult to define, since:

a) the corrosion scale is heterogeneous, loose and brittle;

b) cracking and detachment of scale usually occur. This is a result of the growth of metal chlorides underneath the scale and strain relieving between scale and metal. The strain can be generated by the volume expansion of a growing scale or by the different thermal extension rate between scale and metal, especially in a thermal cycling condition /35-37/;

c) the change of chemical composition and structure of deposit ash with time influences also gas transport and reaction rate. For instance, if ash deposits sinter or melt, the contact and reactions within deposit ash and at scale/metal interfaces will be enhanced.

2.1.2 Thermodynamics of high temperature corrosion

Thermodynamic features in a process determine the possibility and the direction of a spontaneous reaction. In other words, they determine whether a reaction will occur or a substance is stable under certain condition. For example, most metals are not stable at high temperatures in air. They react with oxygen and build up more stable metal oxides, as described in (2.1.3):

$$2x/y\ Me + O_2 \rightarrow 2/y\ Me_xO_y \qquad (2.1.3)$$

The driving force of a reaction is the free enthalpy of the reaction, $\Delta_r G$, which is the difference of the chemical potentials μ (molar Gibbs energy) between the products and reactants at the composition of the reaction mixture /40/:

$$\Delta_r G = \Sigma \mu(products) - \Sigma \mu(reactants) \qquad (2.1.4)$$

The spontaneity of a reaction at constant temperature and pressure is determined by its reaction Gibbs energy $\Delta_r G$:

If $\Delta_r G < 0$, the forward reaction is spontaneous.

If $\Delta_r G > 0$, the reverse reaction is spontaneous.

If $\Delta_r G = 0$, the reaction is at equilibrium.

An important application of the reaction Gibbs energy is to calculate the equilibrium partial pressure of gas species in a gas-metal reaction, in which a certain corrosion product is stable.

The calculation is based on the assumptions that the activity of solid reactants and products are 1, and gas species are perfect gases. The reactant resembly and the product resembly are expressed as A and B respectively.

Since the chemical potential μ of a species is related to its activity by

$$\mu = \mu^o + RT \ln a \tag{2.1.5}$$

(2.1.4) can be also expressed as

$$\Delta_r G = \mu_B - \mu_A = (\mu_B^0 - \mu_A^0) + RT \ln(\frac{a_B}{a_A}) = \Delta_r G^o + RT \ln(\frac{a_B}{a_A}) \tag{2.1.6}$$

Taking the simple metal oxidation in (2.1.3) for example, its reaction Gibbs energy can be expressed as:

$$\Delta_r G = \Delta_r G° + RT\left[\ln(a_{Me_xO_y}^{y/2} /(a_{Me}^{2x/y} \cdot a_{O_2})\right] \tag{2.1.7}$$

The activities of pure metal and pure oxides are 1. When O_2 is considered as a perfect gas, the activity of O_2 can thus be replaced by the partial pressure of oxygen. When the reaction is in an equilibrium *($\Delta_r G = 0$)*, Eq.(2.1.7) can be simplified as:

$$\Delta_r G^\circ = -RT \ln p(O_2) \quad \text{or} \quad p(O_2) = e^{-\frac{\Delta_r G^0}{RT}} \tag{2.1.8}$$

$p(O_2)$ is the oxygen partial pressure at the equilibrium to maintain Me_xO_y stable. When the standard reaction Gibbs energy of the reaction $\Delta_r G°$ is known, the required equilibrium partial pressure of oxygen at temperature T can be calculated according to (2.1.8). In the cases of other gas-metal reactions, such as chlorination, sulphidation of metal, the partial pressure of the involved gas species can also be calculated with the same method.

2.1.3 Oxidation, sulphidation and chlorination in thermodynamic point of view

Gas-metal reactions, such as oxidation, sulphidation and chlorination, could occur alone or simultaneously in flue gas environment. The final corrosion products are dependent on temperature and the partial pressures of involved gas species. The interactions among metal oxides, metal sulphates and sulphides, and metal chlorides are discussed in the following:

Interactions among oxides, sulphates and sulphides

When only oxidation of iron is considered, Fe_2O_3, Fe_3O_4, FeO can be formed from high $p(O_2)$ region to low $p(O_2)$ region in a certain order, corresponding to the atmosphere from the gas/scale interface to the scale/metal interface:

flue gas O_2 | Fe_2O_3 → Fe_3O_4 → FeO | Fe metal

To predict the stabilities of the concerned gas species, the thermodynamic stability diagrams (TDS) in this chapter were calculated by the author with FACTSage program.

If a system contains both oxygen and gas-form sulphur species, according to the Fe-O-S thermodynamic stability diagram (TDS) illustrated in Fig.2.1.1, metal sulphides are stable in the environments where the oxygen partial pressure is low. In flue gas atmosphere, which contains both oxygen and sulphur gas species, such as SO_2, SO_3, the stable solid compounds are metal oxides and metal sulphates in flue gas. However, if SO_2 in flue gas manages to penetrate the scale to the scale/metal interface, where the oxygen partial pressure is low, formation of stable sulphides is possible. By studying the composition of the corrosion scale of iron, it is found that the innermost layer is composed of FeS /32/, and a mixed layer of FeS and Fe_3O_4 is adjacent to the FeS layer /43/.

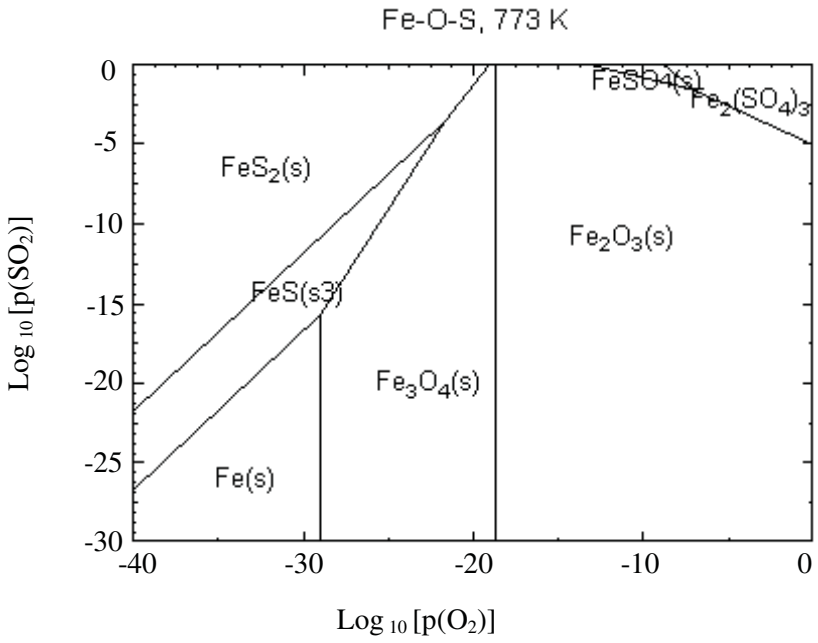

Fig. 2.1.1. Fe-O-S thermodynamic stability diagram at 773K from FACTsage calculation/.

Compared to iron oxides, iron sulphides grow faster, but they are looser. Since the difference of the Gibbs formation energy between various sulphides is smaller than that of oxides,

various forms of sulphides could coexist in a corrosion scale. Loose and heterogeneous metal sulphides are less protective than metal oxides /44/.

Thermodynamics of chlorides and oxides

In oxidizing atmosphere, metal oxides are more stable than metal chlorides. This can be implied by the comparison of the Gibbs Energy of formation between metal oxides and metal chlorides, e.g. at 500°C in Tab.2.1 /34/. This means, under simultaneous attack of oxygen and chlorine, although metal chlorides and oxides could be formed side by side at initial stage, metal chlorides tend to convert to metal oxides with time.

Tab. 2.1. The thermodynamic stability of some metal oxides and chlorides at 500°C /34/

Phase	ΔG°_{773K} *[kJ/mole]*	*Phase*	ΔG°_{773K} *[kJ/mole]*
Cr_2O_3	-955	Fe_2O_3	-631
$CrCl_2$	-304.4	$FeCl_2$	-249.38
$CrCl_3$	-388.5	NiO	-336.8
		$NiCl_2$	-188.6

In reducing environment, solid metal chlorides can be stable. This can be shown in the Fe-O-Cl TDS, e.g. at 773K in Fig. 2.1.2. These regions can locate, for example, under an oxide scale.

The Fe-Cl-O TDS in Fig.2.1.2 also implies that, different as solid metal chlorides, gaseous metal chlorides are possible to form even in oxygen enriched region, when the chlorine gas

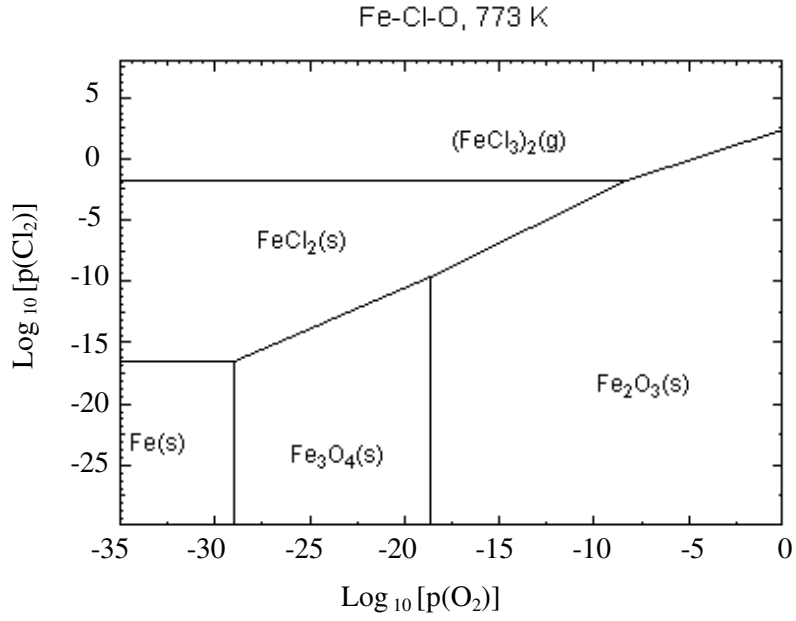

Fig. 2.1.2. Fe-O-Cl thermodynamic stability diagram from FACTsage calculation, T = 773K

pressure is also high enough.

Most solid metal chlorides have high equilibrium vapour pressure. The vapour pressure of metal chlorides increases with temperature. This leads to high evaporation rate of metal chlorides, which is the driving force of chlorine corrosion at high temperature.

Thermodynamics of sulphides, sulphates and chlorides

From above discussion, we know that both metal sulphides and metal chlorides could be thermodynamically stable in reducing environment. The following question is: which is the equilibrium species in reducing environment, when both Cl_2 and S_2 are present? FACTSage calculation has shown that the partial pressure of oxygen is important to determine the equilibrium state of chlorides and sulphur compounds, as shown in TDS diagrams with $\log_{10}[p(O_2)] = -10$ in Fig. 2.1.3, $\log_{10}[p(O_2)] = -15$ in Fig. 2.1.4 and $\log_{10}[p(O_2)] = -30$ in Fig. 2.1.5.

For the same partial pressures of chlorine gas and sulphur gas, metal sulphates are the stable species at relatively higher oxygen pressure region, for example, $\log_{10}[p(O_2)] = -10$. Whereas condensed and vapour metal chlorides and solid sulphides are stable at extreme low oxygen pressure, for example, $\log_{10}[p(O_2)] = -30$. At such low oxygen partial pressure, the stability of chlorides and sulphides depends mainly on the partial pressure of chlorine gases and sulphur gases in the environment, as illustrated in Fig. 2.1.5.

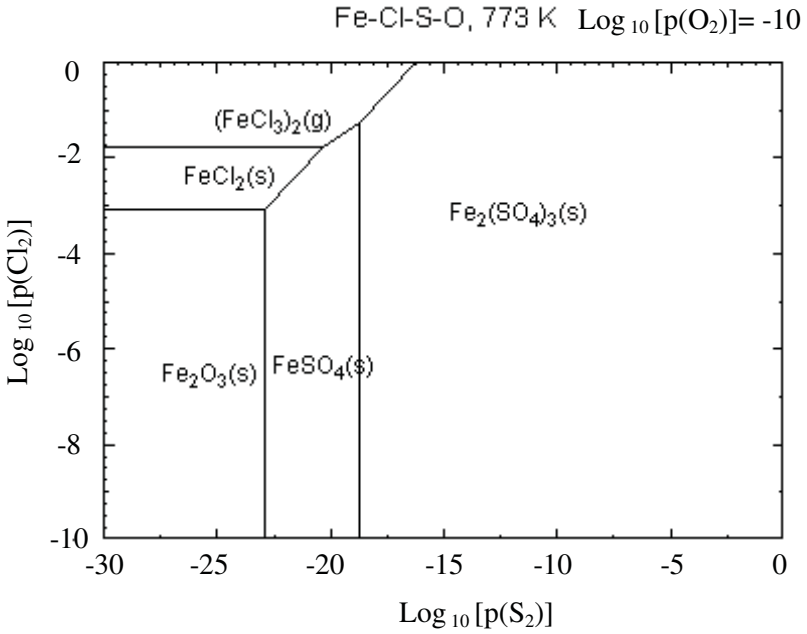

Fig. 2.1.3. TDS of Fe-Cl-S at 773K, $\log_{10}[p(O_2)] = -10$ bar

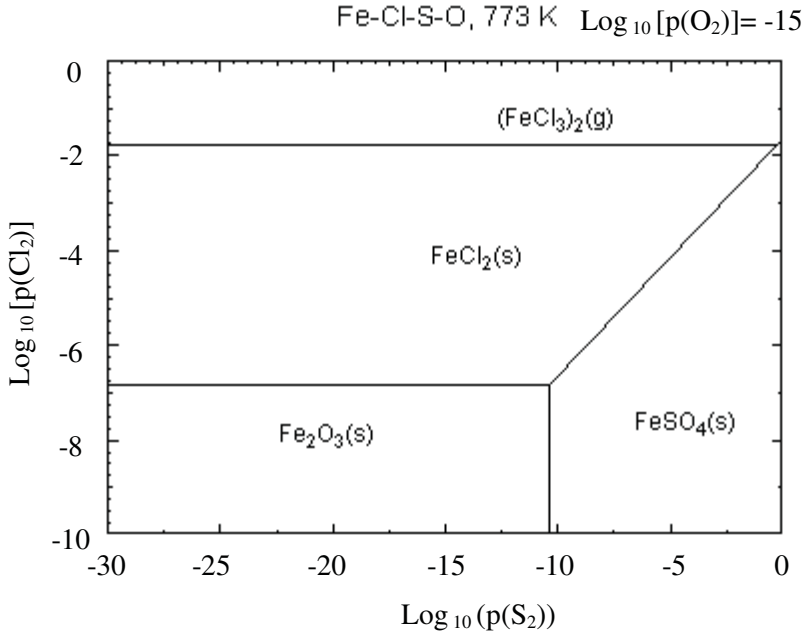

Fig. 2.1.4. Fe-Cl-S thermodynamic stability diagram at 773K, $\log_{10}[p(O_2)] = -15$ bar

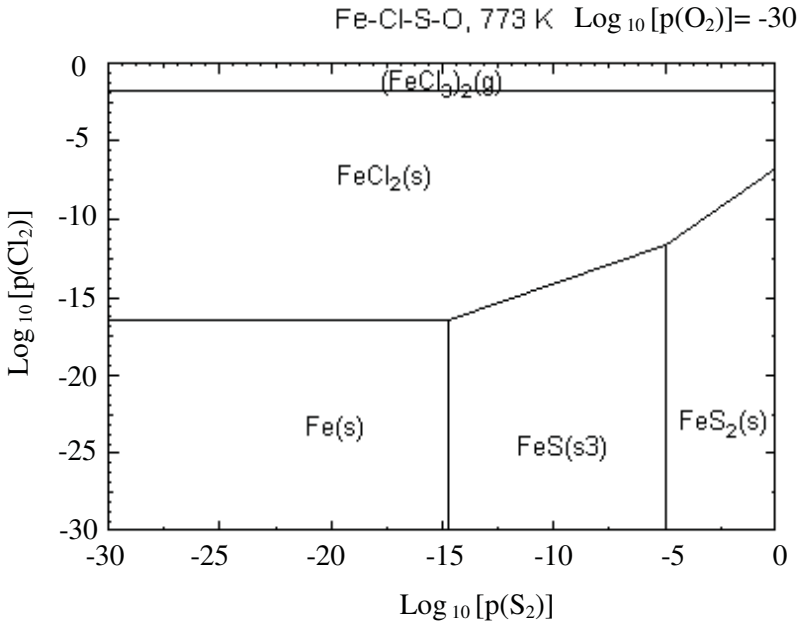

Fig. 2.1.5. TDS of Fe-Cl-S at 773K, $\log_{10}[p(O_2)] = -30$ bar

2.2 Deposit formation and its influence on fireside corrosion

The fate of fuel minerals during combustion and cooling process has direct influence on fireside corrosion. Tube materials covered with deposit ash suffer more serious corrosion than bare tubes. This section gives a brief description of the conversion process of fuel minerals during combustion and different kinds of sulphur-induced fireside corrosion.

2.2.1. The formation and transport of fly ash

Occurrence of mineral matters in fuel

Fuel minerals exist in different chemical and physical forms. According to occurrence, fuel minerals can be classified into excluded mineral grains, included mineral grains in fuel matrix, or organically associated elements /45, 54/. Excluded minerals are added to fuel from extraneous sources during geologic process or during mining. Included mineral grains are inherent minerals in fuel matrix, but they are not chemically bound with fuel matrix. Organically bound minerals are a part of fuel matrix, which come directly from fuel-forming substances. Depending on fuel types, low-rank fuels contain more organically-associated minerals than high-rank fuels. It is often observed that clays and quartz in fuel come from extraneous sources, they are mostly insoluble; alkali and alkaline earth elements are associated with salts or organic acid groups; iron can exist in extraneous pyrite (FeS_2) and siderite ($FeCO_3$), or in organic matters, or in fine-size soluble minerals /61/.

Formation of fly ash

The conversion of fuel minerals to fly ash during combustion and cooling process involves complicated chemical and physical processes. The characters of fly ash depend on the mineral distribution in fuel and the type of combustor. The type of combustor influences the extent of chemical reactions. In the case of pulverized coal combustion, the particle size distribution of fly ash follows a bimodal size model. The ash formation process is illustrated in Fig. 2.2.1 /46, 60, 61/. The intermediate ash species include gases, liquids and solids. Submicron compounds originate from homogeneous condensation of volatile inorganic components during combustion. Volatile minerals can also condense on the surface of entrained ash particles or on ash deposits. Large ash particles originate from the minerals in char particles, which are fragmentised or coalescence during burnout. Excluded minerals evolve into ash particles individually with or without fragmentation; included minerals, which are embedded within coal particles, usually undergo coalescence to some extent, depending on physical closeness within a single char particle.

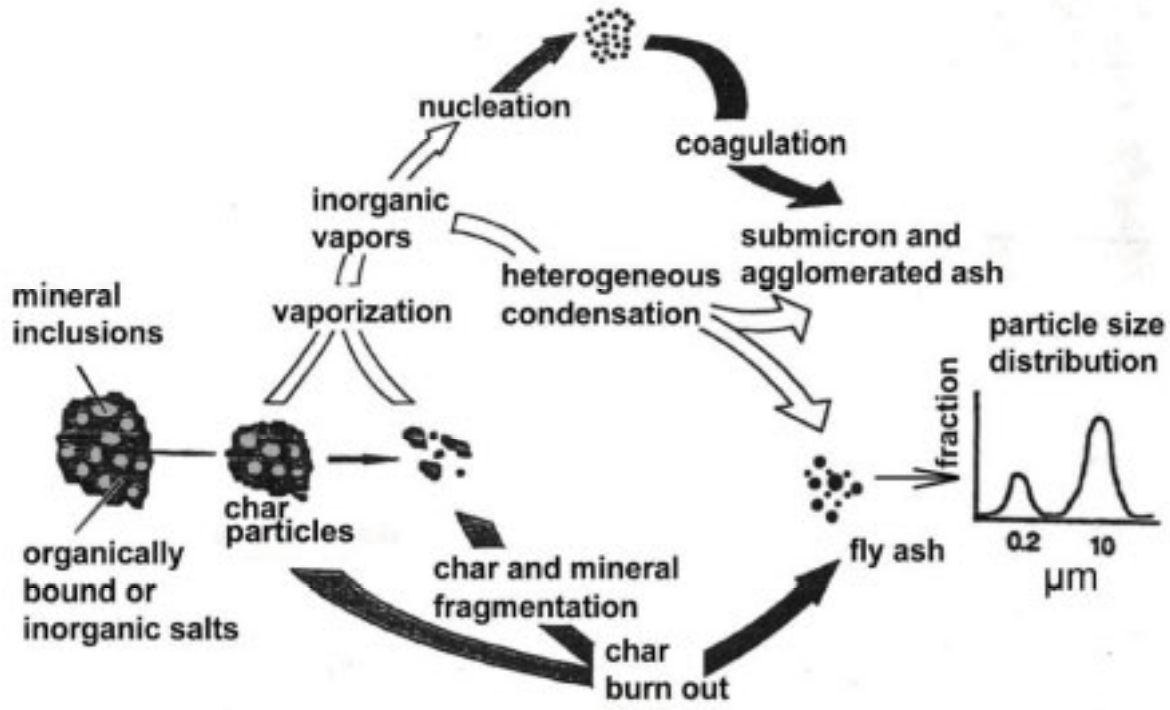

Fig. 2.2.1. Ash conversion process /46/.

The behaviour of mineral matters in biomass can be compared to that in coal. The difference is that biomass contains large quantities of volatile inorganic species. As consequence, condensation of mineral vapours can be more profound in biomass boilers than that in coal boilers. Two important mineral elements in biomass are chlorine and potassium. Detailed studies reveal that chlorine is released into gas phase during volatilization period, whereas most potassium is released into gas phase during char combustion. Potassium chloride (KCl) is the primary gaseous alkali species released from combustion of straw and grasses, whereas KOH(gas) is the most abundant alkali vapour from combustion of biomass with high alkali metal and low chlorine content /47/. When SO_2 is enriched in flue gas, KCl could convert to K_2SO_4 below 850°C /71/. In the flue gas temperature range from 900°C to 650°C, K_2SO_4 condenses homogeneously and acts as the nuclei of fine fly ash particles. The nuclei can further grow by the condensation of KCl /48/.

Combustion temperature exerts significant influence on the fate of chlorine. At low combustion temperature, as in the case of fluidised bed combustion (FBC), KCl is the main form of chlorides; whilst during pulverized fuel (PF) combustion, potassium can be bound with Si-Al minerals. In this case, the free chlorine-ions exist more likely in gaseous HCl /30/.

Deposit formation

The transport of fly ash particles to heat transfer surfaces and the subsequent deposition process depend upon the size and the composition of ash particles, flue gas patterns and tube

surface conditions. The transport of small particles (less than 5 μm) is dominated by thermophoresis, diffusion and condensation, and the transport of large particles (greater than 5μm) is dominated by inertial impaction /50, 54, 56/. The different transport mechanisms are discussed below:

- *Vapour condensation and diffusion*: Due to the temperature difference between flue gas and tube surface, low-dew-point vapour mineral species condense or even solidify at cooler area near heat transfer surface. This generates a pressure gradient of such vapour species from flue gas to tube surface. As result, vapour minerals in flue gas diffuse continuously toward tube surface, condense and deposit there. Vapour condensation and diffusion are the major transport mechanisms for particles less than 1 micron.

- *Thermophoresis*: Small particles (< 3μm) can deposit by means of thermophoresis due to local temperature differences. A small particle is collided by gas molecules from all directions around it. Gas molecules from hot side contain higher average kinetic energy than that from cold side, this results in a net force on the particle towards regions with lower temperature.

Deposit ashes generated by vapour condensation and diffusion, and thermophoresis distribute evenly around the whole circumference of tube. The most corrosive species, such as alkali chlorides and alkali sulphates, are mainly transported to the tube surface by above mechanisms. This phenomenon can be observed during straw combustion: a cooled deposition probe is covered with a white layer of alkali salts right after the insertion in the furnace /10/, /56-58/.

- *Inertial impaction*: Large particles, usually larger than 5 to 10 microns, may have enough inertia to leave gas streamlines and strike straight on the front side of tube surface /56/. The primary factors which dominate the inertial impaction are the velocity of the gas flow and the inertia of an ash particle. The backside of the tube surface is usually deposited by eddy impaction. Eddy impaction acts on particles of medium size. This range of particles is too small to impact on the front side of a tube, but they have sufficient inertia to impact on the backside of a tube by turbulent eddies. The size of these particles is usually less than 10 microns /56/.

The transport of fly ash is also dominated by gas flow patterns. The gas flow field is divided into three zones: a fully turbulent core, a buffer layer and a boundary layer. In the turbulent core and the buffer layer, thermophoresis and diffusion may be negligible due to small

temperature gradients. However, in the boundary layer, thermophoresis and diffusion become much stronger than that in the buffer layer and in the turbulent core /60/.

2.2.2. Deposit growth and strength development

Deposits are often classified into fouling deposit, sintered deposit and slagging deposit. Fouling deposit consists of loosely-bound fly ash. Fouling deposit builds up usually on the heat transfer surface in the convective pass of a boiler. The cohesion in a fouling deposit is resulted by many forces, such as van der Waals effect, surface tension, electrostatic, and interlocking particle effect.

Sintered deposit forms when ash particles stick together strongly. There are several forms of sintering: e.g., liquid state sintering, chemical reaction sintering and solid state sintering. Liquid state sintering occurs through the appearance of melt in a particle. Chemical reaction sintering occurs when a reaction between particles leads to the formation of a third component, which forms the neck between such particles. Solid state sintering may occur through diffusions along particle surface and subsequent condensation. Among above sintering mechanisms, liquid phase sintering is the fastest sintering process and also the dominant sintering mechanism in coal-fired boilers.

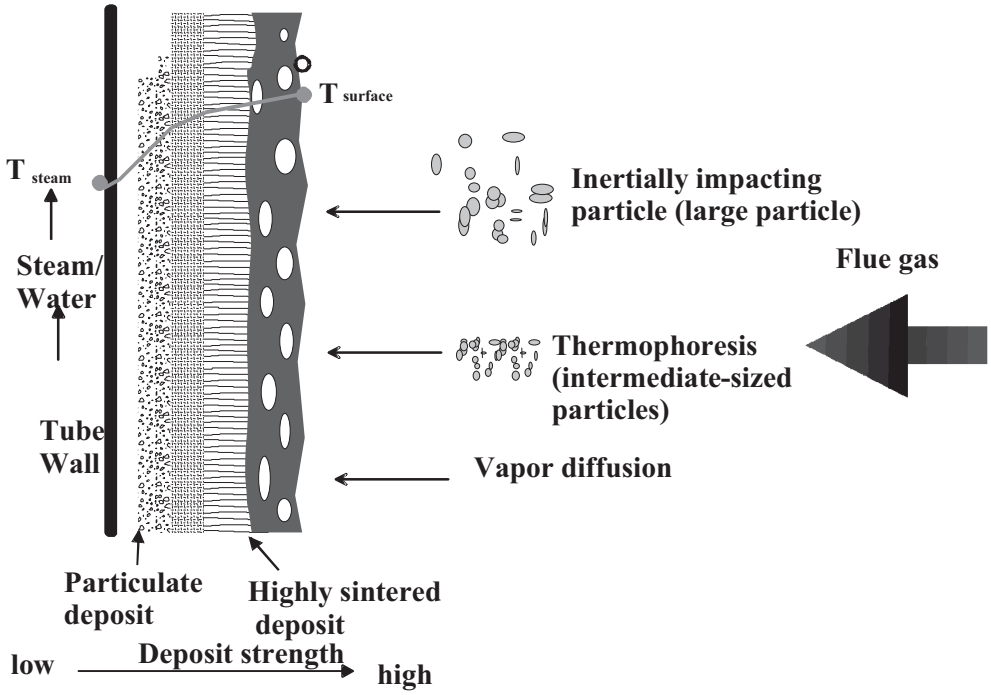

Fig. 2.2.2. Ash transport mechanisms and deposit growth

Slagging deposit can directly build up by inertia impaction of molten or viscous ashes, which is usually the case in the highest temperature zone in a furnace. An outer deposit layer on a

tube surface can also become slagging when the deposit is so thick that the temperature of the outer layer reaches the melting temperature.

The strength development of deposit depends most critically on the formation of low-viscosity melt phases /54/. The growth and the strength development of deposit are illustrated in Fig. 2.2.2 /60/. Initially, a powdery fouling deposit layer forms, which consists mostly of condensed fine particles /45/. The fouling deposit layer acts as an insulator due to its low thermal conductivity. As consequence, the outer layer temperature can be high enough to cause completely fusing. In such way, sintering and slagging occur, and strength builds up in the deposit. The liquid phase then becomes an efficient collector of ash particles, regardless the melting behaviour of these ash particles.

2.2.3. Hot corrosion

Hot corrosion is the most common form of high temperature fireside corrosion in coal-fired boilers. An important character of hot-corrosion is that the combined attack of deposits and gas environment on corrosion rate is more harmful than it would have been by the attack of gas alone. When a deposit ash layer is dry, it is relatively innocuous; but when it is semi-molten, it may corrode most of the alloys that may be used in superheater construction /62/. In coal-fired boilers, the semi-molten deposit component is found to be a sulphate complex. Chlorine corrosion can be troublesome for a bituminous coal when it contains more than 3.5% sulphur and 0.25% chlorine.

Serious hot corrosion is usually observed on the upstream side of a tube, as shown in Fig. 2.2.3 /57, 62/. The greatest metal losses occur usually on the 10 and 2 o´clock positions of the tube, and it tapers off little or none on the back side of the tubes. Since the 10 and 2 o´clock positions on the tube upstream side endure the strongest strike of flue gas streamline, and the heat flux is the highest at such positions. In addition, such positions have easy contact with gas atmosphere and they are continuously deposited with fresh corrosive ashes.

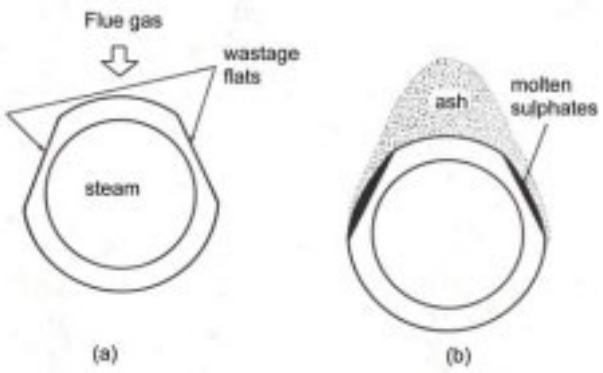

Fig. 2.2.3. Positions of metal wastage by hot corrosion /57/

Metal temperature and flue gas temperature play important roles on the rate of hot corrosion. The corrosion rate as function of metal temperature can be illustrated with a bell-form curve. The peak of corrosion rate locates in the temperature range of 590-720°C, as shown in Fig. 2.2.4 /53, 62/. The starting point of the fast corrosion rate corresponds well to the melting temperature of some alkali complexes; the upper temperature limit corresponds to the decomposition temperature of such alkali complexes /49/.

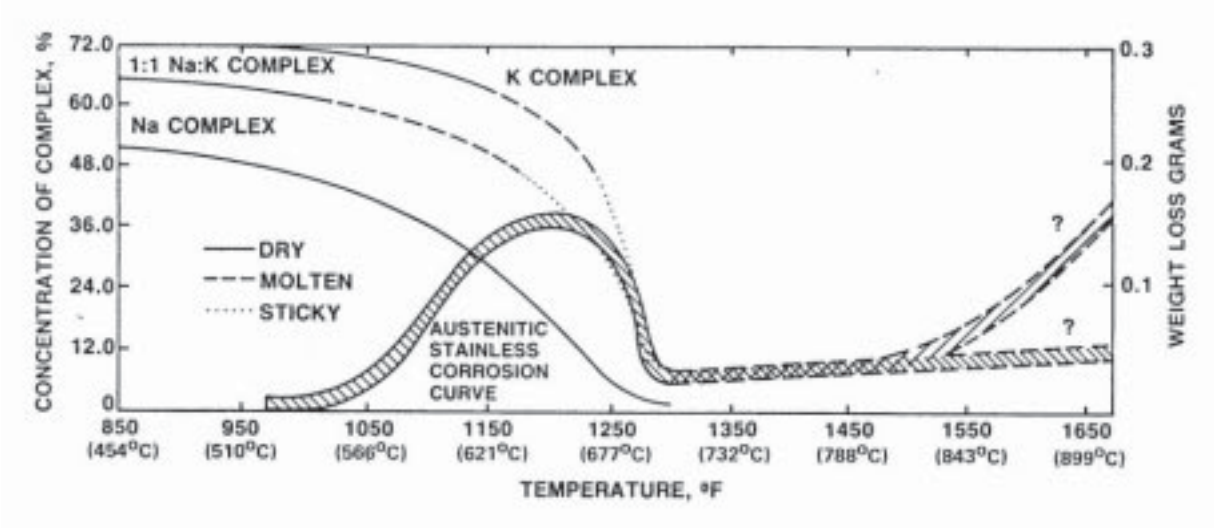

Fig. 2.2.4. Dependence of corrosion rate on metal temperature /59/

The rate of hot corrosion increases with flue gas temperature, as shown in Fig.2.2.5. For a given metal temperature, the higher the flue gas temperature, the higher the temperature gradient between flue gas and metal surface. Corrosive species, such as gaseous alkali chlorides and alkali sulphates, have usually low dew temperatures. They tend to immigrate to cooler tube surface area and condense. Therefore, the temperature gradient between flue gas and tube surface is one of the important driving forces for the continuous inward transport of such corrosive species to tube surfaces /31/.

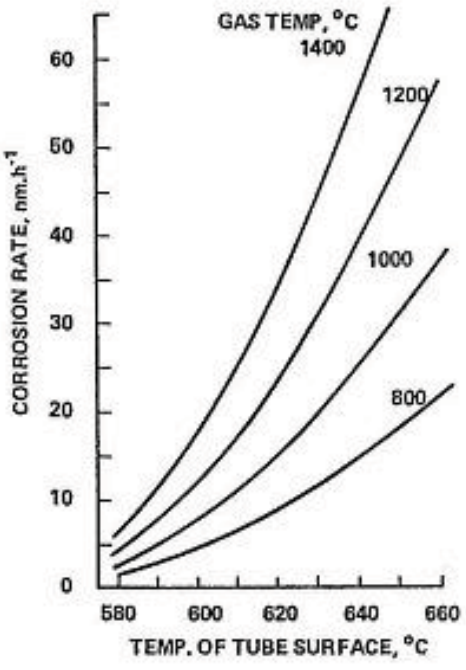

Fig. 2.2.5 corrosion rate dependence on flue gas temperature in coal-fired boilers /31/

The most convincible explanation of hot corrosion is that, SO_3 from the decomposition of alkali-sulphate complex, such as $KAl(SO_4)_2$ or $K_3Fe(SO_4)_3$, acts as direct attack medium to oxide scale and metal /52/. The possibility of the direct attack from solid sulphate complex is excluded, since solid sulphates in the deposit ash are not found directly near the deposit/oxide interface.

The formation of alkali sulphate complexes can be expressed in following reactions:

$$3K_2SO_4\,(s) + Fe_2O_3(s) + 3SO_3(g) \Leftrightarrow 2K_3Fe(SO_4)_3(s)$$

$$K_2SO_4(s) + Al_2O_3(s) + 3SO_3(g) \Leftrightarrow 2KAl(SO_4)_2(s) \qquad (2.2.1)$$

The formation of alkali sulphate complexes in deposit ash requires the enrichment of alkali sulphates and a high local pressure of SO_3. The enrichment of alkali sulphates in deposit is possible in many ways. As described above, alkali sulphates can be either transported to tube surface through vapour condensation and diffusion, or thermophoresis at the initial stage, or through the immigration of gaseous sulphates to the inner cooler deposit layer when the deposit is already built up.

In addition, a high concentration of alkali chlorides in flue gas can also lead to enrichment of alkali sulphates in deposit. Taking KCl for example, there are principally three main reaction routes for gaseous KCl to be converted to solid sub-micron K_2SO_4 particles /46/:

1. KCl is sulphated in the gas phase and then condenses on the heat transfer surfaces or condenses homogenously as sub-micron particles:

$$KCl(g) \xrightarrow{sulphation} K_2SO_4(g) \xrightarrow{condensation} K_2SO_4\,(l,s) \qquad (2.2.1)$$

2. Gaseous KCl condenses on the heat transfer surfaces and is sulphated by a solid-gas phase reaction:

$$KCl(g) \xrightarrow{condensation} KCl(l,s) \xrightarrow{sulphation} K_2SO_4\,(l,s) \qquad (2.2.2)$$

3. Gaseous KCl reacts with SO_2 and forms condensed K_2SO_4:

$$2KCl(g) + SO_2(g) + \tfrac{1}{2}O_2(g) + H_2O(g) \xrightarrow{sulphation} K_2SO_4(l,s) + 2HCl(g) \qquad (2.2.3)$$

On the other hand, the requirement of SO_3 concentration for the formation of alkali sulphate complexes can not be directly satisfied in flue gas atmosphere. Harb and Smith reported, for example, that the mixture of K_2SO_4 and Fe_2O_3 require at least 250 ppm SO_3 to form $K_3Fe(SO_4)_3$ at 538°C, and the equilibrium pressure of SO_3 for the formation of the alkali sulphate complexes is 1000 ppm at 637°C /43/. The SO_3 concentration in flue gas, which seldom exceeds 35 ppm, is too low to meet the formation requirement of the low-melting sulphate complexes. Thus the SO_3 concentration in the local deposit region must be considerably higher than that in the flue gas atmosphere. Experiments done by some researchers have confirmed this possibility: SO_3 can be enormously promoted by the catalytic oxidation of SO_2 and O_2, with catalysts, such as V_2O_5, Fe_2O_3 in deposits /62/. The favour temperature of the catalytic reaction is between 600 and 700°C. It is also observed that the presence of temperature gradient facilitates the adsorption of sulphur from flue gas to ash deposit /43/.

As mentioned above, it is suggested in many studies that the rate of hot corrosion is directly related with the local partial pressure of SO_3, and SO_3 originates from the decomposition of alkali sulphate complexes. Bolt and Pastoors demonstrated that at the metal temperature range of 625-670°C, the corrosion behaviour follows the SO_3-flux behaviour. In this model, SO_3 supply through the deposit is assumed to be the rate-determining step, as shown in Fig. 2.2.7 /49/. Thermo-gravimetric analysis also confirms that $K_3Fe(SO_4)_3$ and $KAl(SO_4)_2$ are not

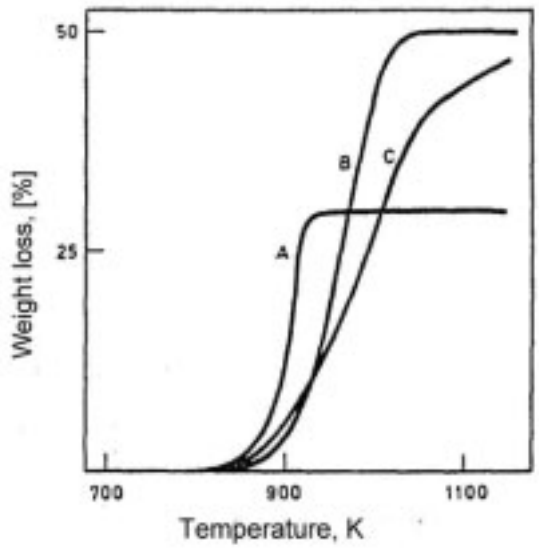

Fig. 2.2.6. Thermogravimetric analysis of complex sulphates and corrosive superheater deposits: A: $K_3Fe(SO_4)_3$, B: $K_3Al(SO_4)_3$, C: sulphates in deposit /43/

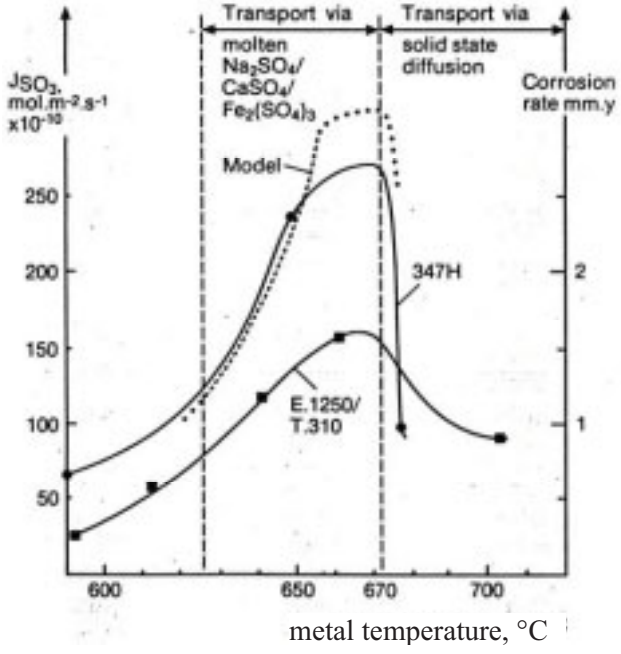

Fig. 2.2.7. SO_3 flux (dashed line) calculated in superheater deposits /49/

thermodynamically stable when the temperature exceeds 600°C. In the case of $K_3Fe(SO_4)_3$, the decomposition starts even at the temperature of about 530°C (Fig. 2.2.6) /43, 49/.

The morphology of hot corrosion in coal-fired boilers is characterized by the formation of metal sulphides at the scale/metal interface. In the case of low-Cr steels, a three-layer structure of the corrosion scale is observed. From gas phase to metal, an outer layer of Fe_2O_3, a medium layer of mixed Fe_3O_4-FeS and an inner layer of FeS can be observed. It is suggested that the medium Fe_3O_4-FeS layer grows by outward diffusion of iron cations, and the inner layer of FeS grows by inward diffusion of oxygen and sulphur to the underneath metal /49/. In the case of high-Cr steels, iron oxides, chromium oxides and sulphides are formed in an order from outer corrosion scale to the metal /41, 42, 49, 67, 68, 70/. The scale structure of austenitic steels, for example, is illustrated in Fig. 2.2.8 /73/.

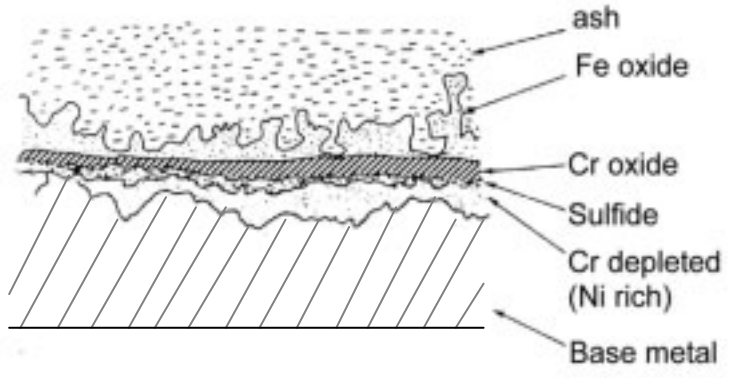

Fig. 2.2.8. Morphology of sulphate hot corrosion of 347H /73/

2.2.4. Waterwall corrosion

Rapid corrosion on waterwall tubes is associated with reducing condition. Reducing combustion atmosphere is often marked with the presence of CO or H_2S, and the poor burnout of fuel particles. Serious fireside corrosion is likely to occur at the areas where the CO concentration is higher than 0.6% /43/. The corrosion rate can be 600nm/hr or more compared to the normal oxidation rate of about 8nm/hr. Such severe corrosion reduces the lifetime of waterwall drastically and may lead to unexpected tube failures. A number of factors may attribute to the high metal wastage: e.g. flame maladjustment, primary NOx-reducing measures, poor milling, high heat flux and molten ash deposits.

Flame maladjustment may cause flame impingement on waterwall tubes. This leads to the transportation of burning particles, volatile species and perhaps molten ashes to the furnace wall. Furthermore, flame impingement creates local alternating reducing/oxidizing atmosphere. Alternating reducing/oxidizing condition is believed to be more dangerous than mono-reducing environment. In the reducing period of the alternating atmosphere, non-oxidized minerals, e.g. FeS, KCl, in flue gas are transported to the tube surface; in the

oxidizing period, such minerals are oxidized and corrosive gases such as SO_3 or HCl are released.

Strategies to limit NOx formation increase the likelihood of corrosion owning to the creation of reducing environment and the enlargement of flame zone. Air staged combustion is regarded to be more corrosive than low-NOx cell burner combustion.

Poor milling can lead to the result that a large amount of large particles impinge on the furnace wall before they are completely burned. During further burnout of such large particles, hot spots and local reducing atmosphere are created.

Heat flux: among all boiler tubes, furnace wall tubes bear the highest heat flux. The great temperature difference between the hot gas in the combustion zone and the relatively cooler waterwall tubes facilitates the transport of low-melting-point chlorides and sulphates to tube areas.

Corrosion by molten iron sulphides

The deposition of molten iron sulphides on waterwall tube surface is one of the important reasons of the local high sulphur concentration. Non-oxidized sulphides can reduce the melting temperature of the whole ash system and release sulphur gases when they are oxidized in ash deposit. Most iron sulphides come from fuel pyrite particles (FeS_2). The conversion process of pyrite during combustion is illustrated in Fig.2.2.9 /66/. Pyrite begins to lose sulphur at about 350°C and decomposes to pyrrhotite (FeS) in reducing environment or iron-oxide in the presence of oxygen /50/, /65/, /73/.

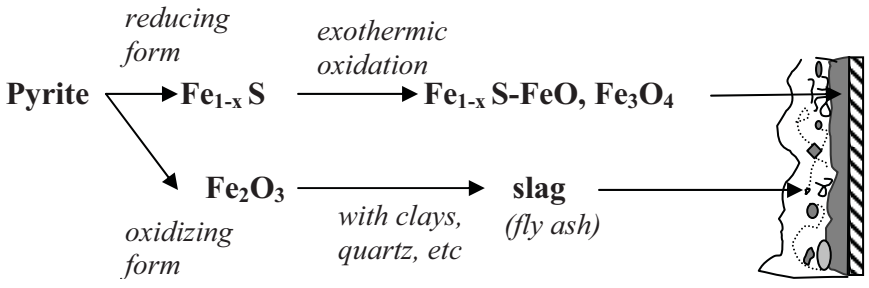

Fig. 2.2.9. Pyrite conversion in reducing and oxidizing environment /66/

Non-oxidized iron compounds are known to melt at low temperature. An enrichment of iron in fuel could reduce the total ash fusing temperature, as shown in Fig. 2.2.10 /62, 64/. A thermodynamic model explains that, during the exothermic oxidation of pyrite, the temperature of iron sulphide particles ($Fe_{1-x}S$) is higher than local temperature, as

consequence, sulphide particles begin to melt in flue gas. In oxidizing condition, pyrite is completely oxidized to Fe_2O_3 in flue gas, which although can also deposit on tube surface, but it is not a further danger of releasing SO_3 gas.

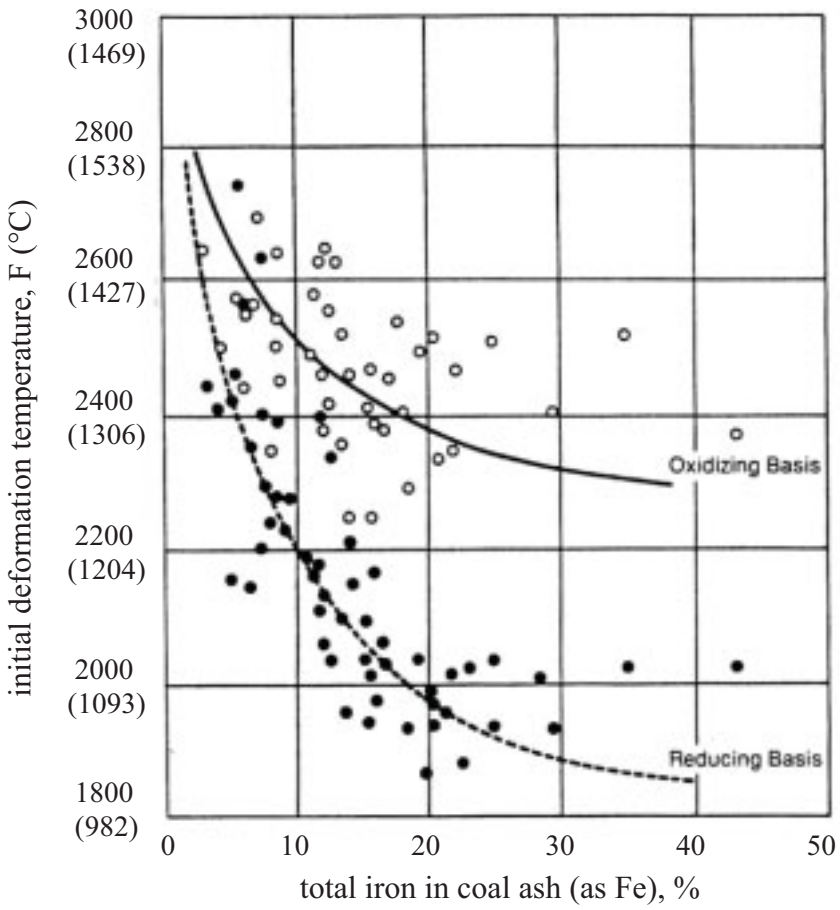

Fig. 2.2.10. Influence of iron on ash fusing temperatures /62/

Both pyrite and pyrrhotite in deposit tend to be oxidized with time. This phenomenon could be verified by author's research of iron slag on a probe surface, as shown in Fig. 2.2.11. The deposition specimen was obtained from a cooled probe which was exposed in the combustion zone of a furnace, in which a high sulphur coal was fired. The tube surface temperature was controlled at 500°C. The probe emitted strong smell of sulphur gas as it was pulled out from the furnace. Molten iron sulphides or Fe-Ca-S complex were observed in the SEM-EDX pictures. Although in the surface-near regions, the molten particles were oxidized, sulphur could still be found in the core of the particles. Furthermore, sulphur was enriched in the corrosion layer. Fig. 2.2.10 suggests that sulphur gases released from molten iron slag diffused to metal surface and built up corrosion product of iron sulphides /63/.

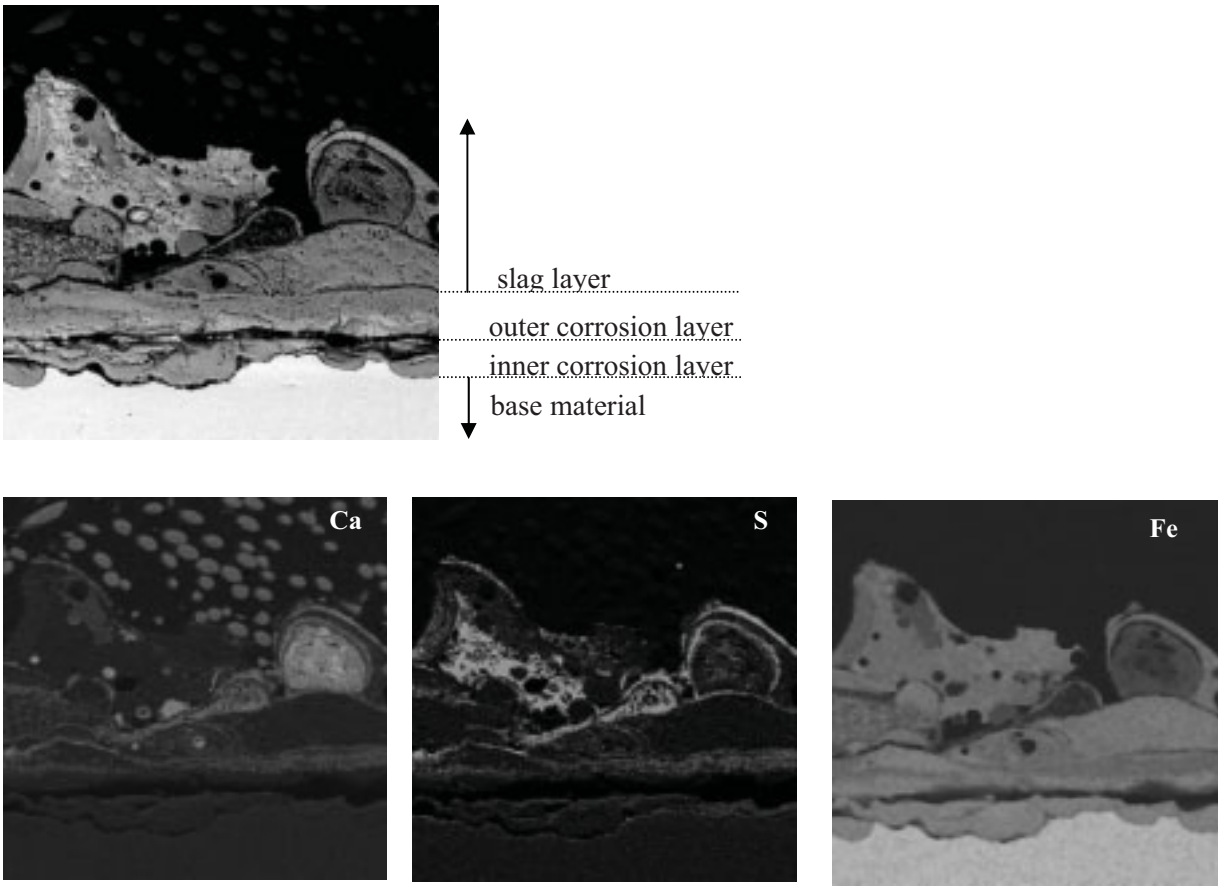

Fig. 2.2.11. SEM-EDX of slag deposit formed by firing a lignite coal

In addition, a molten ash deposit layer on tube surface may promote the activity of sulphide underneath the deposit, since such a compact layer prevents the diffusion of oxygen from flue gas to metal front and thus creates reducing condition underneath the deposit /70/.

Corrosion by molten alkali sulphate

Molten sulphate deposit could be another initiator of waterwall corrosion. Besides the mechanisms of hot corrosion, as described in Chapter 2.2.3, it is also suggested that liquid pyrosulphate ($Na_2S_2O_7$) can attack protective oxide film aggressively according to the following reactions:

$$3Na_2S_2O_7 + Fe_2O_3 \rightarrow 2\ Na_3Fe(SO_4)_3$$

$$3Na_2S_2O_7 + Fe_2O_3 \rightarrow 3Na_2SO_4 + Fe_2(SO_4)_3$$

$$4Na_2S_2O_7 + Fe_3O_4 \rightarrow 4\ Na_2SO_4 + FeSO_4 + Fe_2(SO_4)_3 \qquad (2.2.5)$$

Liquid pyrosulphates can be formed on waterwall tubes by the reaction of SO_3 with alkali sulphates according to (2.2.6) /69/.

$$Na_2SO_4 + SO_3 \rightarrow Na_2S_2O_7\ (l)$$

$$K_2SO_4 + SO_3 \rightarrow K_2S_2O_7\,(l) \qquad (2.2.6)$$

However, the formation of pyrosulphate is limited in waterwall area, since it is not stable above the waterwall tube temperature.

2.3 Chlorine-induced corrosion in biomass or waste combustion facilities

The damage caused by chlorine-induced corrosion in biomass and waste combustion systems is well known. The scale formed during chlorine-induced corrosion is not protective. A number of studies have shown that chlorine gases can even damage normally protective oxide scales /74-75/. Chlorine gases, such as HCl in flue gas atmosphere, are usually present as the second oxidant in oxidizing environment. The combined effect of chlorine and oxygen leads to more damage than the damage done by chlorine alone /44/. Most biomass-fired or waste-fired facilities must limit their steam temperature due to the chlorine-induced fireside corrosion. The maximum steam temperatures allowed for some typical boiler materials in straw-fired facilities are provided in Tab. 2.3.1 /28/.

Tab 2.3.1. max. steam temperature for some superheater alloys in straw-fired boilers

Steel	Cr/Ni, [%]	Maximum steam temperature
15Mo3	- / -	< 450°C
X20CrMoV121	12 / 0.5	< 470°C
TP347HFG	18 / 10	< 540°C

2.3.1 Corrosion mechanisms

Chlorine-induced corrosion is initiated by vapour or solid chlorine species in flue gas or in ash deposit. Harb reported that about 0.8% concentration of HCl in flue gas can completely destroy the integrity of the Fe_2O_3 layer, and 2.0% HCl concentration can destroy the continuity of both Fe_2O_3 and Fe_3O_4 layers /43/. Although HCl or alkali chlorides could be dominant chlorine compounds in flue gas and in ash deposits respectively, Cl_2 is the direct medium to attack metal. The Cl_2 concentration in bulk gas is very low, but it can be increased in ash deposit and at the metal/scale interface, where the oxygen pressure is low /20/. It is even suggested that the oxide scale acts as catalyst in the oxidation of HCl, as shown in (2.3.1). During the reaction, chlorine gas is released /85/.

$$2HCl + ½\, O_2 + MeO \Leftrightarrow Cl_2 + H_2O + MeO \qquad (2.3.1)$$

The equilibrium Cl_2 pressure for above reaction is in the range of 10^{-10} – 10^{-13} bar /95/. When steel surface is exposed in a gas mixture of O_2 and HCl, simultaneous formation of metal oxides and metal chlorides takes place at the initial stage. It can be followed by an overgrowth

of oxides with time. The oxide scale produced under this condition is porous and not protective. Furthermore, when a protective oxide scale is already formed in a pure oxidizing environment, the scale could still be penetrated by chlorine species when the material is exposed in a chlorine-containing gas afterwards. Fast corrosion of a preoxidized metal is observed right after the exposure in chlorine-containing gas, thus, it is more likely that chlorine gas reaches metal surface through shortcuts in the scale, instead of per solid-state diffusion or grain boundary diffusion /95, 96/. For a preoxidized material, the penetration paths for chlorine gas must be created by the reactions of chlorine compounds on the scale.

It is also suggested that the presence of chlorine may change the dynamic equilibrium between crack formation and scale healing: on one hand, crack formation is promoted by the rapid growth of oxide scale; on the other hand, the cracks can be healed with newly formed oxides, but such kind of scale is heterogeneous and porous.

When chlorine gas manages to arrive at the scale/metal interface, metal chlorination takes place according to (2.3.2). Since the oxygen potential at the scale/metal interface is very low, metal chlorides, such as $FeCl_2$ or $CrCl_2$, could be thermodynamically stable there.

$$Me\,(s) + Cl_2\,(g) \rightarrow MeCl_2\,(s) \tag{2.3.2}$$

Simultaneously, metal chlorides evaporate due to their high equilibrium vapour pressures:

$$MeCl_2\,(s) \rightarrow MeCl_2\,(g) \tag{2.3.3}$$

Once the concentration gradient of gaseous metal chloride through the scale is created, volatile metal chlorides tend to diffuse outwards through cracks and pores in the scale. On its way outwards, metal chlorides reach the regions of higher oxygen pressure and are subsequently oxidized:

$$3MeCl_2\,(g) + 2O_2\,(g) \rightarrow Me_3O_4\,(s) + 3Cl_2\,(g) \tag{2.3.4}$$

$$2MeCl_2\,(g) + (3/2)O_2\,(g) \rightarrow Me_2O_3\,(s) + 2Cl_2\,(g) \tag{2.3.5}$$

During above reactions, Cl_2 is released and it can diffuse backwards to the scale/metal interface. In such way, Cl_2 circulates beneath the oxide scale. The circulation of chlorine gas results in continuous transport of metal to oxide scale with little net consumption of chlorine gas. Fig.2.3.1 illustrates the circulation of chlorine gas in the active oxidation process. Such accelerated metal oxidation with the involvement of chlorine gas is called “active oxidation”,

which notifies the difference from the normal passive and protective oxidation. The rate of the active oxidation is catastrophically high and the oxide scale is porous and non-adhering.

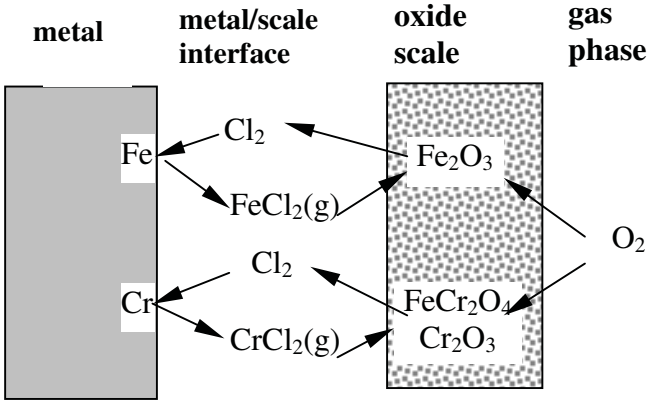

Fig. 2.3.1. Circulation of chlorine gas in the active oxidation process

The rate of active oxidation could be determined by one of the following steps: inward diffusion of oxygen, metal chlorination at the metal surface, vaporization of metal chlorides, outward diffusion of gaseous metal chlorides, and oxidation of gaseous metal chlorides in the scale. Which step determines the corrosion rate depends on the structure of the scale and temperature. Some researchers believe that the rate-determining step after the initial stage is gas transport /95/. After the initial period, when the scale is formed, the driving force of the active oxidation is the pressure gradient of reactants O_2 and the volatile metal chlorides between the metal/scale interface and the gas phase /71/. It is suggested that although the scale is loose and crackly, the free spaces through which $FeCl_2(g)$ or oxygen can diffuse are still rather small. It must take account that the ways for outwards diffusion of $FeCl_2(g)$ are blocked by itself per oxidation /95/.

Other researchers believe that the evaporation of metal chlorides could play an important role. When the vapour pressure of a metal chloride exceeds 10^{-5}Mpa, evaporation of metal chlorides is considered to be profound. The vapour pressure of metal chlorides depends strongly on temperature /34, 82/. Table 2.3.2 lists the melting points and the temperatures at which the vapour pressure of metal chlorides reaches 10^{-5}Mpa. At high temperature, evaporation of metal chlorides could accelerate the total corrosion rate.

Tab. 2.3.2. Melting point (T_m) and temperatures (T_4), at which the chloride vapour pressure is equal to 10^{-5} MPa

Chloride	T_m (°C)	T_4 (°C)
$FeCl_3$	676	536
$FeCl_2$	303	167
$NiCl_2$	1030	607
$CrCl_2$	820	741
$CrCl_3$	1150	611

Similar to the hot corrosion induced by sulphate complex, the corrosion rate of a metal under chlorine-rich deposits is higher than that of a bare metal /93/. The enrichment of chlorides in ash deposits is mainly resulted by condensation and vapour diffusion of gaseous chlorides /97/. Potassium chloride is the dominate chloride species in biomass combustion, whereas the chlorides of sodium, zinc and lead are common in the deposits of waste combustion /71, 88, 98/.

The oxide scale could be firstly attacked by chloride salts according to (2.3.6) and (2.3.7).

$$2NaCl + Fe_2O_3 + 1/2O_2 \Leftrightarrow Na_2Fe_2O_4 + Cl_2\,(g) \qquad (2.3.6)$$

$$4NaCl + Cr_2O_3 + 5/2O_2 \Leftrightarrow 2Na_2CrO_4 + 2Cl_2\,(g) \qquad (2.3.7)$$

During such reactions, chlorine gas is generated. The release of chlorine gas can be especially accelerated by SO_2 in an oxidizing environment, in which chloride salts are converted to sulphates, e.g.:

$$2KCl(s) + SO_2\,(g) + O_2\,(g) \rightarrow K_2SO_4\,(s) + Cl_2\,(g) \qquad (2.3.8)$$

When high water vapour pressure is present, HCl is preferably formed instead of Cl_2 /45/:

$$2KCl(s) + SO_2\,(g) + ½\,O_2\,(g) + H_2O\,(g) \rightarrow K_2SO_4\,(s) + 2HCl\,(g) \qquad (2.3.9)$$

Actually, both SO_2 and SO_3 can convert alkali chlorides to alkali sulphates. However, the reaction goes significantly faster by the involvement of SO_3. The enrichment of SO_3 in deposit is possible by catalytic reactions of SO_2 and oxygen with the involvement of V_2O_5 and Fe_2O_3 in deposits, which is described in Section 2.2.3.

Taking iron and sodium chloride (NaCl) as representatives for metal and chloride salt respectively, the possible reactions in the chlorine-induced corrosion process from gas phase through ash deposits and oxide scales to the metal front are summarized in Tab. 2.3.2.

Chloride salts in deposits can form low-melt-point eutectics with other substances. Tab. 2.3.3 lists the melt point of some chloride eutectics /102/. In waste combustion, formation of a molten slag composed of eutectics of NaCl, KCl and $ZnCl_2$ is usually the cause of accelerated corrosion /21, 89/.

Tab. 2.3.2. Mechanism of chlorine-induced corrosion

important compositions	**reactions**
flue gas: *O_2, SO_2, HCl, NaCl*	$2NaCl\ (g) + ½\ O_2 + SO_2 + H_2O\ (g) \rightarrow Na_2SO_4\ (g) + 2HCl\ (g)$ $2NaCl\ (g) + O_2 + SO_2 \rightarrow Na_2SO_4\ (g) + Cl_2$
ash deposit: *NaCl(s)*	$1/2O_2 + SO_2 \rightarrow SO_3$ $4NaCl\ (s) + O_2 + 2SO_3 \rightarrow 2Na_2SO_4\ (s) + 2Cl_2$
outer oxide layer: *Fe_2O_3*	$4HCl + O_2 + Fe_2O_3 \rightarrow 2H_2O + 2Cl_2 + Fe_2O_3$ $Fe_2O_3 + 2NaCl\ (s) + ½\ O_2 \rightarrow Na_2Fe_2O_4 + Cl_2$ $½\ O_2 + 2Fe_3O_4 \rightarrow 3Fe_2O_3$
inner oxide layer: *Fe_3O_4, FeO*	$3Fe + 2O_2 \rightarrow Fe_3O_4$ $2Fe + O_2 \rightarrow 2FeO$
scale/metal interface: *$FeCl_2$, FeS, Fe_3O_4*	$Cl_2 + Fe \rightarrow FeCl_2\ (s)$ $FeCl_2\ (s) \rightarrow FeCl_2\ (g)$ $3FeCl_2(g) + 2O_2 \rightarrow Fe_3O_4 + 3Cl_2$ $4FeCl_2(g) + O_2 + SO_2 \rightarrow Fe_3O_4 + FeS + 4Cl_2$ $3FeCl_2 + 3H_2O + 1/2O_2 \rightarrow Fe_3O_4 + 6HCl$ $SO_2 + O_2 + 4Fe \rightarrow Fe_3O_4 + FeS$ $3FeS + 5O_2 \rightarrow Fe_3O_4 + 3SO_2(g)$
substrate: Fe	$Fe + S \rightarrow FeS(s)$

Tab. 2.3.3. Melt point of some metal-chloride eutectics /102/

eutectic, mol. -%	*melt t. °C*	*eutectic, mol. -%*	*melt t. °C*
$74\ KCl - 26K_2SO_4$	690	$55ZnCl_2 – 45KCl$	230
50NaCl -50KCl	658	$70ZnCl_2 – 30\ NaCl$	262
$17CaSO_4 –38NaCl_2$-45 KCl	605	$60KCl – 40FeCl_2$	355
$25\ NaCl – 75\ FeCl_3$	156	$58\ NaCl – 42\ FeCl_2$	370
$37PbCl_2 – 63FeCl_3$	175	$70PbCl_2 – 30\ NaCl$	410
$60SnCl_2 – 40\ KCl$	176	$52\ PbCl_2 – 48\ KCl$	411
$70SnCl_2 – 30\ NaCl$	183	$72PbCl_2 – 28FeCl_2$	421
$70ZnCl_2 – 30\ FeCl_3$	200	$90PbCl_2 – 10MgCl_2$	460
$20ZbCl_2 – 80\ SnCl_2$	204	$80PbCl_2 – 20CaCl_2$	475

Alkali chlorides may also facilitate the formation of low-melting $K_3Fe(SO_4)_3$. In the presence of O_2 and SO_2, Fe_2O_3 in ash deposit or in oxide scale reacts with alkali chlorides and form high volatile $FeCl_3$ according to (2.3.10) and (2.3.11). $FeCl_3$ may be further converted to sulphate and release Cl_2 according to (2.3.12):

$$Fe_2O_3(s) + 6\,KCl(s,\,l) \rightarrow 2FeCl_3(g) + 3K_2O(s,l) \quad (2.3.10)$$

$$Fe_2O_3(s) + 6KCl(s,l) + 3SO_2(g) + (3/2)O_2 \rightarrow 2FeCl_3\,(s,l,g) + 3K_2SO_4(s) \quad (2.3.11)$$

$$2FeCl_3(s,l,g) + 3SO_2(g) + 3O_2(g) \rightarrow Fe_2(SO_4)_3(s) + 3Cl_2(g) \quad (2.3.12)$$

Low melting eutectic $K_3Fe(SO_4)_3$ may build up from K_2SO_4 and $Fe_2(SO_4)_3$, which are the products of reaction (2.3.11) and (2.3.12).

High-Cr steels are also sensitive to chlorine attack. It is reported that Cr_2O_3 in the oxide scale is fluxed beneath chloride salts according to reaction (2.3.13) /89, 90, 99/.

$$2Cr_2O_3 + 5O_2 + 8NaCl \rightarrow 4Na_2CrO_4 + 4Cl_2 \quad (2.3.13)$$

The lowest melting temperature of the eutectics of NaCl and Na_2CrO_4 is 557°C. It is considerable difficult to form a protective scale once such melt forms. In contrast, high-Ni alloys are resistant in the chlorine-rich environment, since the reaction product $NiCl_2$ is expected to be stable at the operation temperature /91/.

Furthermore, high-Cr steels are more severely corroded than low-Cr steels in the form of internal corrosion. Chromium carbides at grain boundaries are preferentially attacked, leaving a nickel-rich skeleton behind. This is traced back to the extreme low Gibbs energy of the reactions between chromium carbides and chlorine /19, 21/. The overall reactions can be expressed in (2.3.14) and (2.3.15). Severe internal corrosion usually occurs when the metal temperature exceeds 550°C /77/, /78/, /85/, /90/.

$$Cr_{23}C_6 + 23Cl_2 + 6O_2 \rightarrow 23CrCl_2 + 6CO_2 \quad (2.3.14)$$

$$Cr_7C_3 + 7Cl_2 + 3O_2 \rightarrow 7CrCl_2 + 3CO_2 \quad (2.3.15)$$

2.3.2 The influence of chlorine on sulphur-induced corrosion

The formation of metal sulphides is the result of hot corrosion under sulphate-containing deposits. When chloride salts coexist with sulphate salts in deposit ash, the underlying steel would considerably suffer higher scaling rate and deeper penetration depth than it does in only sulphate-containing deposits /100/. Besides above mentioned reactions for the preferable formation of low melting eutectic $K_3Fe(SO_4)_3$ in the appearance of KCl, alkali chlorides can also facilitate the sulphur-induced corrosion in the following ways:

1). Alkali chlorides are usually enriched in the innermost layer of a deposit due to the initial condensation and inward diffusion of gaseous alkali chlorides. By in-deposit conversion of

alkali chlorides to alkali sulphates, the concentration of alkali sulphates is more enriched near the tube surface area. The study from Boonsongsup showed that the conversion of alkali chlorides to alkali sulphates is more depended on the local partial pressure of sulphur species than other parameters, such as water vapour and O_2 partial pressure /94/. A more accurate argument given by Anderson is that the conversion depends on the partial pressure of SO_3 rather than that of SO_2 /58/.

2). Chlorine corrosion may cause breakdown of the normally protective scale. Through the cracks and porous of the scale, SO_2 or SO_3 could reach easily to the metal surface and the rapid formation of metal sulphides occurs.

3). The coexistence of alkali chlorides and alkali sulphates in deposits decreases the melting temperature of the salt mixture. As results, the bell-shaped curve of corrosion rate in dependence of material temperature in Fig. 2.2.4 becomes wider and higher.

2.3.3 The effect of SO_2 on reducing chloride deposition

A number of studies proved that in the case of firing high-sulphur and high-chlorine fuels, deposits mainly consist of alkali sulphates instead of alkali chlorides. Since gaseous alkali chlorides are thermodynamically not stable in the presence of SO_2, O_2 and water vapour in flue gas, alkali chlorides are sulphated in flue gas and form relative non-critical HCl gas. The overall reaction can be summarized in (2.3.16) /50, 71, 79, 87/.

$$2MeCl(g) + ½\ O_2 + SO_2 + H_2O(g) \rightarrow Me_2SO_4(g) + 2HCl(g) \qquad (2.3.16)$$

where $Me = Na, K$.

Doane applied the mole ratio of SO_2/HCl in flue gas to describe the function of SO_2: in the furnace wall area, the ratio is 2.0, which is sufficient to reduce chlorine corrosion; in the superheater area, the ratio is between 0.7 to 1.5, depending on the alloy composition, to reduce chlorine corrosion /79/. Krause et al completed the result that when the S/Cl- molar ratio is greater than 4.0, chlorine corrosion disappeared completely /101/. Chlorine-induced corrosion is not believed to be severe in coal-fired boilers, since most kinds of coal have a S/Cl molar ratio above 2.2, which can result in a SO_2/HCl molar ratio over 2.4 /79, 80/. However, the deposition of alkali chlorides may be severe during straw combustion, since straw contains generally lower sulphur than coal /19/.

Besides, flue gas temperature, aluminosilicates and calcium contents are found to be important to the deposition of alkali chlorides. Nielsen and Christensen reported that

increasing partial pressure of SO_2 in flue gas only enhances the conversion of chlorides at high temperature (above 900°C) and it has minor influence at low-temperature (below 800°C) /93, 48/. At the hottest flue gas zone in a PF boiler, alkalis are also likely to be bound with aluminosilicates complexes. As consequence, chlorine exists in flue gas as HCl rather than alkali chlorides. During fluidised bed combustion, the flue gas temperature is too low to allow the retention of alkali metals by SO_2 or aluminosilicates, thus the chlorine species in flue gas remain as alkali chlorides. Besides, calcium absorbents can reduce the concentration of SO_2 in flue gas by the formation of $CaSO_4$. This in return promotes the deposition of alkali chlorides. In addition, the deposition of alkali chlorides is expected to be more severe in reducing environment than in oxidizing environment due to the low pressure of reactants O_2 and SO_2.

2.3.4 Conclusion

Chlorine-induced fireside corrosion is characterized by rapid formation of porous oxide scale. This process is so called “active oxidation”. The direct attack medium, Cl_2, is generated from the oxidation of HCl in flue gas, or from the oxidation of solid alkali chlorides in deposits. Cl_2 can penetrate originally protective oxide scale to the scale/metal interface and react with the metal there. Most metal chlorides are high volatile. Gaseous metal chlorides are oxidized on the way outwards to flue gas and release Cl_2 gas. In such way, Cl_2 circulates beneath the oxide scale and attacks the metal in a catalytic way.

Depending on scale structure and temperature, the corrosion rate could be determined by diffusion process or by the evaporation rate of metal chlorides. Chlorination of metal can determine the corrosion rate at the initial stage of an exposure, whereas outward diffusion of gaseous metal chlorides or inward diffusion of oxygen could be the determining step when a thick scale builds up. Increasing temperature exacerbates the corrosion by improving the vapour pressure of metal chlorides.

Considerably faster corrosion may occur when a metal is covered with a chloride-rich deposit than only exposed in gas environment. Corrosion can be severe in oxygen-containing environment, but it can still be further enhanced by SO_2 in flue gas, while the combination of O_2 and SO_2 is more effective to release Cl_2 from alkali chlorides in deposit than O_2 alone.

Alkali chlorides can also reduce the melting temperature of deposit by forming eutectics with other compounds, and enlarge the temperature range of hot corrosion. High concentration of SO_2 in bulk gas and aluminosilicates could suppress chloride deposition, but the effect can be limited by low flue gas temperature (< 800°C), or by the presence of SO_2 absorbents.

2.4 Materials

2.4.1 Evolution of boiler materials

The requirements to tubing material for superheater and reheater application are high temperature strength, good weldability and excellent resistance against fireside corrosion and steam-side corrosion. The development of high-temperature materials is strongly influenced by the worldwide energy supply. In the fifties of the last century, to achieve high power plant efficiency, austenitic materials, e.g. X8CrNiNb 16 13 and X8CrNiMoNb 16 16 were applied for relatively high steam parameters. Fireside corrosion of austenitic steels was reported at that time. As oil supply became sufficient at the beginning of the sixties, ferritic steels, such as 10CrMo9 10 and X20 CrMoV 12 1, were increasingly applied. In the course of the energy crisis, high temperature corrosion during coal combustion became a relevant problem and the interest in using high-temperature-resistance steels arose again. At present, the difficulty to further improve the power plant thermal efficiency lies mainly in the area of material technology. Intensive R&D efforts have been carried out in Japan, USA and Europe in the last years. Tab. 2.4.1 lists the international programs to develop boiler materials for advanced steam power plants /112/.

Tab. 2.4.1 International R&D programs for power plant materials

	Japan	USA	Europe
Project	**EPDC**	**EPRI**	**COST**
involved companies	MHI-Toshiba-Hitachi	GE-Westinghouse	ABB-GECA-MAN-Siemens-NEIGF-VOEST-SV-FEL-Sulzer-VSG-Böhler-ENEL-NP
steam parameters	**50MW pilot power plant** 1989-1990 314 bar 593/593/593°C 1991-1993 343 bar 649/649/649°C 1994-2000 300bar 630/630°C	**Studie 1978-1993** 310 bar 566/566/566°C 310 bar 593/593/593°C 345bar 649/649/649°C **R&D 1986-1993** EPRI-RP1403-15 R&D 300-900MW	1983-1997 300 bar 600/600/600°C 300bar 600/620°C 1998-2003 300bar 620/650°C

Material research in the last decade has focused on the development of cost-effective, high strength ferritic steels that can replace the use of austenitic steels. The existing ferritic-martensitic 9-12%-Cr steels have been further developed for the application of pipes and headers, which are capable to be operated at steam temperatures up to 620°C. Unfortunately, the strongest ferritic steel which can be used up to metal temperature of 620°C are purely

based on the strength point of view. Its applying temperature for superheater is still limited to 593°C due to fireside corrosion. This corresponds to steam temperature of about 565°C, since metal temperature can exceed steam temperature by as much as 28°C. Based on this experience, austenitic steels and Ni-based alloys regain their repute as future materials in the coal-fired power plants /102, 107, 114, 115/. Recently, coating and cladding techniques are encouraging. High-Cr austenitic steels are used as coating materials or cladding materials, whereas low-Cr austenitic steels or ferritic steels are the base materials of the tubes. In such way, the superior corrosion resistance and high-temperature strength are guaranteed /116/.

Evolution of ferritic steels and the role of alloying elements

Material strength at high temperature is the main concern during the development of ferritic steels. The systematic evolution of ferritic steels which bear 10^5 hour creep rapture strength at 600°C is shown in Fig. 2.4.1. The application of 2.25%-Cr steels is limited to the steam pressure up to 60Mpa, whereas optimised 9-12%-Cr steels can be used in the boilers with steam pressure up to 180Mpa. The trend of the alloy development lies in the optimization of high-temperature alloying elements. In each generation, one or two elements are emphasised to be added to the alloys. The roles of alloying element in the development of the ferritic steels have been intensively investigated: W, Mo and Co are primary solid solution strengtheners; V and Nb promote precipitation strengthening by forming fine and coherent precipitate of M(C,N)x carbon nitrides; Cr contributes to solid solution strength; Ni improves the toughness but at the expense of creep strength. Partial replacement of Ni by Cu helps stabilize the creep strength. Carbon is required to form carbide precipitates, but the amount of carbon needs to be optimised for good weldability /101/.

HCM2S (T23), a 2.25Cr-1.5W low carbon steel with V and Nb, is a cost-effective steel with higher creep strength than T22 (2.25Cr-1Mo). Because of its excellent weldability without pre- or post-weld heat treatment, it is a good candidate for waterwall tubing. Among the commercialized 9%-Cr steels, T91 possesses the highest allowable strength and has been extensively used as a material for headers and steam pipes operated in steam temperature up to 593°C. Alloy NF616 (P-92), developed by substituting part of Mo in P91 by W, has even higher allowable strength and can be operated up to steam temperature of 620°C. E911 is an European alloy similar to NF616 /112/. Beyond 620°C, 9%-Cr steels are limited by their corrosion resistance, thus 12%-Cr ferritic steel and austenitic steels have to be used. /100, 101, 105, 108, 109, 110/. Among 12%-Cr steels, HT91(X20CrMoV121) has been widely used for tubing, headers and piping in Europe. HCM12 is an improved version of HT91 with 1% W and 1%Mo. It possesses improved weldability and higher creep strength. Further

improvement in creep strength by substituting more Mo with W and by the addition of Cu has resulted in alloy HCM12A(P-122). Two alloys, NF12 and SAVE12, which possess even higher creep strengths than HCM12A by adding more Co and W, are in the developing stage.

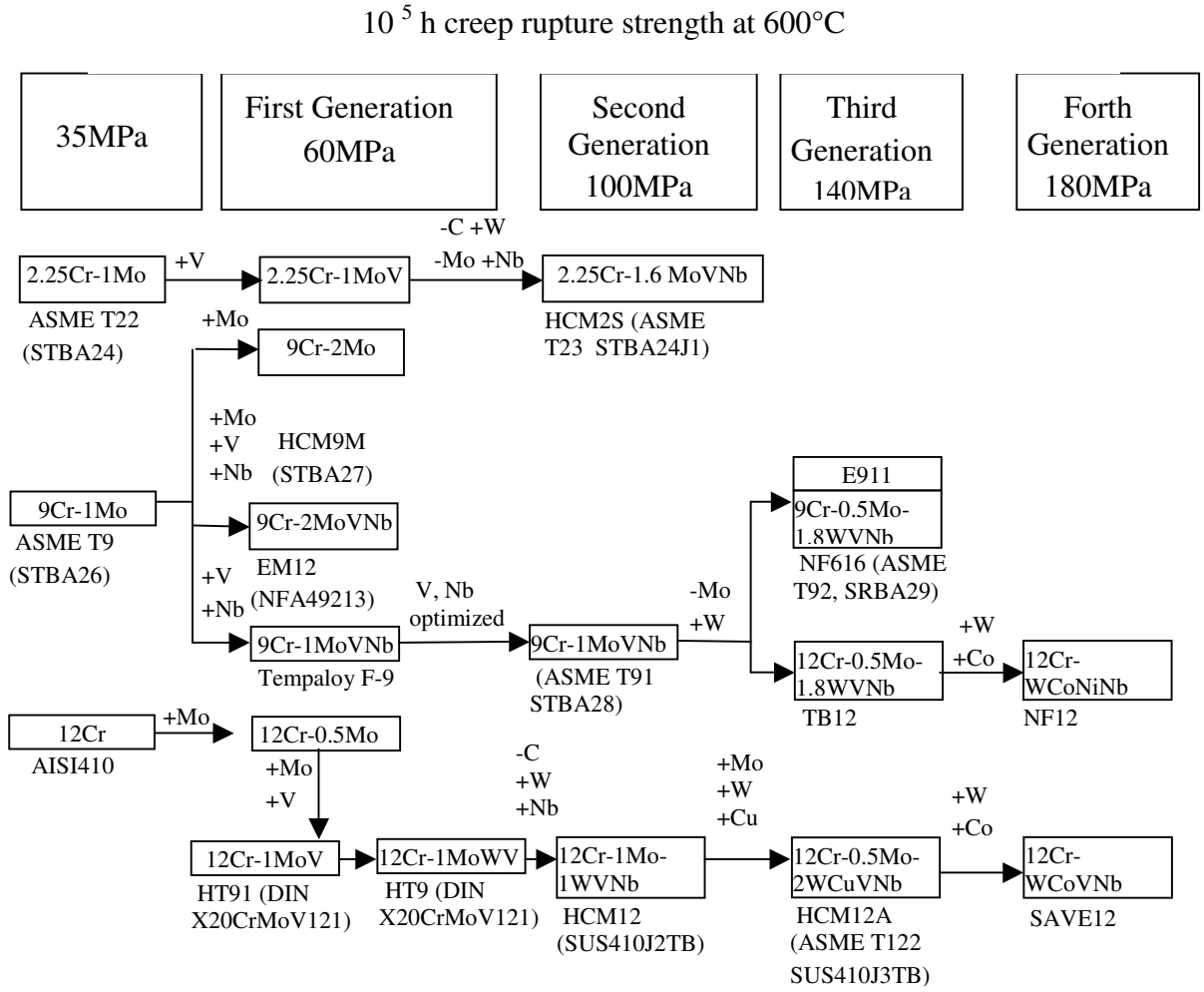

Fig.2.4.1. Evolution of ferritic steels /107/

Evolution of austenitic steels

Austenitic steels are candidates primarily for the end stage of superheater/reheater tubing. At this stage, resistances against fireside corrosion and steam side oxidation become important in addition to creep strength. From the corrosion point of view, when steam temperature is above 593°C, austenitic steels are required. Fig. 2.4.2 illustrates the evolution of austenitic steels.

The evolution of these steels comprises following stages:

- initially adding Ti and Nb to stabilize the steels from corrosion point of view;
- then reducing Ti and Nb to promote creep strength rather than corrosion consideration;

- followed by Cu addition for increasing precipitation strengthening by fine precipitation of a Cu-rich phase;
- further trends include increasing austenite stabilization using 0.2% N and W addition for solid solution strengthening.

Among the 18Cr-8Ni alloys, SS304M and SS347 are widely used instead of T91 in superheater, mainly because they are easier to weld, and the cost difference is relatively small.

According to the phase of material development for USC plants /101, 111, 113/, material selections for waterwall and SH/RH piping are generalized in Tab.2.4.2.

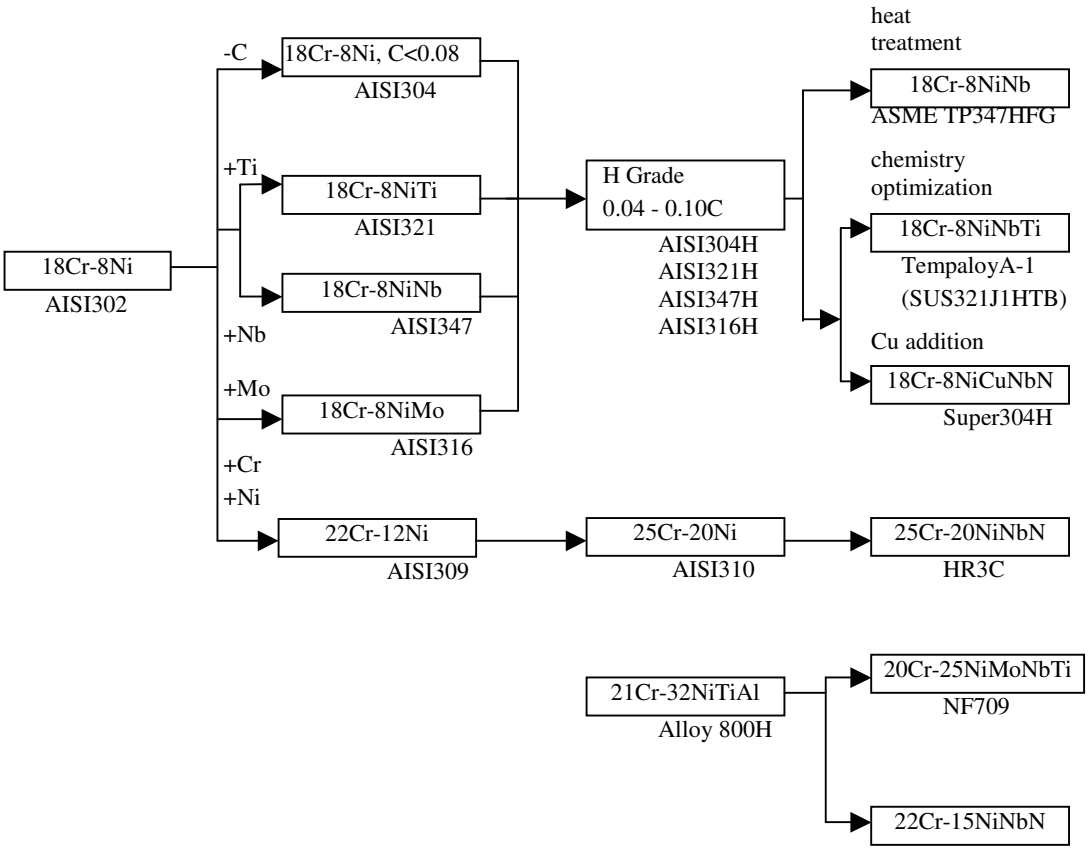

Fig.2.4.2. Evolution of austenitic steels /107/

Tab. 2.4.2. Candidate materials for advanced supercritical plants for various steam conditions

Component	Phase 0 31MPa 565/565/565°C	Phase 1 31MPa 593/593/593 °C	Phase 1B 31MPa 620/620/620 °C	Phase 2 34.5MPa 650/650/650
Headers/steam pipes	P22, HCM2S(P23) P91, P92, P122	P91, P92, P122, E911	P92, P122, E911, NF12, SAVE12	SAVE12*, NF12*
Finishing SH				
Non-corrosive	T91, 304H, 347	TP347HFG Super304	NF709 Super 304H	NF709 Inconel 617
Corrosive	310NbN(HR3C)	310NbN(HR3C) SS347	310NbN(HR3C) Super304H	Cr30A NF709
Finishing RH	Same as SH	Same as SH	Same as SH	Same as SH
Waterwall				
Lower wall	C steel	T11, T12, T22,	Same as phase 1	
Upper wall	T11, T12, T22	T23, HCM12	Same as phase 1	
Low NOx boilers + high S coal	Clad with alloy containing >20% Cr or chromized	Same as phase 0	Same as phase 0	Same as phase 0

* alloy in development

2.4.2 Corrosion resistance

Resistance of boiler steels against hot corrosion

Hot corrosion in coal-fired boilers described in Section 2.2.3 is the main concern for superheater/reheater materials. The resistance of a steel against hot corrosion increases with increasing chromium content in the steel. As shown in Fig. 2.4.3, the 9-12%-Cr ferritic steels

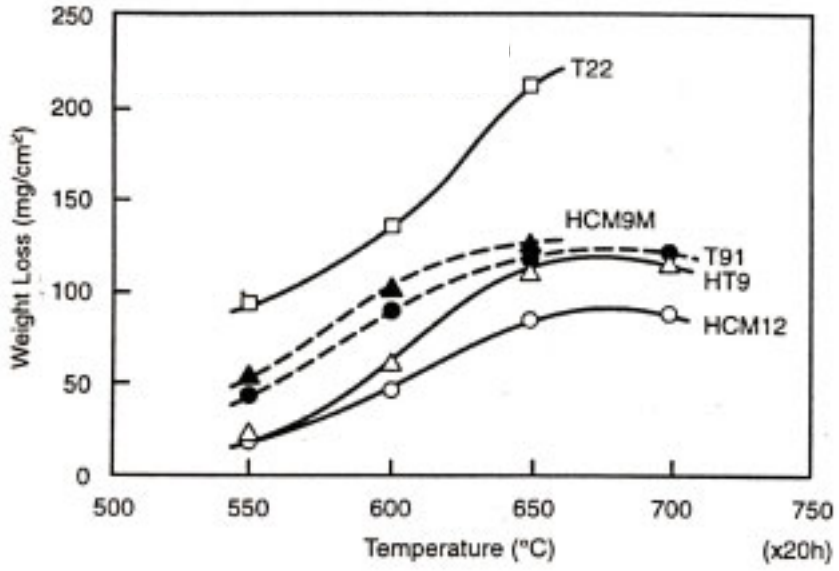

Test conditions:

Ash: $1.5^{M}Na_2SO_4$ – $1.5^{M}K_2SO_4$ – $1^{M}Fe_2O_3$

Gas: 1% SO_2 –5%O_2 – 15%CO_2 – Bal. N_2

Fig.2.4.3. Relationship between hot-corrosion weight loss and temperature for ferritic steels /101/

are more resistant than 2.25%-Cr steels; 12%-Cr steels show better resistance than the conventional 9%-Cr steels. Austenitic steels possess overall better corrosion resistance than 9-12%-Cr ferritic/martensitic steels. The influence of chromium content in austenitic steels on corrosion resistance is illustrated in Fig.2.4.4. Increasing chromium content beyond 30% results in a saturation effect on corrosion resistance. For practical purpose, when corrosion conditions are present, fine distinction of ferritic steels may be academic, it is usually necessary to use austenitic steels containing Cr in excess of 20% /101/.

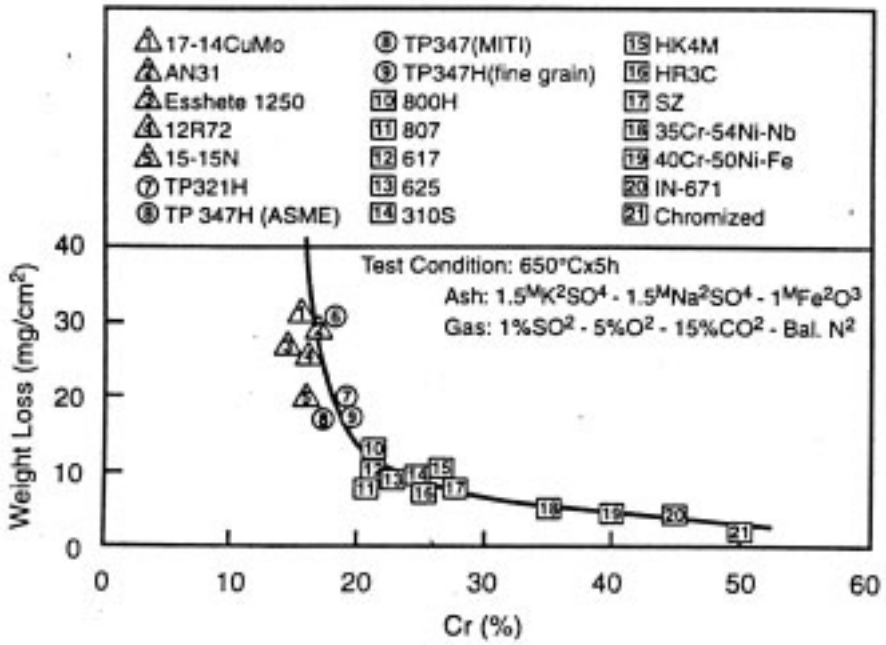

Fig. 2.4.4. Relationship between hot-corrosion weight loss and Cr content for austenitic alloys /107/

The corrosion rate of austenitic steels in dependence of temperature follows a bell-shape curve, as shown in Fig. 2.4.5. The highest corrosion rate locates in the material temperature range between 600 and 750°C. When austenitic steels contain Cr more than 20%, such as type 310 stainless steel, Incoloy 800H (Cr/Ni = 21/32, %), they possess considerably higher corrosion resistance than the austenitic steels with Cr-content lower than 20%. Incoloy 671 (Ni-50Cr) is virtually immune to hot corrosion, whereas 17-14CuMo seems to be the most sensible austenitic steel to hot corrosion.

Kihara and co-workers /73/ reported that the peak point of the corrosion rate curve tends to shift to lower temperatures for alloys with higher corrosion resistance. They provided an order of alloys with increasing corrosion resistance: T91, HCM12, Type 347 and Incoloy 800.

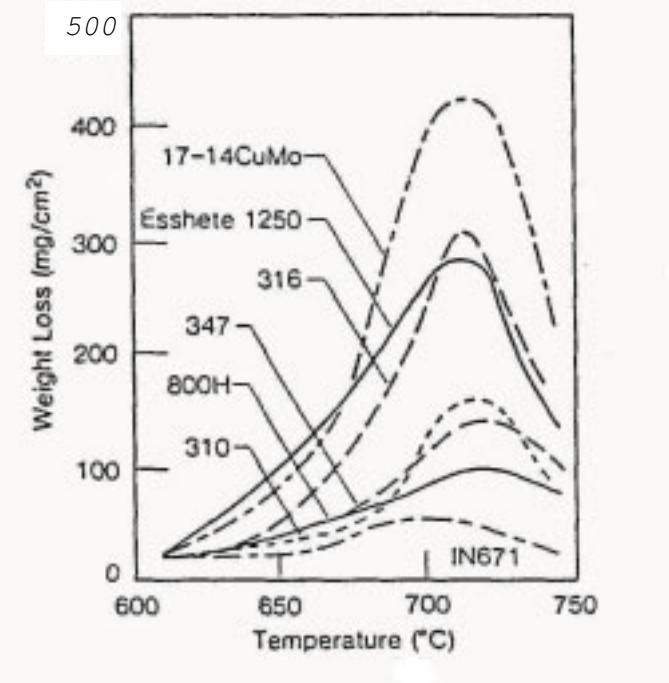

Fig. 2.4.5. Temperature dependence of hot corrosion of austenitic steels /107/

In addition, concern is also given on the mechanical performances of oxide scale. The development of thin, dense and stable oxide scale is necessary but insufficient prerequisite to prevent material wastage. Other decisive attributions of oxide scale to protect its substrate material are mechanical performances under isothermal or thermal cycling conditions. These performances include heat expansion rate, strength, elasticity and adhesion behaviour of the oxide scale. The process of stress producing and relief during scale growth or thermocycling condition can result in scale defects, such as cracking and detachment. Regarding the heat expansion rate of scale, iron oxides formed on ferritic steels have similar expansion rate as their alloy. However, this advantage is often counteracted by thicker oxide scale, which reduces the scale elasticity /1/. Recent researches of the "reactive element effect" (REE) have shown that by adding small amount of certain rare-earth metals to an alloy, the adhesion between oxide scale and substrate material can be enhanced /32, 117, 118/.

Resistance of boiler steel against chlorine corrosion

Different from the conventional hot corrosion induced by sulphate complexes, the alloy chromium content does not correspond to the resistance against chlorine corrosion. A large number of austenitic steels with Cr content lower than 20% suffer both rapid scaling and deep internal corrosion in chlorine-containing environment. Many studies reported that chromium carbides are more ready to react with chlorine gas (Cl_2) than iron carbides do, and the corrosion products are high volatile. The internal corrosion of austenitic steels presents

typically in the form of grain boundary corrosion. This is the result that chromium carbides tend to precipitate at grain boundaries /119, 57, 32/.

Some austenitic alloys are particularly sensitive to internal chlorine corrosion in the temperature range between 500°C and 600°C. Vander Voort /125/ reported that, in such temperature range, chromium carbides precipitate extensively along grain boundaries after certain period. This can lead to heavy attack of chlorine gas along the grain boundaries /103/. The generally accepted interpretation is that carbon in the alloy is promoted to react with chromium and forms of $Cr_{23}C_6$ at such practice temperature. Another negative effect of the chlorine attack is that, the area near grain boundaries is depleted of chromium, and becomes weak against other corrosive gases.

Besides, protective Cr_2O_3 may also be dissolved by acid fluxing in chloride salts. Otsuka reported that the corrosion product is CrO_2Cl_2, which is highly volatile above 350°C /91/. Consequently, the accelerated oxidation is self-sustaining for Cr_2O_3-forming alloys. In contrary, Ni-based alloys possess low corrosion rate in such condition. This behaviour can be attributed by the stability of NiO scale. Dissolution of NiO by an acid fluxing results in the formation of $NiCl_2$, however, $NiCl_2$ is not volatile. The corrosion reaction is therefore not self-sustaining.

In summary, to minimize chlorine corrosion by material selection: either 9-12%-Cr ferritic/martensitic steels, or austenitic steels with high-Cr content (>20% Cr), or Ni-based alloys could be selected. Since the use of high-Cr austenites and nickel alloys is often limited by cost factor, the choice of 9-12%-Cr ferritic steels with moderate steam temperature (not high than 550°C) is recommended /97/.

2.4.3 High temperature strength of boiler materials

The allowable strengths of ferritic steels, austenitic steels with Cr below 20%, austenitic steels with Cr above 20% and Ni alloys are illustrated in Fig. 2.4.6, Fig. 2.4.7 and Fig. 2.4.8 respectively /101/.

Among ferritic alloys, HCM12A (P122), NF616 (P92) and E911 are distinguished with the highest strength. They are suitable for steam temperature up to 620°C. T91, HCM12, EM12, HCM9M and HT91 (X20CrMoV) are suitable for intermediate temperatures up to 593°C. T22 and T9 show the lowest strength, which can only be used below 565°C /13/.

Among austenitic alloys with chromium below 20%, Tempaloy A1, Esshete 1250 and 17−14CuMo are found to be superior to the 300 series stainless steels in allowable strength.

Among the austenitic steels containing more than 20% Cr, NF709 and HR3C are the leading candidates for high temperature application. The highest strength is achieved by the nickel alloy Inconel 617. It is also likely the most expensive alloy to use, due to its high nickel content.

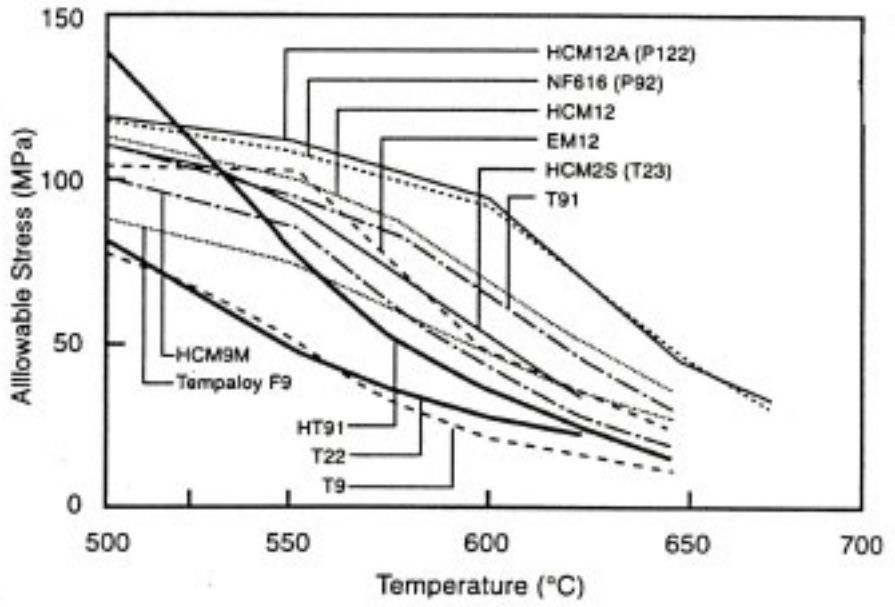

Fig.2.4.6. Allowable stresses of ferritic steels /107/

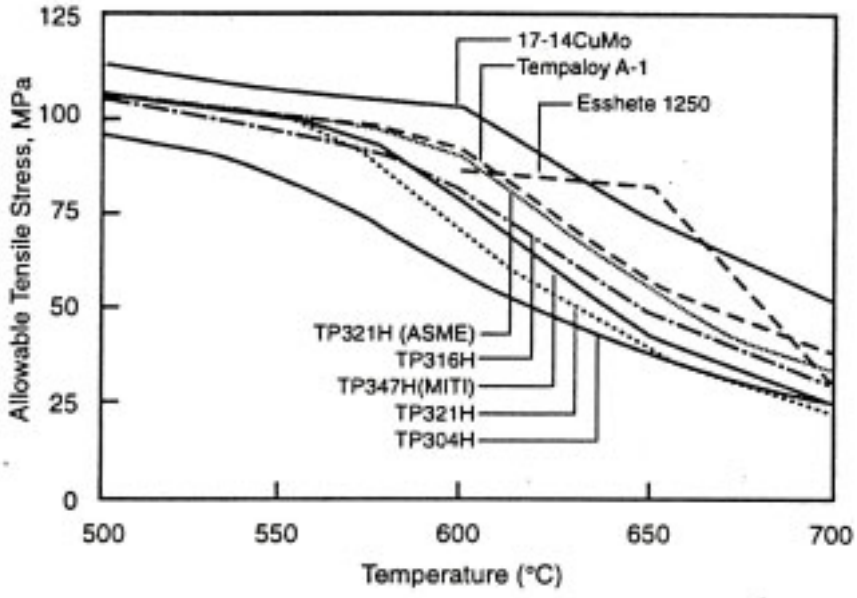

Fig. 2.4.7. Allowable stresses for 18Cr-8Ni and 15Cr steels /107/

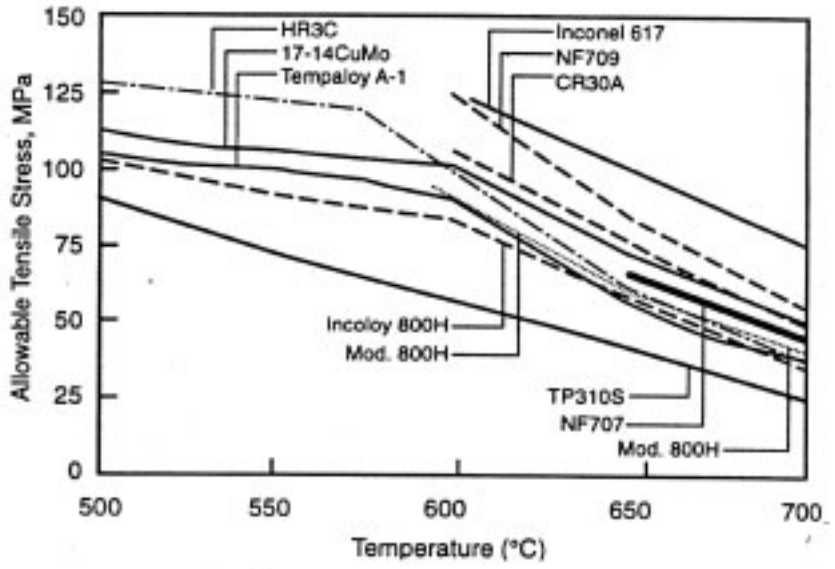

Fig. 2.4.8. Allowable stresses for high-Cr austenitic steels and nickel alloys /107/

Criteria of selection of high-temperature tubing materials

A combined consideration should be taken for the material selection for the hottest part of boiler tubing. The main criteria of material selection are listed as follows:

1. High temperature strength
2. High resistance against fireside corrosion and steam side corrosion,
3. Excellent weldability and necessity of postweld heat treatment (PWHT), including the sensibility of cracking at heat treatment affected zone (HAZ)
4. Low thermal expansion, high heat conductivity and acceptable wall thickness
5. Acceptable cost

2.5 Measurement Technique

There is a diversity of measurement principles for fireside corrosion. The methods to determine corrosion rate can be generally classified into laboratory measurements and field tests, depending whether the measurement is carried out in a simulated combustion environment or in a real combustor. Laboratory tests, due to the difficulty to simulate whole combustion parameters, put usually emphases on specific aspects of corrosive condition, such as gas environment (in air or in simulated flue gas environment), the presence and the composition of ash deposit, material surface preparation and heat treatment, etc. The material degradation can be examined according to many physical and chemical changes of the specimen. The measurements of physical change include weight change of a specimen, thickness change of a scale or of a specimen, and the change of material microstructure. The microstructure analyses comprise surface etching, optic microscopy and electron microscopy. Some electron microscopy can also reveal chemical composition of corroded zone. In field tests, testing specimens are usually mounted on the furnace wall, or on a probe, which is exposed in combustion zone. The material temperature is controlled and the local gas composition is usually also measured for reference. In case of online measurements, electro-chemical sensors are applied to provide online signals corresponding with the corrosion events. Brief descriptions of each measurement technique are given below.

2.5.1 Laboratory measurements

Thickness measurement

Thickness measurement is the most common method to evaluate corrosion rate. By examination of the cross section of a specimen after exposure, both the thickness of scale and the depth of the internal corrosion can be determined. Thickness measurement can provide accurate assessment of scaling rate of low-ferritic alloys. Difficulty usually appears by examining a material with high corrosion resistance, since its scale is too thin to be measurable.

Weight change measurement

Weight change measurement is another traditional method to determine corrosion rate. A metal specimen can gain weight by absorption of gas reactants from environment or lose weight by formation of volatile corrosion products. Weight change is a simple and effective method to provide general information. But it is unable to examine microstructure changes. Complexity may arise when a corrosion process involves both weight gain reactions and

weight loss reactions, such as the case of chlorine-induced corrosion. Weight change measurement can be carried out either offline or online. Precise online weight change measurements comprise thermogravimetric analysis (TGA) and differential thermoanalysis (DTA). During such measurements, a specimen (< 20g) is hung on a precise balance in an electrical-heated furnace. The test cell can be filled with simulated corrosive gas, and the balance area is isolated with inert gas to protect the balance.

Metallographic analytic techniques

- **Etching**

Metallographic etching is applied to reveal the microstructure of an alloy, which is otherwise not evident in the as-polished condition. The principle of etching is based on the preferential attack or preferential staining of one or more phases in an alloy, owning to their differences in chemical composition or in orientation. The microstructure characteristics, such as form, size, distribution, segregation, and inclusions of special metallurgical phases, can be clear revealed with etching on a well-polished specimen. Chemical etching, electrolytic etching and heat tinting are the mostly applied procedures. There are specific etchants and procedures for specific steels or even phases /125, 130/.

- **Optic microscopy (OP), scanning electron microscopy (SEM) and transmission electron microscopy (TEM)**

For metallographic studies of corrosion structure, low-resolution optic microscopy is usually the first step to examine the features of a specimen by light reflectivity difference, colour difference or polarization effects. SEM is necessary for high-resolution images with extensive field depth and wide range of magnification. Another feature of SEM is that the image can be produced by atomic number contrast or electron channelling contrast. This provides very useful information of material chemical composition. TEM is a powerful tool to study detailed metallurgic features, such as lattice defects, phase dislocations and crystal structures /126/. A well-prepared thin-foil specimen is the prerequisite for the TEM analysis.

2.5.2 Field tests

Field test constitutes a very important part of corrosion rate determination. Since realistic combustion condition, such as flue gas composition, temperature difference between flue gas and material, and the structure of deposit ash, exert direct influence on corrosion rate. According to the complexity of the measuring technique, corrosion monitoring methods during field test can be generalized as following:

- Thickness controlling

- Ultrasonic controlling
- Electrical Resistance
- Impedance Spectrometry
- Electrochemical noise

Among the electrochemical methods, electrical resistance measurement is the simplest method, whereas the electrochemical noise is the most advanced and accurate electrochemical technique.

Temperature-controlled material probe for thickness controlling

Thickness controlling is the most applied and the simplest method. By exposing a material probe in combustion environment, both material exposure test and deposit sampling can also be carried out simultaneously. The difference of corrosion rate on wind side and leeside of a tube can also be identified. The disadvantage of the thickness measurement lies in its offline feature. Therefore multiple measurements are needed for the determination of corrosion rate.

Ultrasonic measurements

Ultrasonic controlling is applied to examine a large tubing area. The technique is a traditional method of material quality control. It can be applied to check the thickness of installed boiler tubes. Contour map of wall tube thickness can be obtained by ultrasonic survey. The advantage of this technique is the possibility of large area control, its drawback is that the measurement can only be done during boiler still time /123/.

Electrical Resistance (ER)

ER technique is used to measure the change in ohmic resistance of a metal element exposed in a corrosive environment. The scaling on the surface of a specimen produces a decrease in the specimen cross-sectional area, corresponded with an increase in its electrical resistance. The increase in electrical resistance can be related directly to metal scaling rate. Electrical resistance measurement is applicable to all working mediums, such as gases, liquids, solids and particulate flows. It could respond quickly to corrosion upsets and can be used to trigger an alarm. ER probes are available in a variety of element geometries /123/.

Electrochemical methods

Electrochemical methods record continuously the current and the voltage signals which are generated spantaneously from corrosion events. The signal implies the mechanism and the intensity of a corrosion event. Electrochemical measurements are especially usefull to identify pit corrosion and crevice corrosion. The typical electrochemical measurement techniques are EPN (Electrochemical Potenitial Noise), ECN (Electrochemical Current Noise) and ZRA

(Zero-Resistance Ammetry). The detailed working principles of above techniques are given in /120, 121, 124/.

Comparison

There are differences in complexity and accuracy between conventional measuring techniques and advanced electrochemical measurements. Simple methods, such as weight and thickness measurements, are usually offline measurements, but they can provide accurate results; online electrochemical methods can provide online corrosion events, but fail to signify general metal loss. Therefore, the traditional measurements have not lost its signification. There is often a compromise between absolute accuracy and the degree of control over the system. Fig. 2.5.1 illustrates proximately the control complexity and the accuracy of each method /122/.

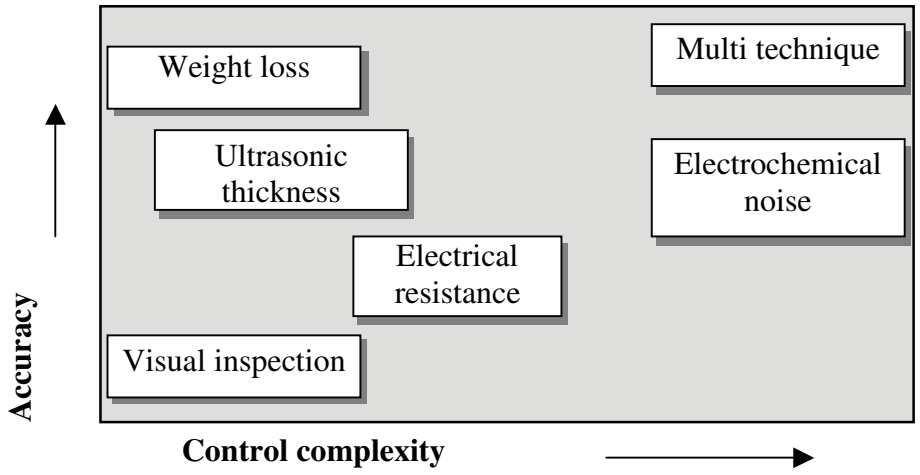

Fig. 2.5.1. control complexities and accuracies of measurement methods /122/

3. Experimental Techniques

3.1 Description of experimental methods

The experimental investigation of fireside corrosion at Institute of Process Engineering and Power Plant Technology (IVD), University Stuttgart, comprises combustion tests, laboratory tests and laboratory analyses. The reciprocal benefits of these three activities are illustrated in Fig.3.1. The 500 kW combustion test rig can provide combustion conditions, which are identical to conventional power plant boilers. The test rig possesses the flexibility to burn different kinds of fuel or fuel blend. Comprehensive measurements and ash sampling can be carried out during combustion tests. Regarding fireside corrosion, which is influenced by complicated interactions between flue gas and deposit ash, combustion tests can provide material exposure, flue gas data, and deposit ashes for laboratory corrosion tests and laboratory analyses. Laboratory analyses comprise ash analyses and metallographic examinations. Laboratory analyses can provide laboratory tests a guide for the optimisation of test conditions. The laboratory tests were carried out in an electric-heated furnace. The advantage of the laboratory test is the well-controlled test conditions, such as gas composition, deposit ash composition and material temperature. These allow precise determination of corrosion mechanism and corrosion rate. In addition, a large number of

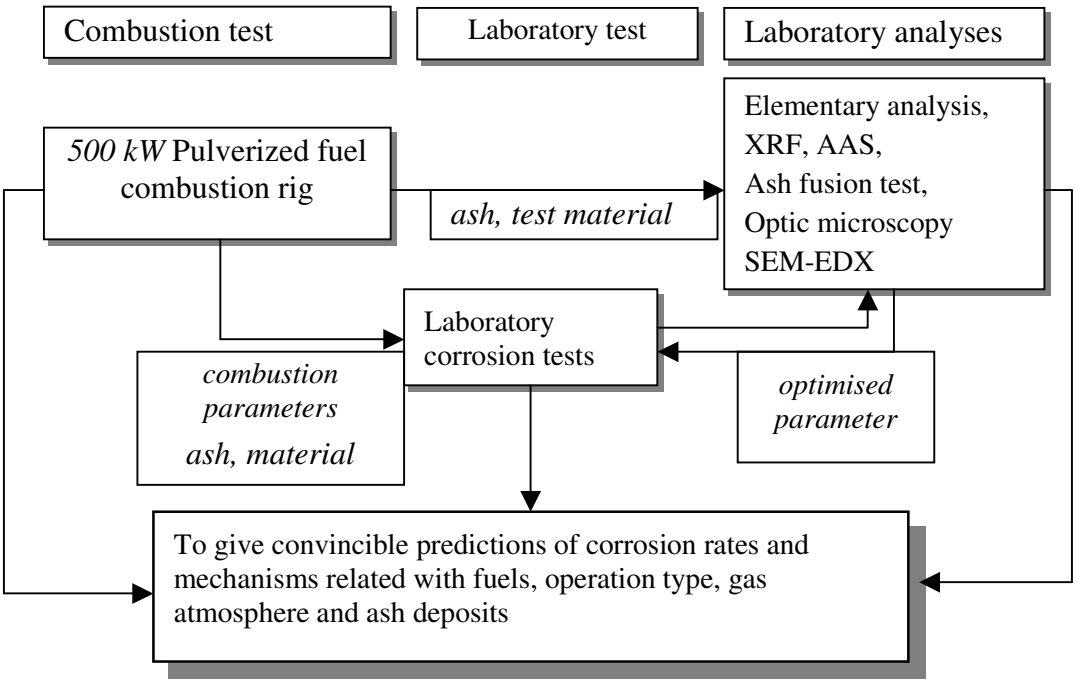

Fig. 3.1. Experimental methods in this study

metallic species can be tested at same time. By integrating combustion test, laboratory tests and laboratory analyses, convincible results regarding corrosion mechanisms, corrosion rate and influence factors can be obtained.

3.2 Combustion Tests

Description of the facility

The pulverized combustion test rig at IVD is suitable for firing coal or fuel blends of biomass, refuse-derived fuel or sewage sludge. The thermal input is 300-500 kW. Fig. 3.2 illustrates the scheme of the furnace. The furnace is vertically installed to minimize the asymmetry effects of flame, particle deposition and slagging. This structure also facilitates profile measurement and fly ash sampling. The down-fired design provides the advantage of ash removal. The furnace is 7.5 m high, its 4 m upper section is refractory-lined and water-cooled, simulating the furnace of a boiler, and its 3.5 m lower section is only water cooled, simulating the

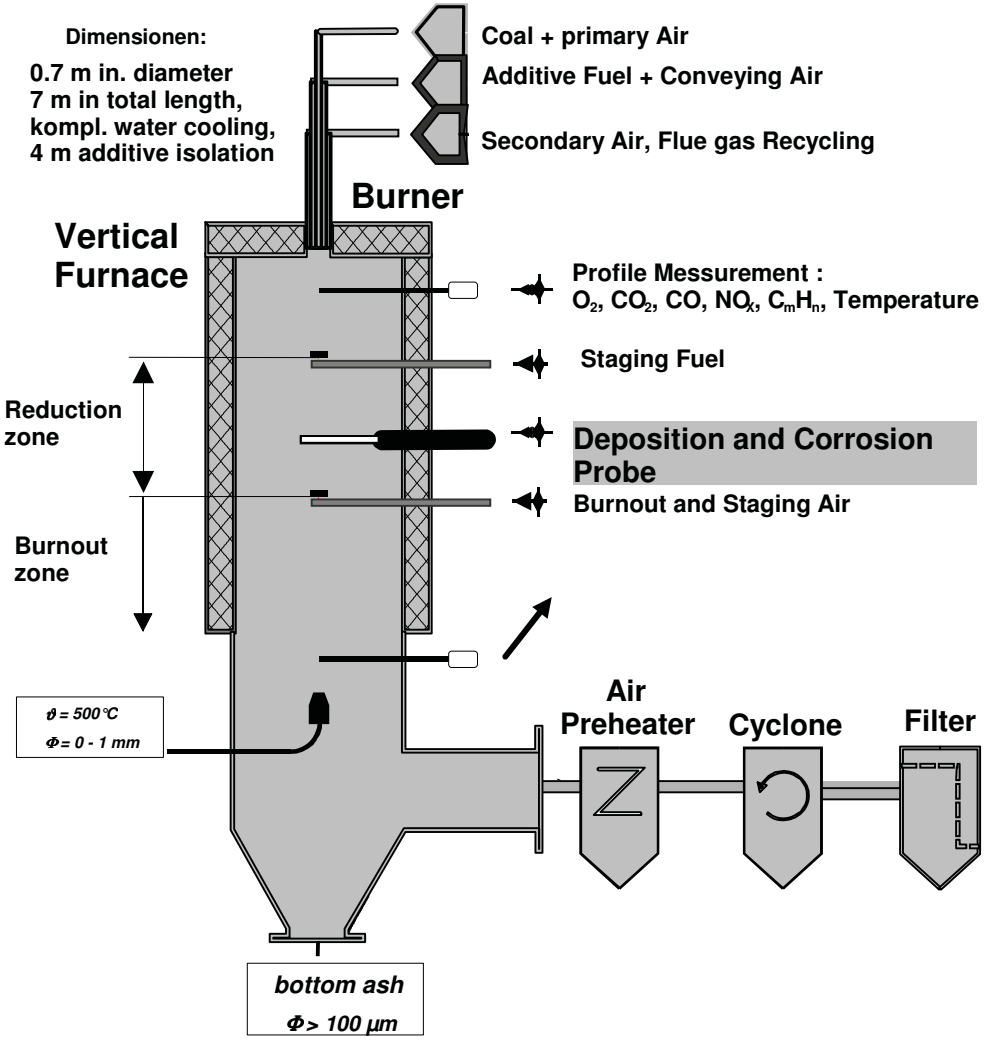

Fig. 3.2. Sketch of the 500 kW pulverized fuel test rig at IVD

burnout section in a boiler. The diameter of the furnace is 0.75 m in the refractory part and 0.85 m in the non-refractory part. The similarity of the combustor with conventional power plant boilers guarantees identical combustion conditions as in utility boilers.

Fly ashes generated during combustion are captured either in the furnace bottom or in the convection pass. While large slag particles fall down directly to the furnace bottom, fine ash particles are carried away by flue gas to the convective pass and are captured in air preheater, cyclone and bag filter, depending on their inertia. Fly ashes can be gathered in above positions /26, 131, 132, 133, 134/.

Along the furnace height, three vertical rows of access port on the furnace wall allow detailed measurement of flame characteristics and the insert of corrosion and deposition probes. They also provide the possibility of air staging and fuel staging at different furnace height.

Vertical and horizontal profile measurements of flue gas composition and temperature can be carried out in the upper part of the furnace. The measurable gas species include O_2, CO_2, CO, NO_x, SO_2, C_mH_n. At the same positions of flue gas extraction, furnace global temperature can be measured by ceramic-covered Pt-Ph thermal couples. At the lower part of the furnace, about 5.5m from the furnace top, flue gas composition and temperature are continuously monitored.

Corrosion/deposition probe

Temperature-controlled probes were applied to expose test materials as well as to gather deposit ash. By inserting the probe in the flame centre or in the burnout zone, fireside corrosion and deposition in these areas were examined.

The sketch of the water-and-air-cooled probe is shown in Fig. 3.3. Several test material rings are installed at the front part of the probe. The probe construction provides the possibility for

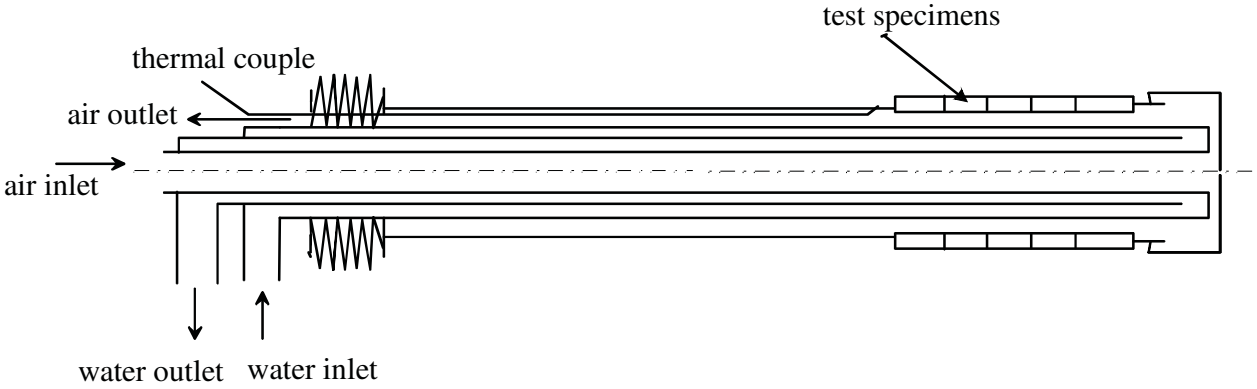

Fig. 3.3. Sketch of the temperature-controlled Corrosion/Deposition probe

material exchange at short breaks between two combustion tests. Pressure air is used as direct coolant to control the tube surface temperature, whilst water is used as indirect coolant to extract the heat from cooling air, so that sufficient cooling effect can be achieved. The tube surface condition of waterwall or superheater can be simulated by adjusting the probe surface temperature with air flow. An air-flow control device with emergency cooling bypass regulates the probe surface temperature automatically to the given temperature. The surface temperatures around the probe are continuously monitored and recorded with three thermal couples mounted around the outer tube adjacent to the test material.

After combustion test, the deposit ash on the probe surface was gathered separately from different positions. The possible positions for ash collection are illustrated in Fig. 3.4. Generally, deposit ash was separated from wind-side and leeside of the probe, and from the outer layer and the inner layer of a wind-side deposit. Metal rings, together with the inner deposit ash layer, were reserved in an exicator right after each combustion test for laboratory analyses.

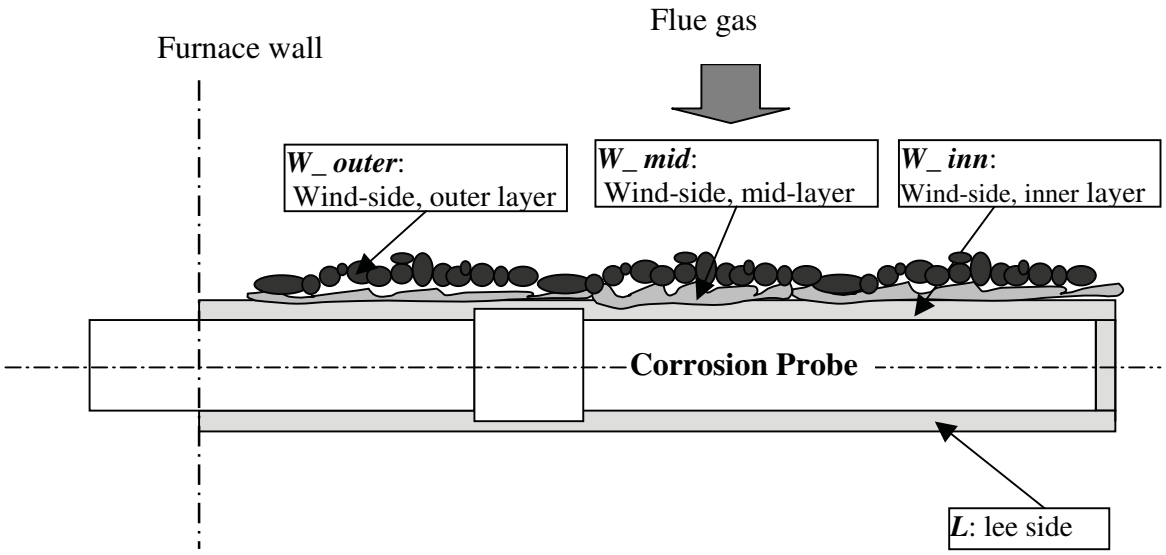

Fig. 3.4. Sketch of possible ash sampling positions from the Corrosion/deposition probe

During some combustion tests, besides the temperature-controlled probe, water-cooled probes with non-cooled ceramic front part were also exposed in the furnace. Deposit ashes or slags on the non-cooled ceramic part as well as on the water-cooled part of the probe were collected, so that comparison of the deposit mechanism can be made regarding different tube temperature.

3.3 Laboratory corrosion tests

Laboratory furnace

An electric-heated furnace was constructed at IVD for long-term corrosion exposure tests. The furnace is equipped with a gas mixture system and a precise temperature control unit. The sketch of the furnace is given in Fig. 3.5. The furnace body is composed of two half-cylinder electric heaters with the total output of 3.8 kW. The interior furnace wall is constructed with stainless steel with the dimension of $\phi 114 \times 2.5$ mm. The furnace is gas tight: gas inlet, gas outlet and furnace wall were welded to a whole unit to prevent gas leakage. The sealing between furnace door and furnace body was achieved with a high-temperature sealing material. The whole furnace system is illustrated in Fig. 3.6. The gas mixture station could supply gas mixtures of air, N_2, HCl, H_2O and SO_2 to the furnace. Air and N_2 were provided by pipelines in the experimental building; a HCl-generator can supply precise amount of water vapour and HCl vapour solution; SO_2 was supplied by a gas bottle. To guarantee a slight positive pressure in the furnace, all the gas components were depressurised and regulated to 1.2 bar before led to the furnace. The gas flow rate can be varied. It was controlled at about 500 litre/hour for the corrosion tests in this study. To prevent vapour condensation in the furnace, the gas mixture was preheated to 170°C. The hot gas after the furnace outlet was cooled and neutralized before released to the stack. For the sake of personal safety in the working area, the furnace is enclosed in a hood with air extraction.

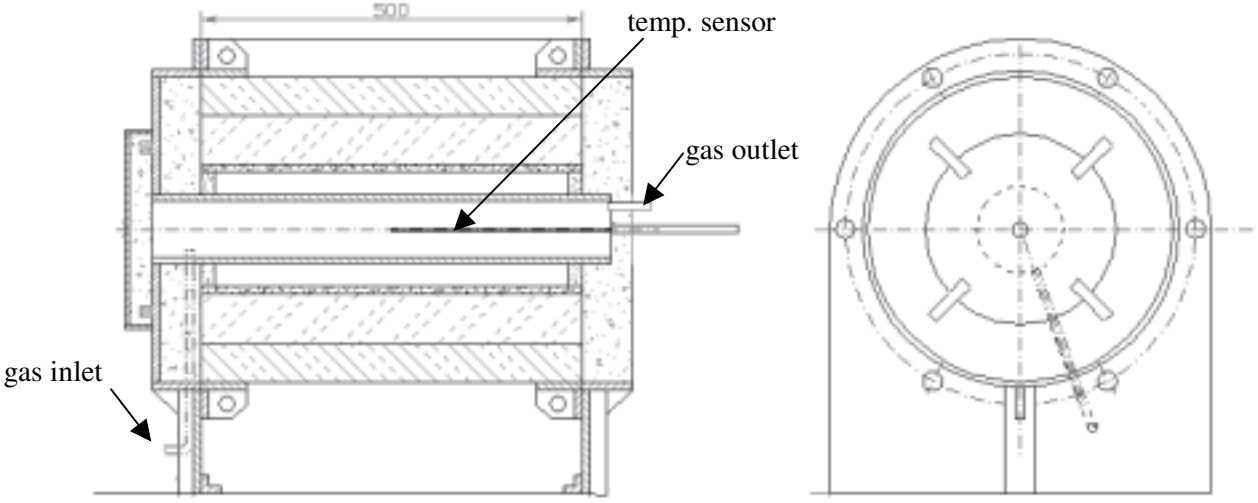

Fig. 3.5. Sketch of the laboratory furnace

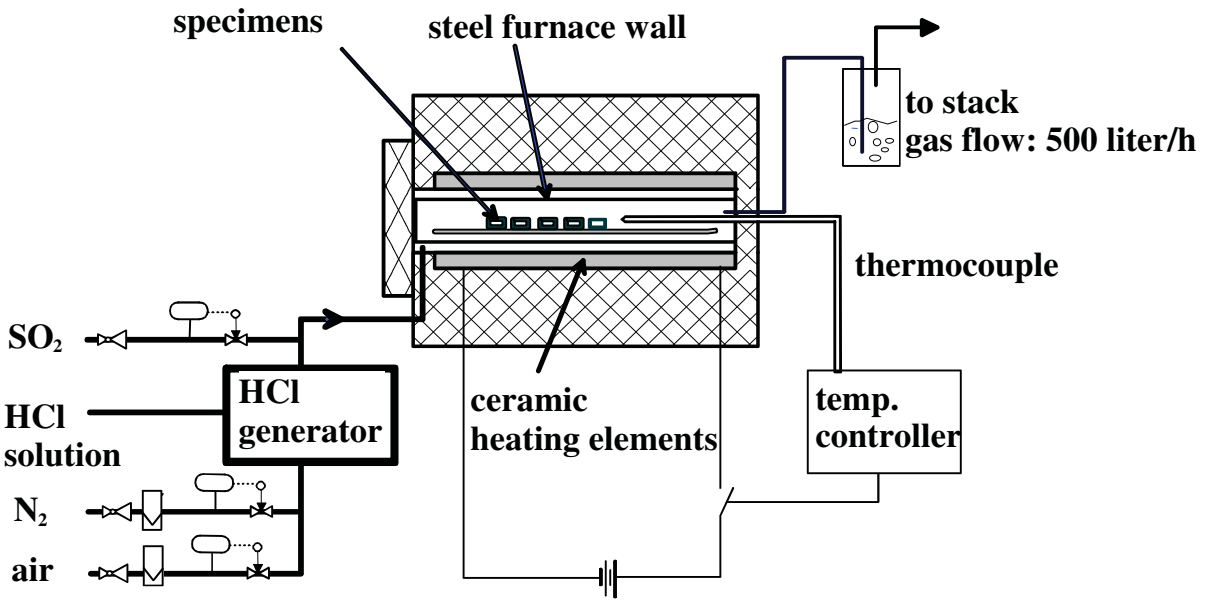

Fig. 3.6. laboratory furnace system

The heating period takes generally about 20 minutes. During the operation, the temperature fluctuation is within 1°C. Prepared test specimens, either bare, or covered with ashes, were put in crucibles and exposed in the middle zone of the furnace. In order to minimize undesired chemical changes of corrosion products on test specimens during heating period and cooling period, only N_2 flew through the furnace during these periods.

Preparation of material specimens before and after laboratory corrosion tests

Before a furnace exposure, thin plates of test material were cut from as-received tubes, double side polished and cleansed. The weight and surface area of the specimens were measured. For the tests without ash deposit, the plates were put in the crucibles in such a way that the whole surface of the plates was exposed in the gas atmosphere; for the tests with deposit ash, the metal plates were embedded in finely milled ashes in the crucibles.

After exposure, the weight change of material specimens was firstly measured with corrosion products. Then the corrosion scale was cleansed with a thin HCl solution in an ultrasonic bath. Afterwards, the weight of the cleaned specimen was measured. The weight gain of the specimen with corrosion products indicates the growth rate of corrosion products, whereas the weight loss of a specimen without corrosion products reflects the real metal loss. In the case of the exposure tests with ash deposit, only the weight of specimen after descaling can be measured.

3.4 Laboratory Analysis

Fuel and ash analysis

Comprehensive fuel and ash analysis were carried out for combustion tests in this study (Chapter 5). The fuel analysis comprises:

- water, volatiles, ash and fixed C
- elemental analysis C, H, N, S
- low heating value and high heating value
- chlorine and sulphides
- particle size distribution
- major and minor ash elements

According to ISO 1171, the ash content of fuel in the combustion test is determined at 815°C. It is need to mention that at this temperature, some alkali metals and chlorine in biomass can be already evaporated and not be measured.

It is of special interest in this study to analyse the composition of fly ash and of deposit ash in the combustion test, because such analysis can provide information of the selective deposition of corrosive components and so that the analysis results can indicate the potential of corrosion. In addition, the ash composition was also examined for the deposits in laboratory test before and after exposure. The main elements and trace elements were analysed with XRF (X-ray Fluorescence Analysis) /131/. Three types of preparation for XRF are available according to ash characteristics: to produce molten ash tablet, to produce press tablet or to measure loose ash enclosed in a plastic foil. The molten tablet method distributes ash most homogeneously, followed by the press tablet method, and ash in the plastic foils is untreated. Therefore, the molten tablet could deliver the most accurate assessment. However, it has also drawback: during the preparation of molten tablet, some volatile elements, such as part of sulphur and some heavy metals, are volatised. Thus they could not be bound in the molten tablet. Press tablets, which are produced in room temperature, will be an alternative for such problem. When ash amount is not adequate to produce molten tablet or press tablet, which is especially the case of deposit ash, the foil measurement is a proper method. The molten tablet method was applied in the analysis of combustion test, whereas the pressed tablet method was applied to the simulated deposits in laboratory test, so that the major part of the chlorides in the deposits can be conserved. Chlorine content in the ash was extra analysed by a bomb digestor with subsequent titration.

The molten behaviour of some fuel ashes and deposit ashes generated in combustion test described in Chapter 5 was investigated by recording the continuous deformation of an ash pyramid with increasing temperature. In comparison with ASTM standard point measurements /37/, the continuous measurement provides a complete view of the ash melting behaviour.

Microstructure analysis of metallic and ash specimen

A polished surface of a specimen is required for microscopic examination. Such examination is needed e.g. for the corrosion depth determination in laboratory test as well as for the examination of the deposit on metal rings in combustion test. This polished surface must be representative of the microstructure of the metal or ash, not of the method of preparation. A successful preparation depends not only on the selection of proper procedure and help materials, but also on the property of investigated materials. The general procedure for mounting specimen preparation includes cutting, mounting, grinding, polishing, cleaning and etching.

Cutting and mounting

Cutting is necessary for a specimen, whose original form is larger than the mounting form. During cutting, the representative surface for the examination should not be destroyed. Cooling fluid should be used cautiously or not be used when water-soluble substances are going to be examined. When the cut surface is prepared to be examined, an even and smooth surface can save time and work of the followed grinding step.

Mounting is the process to cast the investigated specimen in fluid or powder substance, which will be solidified after certain time. Besides the function to protect specimen surface, mounting is also a necessary step to fix small pieces of specimen before grinding. In this study, metallic specimens were cut to thin plates and polished to 1200 grit. The dimension of the plates is about 1cm x 1.5 cm x (1~1.5) mm. In the case of metal ring from combustion test, the whole ring with the inner deposit ash layer was mounted after combustion test. For the slag which sticks on ceramic holders, a piece of the ceramic tube with adherent slag layer was cut off as mounting specimen.

There are basically two mounting methods: cold mounting and warm mounting. Cold mounting can be carried out in normal room temperature, the procedure of which is similar with cake baking, but in normal temperature. Firstly, the inner surface of the form is creamed. Then, one or several specimens are so positioned in the mounting form that the surfaces to be ground face the bottom of the mounting form. In the next step, mounting fluid or mounting

powder is mixed with corresponding fluid harder. Finally, the fluid immerses the examined specimen in the mounting form usually to a height about 1 cm. The mounting fluid is solidified after certain time and the solid mass can be pushed out of the form. The selection of mounting material and the proper handling are important. For porous specimens, such as corroded material or ash, the mounting fluid should be as thin as possible. So that it can reach pores and fissures in the specimen, and fix the small parts together. The mounting material used in this study is a super thin epoxy resin (Epothin from Buehler). To get a good effect of penetration and adhesion of the epoxy resin, it should be well mixed with its fluid harder by slowly stirring for at least 1 minute. A better effect can be achieved by putting the cup of the mounting mixture in a warm water bath during stirring. Cold mounting is easy for handling. The drawback of the cold mounting method is that the mounting materials are not electrical conductive. Therefore, extra surface handling with conductive material is needed before electrical microscopy examinations.

For the procedure of warm mounting, a warm press machine is required. Test specimen is embedded with warm mounting material in a cell in the press machine. Under certain heating temperature and pressure, the mounting material is molten, and bound with the test specimen. After about 20 minutes of cooling, a mounting tablet is formed. The advantage of warm mounting is that conductive mounting materials can be applied. However, warm mounting can not guarantee a good adherence of mounting material with porous specimen. Most mounting specimens in this study were prepared with cold mounting procedure, since the ash specimen and corroded metallic specimen require superior contact with mounting material.

The arrangement of metallic specimen in a mounting form is also important to achieve good polishing. Since mounting materials are usually softer than metal or ceramic, more mounting material could be polished away than test specimens. This leads to uneven interfaces between

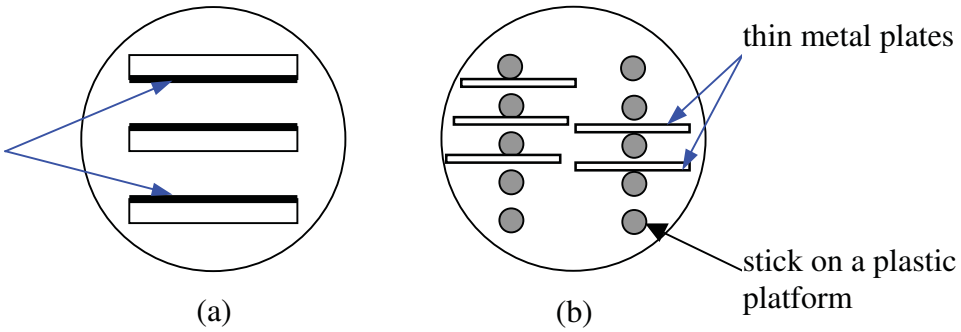

Fig. 3.7. a) arrangement of several test specimens in one form; b) the cross section of a cramp device to support thin plates of testing specimen

specimen and the mounting material. Such unevenness is undesired, since the interface area is especially important for corrosion examination. This case can be happened during polishing a part of metal rings after the combustion test. To avoid this, several metal species can be evenly settled in a mounting form, with the interface in question toward inside, as shown in Figure 3.7 (a). In such way, the hardness of the grinding surface is evenly distributed. To examine the cross section of thin plates, which is the case of the metallic specimen after exposure in laboratory furnace, some cramp devices are helpful to support or to fix such thin plates. An example is given in Figure 3.7 (b): thin metal plates are supported by many parallel sticks on a plastic platform.

Mounting of ash: to observe the cross section of fine ash particles, it is desired that many ash particles are ground at one surface, and ash particles should be fixed tightly by the mounting material. Such requirements can be met by a two-step mounting procedure: in the first step, the ash is mixed with a little mounting fluid (one or two drops) and let it solidify on the bottom of the mounting form; in the second step, the mounting form is filled to the standard level.

Grinding

Grinding can be carried out by hand or machine with successively finer and finer grinding paper. In proceeding from one grade of grinding paper to the next, the new scratches should be put on the surface perpendicular to those from the previous paper. One grade grinding is finished if the scratches in this stage slightly pass the point of the previous step. By using a number of papers that cut finer and finer scratches, the surface become smoother and, at the same time, the distorted layer on the metal surface becomes thinner /127/. Four stages of grinding were applied in this work. The roughness order of the SiC grinding papers was 60/180, 500, 1000, 1200 grade, corresponding to the coarse grade of 100/80, 28, 20 and 15 micron respectively /130/.

Polishing

Polishing is done by holding the specimen against a cloth-covered wheel charged with polishing compound. Polishing consists of two steps: rough polishing and final polishing. Rough polishing is not a true polishing, but rather a super-fine grinding step, which leaves very fine uniform scratches on the surface. If properly carried out, rough polish can effectively eliminate the distorted surface layers from the previous grinding step. The purpose of the final polish is to produce a smooth, level surface free of scratches and irregularities. In this study, for the rough polishing, 6 micron and 3 micron diamond suspensions with

lubricating fluid were applied; for the final polishing, finely powdered aluminium oxides of 1 micron was used.

To achieve a final scratch-free surface, some disturbing factors should be carefully prevented. These factors could be that, e.g. coarse dust particles in the environment settle on fine grinding papers or cloth lap; coarser particles from the previous step are carried on the specimen to the next finer paper or lap; fine abrasive particles stick together on the lap with time; or hard particles from embedded specimens are detached from the mount tablet. All these possibilities could ruin the surface of the specimen. The hand-holding pressure to the specimen on the cutting papers or laps has also a considerable influence on the results. Too little pressure retards the rate of polishing and leads to pits in the final surface. Too much pressure causes local overheating and severe distortion to an appreciable depth. The suitable pressure varies with different metals and it can be only learned by practise /129/.

Cleaning

Cleaning of the specimen between each grinding or polishing step is very important to avoid the disturbance of the grinding residues from the previous step to the next. The whole specimen and the hands should be cleaned when a step is finished. Distilled water can be used for a bare metallic specimen. For specimens covered with ash or corrosion products, the dissolution of water-soluble elements should be considered. As an alternative, ethanol is a proper wash medium for water-soluble specimens.

Etching

Etching is a useful method to reveal the microstructure of metallic crystals of metallic alloy, e.g. the materials shown in Fig. 4.2.21 in this study. Etching is performed by immersing a polished metallic surface in a weak acidic or basic solution that attacks the metal surface at a rate varying with crystalline orientation or phase composition. It is easier to control the etching rate by spreading the etching solution with a cotton watt on the polished surface from one side to the other with varying spreading frequency and exposure time. Three groups of etching solutions were selected to reveal ferrite, martensite and austenite in this study:

- Ferrite: 100ml 95% ethanol + 5ml 65% nitric acid /130/
- Martensite: 80ml 96% ethanol, 10ml 65% nitric acid (HNO_3), 10ml 37% hydrochloric acid (HCl), 1g pirkin acid /130/
- Austenite: king water (HCl : HNO_3 = 3:1), then 5 minutes oxidation in air at 500°C /128/

Optic microscope with digital image photography

Optic microscope is the most applied equipment to examine material microstructure at the first step. Optic microscope is also used for some basic measurements, such as grain size and corrosion depth determination. Average and maximum corrosion depth were measured in this study according to the method described in /128/: average corrosion depth is determined by averaging a number of corrosion depths localized in a horizontal constant distance, for example, which are marked with " ° " in Fig. 3.8.

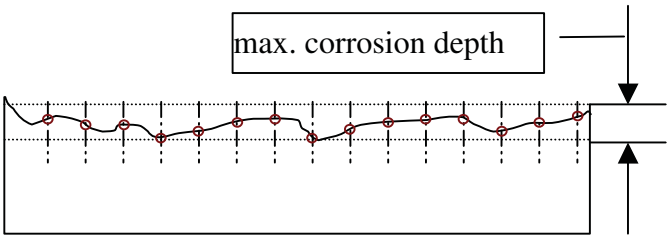

Fig. 3.8. average corrosion depth determination

A Zeiss reflected-light microscope with 5 objectives was used in this study. Images with 50x, 100x, 200x, 500x and 1000x magnification can be obtained. A light filter proved to be helpful to distinguish metal or ash substance from mounting material. A digital camera Nikon 990 with 3.4 million pixel resolution set on the microscope enabled comfortable photography and digital image processing.

Scanning Electrical Microscope (SEM) and Energy Dispersive X-ray (EDX)

SEM: SEM can obtain images with higher magnification than optic microscope can do. The working principle of SEM is described in /131/. Electron images can be taken as secondary electron image (SE) or back-scattered electron image (BE). Secondary electron image has very high depth sharpness even for high magnification, which can reveal the details of the specimen. Back-scattered electron image has low depth sharpness, but it shows the density and the composition of a top surface. The elements with a higher number in the periodic table are shown with brighter colour than elements with lower periodic number.

EDX: EDX is a powerful tool usually equipped with SEM. Element distribution at a point, along a line or of an area can be qualitatively identified by EDX measurement. The element distribution of an area (mapping) is especially useful to evaluate specimens with heterogeneous character, such as deposit specimen. By comparison of elemental distribution of a local phase, the chemical composition on this area can be roughly determined. SEM-EDX analysis were applied both for the corrosion production examination in laboratory test and for the deposit examination in combustion test.

4 Laboratory Investigation

In the laboratory investigation, emphases were given both on the mechanism of chlorine-induced corrosion and the influences of flue gas and deposit on corrosion rate. Therefore, the results of the investigation comprised two parts:

1. mechanisms of chlorine-induced corrosion;
2. combined influence of gas and deposit ash on corrosion rate of advanced boiler materials.

4.1 Mechanisms of chlorine-induced corrosion

For the fundamental investigation of chlorine-induced corrosion, the influences of HCl gas on metal specimen in slight reducing environment and in oxidizing environment were firstly studied.

In oxidizing environment, besides corrosion mechanisms and corrosion structures, corrosion kinetics, influences of temperature, and the concentration of HCl and H_2O on corrosion rate were investigated.

Low-Cr ferritic steels, 9-12%-Cr ferritic/martensitic steels und austenitic steels were selected as test materials. The material compositions are listed in Tab. 4.1.

Tab. 4.1. Composition of test materials in Section 4.1

Test materials	*C*	*Si*	*Mn*	*Cr*	*Ni*	*Mo*	*V*	*rest*	*Fe*
13CrMo44 (ferr.)	0.13	0.2	0.51	0.87	-	0.5	-		rest
7CrMoVTiB 10 10 (ferr.)	0.08	0.21	0.53	2.44	0.175	0.95	0.26	Ti: 0.05, Nb: 0.002	rest
HCM2S (ferr.)	0.08	0.073	0.365	2.58	0.053	0.281	0.23	W: 1.58, Nb: 0.046	rest
10CrMo9 10 (ferr.)	0.13	0.25	0.43	2.28	-	0.92	-		rest
T91(ferr.)	0.10	0.38	0.46	8.1	0.33	0.92	0.18	Cu: 0.06, Nb: 0.07	rest
X20 (marten.)	0.18	0.18	0.57	10.3	0.79	0.9	0.25		rest
HCM12A(ferr. /marten.)	0.15	0.28	0.89	12.21	0.26	0.29	0.21	Cu: 0.51, W:1.84, Nb: 0.06	rest
ASI 304 (austen.)	0.07	max. 1	max. 1	17-19	8.0-12.5	-	-		rest
NF709 (austen.)	0.10	0.16	1.57	22.09	24.7	1.30	0.05	Cu: 0.06, Nb: 0.17	rest

4.1.1 Corrosion mechanisms in slight reducing environment

Test condition

Two tests were carried out in a gas mixture of HCl, water vapour and N_2. Slight reducing environment was created by supplying N_2 and pyrite powder in the test chamber. Various HCl-concentrations were selected to check the influence of HCl on the corrosion rate. The water content was set to about 5%, as the normal case in the combustion zone. N_2 was used as balance gas. The test conditions are listed in Tab. 4.2.

Tab. 4.2. Test condition exposed for 24 hours in the laboratory furnace

	HCl [vppm]	*H_2O [%]*	*Temperature [°C]*	*exposure time [hour]*
Test 1	200	5.01	600	24
Test 2	1000	5.69	700	24

Four materials, 13CrMo44, 10CrMo910, X20 and ASI 304, were selected as testing materials, their chemical compositions are listed in Tab. 4.1.

Results

In both tests, the surface of 13CrMo44 and 10CrMo9 10 turned grey and rough after exposure. In some cases, the scales on 13CrMo44 and 10CrMo9 10 exfoliated. X20 showed only point attack in gas atmosphere containing 200ppm HCl, but it suffered general attack all over the surface in gas containing 1000 ppm HCl. The austenitic steel ASI304 exhibited the best corrosion resistance among the four materials. Almost no corrosion could be observed on it.

Microstructure examination of the specimens after exposure was undertaken with optic microscope and SEM. The grey scale of the low Cr and medium Cr alloys (here 13CrMo44, 10CrMo9 10 and X20) revealed a honeycomb structure (Fig. 4.1.1). EDX elemental analysis implied that the porous scale was composed of iron oxides. The particles on the surface of X20 in Fig. 4.1.1 were composed of both iron oxides and chromium oxides.

Based on above observation, the author suggests that simultaneous formation of solid metal oxides and solid metal chlorides take place at the initial stage of exposure. The holes on the oxide scale were likely generated by the evaporation of the iron chlorides afterwards, which could not be oxidized due to the low oxygen potential. The densely and evenly distributed

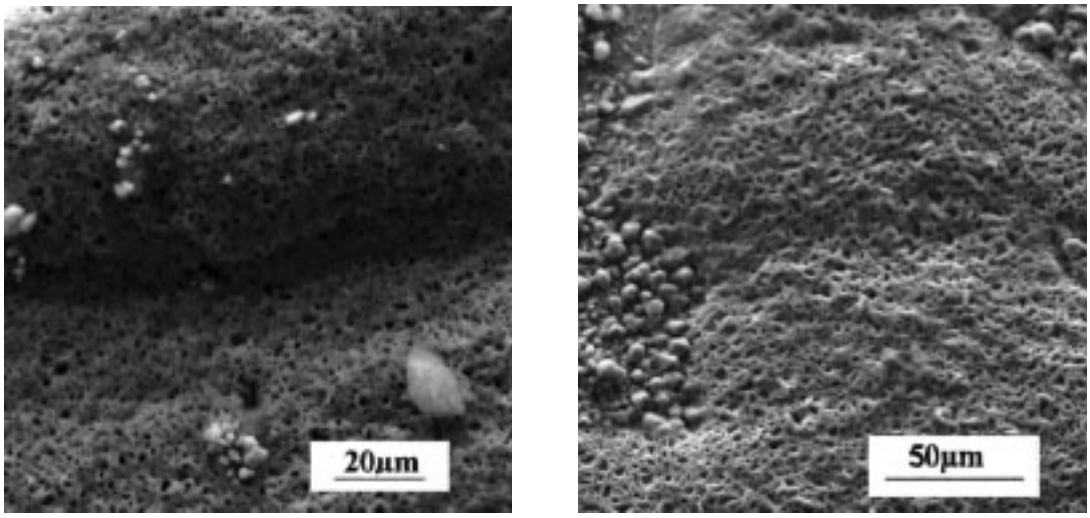

Fig. 4.1.1. SEM, left: 13CrMo44 in gas containing 200ppm HCl at 600°C, right: X20 in gas containing 1000 ppm HCl at 700°C.

holes in the oxide scale created shortcuts between flue gas and metal. As result, there was no concentration gradient of reactants and products through the scale, and the corrosion rate remained relatively constant.

The simultaneous attack of chlorine and oxygen at the initial stage of reaction was also observed by Reese and Müller /97/. They found that oxides and chlorides were formed side by side at the early stage of reaction, although the chlorides were not in stable equilibrium with the gas phase. Salmenoja reported that there is no memory effect of chlorination in reducing environment: the corrosion process stops when the gas supply is shut down /82/. This phenomenon indicates that the oxide scale formed in reducing condition is not a barrier between bulk gas and metal, thus the circulation of chlorine gas under the scale can not maintain for a certain time, as the "active oxidation", does in the oxidizing environment, which is described in chapter 2.3. This kind of corrosion can occur on the furnace wall tubes when chlorine-containing fuels are applied.

4.1.2 Corrosion mechanisms in oxidizing environment

Three test series were carried out in oxidizing atmospheres with following emphases:

- Test Series I: mechanisms of chlorine corrosion;
- Test Series II: corrosion kinetics and the influence of temperature

- Test Series III: the influences of HCl concentration and H_2O concentration on corrosion rate

Test Conditions

- **Test Series I**

Exposure tests were carried out in constant gas environment with varying temperature and exposure time. The gas environment was composed of:

- HCl: 1000vppm
- H_2O: 5.69%
- O_2: 3%
- N_2: balance gas

The temperature and exposure time of tests in Test Series I are listed in Tab. 4.3.

Tab. 4.3. Test conditions of the Test Series I

Temperature, /°C/	400	500	600	700	500
Time, /hours/	24	24	24	24	72

Four low-Cr steels: 13CrMo44, 7CrMoVTiB 10 10, HCM2S and 10CrMo9 10, and two medium-Cr steels: T91 and X20, were studied. The chemical compositions of the testing materials are shown in Tab. 4.1.

- **Test Series II**

Test Series II was carried out at gas temperature ranging from 400°C to 650°C. The exposure time varied from 10 hours to 100 hours. The test schedule is listed in Tab. 4.4. To obtain detailed information, more tests were conducted at 550°C with closer exposure time intervals than at other test temperatures.

Tab. 4.4. The test schedule of Test Series II (The tests were carried out at conditions marked with "•")

time	*temperature*			
	400°C	*450°C*	*550°C*	*650°C*
10 h	•	•	•	•
20 h			•	
30 h	•	•	•	•
60 h			•	
100 h	•	•	•	•

The gas composition was constant in all the tests, which contained:

- HCl: 1000 vppm
- H_2O: 5.69%
- O_2: 3%
- N_2: balance gas.

For each test condition, the test was carried out without cooling and heating interruption.

Four kinds of boiler steel were selected. They are two low-Cr ferritic steels 13CrMo44 and 7CrMoVTiB10 10; a medium-Cr ferritic/martensitic steel HCM12A and a high-Cr austenitic steel NF709. 13CrMo44 is a commercial boiler steel, which was applied as a reference material in this study; the other steels are either newly developed or newly commercialized. The material composition is listed in Tab. 4.1.

The specimen weight before test, after test with scale and after descaling was measured. In some cases, very adhering scale could not be cleansed by thin HCl solution. The weight change of specimens was determined by the weight difference before tests and after tests with corrosion products; the metal loss was determined by the weight difference of metal specimens before test and after descaling. The weight change with corrosion products can give information about the growth rate of the corrosion products, and the metal loss is an indicator of the actual material wastage.

- **Test Series III**

For the investigation of the influence of HCl concentration and H_2O concentration on the corrosion rate, exposure tests with following test conditions were carried out:

Tests with various HCl concentrations:

HCl:	100ppm, 250ppm, 500ppm, 1000ppm, 2000ppm
Other gas composition:	O_2: 3%, H_2O: 5.54%, N_2: balance gas
Exposure time:	30 hours
Furnace temperature:	550°C
Test materials:	13CrMo44, 7CrMoVTiB 10 10, HCM12A, NF709

Tests with various H_2O concentrations:

H_2O:	2.8%, 5.7%, 11.6%, 23.4%
Other gas composition:	O_2: 3%, HCl: 1000ppm, N_2: balance gas
Exposure time:	30 hours

Furnace temperature: 550°C

Test materials: 13CrMo44, 7CrMoVTiB 10 10, HCM12A, NF709

Other test procedures, such as specimen preparation and weight change measurements, were the same as the methods described in the Test Series II.

Corrosion mechanisms

At the initial stage of exposure in the oxidizing atmosphere, compact scale began to form. However, fast growth of solid metal chlorides was observed. They destroyed the continuity of oxide scale. The corrosion topography and corrosion product composition are shown in Fig. 4.1.2. and in Fig.4.1.3. respectively.

Increasing temperature can accelerate scale growth dramatically in HCl-containing gas. Fast scale growth was not observed when the specimens were exposed in environment without

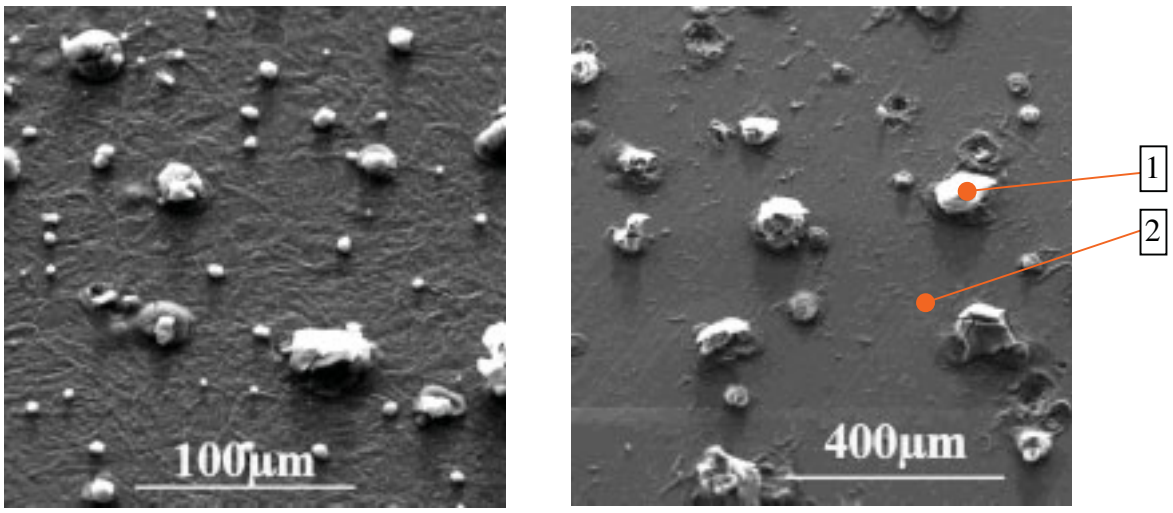

(a) 7CrMoVTiB1010 (b) X20

Fig. 4.1.2. Surface morphology of (a): 7CrMoVTiB 1010 and (b)X20, after 24 h in 400°C in gas containing 1000ppm HCl, 5.56% H_2O and 3% O_2

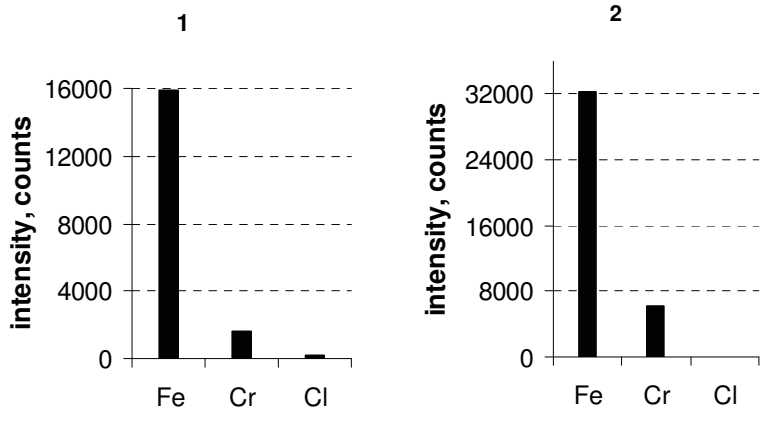

Fig. 4.1.3. EDX point analysis of X20 in Fig. 4.1.2 (b)

HCl. This implies that the rapid formation of oxide scale in chlorine-containing gas is a result of the oxidation of metal chlorides. In this process, temperature plays a very important role.

Fig. 4.1.2, Fig. 4.1.4 to Fig. 4.1.6 show the development of the scale with increasing temperature. At 400°C (Fig.4.1.2), the scale grew slowly, this enabled the underlying metal chlorides to penetrate the scale easily; at 500°C, a complete scale formed on low-Cr and middle-Cr steels. The local attack of chlorine could not be observed over the scale, but the formation of alkali chlorides was profound underneath the scale. As result, the scale was

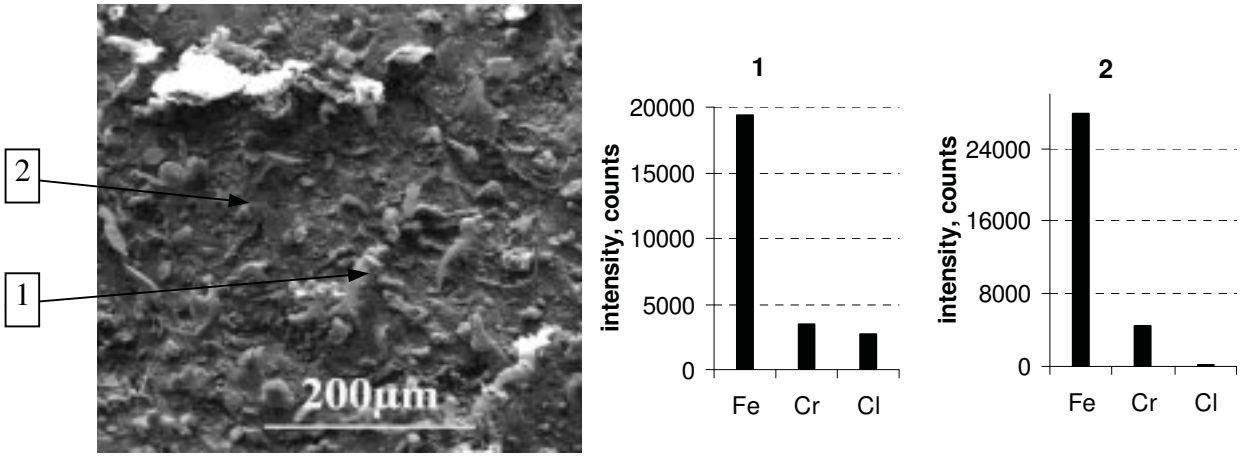

Fig. 4.1.4. Morphology of T91 beneath the spalled oxide scale after 24 h in 500°C in gas containing 1000 ppm HCl, 5.56% H_2O and 3% O_2

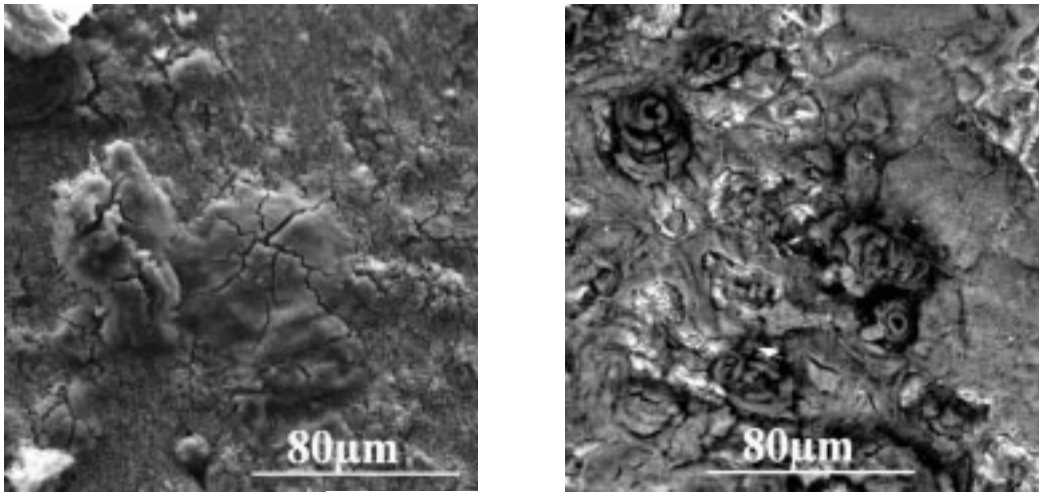

13CrMo44 HCM2S

Fig. 4.1.5. Morphology of 13CrMo44, HCM2S beneath scale after 72 hours exposure in 500°C in gas containing 1000ppm HCl, 5.56% H_2O and 3% O_2.

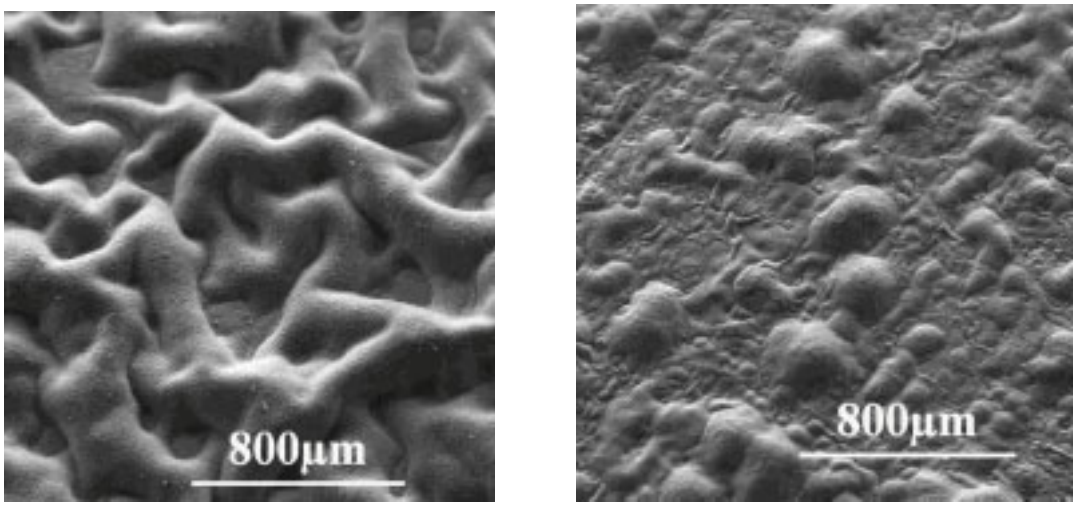

13CrMo44 X20

Fig. 4.1.6. surface morphology of 13CrMo44, X20 after 24 hours exposure in 700°C in gas containing 1000ppm HCl, 5.56% H_2O and 3% O_2.

poorly adherent and partially broken. The corrosion morphologies of T91, 13CrMo44, HCM2S under scale are shown in Fig. 4.1.4 and Fig. 4.1.5.

At 700°C, the oxide scale of low-Cr and middle-Cr steels grew so overwhelmingly, that it corrugated, as shown in Fig. 4.1.6. The different morphologies of chlorine attack with increasing temperature implies that at high temperature, the scale growth is speeded up by the

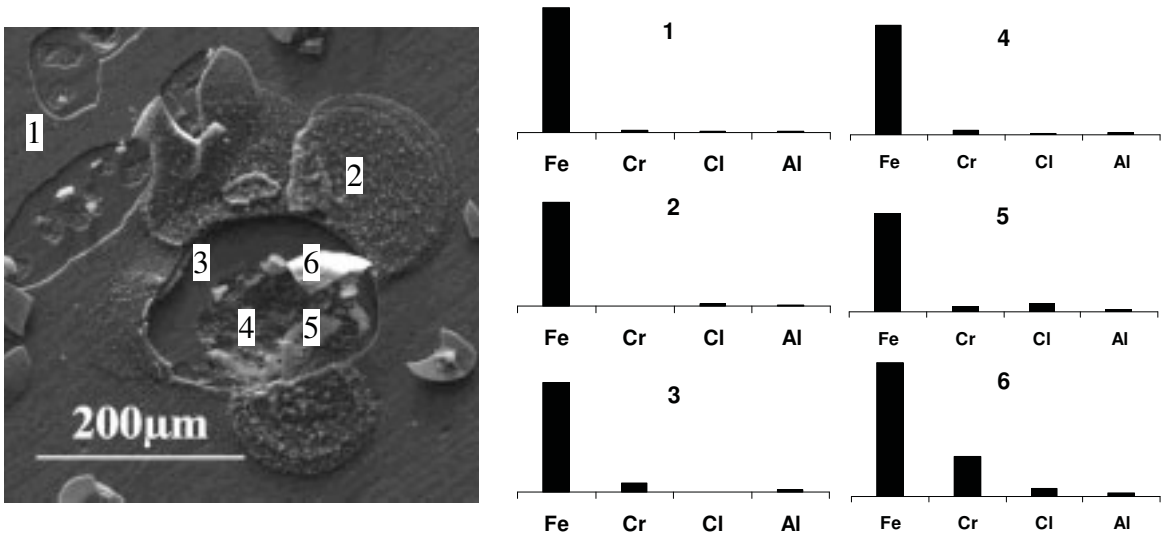

Fig. 4.1.7. 7CrMoVTiB 1010, left: corrosion surface, Secondary Electron picture, 450°C, 10h; right: EDX point analysis

evaporation and the oxidation of metal chlorides, whereas at low temperature, the formation of solid metal chlorides is the main reaction in chlorine corrosion. The form of metal chlorides can be either outgrowing sticks (T91 in Fig. 4.1.4) or buds with cracking or central pass way. Such structure provides shortcut for the outwards diffusion of vapour metal chlorides (13CrMo44 and HCM2S in Fig. 4.1.5).

More detailed information of the corrosion mechanism is revealed by the analysis of 7CrMoVTiB1010 (Fig. 4.1.7). Around corroded pits resulted by chlorine attack, non-protective oxides grew rapidly. Such oxide scale was disrupted by the growth of underlying metal chlorides (Point 5). High chlorine concentration could be detected at the scale/metal interface, as shown in Point 6, which was the downside of the scale. The scale surface around corrosion pits was composed of Fe_2O_3 whiskers (Point 2). This is the typical morphology of oxides converted from gaseous reactants. The outer layer of the scale was mainly composed of iron oxides, but the inner layer was enriched in chromium (Point 3, 4, 6).

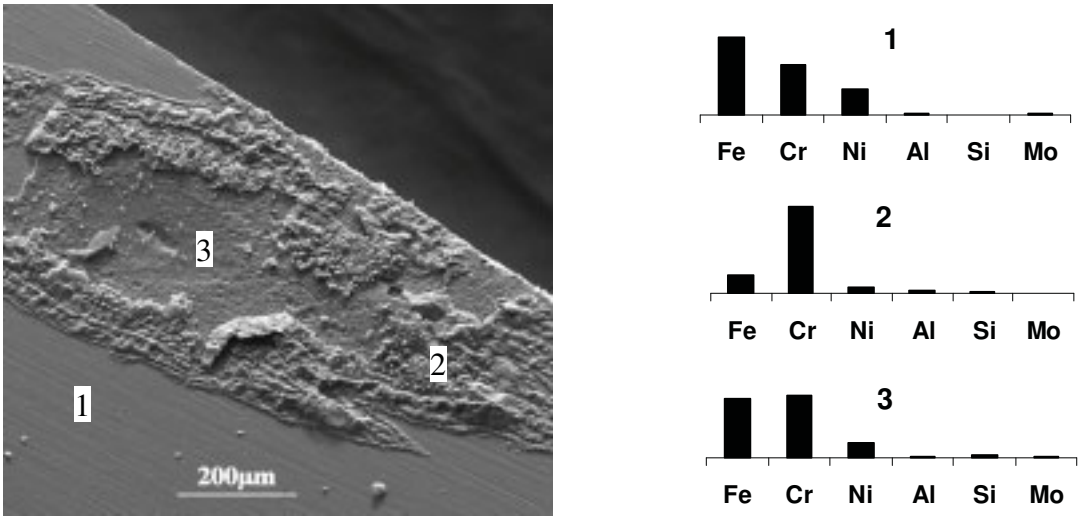

Fig. 4.1.8. NF709, 650°C, 100h, left: corrosion surface; right: SEM-EDX point analysis

Higher Cr content in alloy does not change the corrosion mechanism, but leads to the build up of thinner scale due to the compactness of chromium oxides, as the case of NF709 shown in Fig.4.1.8. Similar to the corrosion feature of low-Cr steels at low temperature, local chlorine corrosion was obvious on NF709, which destroyed the completeness of the scale. On the compact and protective scale surface, the content of iron, chromium and nickel was proportional to the composition of the steel (Point 1). But at the area where the scale was

broken due to the chlorine attack, chromium was dominant. This implies that chromium is preferentially to react with chlorine (point 2 of Fig. 4.1.8). Chlorine could however not be found after the test. Very probably the metal chlorides at the metal/scale interface were oxidized, since oxygen could approach the scale/metal interface easily through the broken scale.

Discussion of corrosion mechanisms

The corrosion morphologies in HCl-containing oxidizing environment have demonstrated the typical features of chlorine-induced "active oxidation". It is characterized by: a) the formation of solid metal chlorides at metal/scale interface, b) the evaporation of metal chlorides and c) the oxidation of vaporized metal chlorides on the way outwards to bulk gas. The oxide scale formed by "active oxidation" grows rapidly, and tends to be disconnected from its bulk alloy.

Chlorination of metal can occur either locally or evenly on metal surfaces at the initial stage. The local pit corrosion may firstly occur at the positions of metal matrix defect, where chlorine gas can penetrate the metal to a certain depth, and to form stabilized metal chlorides in the micro-environment. The evenly distributed metal chlorides on metal surfaces, however, are not stable in the bulk gas environment and are consequently converted to metal oxides. Under oxide scales, where lower O_2 partial pressure and higher Cl_2 partial pressure present, metal chlorides can grow rapidly.

The growth rate of oxide scale in the active oxidation process can be dramatically enhanced by increasing temperature, since the evaporation rate of metal chlorides depends strongly on temperature. The equilibrium vapor pressure of metal chlorides as function of temperature at

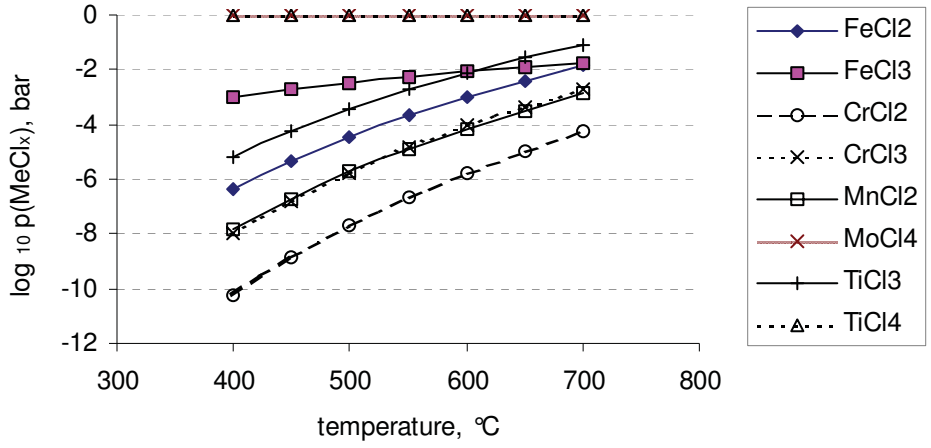

Fig. 4.1.9. Equilibrium vapor pressure of metal chlorides in gas containing 3% O_2, 5% H_2O and 1000vppm HCl

the test gas environment and the equilibrium oxygen partial pressure for the conversion between metal chlorides and metal oxides were calculated with FACTSage in this study. The input gas data correspond the test condition: 3% O_2 , 5% H_2O and 1000 vppm HCl. The results are illustrated in Fig. 4.1.9 and Fig. 4.1.10 respectively.

$MoCl_4$ and $TiCl_4$ could only exist in gas form in the calculated temperature range (Fig. 4.1.9). The equilibrium vapour pressure of other solid metal chlorides increases with temperature. This result indicates that the evaporation of most metal chlorides become stronger at higher temperature, which could lead to faster growth of oxide scale. The equilibrium oxygen partial pressure for the conversion from chlorides to oxides shown in Fig. 4.1.10 could imply the scale structure and composition: when a metal chloride converts to the metal oxides at low oxygen partial pressure, then the oxides should locate at the inner layer of scale; and a high oxygen partial pressure for the conversion implies that the converted oxide locates at the outer layer of the scale. Therefore, according to the equilibrium oxygen pressure in Fig. 4.1.10, the order of the metal oxides, which are enriched from the inner scale to the outer scale, could be the oxides of Ti, Cr, Mo, Fe and Mn. It should be noted that above prediction is based on the formation of pure metal oxides.

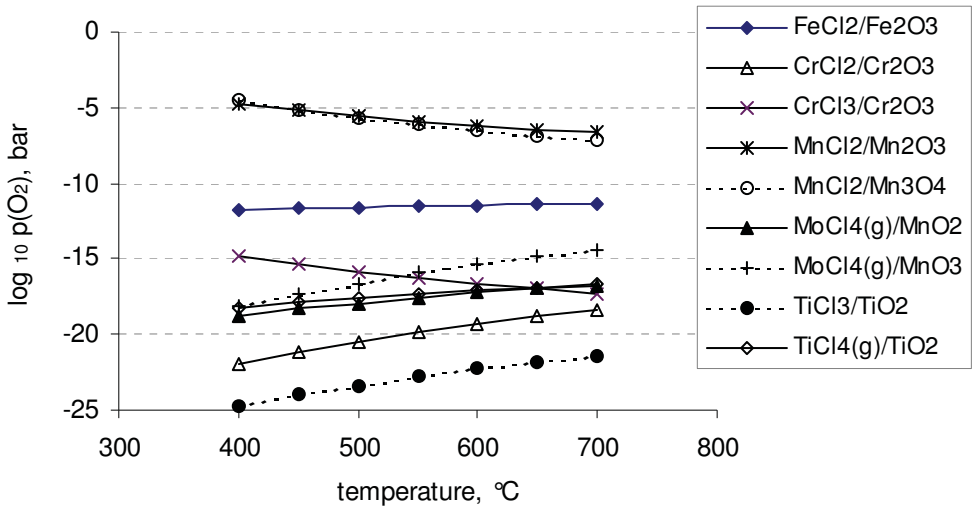

Fig. 4.1.10. Equilibrium oxide partial pressure of gaseous chlorides to solid oxides in gas containing 3% O_2 , 5% H_2O and 1000vppm HCl

Nevertheless, the morphologies of chlorine attack shown in Fig. 4.1.4, Fig. 4.1.7 and Fig. 4.1.8 confirm the calculation results: when the scale is thick enough, iron oxides locate at the

outer side of the scale, whereas chromium oxides are concentrated at the inner side of the scale.

4.1.3 Corrosion kinetics

In this section, the kinetic features of chlorine-induced corrosion are studied. A correlation between weight change and metal loss was defined. Based on the correlation and experimental data from Test Series II, the corrosion kinetics of chlorine-induced corrosion were discussed.

As introduced in Section 2.1, due to the simultaneous weight gain and weight loss during chlorine-induced corrosion process, the general measurement of weight change can not predict the corrosion rate accurately. In the study of Prescott /74/, a comparison was given between the values of weight change and metal loss of advanced steels after exposure in a chlorine containing gas. The results showed that the weight change data are not representative for the corrosion rate.

In such case, more useful information can be obtained from actual metal loss after the corrosion products are cleansed.

Correlation between weight change and metal loss

"Metal loss" in this study is defined as the amount of metal, which is involved in corrosion reactions. "Metal loss" can be determined by:

Metal loss = initial weight of specimen – Weight of specimen after descaling

Assuming that a certain amount of metal of a specimen is consumed to form corrosion products, and the corrosion products are solid and adhering, then the total weight change of the specimen could be expressed in (4.1):

$$\textit{total weight change} = \textit{weight of corrosion products - metal loss} \tag{4.1}$$

Taking the simple oxidation of iron for example:

$$4Fe\,(s) + 3O_2\,(g) \rightarrow 2Fe_2O_3\,(s) \tag{4.2}$$

the total weight change of a specimen, ΔM, for 1 molar iron consumption in reaction (4.2) is:

$$\Delta M = \tfrac{1}{2} M_{Fe2O3} - M_{Fe} = 3/4 M_{O2} \tag{4.3}$$

where M_{Fe2O3}, M_{Fe}, M_{O2} are the molar weight of Fe_2O_3, Fe and O_2 respectively. It is clear that the weight change resulted by iron oxidation is the weight of oxygen involved in the oxidation process. Since the measurement of weight change is easier than the determination of metal loss, which must be conducted after the removal of corrosion products, a correlation between weight change and metal loss is desired, in which the metal loss can be expressed by the weight change of a specimen. Here, a parameter "R" is defined to correlate weight change and metal loss:

$$R = (\text{weight of corrosion products}) / \text{metal loss}$$
$$= (\text{weight change} + \text{metal loss}) / \text{metal loss} \quad (4.4)$$

According to the definition in (4.4), "R" of iron oxidation in (4.2) can be calculated:

$$R_{Fe2O3} = \tfrac{1}{2} M_{Fe2O3} / M_{Fe} = 1.429 \quad (4.5)$$

Chlorine induced active oxidation involves complicated interactions of oxidation, chlorination and evaporation of metal chlorides. Taking pure iron for example, the whole process of chlorine induced "active oxidation" can comprise following reactions:

a) Oxidation of Fe to Fe_2O_3, weight gain, $R = 1.429$

b) Chlorination of Fe, which can be separated into following steps:

   (i). Chlorination of Fe to solid $FeCl_2$: weight gain, $R = 1.607$;

   (ii). Chlorination of Fe to solid $FeCl_2$, then the solid $FeCl_2$ is vaporized and oxidized: weight gain, $R = 1.429$;

   (iii). Chlorination of Fe to solid $FeCl_2$, then the solid $FeCl_2$ is vaporized and escapes into bulk gas: weight loss, $R = - 1.607$.

The R-value for low-Cr steels can give important information about the dominant reaction in a chlorine involved corrosion process:

a) when $R > R_{Fe2O3}$ (1.429), chlorination of iron to solid $FeCl_2$ may be dominant;

b) when $R < R_{Fe2O3}$ (1.429), evaporation of solid $FeCl_2$ may be the dominant;

c) when R is close to R_{Fe2O3} (1.429), iron oxidation is the main reaction. This can be either the direct oxidation of metal, or the active oxidation, in which iron oxides are formed firstly, and then they are oxidized to iron oxides;

d) when R is close to 1, no weight change occurs. This can be a result of two different processes: either the growing rate of corrosion products is very low, indicating the formation of protective scale; or the weight gain of a reaction is discounted by the weight loss of another reaction, so that the whole system locates in an equilibrium state of weight change.

Corrosion rate and R-Value determined by experiments

The weight changes of test materials after different exposure periods at 550°C and the actual metal losses after descaling are shown in Fig. 4.1.11. The R-values defined in Eq. 4.4 were calculated from the experimental results and are also shown in Fig. 4.1.11. The "R" of NF709 is not shown in the diagram, since the metal loss of NF709 was too low to give an accurate

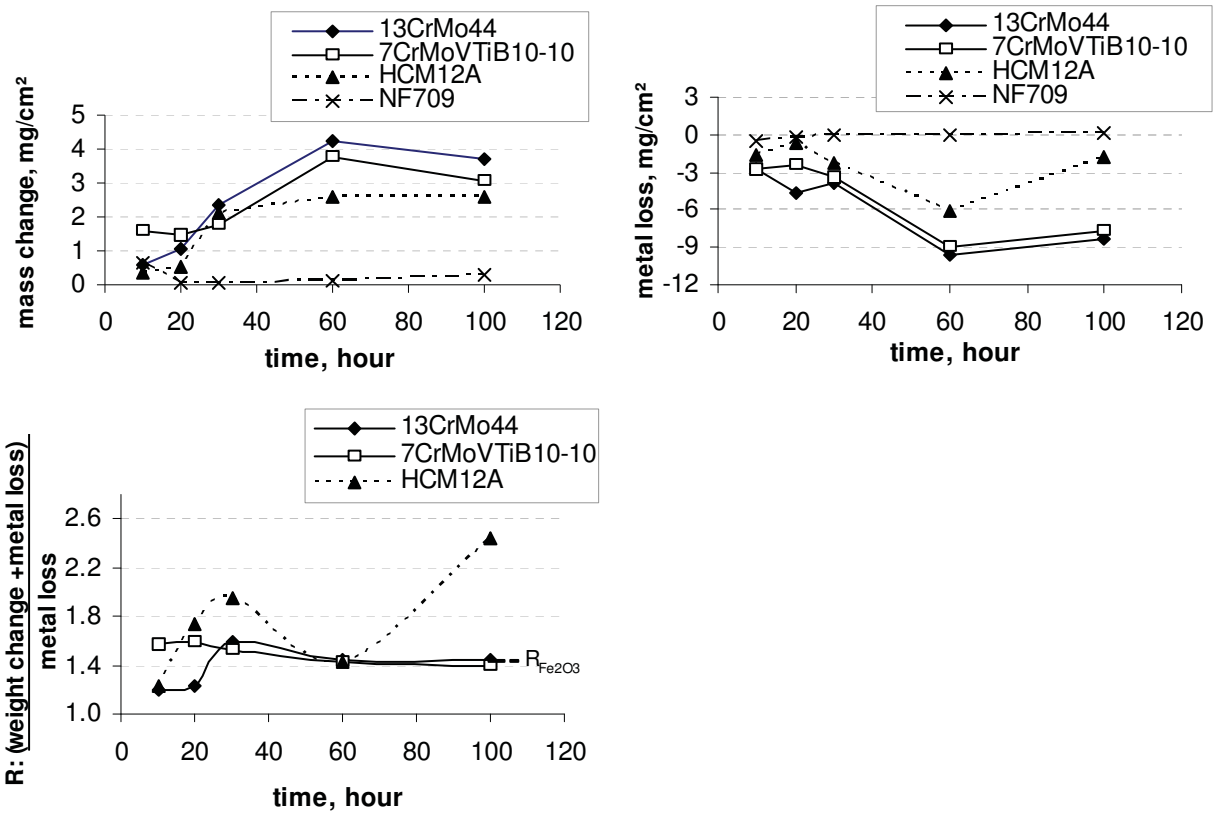

Fig. 4.1.11. Weight change, metal loss and R values at 550°C

evaluation.

Except NF709, the test specimens exhibit rapid weight gain at the first 60 hours of exposure, but the weight gain slows down after this initial stage. R-values of 13CrMo44 and 7CrMoVTiB1010 show very interesting results: they are very fluctuating in the first 60 hours,

but approach R_{Fe2O3} afterwards. The corrosion layers of NF709 and HCM12A were very compact, which were difficult to be cleansed in HCl solution, therefore their R-value can not be precisely calculated.

The fluctuating R-values indicate that, according to material and exposure period, one reaction from chlorination, oxidation and evaporation of metal chlorides can be dominant at the initial stage, even though metal chlorides are less stable than oxides in such environment. The irregularity of corrosion kinetics of the active oxidation was also observed by other researchers /139, 135/. Reesem suggested that the growth rate of oxides is not determined by one slowest step of a diffusion-determined process, but by the interaction of several steps, the conversion rates of which are comparable.

The approximation of R-values from 13CrMo44 and 7CrMoVTiB1010 to the R_{Fe2O3} after the initial period indicates that metal oxides become gradually the main products in the process. From the observation of corrosion morphologies of above materials, the rapid growth of such metal oxides is attributed by the "active oxidation" process. However, a slow down of the weight gain and metal loss were also detected, as shown in Fig. 4.1.11. A likely explanation is that the oxide products formed during "active oxidation" could also supply some degree of protection to metal.

Influence of temperature on corrosion rate

The weight change with time at different temperature was also studied, as illustrated in Fig. 4.1.12. Below 450°C, the weight gains of all steels are quite low, and they slow down with time. At 550°C, the weight gain of low-Cr steels and medium-Cr steels becomes considerably higher. 13CrMo44 and HCM12A showed slow down of scale growth with time, but the scale growth of 7CrMoVTiB 1010 kept almost linear. NF709 exhibited almost no weight change at 550°C and at 650°C. Combining the corrosion morphologies shown in Fig. 4.1.2 to Fig. 4.1.7 with the weight gain data, it is reasonable to assume that below 450°C, chlorine corrosion is not severe, whereas above 550°C, chlorine-induced active oxidation dominates the process. Similar observation was reported by Valente /136/.

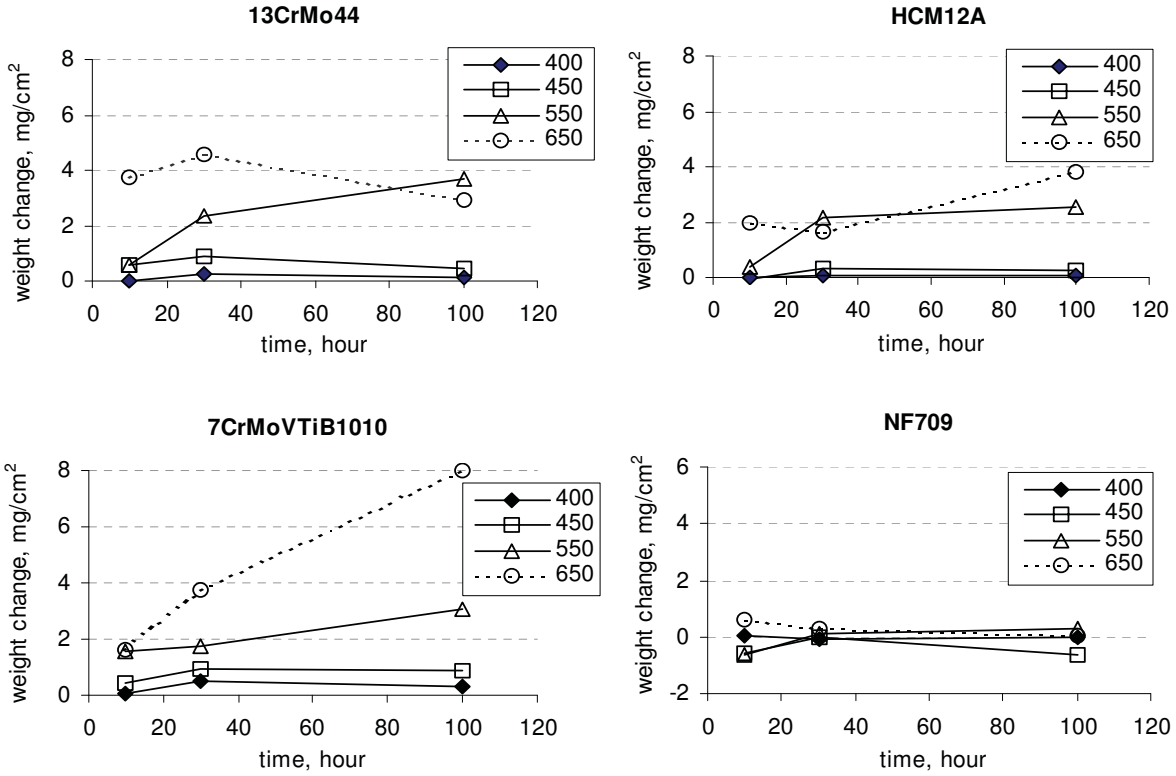

Fig. 4.1.12 the influence of temperature on corrosion rate in term of weight change

4.1.4 Influence of HCl and H_2O on corrosion rate

Influence of HCl concentration

The corrosion rates in gases containing different HCl and H_2O concentration were investigated in the Test Series III. Fig. 4.1.13 shows the dependence of corrosion rate on HCl concentration in gas atmosphere. In the HCl-concentration range of 100ppm to 500ppm, except NF709, obvious increase of weight gain and metal loss were observed with increasing

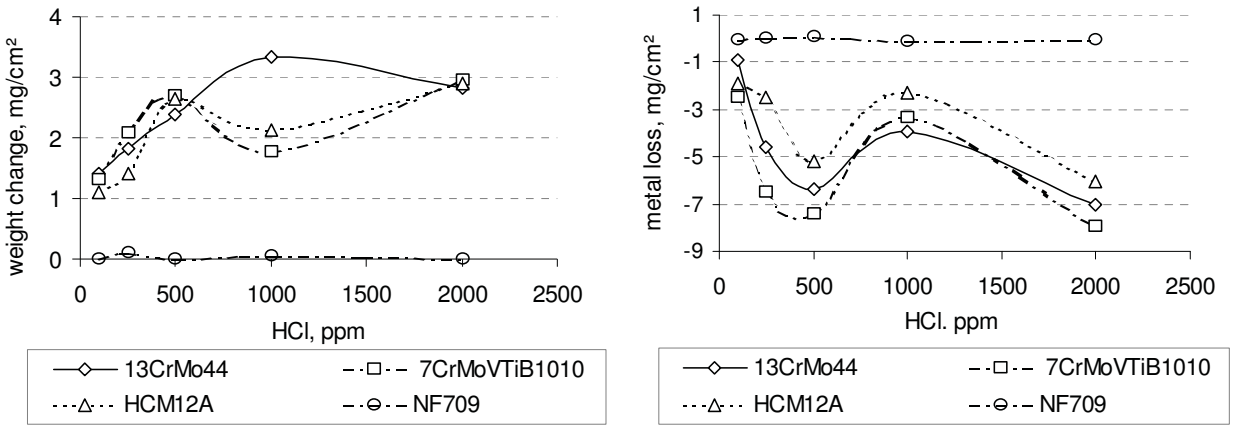

Fig. 4.1.13. Influence of HCl concentration on corrosion rate at 550°C, 30 h.

HCl concentration. Above 500ppm, the corrosion rate decreases again. Other researchers reported similar results. Spiegel showed that a high rate of weight gain of high-alloyed steels takes place with HCl up to 500vppm, above this HCl concentration in gas, the rate of weight gain slows down /137/. Besides, it seems that a certain concentration of HCl in flue gas is required to activate chlorine corrosion. Valente /136/ reported that, when HCl concentration is higher than 200mg/Nm^3 (equals to 123 vppm) and the material temperature is higher than 500°C, the kinetic curve of corrosion attack is linear rather than parabolic. These results may be convincing for coal-fired power plants, in which HCl concentration in flue gas is seldom higher than 500 vppm.

Influence of H_2O concentration

Fig. 4.1.14 shows the weight change and the metal loss with increasing of water vapour concentration. It demonstrates that NF709 has superior corrosion resistance against chlorine corrosion and is not sensible to H_2O concentration. In the case of other materials, the peak values of corrosion rate locate around 12% of H_2O in gas. There is no obvious influence of H_2O on corrosion rate of different materials when H_2O concentration is lower than 5%. On the other hand, a high H_2O concentration, e.g. 25% in flue gas, seems to depress the chlorine-induced corrosion effectively.

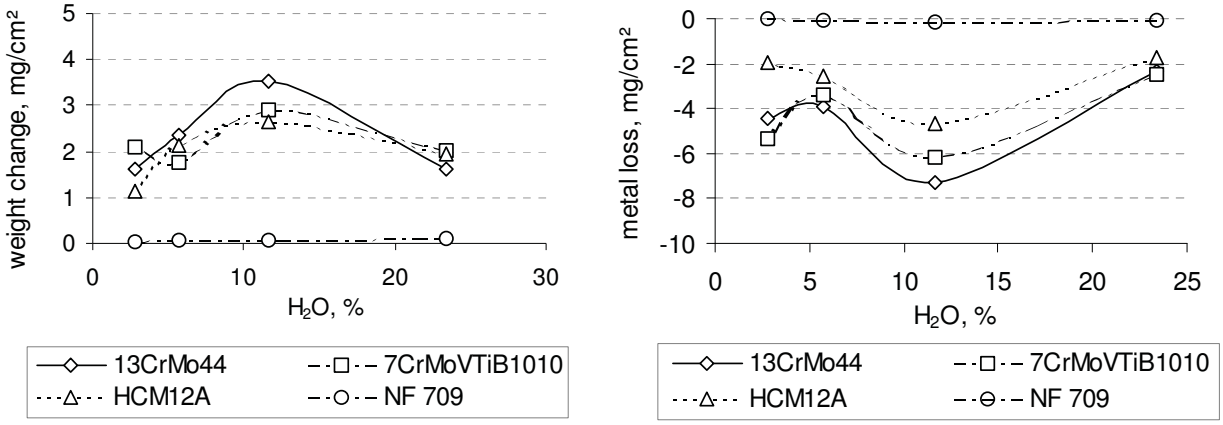

Fig. 4.1.14. Influence of H_2O concentration on corrosion rate at 550°C, 30 h.

4.1.5 Conclusion

The morphologies and corrosion mechanisms of chlorine corrosion are different in different gas environment and temperature, which can be generalized in following points:

1. In reducing atmosphere, honeycomb-like scale is formed on the metal surface due to the formation of solid metal chlorides and the evaporation of such metal chlorides afterwards.

2. In oxidizing atmosphere, temperature plays an important role in the chlorine corrosion. Below 450°C, the corrosion morphology is characterized by the fast growth of solid metal chlorides on a thin metal oxide layer. The corrosion rate is relatively low. Above 550°C, oxide scale growth fast, which tends to break down and spallling. Chlorination of metal after the initial stage occurs mainly beneath the oxide scale. The high corrosion rate is resulted by the increased equilibrium vapour pressure of metal chlorides at high temperature, which leads to rapid evaporation of metal chlorides and oxidation of such vapour metal chlorides to metal oxides.

3. For low-Cr steels and medium-Cr steels, the outer side of the scale is enriched with iron oxides, and the inner side of the scale is enriched with chromium oxides. High-Cr austenitic steels, such as NF709, did not show obvious metal loss during chlorine attack, but, it can still suffer local attack in form of corrosion pit.

The rate of metal loss during chlorine corrosion in oxidizing atmosphere can be revealed by the R-value, which correlates metal loss and weight change of a specimen. R-value can be calculated for a certain single reaction. “R”-value of a whole process, which involves many uncertain reactions, can be measured by laboratory tests, and it can be used to predict the dominant reaction in this process. For example:

1. The different “R” curves of test materials during the first 60 hours exposure in HCl containing gas indicates that, there is no common corrosion kinetics for the corrosion rate of low-Cr and medium-Cr steels. Depending on materials and exposure period, the corrosion rate can be dominated by one of the following reactions: metal oxidation, metal chlorination, evaporation of metal chlorides, and oxidation of vapour metal chlorides. The approach of all “R”-curves to “R”$_{Fe2O3}$ after this initial period suggests that, the weight change of test specimens is mainly attributed by the oxidation of metal chlorides.

2. Although the oxide scales formed on low-Cr steels and middle-Cr steels are poorly adherent, they can still work somewhat as a barrier between metal and flue gas to slow

down gaseous diffusion. In case of austenitic steel with Cr-content more than 20%, the corrosion rate is very low.

The influence of HCl concentration and water vapour in flue gas can be generalized as following:

- Corrosion rate increases with HCl concentration in the range of 0-500 vppm. Above this range, there is no clear dependence of weight change and metal loss on HCl concentration. Regarding the water vapour content, a peak value of the corrosion rate locates at the water vapour concentration around 12%.

4.2 Combined influences of gas and deposits on chlorine corrosion

It is known that under chlorine-rich or sulphur-rich ash deposits, boiler steels suffer much higher corrosion attack than they could be only in corrosive gas environments. The general explanations of the interactions between gas and deposits in oxidizing environment were given by some researchers, but the interactions between gas and deposits in reducing environment are seldom reported. Also seldom reported are the effective ash components and their concentration to trigger high corrosion rate in reducing atmosphere and in oxidizing atmosphere. Concerning the internal corrosion induced by chlorine attack, the morphology differences of internal corrosion caused by material metallurgical features are still not given enough attention. Targeting at above questions, intensive investigations were carried out on following topics:

- Chemical changes of deposit composition with time in reducing and oxidizing atmospheres,
- Influences of ash deposit on corrosion rate in reducing, oxidizing and sulphur-containing atmosphere,
- Metal loss and internal corrosion depth of advanced boiler materials at high temperature.

4.2.1 Test conditions

Two test series were carried out with following emphases:

- the first test series: the combined influences of gas and deposit on corrosion rate. The gas temperatures were 550°C and 650°C;
- the second test series: the corrosion resistance of advanced boiler steels regarding metal loss and the depth of internal corrosion. The gas temperatures were 650°C and 700°C.

Thin plates of test material were covered with ash deposit and exposed for a period between 100 hours to 300 hours. Metal loss of specimens after exposure was determined. Afterwards some specimens were mounted and polished for microstructure analysis.

Deposit ash

Following five ashes were selected as deposit ashes:

1. 100% KCl (synthetic ash)

2. 50 wt. % KCl + 50 wt. % K_2SO_4 (synthetic ash)
3. straw ash (from 100% straw combustion)
4. wood ash (from a co-firing of 50% wood + 50 % lignite of thermal basis)
5. coal ash (from 100% lignite combustion)

For the first test series, all the five ashes were applied, whilst for the second test series, only straw ash and coal ash were applied. The real ashes from combustion process were collected from filter container, since the chlorine content and the sulphur content of filter ash are most similar to those of deposit ash on SH/RH tube surfaces. All ashes were finely milled before use.

The ash chemistries of real ashes are illustrated in Figure 4.2.1. The main elements in straw ash are potassium, chlorine and silicon, in wood ash are calcium, sodium, iron and sulphur, and in lignite ash are earth alkalis, iron, silicon and aluminium. It is to note that sulphur content in wood is usually low. The high sulphur content in wood ash comes actually from the coal, which is co-fired with wood. Besides, unburned carbon in coal ash was much higher than that in other ashes. This could create local reducing atmosphere during exposure in laboratory tests.

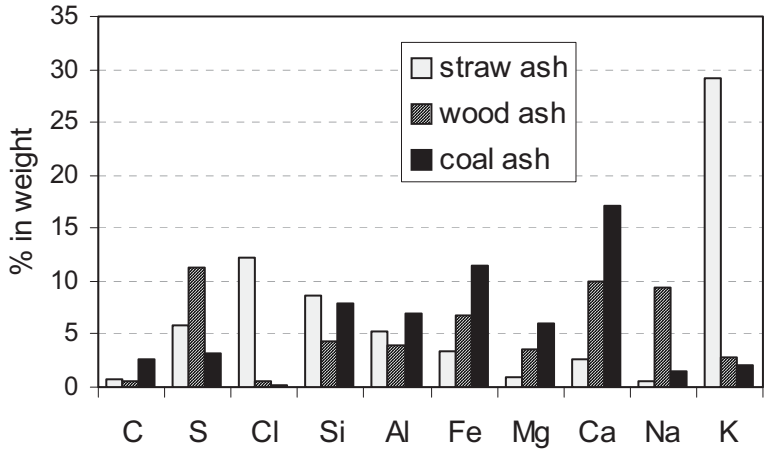

Fig. 4.2.1. Chemical composition of straw ash, wood ash and coal ash

Gas composition

Following three gas compositions were applied in the investigation, corresponding to slight reducing, oxidizing and oxidizing-sulphating atmospheres:

- N_2 (slight reducing atmosphere)
- $3\%O_2 + N_2$ (oxidizing atmosphere)
- $500mg/m^3\ SO_2 + 3\%O_2 + N_2$ (oxidizing-sulphating atmosphere)

The furnace atmosphere filled with N_2 is regarded as slight reducing during the exposure of carbon-containing ashes, since the oxidation of unburned carbon during exposure creates local reducing atmosphere.

Testing materials

Nine boiler steels were selected for the investigations. The chemical compositions of them are listed in Tab. 4.2.1.

Tab. 4.2.1 Elemental composition of tested materials

materials	*C*	*Si*	*Mn*	*Cr*	*Ni*	*Mo*	*Al*	*Cu*	*V*	*Nb*	*Rest*	*Fe*
13CrMo44	0.13	0.2	0.51	0.87	-	0.5	-	-	-	-		bal
T91	0.1	0.38	0.46	8.1	0.33	0.92	-	0.06	0.18	0.073		bal
X20	0.18	0.18	0.57	10.3	0.79	0.9	-	-	0.25	-		bal
HCM12A	0.1	0.28	0.89	12.21	0.256	0.29	-	0.507	0.21	0.059	W: 1.84, Pr: 0.07, Ce: 0.03	bal
Esshete1250	0.12	0.36	8.13	15.19	8.91	0.91	-	-	0.249	0.925	Ti: 0.05	bal
TP347HFG	0.1	0.41	1.50	18.10	11.84	0.21	0.20	0.24	0.07	0.93	W: 0.01, Ti: 0.01, Co: 0.22	bal
S304H	0.09	0.15	0.88	18.50	9.2	0.34	0.01	2.92	0.07	0.6	Ti: 0.007, Co: 0.16	bal
NF709	0.08	0.156	1.57	22.09	24.7	1.3	-	0.058	0.048	0.174	Pr: 0.071, Co: 0.125, Ce: 0.058	bal
HR3C	0.07	0.252	1.52	24.32	19.82	0.07	-	0.045	0.067	0.442	Pr: 0.092, Co: 0.348, Ce: 0.066	bal

13CrMo44, T91 and Esshete1250 were selected for the first test series, which are typical low-Cr-ferritic steels, medium-Cr ferritic/martensitic steels and low-Cr austenitic steels respectively. For the second test series, only 9-12%-Cr ferritic/martensitic steels and austenitic steels were selected.

An overview of the test conditions including exposure time, temperature, deposit ash, gas composition and material selection is given in Tab 4.2.2.

Tab. 4.2.2. Test condition for corrosion test under ash deposits

	Temp. [°C]	*time [hour]*	*Deposit ash*	*Materials*	*Gas environment*
Test Series I	550	100	100% KCl, 50%KCl +50% K_2SO4	13CrMo44, T91, Esshete1250	N_2, O_2+N_2, SO_2+O_2+N_2
	650	100	100% KCl, 50%KCl +50% K_2SO4 straw ash, wood ash, coal ash	13CrMo44, T91, Esshete1250	N_2, O_2+N_2, SO_2+O_2+N_2
Test Series II	650	300	straw ash, coal ash	T91,X20, HCM12A, Esshete1250, TP347HFG, S304H, NF709, HR3C	N_2, O_2+N_2
	700	100	straw ash, coal ash	T91,X20, HCM12A, Esshete1250, TP347HFG, S304H, NF709, HR3C	N_2, O_2+N_2, SO_2+O_2+N_2
		300	straw ash, coal ash	T91,X20, HCM12A, Esshete1250, TP347HFG S304H, NF709, HR3C	N_2, O_2+N_2

4.2.2 The change of ash deposition with time in reducing and oxidizing atmospheres

Results

The understanding of the interactions between gas and ash deposit during exposure is important, since the corrosion rate is directly depended on the corrosive gas species, which are released from such interactions. The changes of chlorine and sulphur concentration in ash deposits after the exposure in slight reducing, oxidizing and oxidizing-sulphating atmospheres are illustrated in Fig. 4.2.2.

In slight reducing atmosphere, there is a minor decrease of sulphur in straw ash and in wood ash after exposure. Chlorine concentration is also slightly reduced in straw ash. The reduction of chlorine concentration in deposit was caused by the evaporation of solid chlorides, since it was observed that evaporated KCl condensed again on the front part of the furnace wall when it met relatively cooler gas stream, as shown in Fig. 4.2.3. Sulphides were found in the coal ash after exposure in N_2, but there were no sulphides in the original coal ash. This implies that local reducing atmosphere was created during test period, in which sulphate compounds converted to sulphides. Due to the formation of sulphides in coal ash, the chlorine analysis by potentiometric titration with $AgNO_3$ showed an inaccurate high concentration of chlorine in coal ash (Fig. 4.2.2, “Coal ash” diagram: N_2, 650°C).

After exposure in the oxidizing gas at 550°C and at 650°C, straw ash and wood ash were slightly sintered. The chlorine concentration in the chlorine-rich straw ashes reduced slightly.

However sulphates in all the ashes were relatively stable in the oxidizing atmosphere.

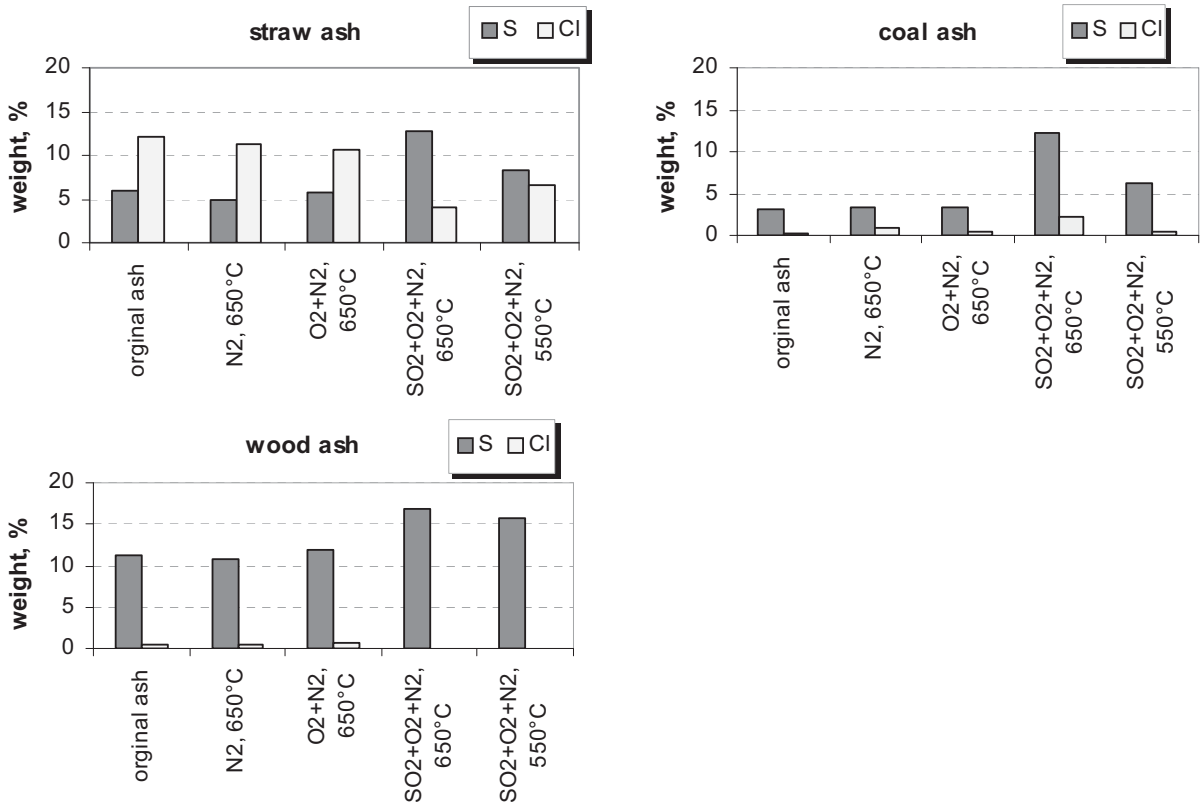

Fig. 4.2.2. The changes of ash chemistry after exposure in slight reducing, oxidizing and oxidizing-sulphating gases for 100hours.

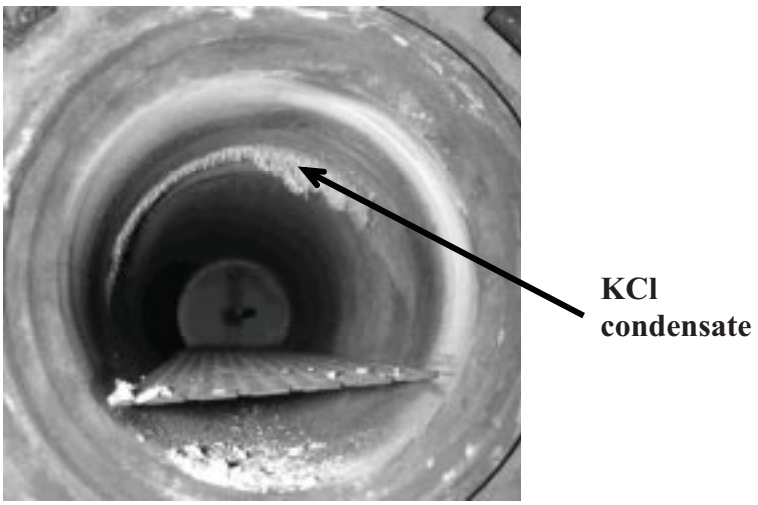

Fig. 4.2.3. KCl condensate after 100 hours exposure of Cl containing ash in N_2 at 650°C

After the exposure in the oxidizing-sulphating gas, sulphur content in all ashes increased dramatically, but chlorine concentration showed the opposite trend. The decrease of chlorine concentration in ash deposits in SO_2-containing atmosphere was more apparent than it did in the only oxygen-containing atmosphere.

Discussion

Due to the high equilibrium vapour pressure of alkali chlorides at high temperature, solid chlorides tend to vaporize, for example, according to the following reaction:

$$KCl(s) \rightarrow KCl\ (g)\ or\ K_2Cl_2(g) \qquad (4.2.1)$$

In reducing atmosphere, few oxygen or SO_2 is available to oxidize evaporated chlorides, therefore, the evaporated alkali chlorides are more apparent to be observed than that in oxidizing atmosphere. The decomposition of sulphate compounds is possible in N_2 gas, since unburned carbon in ash can create local reducing atmosphere by carbon oxidation. The decomposition products of sulphate can be oxides or sulphides, depending on the local oxygen partial pressure in deposits: e.g. iron sulphate can be decomposed either to Fe_3O_4 according to (4.2.2) or to FeS according to (4.2.3). Results of FACTSage calculation at 650°C show that, $FeSO_4$ is decomposed to FeS at $p(O_2) = 0.87E^{-17}$ Mpa and $CaSO_4$ is decomposed to CaS at $p(O_2) = 0.157E^{-18}$ Mpa. Above reactions can be described in (4.2.3) and (4.2.4):

$$3FeSO_4 \rightarrow Fe_3O_4 + 3SO_2 + O_2 \qquad (4.2.2)$$

$$FeSO_4 + 2C \rightarrow FeS + 2CO_2,\quad p(O_2) = 0.87E^{-17}\ \text{Mpa},\ p(S_2) = 0.85E^{-2} \qquad (4.2.3)$$

$$CaSO_4 + 2C \rightarrow CaS + 2CO_2,\ p(O_2) = 0.157E^{-18}\ \text{Mpa},\ p(S_2) = 0.992E^{-4} \qquad (4.2.4)$$

In the oxidizing atmosphere with 3% oxygen, another mechanism dominates the ash conversion process, which can be generalized in following points:

a) oxygen in gas atmosphere stabilizes sulphates in deposit, therefore there is almost no change of sulphur concentration in deposit after exposure;

b) the release of Cl_2 gas from ash chlorides depends not on the decomposition of sulphates in deposit, but depends directly on the O_2 concentration in gas atmosphere;

c) when enough O_2 is available for the oxidation of chlorides, the rate of Cl_2 formation is mainly related with the chlorine concentration in ash deposits.

The changes of sulphur and chlorine concentration in ash deposits after exposure test in the oxidizing-sulphating gas imply that chlorides in ash deposits can be effectively sulphated by

SO_2 in flue gas, and the combination of O_2 and SO_2 in gas atmosphere is more effective to release Cl_2 from chlorides than oxygen alone.

4.2.3 The influences of ash deposit on corrosion rate in reducing, oxidizing and oxidizing-sulphating atmosphere

In slight reducing atmosphere

Metal losses of the test material at 550°C and at 650°C in slight reducing atmosphere are shown in Fig. 4.2.4. The metal losses were generally low in the reducing atmosphere. Straw ash and wood ash were considerably more corrosive than synthetic ashes. In all the cases, the corrosion resistance of test materials was improved with increasing alloy chromium content.

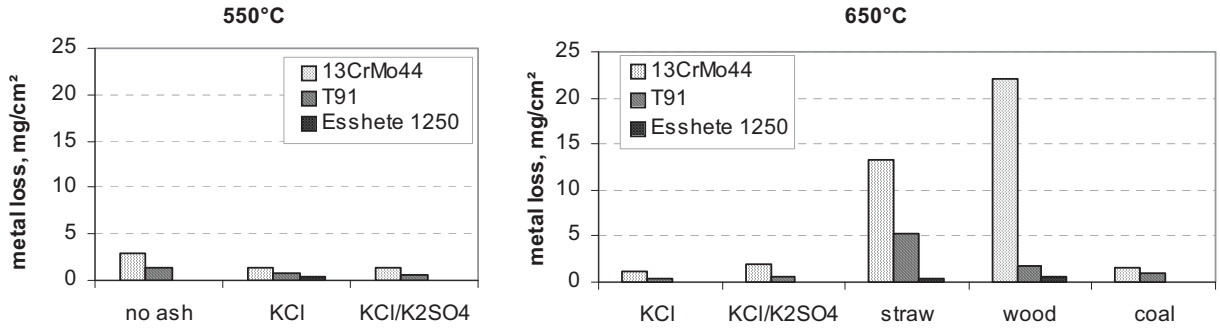

Fig. 4.2.4. metal loss in slight reducing atmosphere

In oxidizing atmosphere

In oxidizing atmosphere, the corrosion morphologies under deposit ashes are different. Under chlorine-enriched ashes (the two synthetic ashes and straw ash), a porous outer scale and a relatively compact inner corrosion layer were formed on the low-Cr steels and medium-Cr

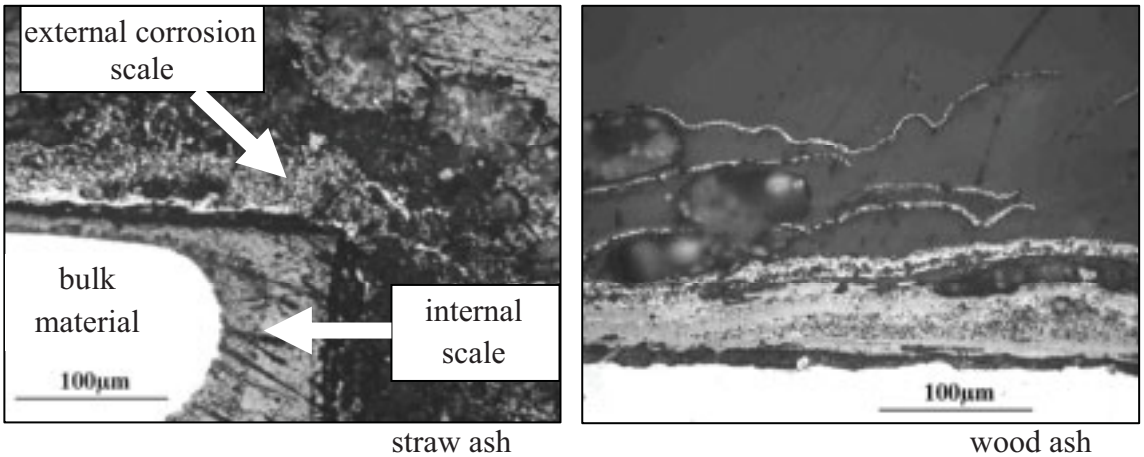

straw ash wood ash

Fig. 4.2.5. The cross section of T91 covered with straw ash and wood ash and after 100 hours exposure at 650°C.

steels. The porous outer oxide scale under straw ash is an evidence of the outwards diffusion of $FeCl_2$, which is oxidized to Fe_2O_3 afterwards. Under wood and coal ash, only compact scales were formed. However, such compact scales exfoliated with time. Fig. 4.2.5 shows, for example, the corrosion morphologies of T91 under straw ash and wood ash at 650°C.

The metal loss rates in oxidizing atmosphere are shown in Fig. 4.2.6. Generally, chlorine-rich deposits resulted in considerably higher metal loss than bare materials alone, furthermore, synthetic ashes, which contained more chlorine than real ashes, were correspondingly more corrosive than real ashes.

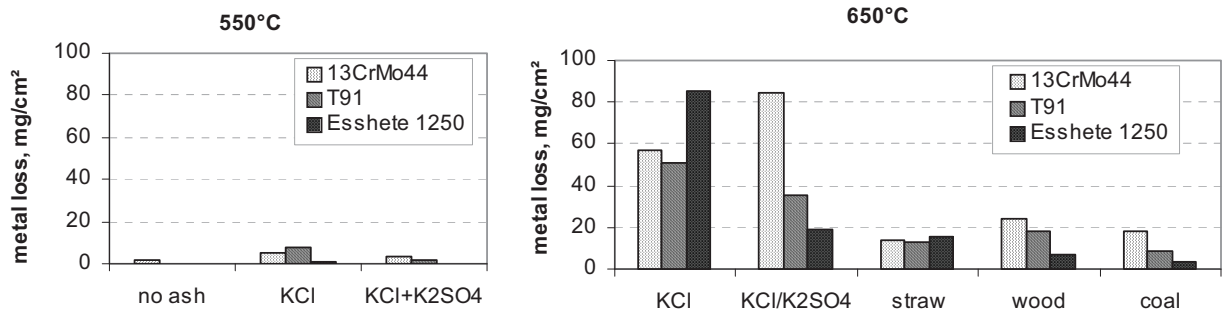

Fig. 4.2.6. metal losses in oxidizing atmosphere

Metal losses increased dramatically as gas temperature raised from 550°C to 650°C. There was no clear dependence of metal loss on alloy chromium content by chlorine attack. For example, austenitic steel Esshete 1250 did not show better corrosion resistance than ferrite steels. However, under wood ash and coal ash, metal wastage corresponded to alloy chromium content again.

No internal attack was observed on all test materials at 550°C. At 650°C, internal corrosion by chlorine attack was observed on T91 and Esshete 1250. Figure 4.2.7 shows the internal corrosion of T91 in the form of point attack under KCl ash after the oxide scale was removed. In the case of Esshete 1250, the chemical composition on the internal corroded zone was analysed with SEM-EDX mapping and the detached scale was analysed with SEM-EDX point analysis, as shown in Fig. 4.2.8 and Fig. 4.2.9 respectively. The mapping pictures in Fig. 4.2.8 imply that chromium is depleted along some fissures in the metal matrix, which are probably generated by chlorine attack. Another observation is the enrichment of nickel and sulphur at the oxide/metal interface (Fig. 4.2.8), which implies the formation of nickel sulphide. This should give enough attention, since nickel sulphide is able to form low temperature melts. The missing chromium was found in the detached oxide scale (Fig.4.2.9). Chromium was enriched in inner scale, whereas only iron oxides could be found in the porous outer scale. KCl ash and

metal oxides were mixed together at the outer layer, as shown in elemental analysis of Point 2 and Point 3 in Fig. 4.2.9. This can be a result of the oxidation of gaseous metal chlorides in the deposit ash.

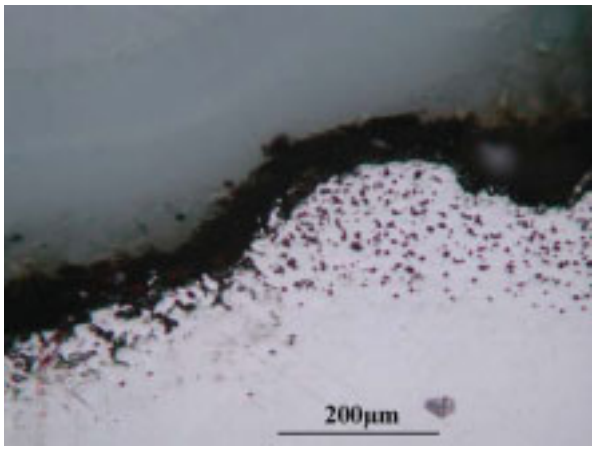

Fig. 4.2.7. T91 under KCl ash after exposure at 650°C in 3%O_2 +N_2

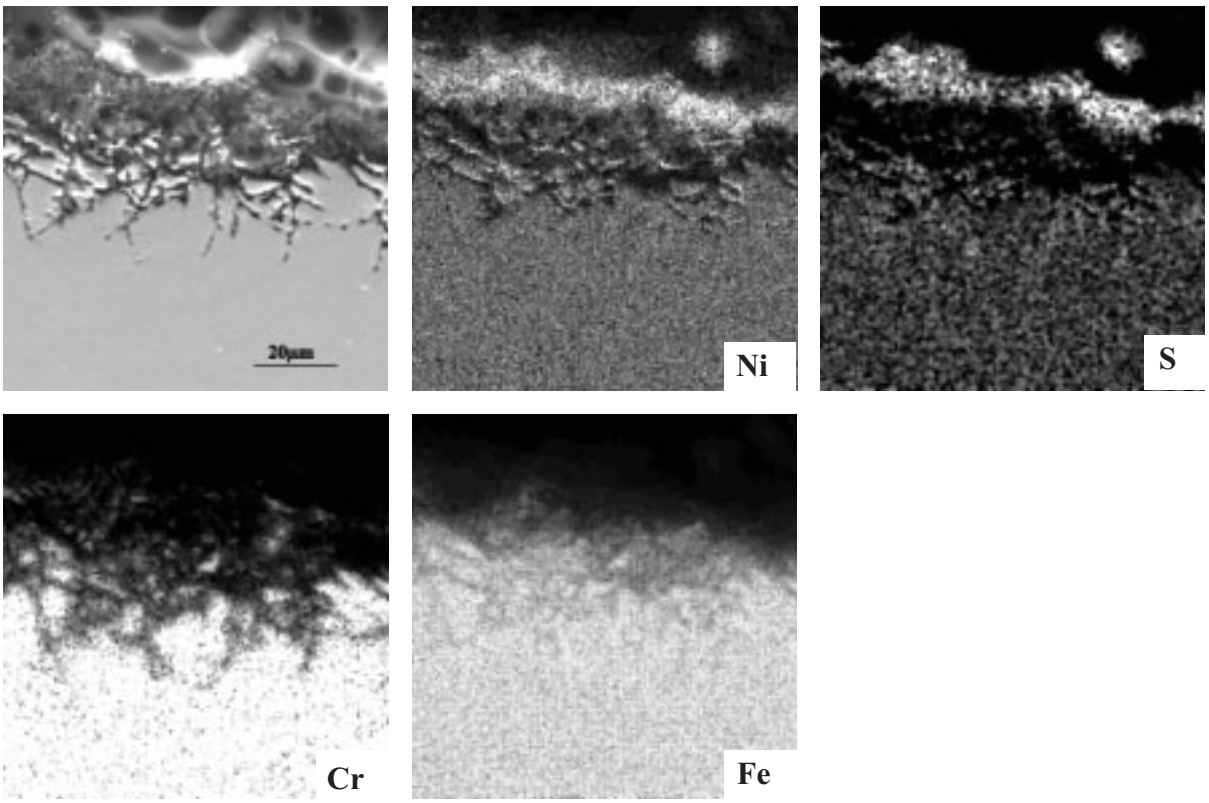

Fig. 4.2.8. Esshete1250 after 100h exposure in 3%O_2+N_2, at 650°C, covered with 50%KCl+50%K_2SO_4. SEM-EDX mapping of cross section without spalled oxide scale.

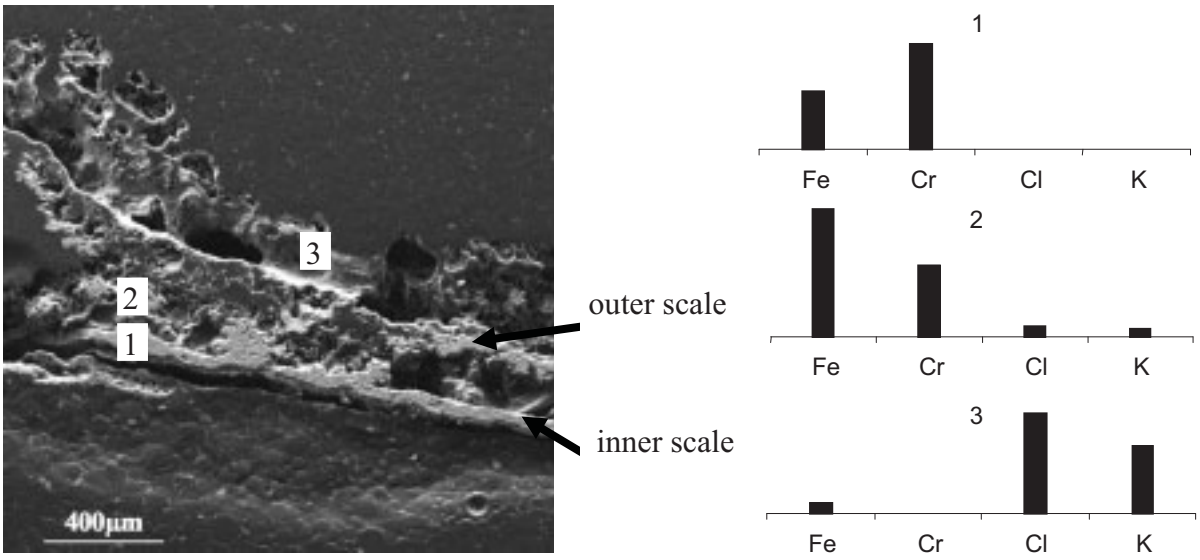

Fig.4.2.9. detached oxide scale of Esshete 1250, corresponding to the specimen in Fig.4.2.8.

In oxidizing-sulphating atmosphere

In oxidizing-sulphating atmosphere, the test specimens showed different trends of metal loss at 550°C and at 650°C, as shown in Fig. 4.2.10. At 550°C, metal losses increased with increasing chlorine content in ash, and the corrosion resistance was improved by high chromium content in an alloy; at 650°C, such trends disappeared: similar as the case in oxidizing atmosphere, the metal loss of austenitic Esshete 1250 was higher than that of ferrite/martensitic T91 under high-chlorine ashes and under coal ash.

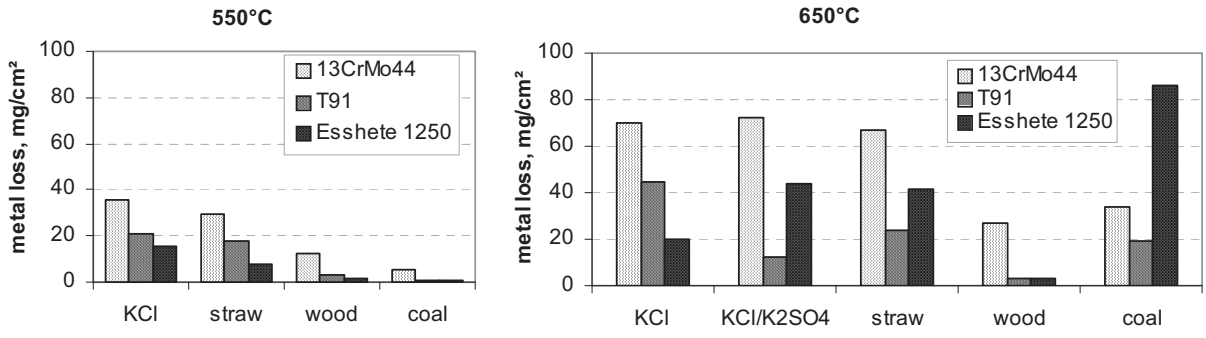

Fig. 4.2.10. Metal loss in oxidizing-sulphating atmosphere

In addition, serious internal corrosion was observed on Esshete 1250 and T91 under chlorine-containing ashes at 650°C. In the case of low-Cr ferrite steel 13CrMo44, no internal corrosion was detected. The internal corrosion of Esshete1250 and T91 are shown in Fig. 4.2.11 and Fig. 4.2.12 respectively. The internal attack to the austenite Esshete 1250 occurred mostly along grain boundaries; whereas the internal attack to the ferrite/martensite T91 targeted to some metallurgical phases in the alloy. No apparent grain boundary attack of T91 could be

found. Furthermore, the depth of the internal corrosion in T91 was smaller than that in Esshete 1250.

Besides, Esshete 1250 suffered also internal attack under coal ash, but the corroded zone was

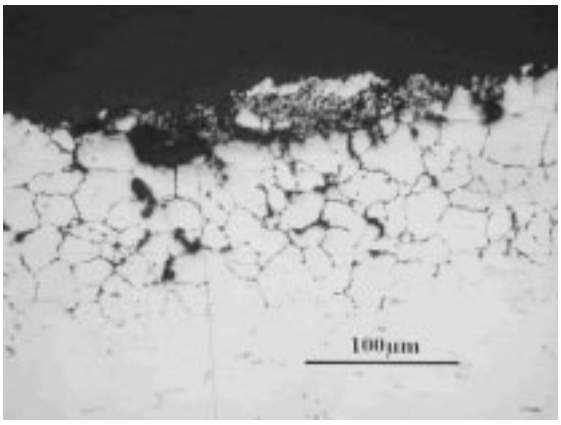

Esshete1250 , KCl ash

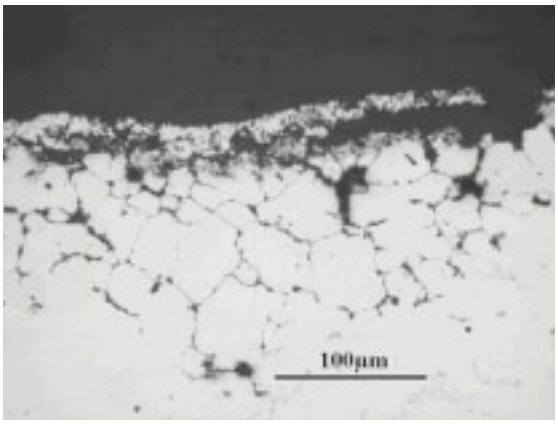

Esshete 1250 , straw ash

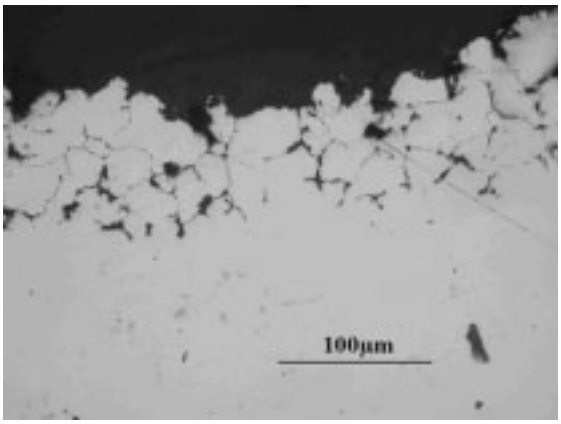

Esshete 1250, $KCl+K_2SO_4$ ash

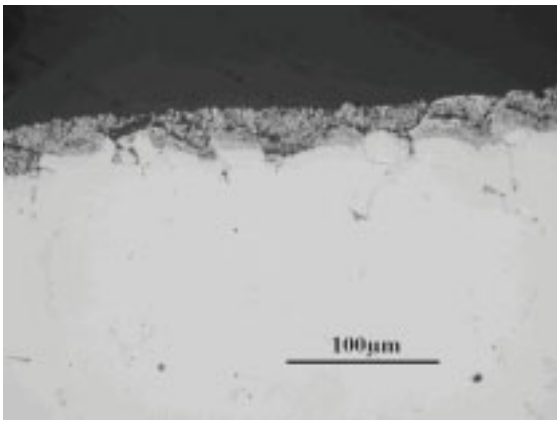

Esshete 1250 , coal ash

Fig. 4.2.11 Esshete 1250 after exposure at 650°C in 500mg/m^3 SO_2+3%O_2+N_2

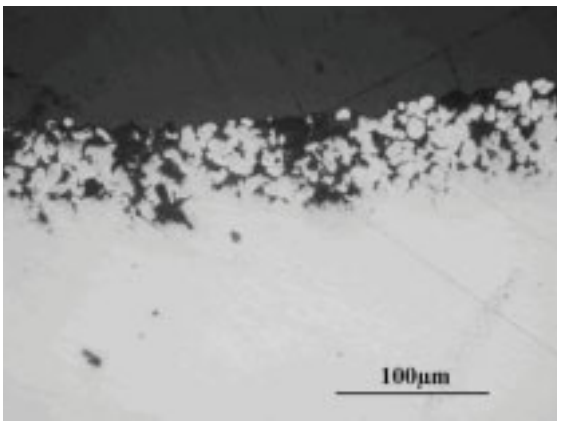

T91, KCl ash

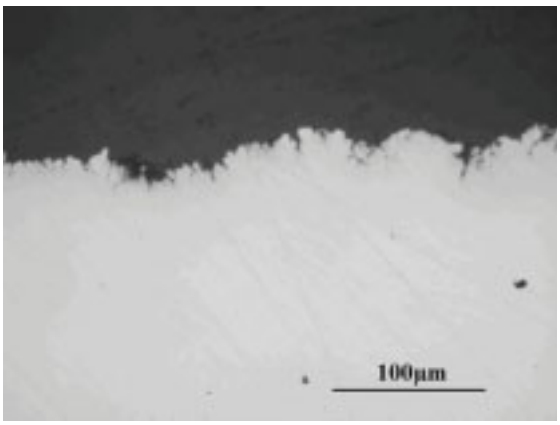

T91, straw ash

Fig. 4.2.12. T91 after exposure at 650°C in 500mg/m^3 SO_2+3%O_2+N_2.

considerably smaller than that under chlorine-enriched ashes (Fig.4.2.11). Specimens under wood ash showed no sign of internal corrosion.

Discussion

- In reducing atmosphere

The interesting fact of the low metal loss rate in reducing atmosphere under chlorine-rich ashes indicates that solid alkali chlorides in ash deposit are not the direct attack medium in chlorine-induced corrosion. Fast chlorine corrosion will be triggered when alkali chlorides in ash deposits are oxidized. The direct attack medium is chlorine gas, which is released from the alkali chlorides during oxidation.

Due to the lack of oxidants, such as O_2 or SO_2 in gas atmosphere, the rate of chlorine corrosion is low. In a multi-compound ash deposit, which contains chlorides, sulphates and oxides, O_2 and SO_2 can be available through the decomposition of sulphates and oxides in ash deposit. The corrosion rate depends on the rate of the decomposition rate of such ash components, which is a function of the partial pressure of O_2 and SO_2 in the local environment.

Real ashes can be more corrosive than simplified synthetic ashes in reducing environment. Following points could attribute to this result:

a). unburned carbon in real ash can produce a strong local reducing atmosphere, this facilitates the decomposition of sulphates and oxides in the real ash;

b). the decomposition of sulphates in real ash can be enhanced by other ash components as catalysts, such as Fe_2O_3;

c). a multi-compound system tends to lower its melting temperature due to eutectic formation, this promotes interactions among ash components.

It is interesting to note that in reducing gas, the highest metal loss for low-Cr steels is found under the wood ash in this study. The wood ash, which is originated from the co-combustion of wood and high-sulphur lignite, contains a high level of sulphates (Fig.4.2.1). Therefore it is reasonable to suggest that decomposition of sulphates to SO_2 and O_2 facilities the release of chlorine gas in the wood ash. The coal ash contains a high level of sulphur, but its chlorine level is very low, as consequence, there is no sign of strong metal loss under the coal ash. From above analysis, conclusion can be drawn that in reducing atmosphere, ashes containing high sulphur and moderate chlorine is more aggressive than ashes only enriched in chlorides

or in sulphates.

A general reaction, in which oxide scale, expressed as Me_2O_3, is consumed under the combined attack of alkali chlorides, sulphur and unburned carbon, is suggested by Cutler et. al. /138/:

$$Me_2O_3 + 4NaCl + S_2 + 3C \leftrightarrow 2MeCl_2 + 3CO + 2Na_2S \qquad (4.2.5)$$

It is also needed to mention that after long exposure time in reducing atmosphere, corrosion rate in the form of metal loss and internal corrosion can be exacerbated by another form of corrosion: metal dusting of chromium carbides. The material damage created by metal dusting would facilitate the inwards diffusion of chlorine and sulphur /145/. Since metal dusting is usually a phenomenon after long exposure time (more than 1000 hours), its influence was not observed in this study.

- In oxidizing atmosphere

In oxidizing atmosphere, oxygen pressure in gas atmosphere is high enough to oxidize alkali chlorides. Sulphates in deposits are stabilized by oxygen and do not play an essential role for chlorine corrosion as they do in reducing atmosphere. Metal loss is more correlated with the chlorine concentration in deposit ash than the partial pressures of O_2 and SO_2 in local gas environment.

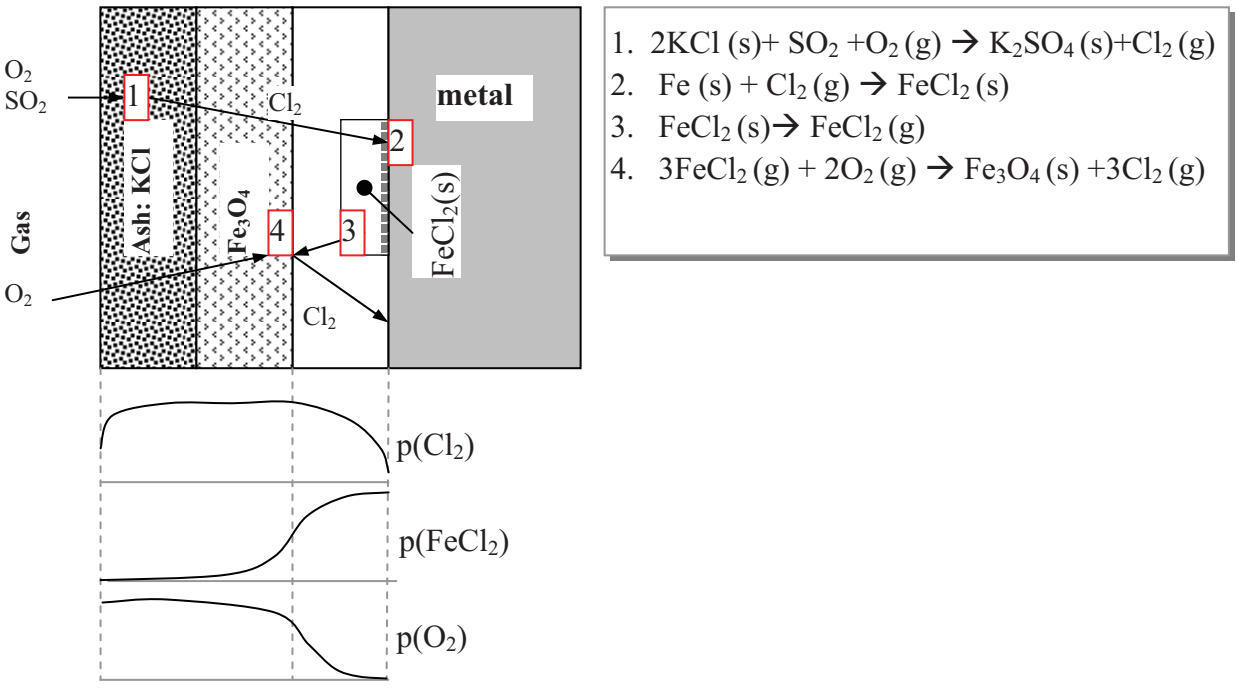

Fig. 4.2.20. possible reactions and gas partial pressure within and underneath ash deposits and oxide scales.

Fig. 4.2.20 illustrates the oxidation of alkali chlorides in ash deposits and the consequent chlorine-induced active oxidation. The changes of gas pressure of reactants and products through ash deposit and oxide scale are also illustrated.

It was discussed in Section 4.1 that without considering the influence of ash deposits, the corrosion rate depends on the evaporation rate of metal chlorides or the rate of gas transport through the scale. This conclusion is drawn under the assumption that sufficient Cl_2 is available for metal chlorination. This could be the case when chlorine gas in local gas atmosphere is high enough to maintain the rate of metal chlorides formation (corresponding to HCl ≥ 500vppm in this study). But in low-HCl oxidizing environment, the supply of chlorine gas near heat transfer surfaces is strongly dependent on the chloride content in ash deposits. The test results shown in Fig. 4.2.6 imply that increasing chloride concentration in ash deposits could enhance chlorine corrosion, or more clearly, the rate of chlorine gas generation from alkali chlorides plays an important role on the overall corrosion rate.

Another desirable property of a material is the non-sensibility to the ash chlorine concentration. The sensibility of materials to ash chlorine concentration is different: Ferritic/martensitic steels are not sensible to small differences of chlorine concentration in ash deposits, they showed only notable difference of metal loss between high-chlorine synthetic ashes and low-chlorine real ashes. The behaviour of austenitic steel is in opposite, their metal loss rate showed even clear dependences on chlorine concentration in ash deposits, even when the chlorine concentration in ash is low. For example, the metal losses of austenitic steels are very different under straw ash, wood ash and coal ash (Fig.4.2.6).

The different influences of the ash chlorine concentration on metal loss of ferritic steels and austenitic steels were explained by Alexander /90/. He examined the influence of NaCl concentration from 1% to 100% in ash deposits on the corrosion rate of 2.25 Cr steel and 18Cr-8Ni steels, and found out that the oxidation rate of austenitic steels increased rapidly at 650°C by increasing the proportion of chloride. When NaCl concentration was above 5%, there was a linear relationship between weight gain and time during initial period of the test, later it changes to parabolic. The period before the change from linear to parabolic prolonged with increasing chloride content. Whereas small amount of chloride can significantly change the oxidation rate of the austenitic steel, only large increase in chloride concentration has any noted effect on the ferritic steel. He proposed the corrosion mechanism of austenitic steels according to the following reaction:

$$24KCl + 10Cr_2O_3 + 9O_2 \rightarrow 12K_2CrO_4 + 8\,CrCl_3 \qquad (4.2.6)$$

Alexander suggested that the sensibility of austenitic steels to chloride concentration is traced back to the behavior of chromic chlorides formed in above reaction. As the chromic chloride is volatile, it will be continually removed from the reaction site, the reaction will proceed until all the chloride has reacted. The breakdown of the normally protective layer due to the formation of non-protective chromate can account for the linear oxidation rates observed on austenitic steels. And the change from linear to parabolic oxidation rates corresponds to the consumption of all the chloride.

- Influence of SO_2 on metal loss

SO_2 in flue gas could exert completely different influences on chlorine corrosion. Although SO_2 is regarded to be able to react with gaseous alkali chlorides in gas atmosphere, and thus suppress the deposition of alkali chlorides on heat transfer surfaces, a reverse effect of SO_2 in oxidizing atmosphere works when alkali chlorides are already deposited on heat transfer surfaces. That means, SO_2 in flue gas can enhance the chlorine corrosion dramatically when deposit ash contains alkali chlorides, since a high concentration of chlorine gas near the tube surface can be created through the conversion of alkali chlorides to alkali sulphates. This phenomenon was also observed by other researchers /85/. The two effects have the same thermodynamic background: alkali chlorides, either in gas form or in solid form, are less stable than alkali sulphates. This explains also why in straw-firing plants, high level of alkali chlorides are detected in fresh deposit after short operation time, but alkali sulphates are dominant alkali species in the ash deposit after a long exposure time /72/. The results in Fig. 4.2.2 have show that SO_2 is an effective oxidant to release Cl_2 gas from alkali chlorides in ash.

- Influence of temperature on metal loss rate

Increasing temperature from 550°C to 650°C is very effective to accelerate the rate of metal loss in many aspects:

a). the reaction rates of oxidation, sulphation, and chlorination are promoted with temperature;

b). the vapour pressure of alkali chlorides and metal chlorides increase dramatically with temperature (Fig. 4.1.8);

c). increase of temperature enhances the contact among ash components due to the formation of eutectic ash molten complexes.

4.2.4 Corrosion resistance of advanced boiler materials

Eight martensitic and austenitic steels were tested at 650°C and 700°C under straw ash and coal ash. The test conditions were described in Section 4.2.1, corresponding to the second test series. The corrosion morphologies, metal losses and depths of internal corrosion were investigated in this test series.

Corrosion morphologies

Different corrosion morphologies were observed under straw ash and coal ash. Under straw ash, a thick, porous and non-adherent outwards-growing scale formed, under which internal corrosion to certain metallurgical phases or along grain boundaries occurred. Three types of the internal corrosion can be generalized: a) on 9-12% Cr steels, such as T91, X20 and HCM12A, there were local attacks to certain metallurgical phases; b) in cases of austenitic steels with chromium content ranging from 15% to 20%, such as Esshete 1250, TP347HFG, S304H, grain boundaries were firstly attacked, followed by selective corrosion to certain metallurgical phases; c) concerning austenitic steels with more than 20% chromium, an internal affected zone was observed instead of clear boundary attack. The internal corrosion morphologies of test materials under chlorine containing ashes are shown in Fig. 4.2.13. Under coal ash, the oxide scale is compact and adherent, little internal corrosion was observed.

Metal loss

In both oxidizing environment and oxidizing-sulphating environment, the metal losses under straw ash were significantly higher than those under coal ash, as shown in Fig. 4.2.14. SO_2 in gas environment aggravated generally the metal loss under straw ash, in comparison, under coal ash, SO_2 had no apparent influence on the metal loss of these materials.

Under coal ash, austenitic steels showed generally better corrosion resistance than ferritic/martensitic steels; under straw ash, however, there was no clear advantage of austenite steels against chlorine corrosion (Fig.4.2.15). Another interesting fact is the different influence of temperature on the metal loss of test materials under chlorine-containing ash. Under straw ash, ferrite/martensite steels X20 and HCM12A presented higher metal loss at 650°C than at 700°C. An opposite trend was found in case of austenite steels with chromium content above 18%. This group of materials have shown higher metal loss at 700°C than 650°. Under coal ash, ferrite/martensite materials have shown significantly higher metal loss rate at 700°C than at 650°C, whereas austenite materials have not shown clear increase of metal loss with the rising temperature.

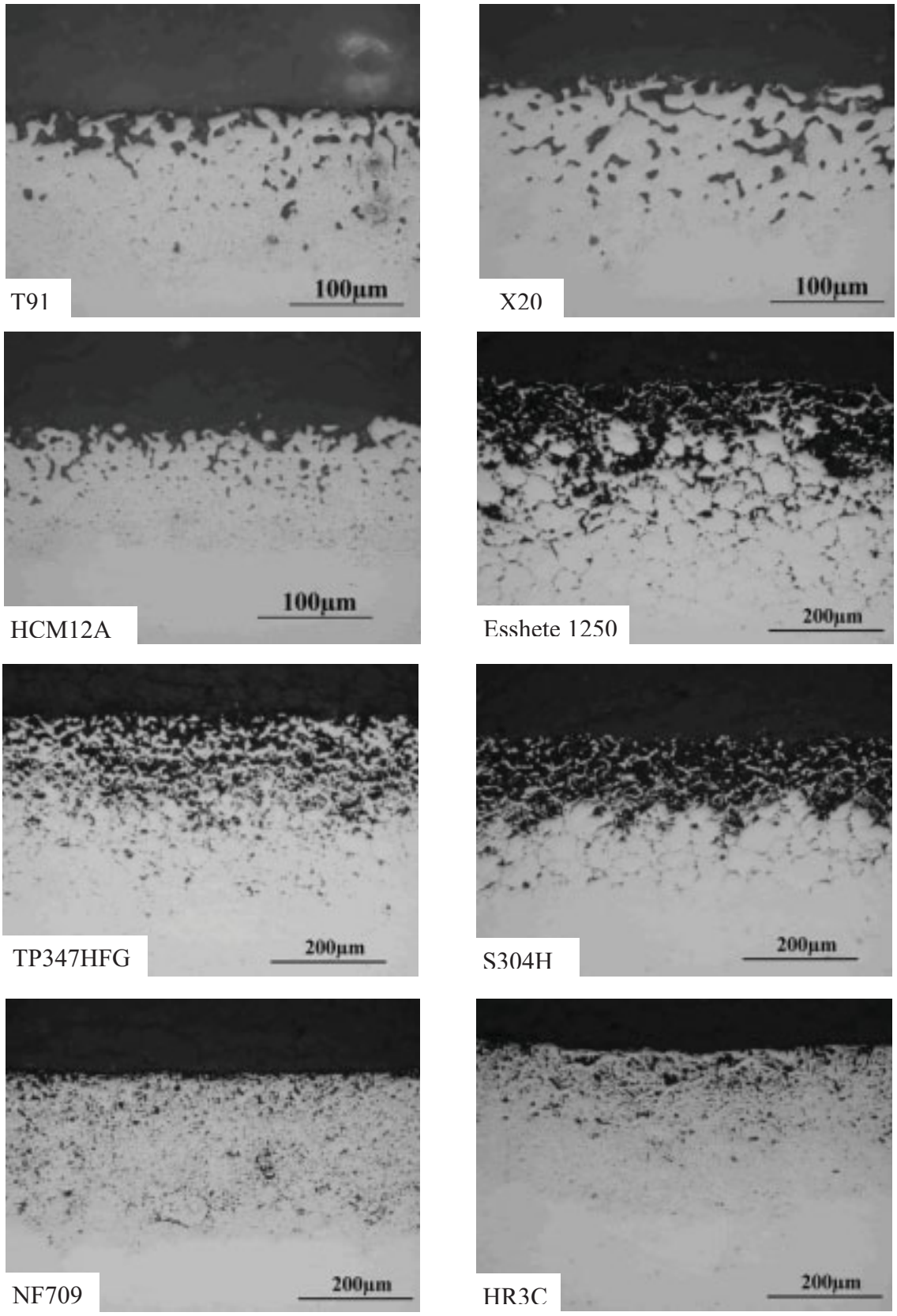

Fig. 4.2.13. Internal corrosion under straw ash after 300h in 700°C in 3% O_2

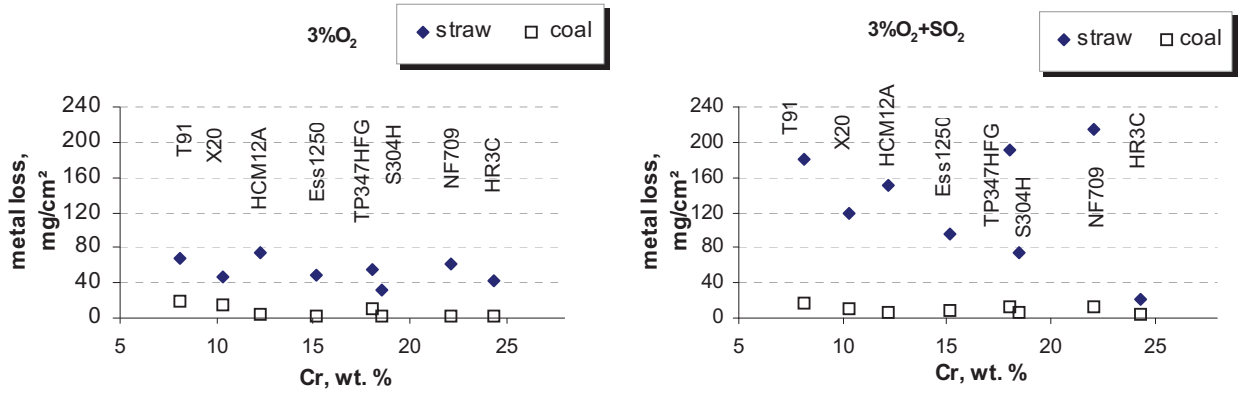

Fig. 4.2.14. Metal losses at 700°C after 100 hours exposure.

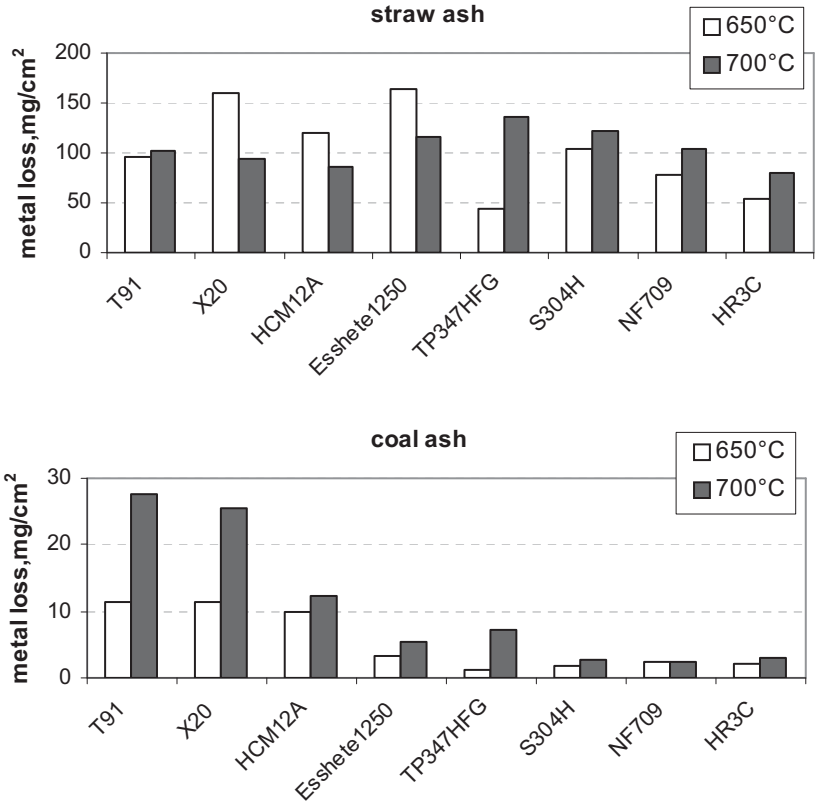

Fig. 4.2.15. Metal losses at different temperature in oxidizing environment

In addition, the corrosion rate as function of exposure time is illustrated in Fig. 4.2.16. Extending exposure time from 100 hours to 300 hours resulted in increases of metal loss under both straw ash and coal ash. However, the growth rate of metal loss is slower than linear rate law. Since the linear rate law describes the formation of a completely non-protecting oxide scale, the metal loss in this study indicates that although the oxide scale formed under the chlorine attack is not compact, it still works somewhat as a barrier between flue gas and metal surface.

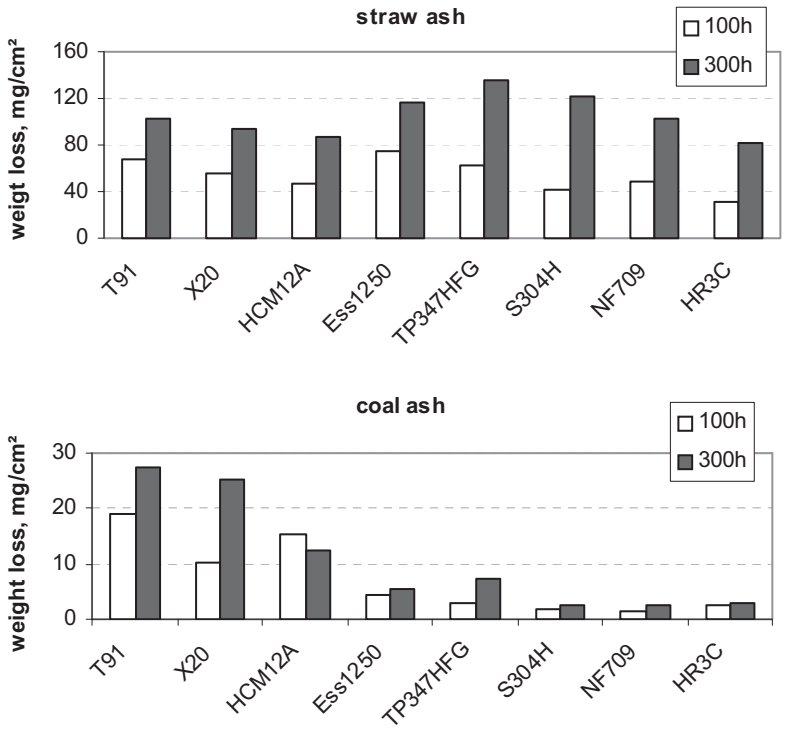

Fig. 4.2.16. Metal losses after different exposure time at 700°C in oxidizing environment

Internal corrosion

Since almost no internal corrosion was detected under coal ash, only the internal corrosion under straw ash is discussed in this study. The maximum, minimum and average internal corrosion depths at 700°C in oxidizing atmosphere are illustrated in Fig. 4.2.17. All ferritic/martensitic steels showed better resistance against internal corrosion than austenitic steels. Among austenitic steels, Esshete 1250 and TP347HFG suffered the deepest internal corrosion.

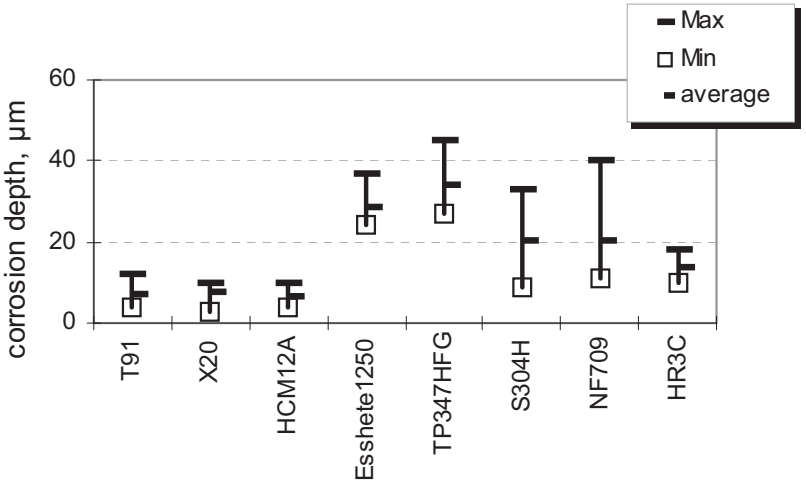

Fig.4.2.17. Internal corrosion depths of test materials under straw ash after 100 hour exposure at 700°C

SO_2 in flue gas enhanced the internal corrosion of almost all materials. An exception is TP347HFG. Fig. 4.2.18 illustrates the influence of SO_2 on the internal corrosion depth after 100 hours exposure at 700°C. In comparison to austenitic steels, martensitic steels were not sensitive to the SO_2 in gas atmosphere.

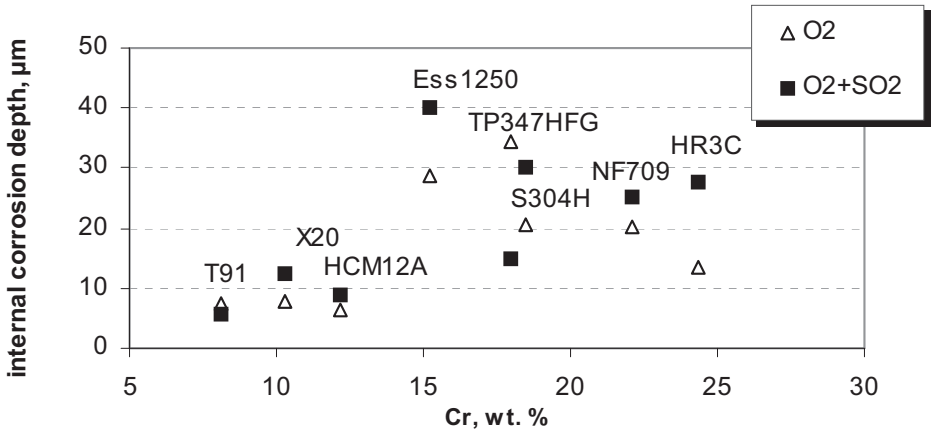

Fig. 4.2.18. Internal corrosion of test materials in oxidizing and oxidizing-sulphating atmospheres after 100 hours at 700°C

The influence of exposure time and exposure temperature on the rate of internal corrosion is illustrated in Fig. 4.2.19. Again ferritic/martensitic steels showed better resistance against internal corrosion than austenitic steels for different exposure times and in different temperatures. Among austenitic steels, although the corrosion depths of some materials after 300 hours exposure were a little higher than those after 100 hours exposure, such as Esshete 1250 and HR3C, the corrosion depths for the two exposure periods were in the same

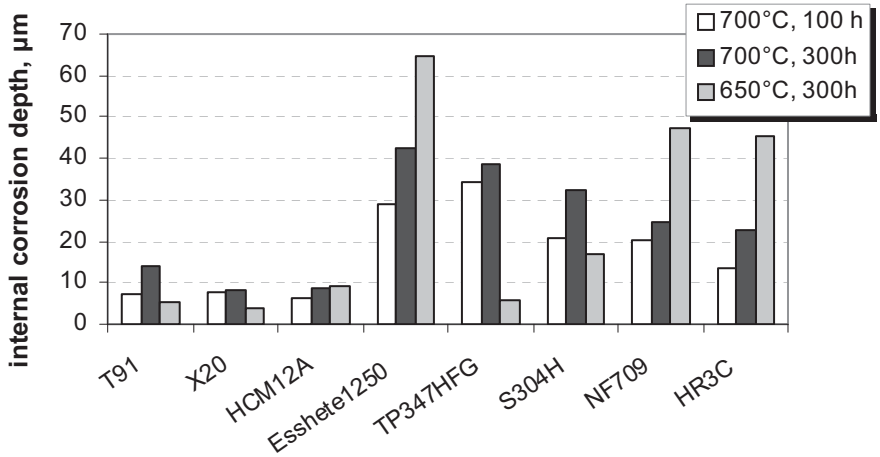

Fig.4.2.19. Internal corrosion depth in oxidizing atmosphere for different exposure time and exposure temperature.

magnitude. Increasing temperature from 650°C to 700°C did not exacerbate internal corrosion for all austenitic steels. Esshete 1250, NF709 and HR3C were more sensible to internal corrosion at 650°C than at 700°C. At 650°C, the best austenitic steels against internal corrosion are 18%-Cr austenite TP347HFG and S304H, whereas the best austenitic steels at 700°C are high-Cr NF709 and HR3C.

Discussion

- Mechanisms of internal corrosion

Internal corrosion is resulted by selective attack to certain metallurgical phases in a metal. Whilst corrosion attack to all metal phases results in homogenous metal loss in form of corrosion scale, which can be removed and the corresponding metal loss can be measured, internal selective corrosion has almost no sign on mass change. However, internal corrosion should not be ignored due to its consequence of material availability loss.

Chlorine-induced internal corrosion is a kind of selective corrosion of chromium carbides either along grain boundaries or within grains matrix. For the formation of chromium carbides, sufficient carbon must be available in alloy itself or from gas environment. McNallan reported that no internal oxidation occurs when no carbon exists in an alloy or in a gas environment /146/. He observed an accelerated internal corrosion of Alloy 800H in oxygen-chlorine environment when oxygen is replaced by carbon dioxide. Shinata and Prescott gave similar argument that the availability of carbon is especially the prerequisite for the internal attack of high-chromium austenitic steels /74/, /141/.

The morphologies of the internal attack by chlorine, within grains or along grain boundaries, depend strongly on the metallurgical characteristics. Low Cr ferritic steels usually do not suffer such kind of corrosion due to their low chromium concentration.

- Metallurgical background of the internal corrosion morphology

The different metallurgical features between austenitic steels and martensitic steels lead to different morphologies of internal corrosion.

In the case of austenitic materials, it is noted that chromium carbides are firstly consumed along grain boundaries and then inside grains. Douglass explained that grain boundaries act as short-circuit or rapid diffusion paths for heterogeneous nucleation. Thus, the precipitation of carbides should firstly occur in grain boundaries /44/. Another argument of the grain boundary corrosion is that the diffusion of chromium to the grain boundary creates a chromium-depleted zone near the boundary, where is less resistance than the core matrix due

to the lower chromium concentration /77/.

Martensitic steels possess a different metallurgical structure to austenitic steels. Chromium carbides in martensitic matrix are more evenly distributed and there are no clear grain boundaries. The diffusion of gas and solid substance in martensitic matrix is difficult. Therefore, the corrosion depth is low. The middle-Cr steels (containing 9-12%-Cr) are ferritic/martensitic steels. The chromium carbides in the metal matrix are usually selective corroded.

The microstructures of the testing materials are shown in Fig.4.2.20. Taking the morphologies of internal corrosion in Fig.4.2.13 as reference, the internal corrosion mechanisms by chlorine attack of each material are suggested:

a). 13CrMo44 is composed of ferrite grains (bright fields) and carbides (dark points), the most carbides are precipitated along grain boundaries. Since the chromium content in 13CrMo44 is very low, no internal corrosion takes place in 13CrMo44.

b). T91 and X20 are ferritic/martensitic steels. Fine chromium carbide particles are precipitated evenly in the matrix. As result, the selective attack of T91 and X20 locates at such evenly distributed chromium carbides.

c). Austenitic steels with chromium less than 20 wt.% and the austenitic steels with chromium more than 20 wt. % have different morphologies. The austenitic steels with chromium less than 20%, such as Esshete1250, S304H, S347HFG, have a deep front of grain boundary fissures, followed by massive corrosion within metal grains. The mechanism of grain boundary corrosion is already discussed in above section. The selective corrosion within grains could be a result of many influences, for example, a) the chromium concentration inside grains falls after the chromium diffusion toward grain boundaries, b) the pores and fissures behind the selective corrosion facilitates a rapid diffusion of chlorine gas into grain lattice.

d). In the case of austenite with chromium more than 20%, such as NF709 and HR3C, the overall chromium content in such alloys is likely high enough to reduce grain boundary corrosion and the selective corrosion within grains. However, they are not immune to chlorine corrosion, the deep corrosion zone of such alloys implies that chlorine is very diffusive in such alloys.

- Influence of sulphur gases on internal chlorine corrosion

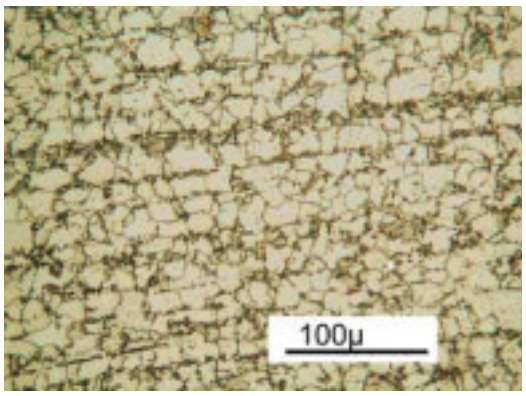

13CrMo44

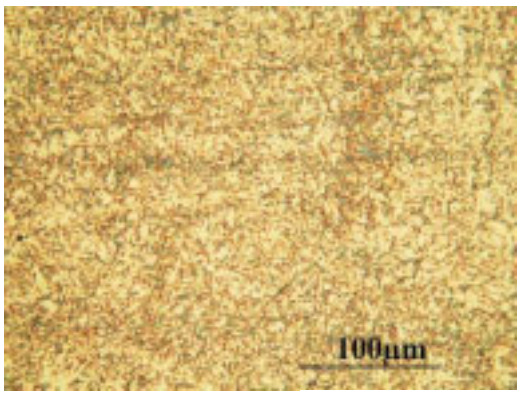

T91

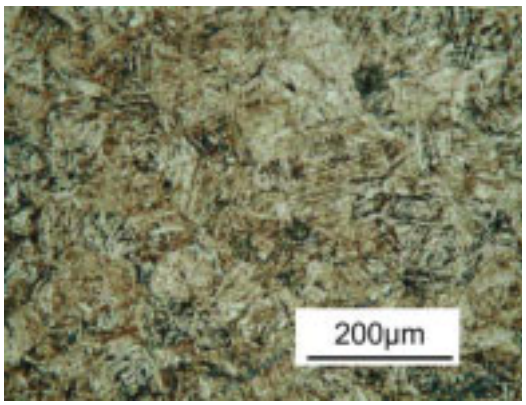

X20CrMoV121

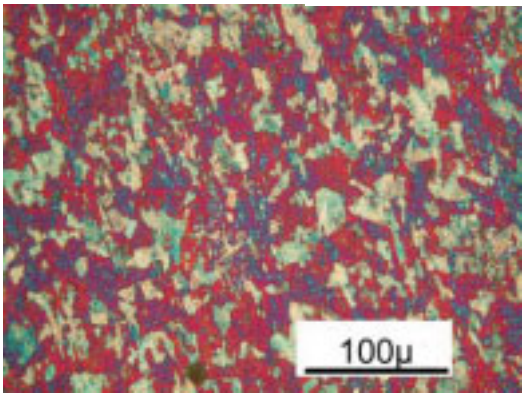

Esshete 1250

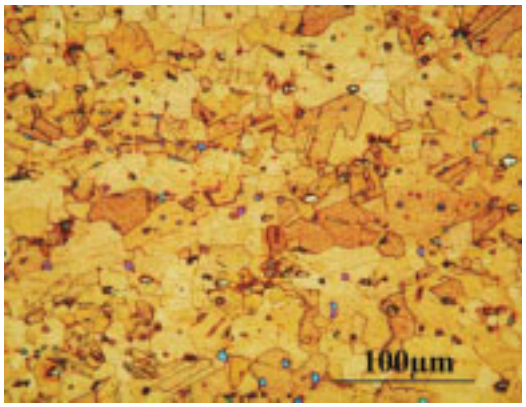

S347HFG

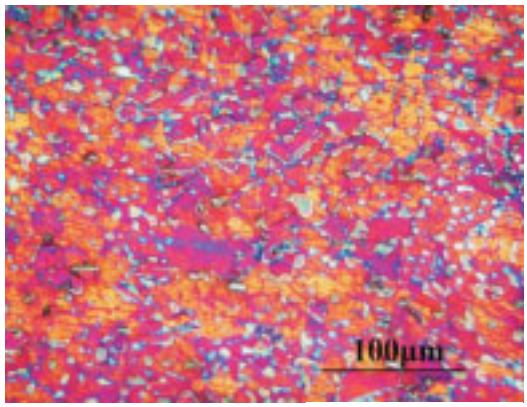

S304H

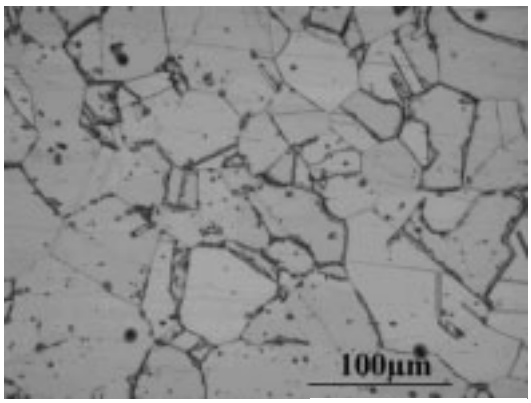

HR3C

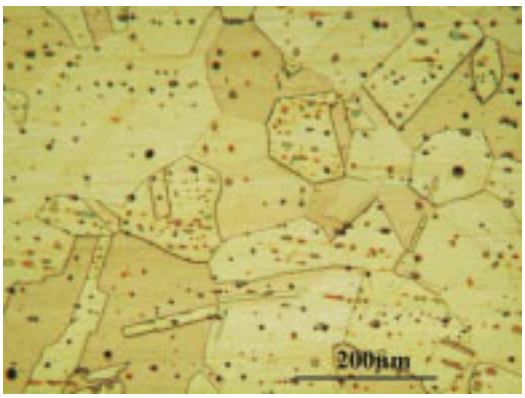

NF709

Fig.4.2.20. Microstructure of testing materials

Sulphur gases, such as SO_3 or S_2, can facilitate chlorine gas to diffuse along grain boundaries. This could be explained by a "dual oxidant" effect, which is suggested by Douglass /44/: two gases may diffuse simultaneously and each forms its own product with the metal. The thermodynamically most-stable compound forms near the surface, and the less-stable compound forms deeper in the alloy. The less-stable compound is subsequently converted to the more-stable compound with a concomitant release of the second oxidant. In this investigation, metal sulphides and metal chlorides are the corrosion products in the metal substrate when both sulphur gases and Cl_2 gas manage to diffuse into the metal. Metal sulphides are more stable than metal chlorides in an extreme reducing environment. This fact is verified by the phenomenon that only sulphur is detected in the voids of the substrate material in the chlorine-induced corrosion. Chlorine corrosion could firstly create voids along grain boundaries for the sulphur gas penetration, sulphur gas converts metal chlorides to metal sulphides and release chlorine gas, which diffuses deeper into the alloy. Without chlorine in ash or without SO_2 in gas, the grain boundary attack is somewhat dampened.

Other uncomfortable corrosion products, the nickel-rich sulphides, can be formed on austenitic steel surface when high potential of sulphur gas reaches the metal front. It was often reported that nickel-rich sulphides are likely melt at application temperature /41, 142, 143, 144/: for example, an eutectic of the Ni-S system has the melt temperature of 635°C when the share of sulphur is 21.5 wt. %. When this kind of melt is present, even former protective scales could be destroyed.

- Influence of temperature on internal corrosion

Temperature can exert heat treatment effect on austenitic metallurgical structure, which could facilitate internal corrosion attack. It was observed from this study and other reports /141-143/, that austenite steel has a temperature sensible range between 550°C-650°C. In this temperature range, either during heat treatment or in practical service, chromium carbides undergo changes towards equilibrium in the way that they segregate on grain boundaries and form coarse chromium carbide grains. The beginning temperature for the segregation of Esshete 1250, for example, is at 550°C in this study. In other studies with long-term exposure, grain boundary attack starts even at 515-525°C /22/.

4.2.5 Conclusion

Influence of gas atmosphere on deposit ash and corrosion rate

Different influences of reducing atmosphere and oxidizing atmosphere are observed on ash

deposits and on corrosion mechanisms:

- In reducing atmosphere, alkali chlorides in ash deposit are not active and exert no deteriorate influence on corrosion rate until they are activated by oxidants, such as oxygen and SO_2. Such oxidants come from the decomposition of other components in ash deposits. Sulphates in ash deposits are one kind of such oxidant suppliers. The rate of chlorine-induced corrosion is determined by the local partial pressure of oxygen and SO_2. Deposit ash containing moderate chlorine and high sulphur could be corrosive in reducing gas environment.

- In oxidizing atmosphere, the pressure of oxidants in the gas atmosphere is high enough to oxidize metal chlorides. Therefore, the rate of chlorine corrosion depends more strongly on the chlorine concentration in deposits than the local concentration of O_2 and SO_2. SO_2 in bulk gas facilitates chlorine-induced active oxidation in both form of metal loss and internal corrosion.

Material behaviour under chlorine-rich ash deposits

- Austenitic steels suffer generally higher metal loss and deeper internal corrosion than 9-12%-Cr ferritic/martensitic steels under chlorine-rich deposits. Austenitic steels are also sensible to chlorine concentration in ash deposits. Even slight increasing of chlorine content in ash deposits results in notable weight loss on austenitic steels. In comparison, ferritic and martensitic steels are not as sensitive to ash chlorine concentration as austenitic steels.

- SO_2 in gas atmosphere is very effective to enhance metal loss of all materials. Regarding internal corrosion, 9-12% Cr steels are not sensitive to SO_2; whilst austenitic steels suffer aggravated internal corrosion under the influence of SO_2 in gas atmosphere.

- Some austenitic steels have a sensible temperature range for the aggravated grain boundary corrosion which lies between 525°C-650°C.

- Austenitic steels with Cr lower than 20%, which are generally superior against other kinds of corrosion, are week against chlorine attack. This is traced back to the preferable reaction between chlorine gas and chromium carbides. Since chromium carbides tend to immigrate to grain boundaries in austenite to reach their equilibrium state, grain boundary is firstly attacked by chlorine gas. Austenitic steels with Cr higher than 20% have moderate resistance against chlorine corrosion due to their

overall high chromium content in metal matrix. In case of 9-12%-Cr ferritic/martensitic steels, deep diffusion of chlorine gas is blocked since no grain boundaries with enriched chromium carbides can be formed, thus the invasion of chlorine only takes place in evenly distributed chromium carbide phases in metal matrix.

- Concerning material selection for the facilities firing chlorine-rich biomass or waste materials, 9-12%-Cr steels are the favourable candidates. Although low-Cr steels (Cr<2.5%) show no sign of internal corrosion, the high metal loss rate of such steels is unacceptable. Austenitic steels should be only applied under 600°C. Above this temperature range, their internal corrosion depth is unacceptable. For the coal combustion, austenitic steels are still the materials with superior fireside corrosion resistance.

5. Combustion Test

Combustion tests constitute a non-negligible part of the investigation of fireside chlorine corrosion, since they can provide information about influence factors on chlorine deposition during combustion. Such information from combustion tests can also give laboratory tests guideline for the selection of ash deposits in the material exposure tests.

The purpose of combustion tests in this study is to investigate deposition and corrosion tendencies in PF boilers during firing various fuel blends. Two combustion test series were carried out in this study: the first test series was co-firing lignite with paper sludge and co-firing lignite with compost waste, the second test series was co-firing a kind of South Africa bituminous coal with olive husk. Flue gas parameters, fly ashes and deposit ashes were extensively investigated regarding their influences on fireside corrosion.

5.1 Co-combustion of lignite with paper sludge and compost waste

5.1.1 Fuel characteristics and test program

Two kinds of waste fuels, paper sludge (PS) and compost (CP), were co-fired with two kinds of lignite (Lig1 and Lig2). Paper sludge is mainly composed of cellulose material. The compost is a waste material from mushroom plantation, which is composed of straw and chicken manure. The lignite fuels come from Rheinland area in Germany, which has low ash content and very low sulphur and silicon content. All the fuels were milled and dried before conveying to the burner. The fuel features and ash composition after drying are listed in Tab. 5.1 and Tab. 5.2 respectively.

Comparing to lignite, paper sludge and compost are characterized with considerable low heating value and high ash content. Furthermore, there are notable differences in fuel ash composition: the main elements in the lignite ash are Ca, Mg, and Fe. The contents of Si and Al in lignite fuel ash are very low. The fuel ash of paper sludge contains high Ca, Si and Al, but extreme low Fe, Mg and S. Compost is similar to straw, characterized with high Cl, S, K and Si, middle level of Ca and low Al. Leaching test of compost revealed that 60-70% potassium in compost is water soluble. In addition, there is significant difference in alkali content between the two lignite fuels: the sum of alkali metals in Lig 1 is almost 7%, whereas only 1.5% of alkali metals is present in Lig 2.

Tab. 5.1. Fuel data after mill drying

		unit	Lig 1	Lig 2	PS	CP
Heating value	HHV	MJ/kg	23.71	23.11	7.01	9.75
	LHV	MJ/kg	22.66	21.47	6.26	8.76
	HHV	MJ/kg, dry	25.53	25.3	7.19	10.97
	LHV	MJ/kg, dry	24.58	23.75	6.48	10.17
Immediate analysis	Water content	% analyse	7.12	8.7	2.47	11.09
	volatiles	%, dry	51.18	51.42	53.05	51.84
	Ash content	%, dry	3.87	4.6	42.54	45.74
	Fixed carbon	%, dry	44.95	43.99	1.23	5.62
Element analysis	C	%, dry	65.44	63.59	23.79	29.93
	N	%, dry	0.66	0.39	0.09	2.17
	S	%, dry	0.13	0.11	0.19	2.76
	H	%, dry	4.35	7.18	3.25	3.63
	O	%, dry	25.47	24.09	26.87	18.53

Tab.5.2 Fuel ash analysis

		unit	Lig 1	Lig 2	PS	CP
Ash composition at 815 °C	Cl	% wf	0.05	0.03	0.07	0.45
	Al_2O_3	%	3.4	4.8	19.4	2.0
	CaO	%	39.0	35.9	45.0	27.9
	Fe2O3	%	12.2	24.4	1.2	1.3
	K_2O	%	2.1	0.6	0.7	6.0
	MgO	%	16.7	14.2	2.4	1.9
	Na_2O	%	4.7	0.9	0.4	1.1
	SiO_2	%	4.6	4.4	27.8	39.6
	SO_3	%	14.6	13.8	0.29	17.2
	TiO_2	%	0.2	0.3	0.5	0.2
Ash melting temp.	$T_{0,95}$	°C	1160	1050	1245	1195
	$T_{0,5}$	°C	1420	1350	1480	1290
	$T_{0,2}$	°C	1450	1370	1490	1305

Since the ash content in paper sludge and compost are about 10 times the amount of that in the lignite fuels, the minerals in paper sludge and compost can have over-proportional influence on the fly ash formed in the co-firing tests. For example, even for a low mixing rate, e.g. 8% of compost, about 50% of the fly ash comes from the compost.

Five tests with different fuel mixing ratios were carried out. The fuel mixing ratios are listed in Tab. 5.3. Each test period took about 8 hours. The waste fuels were premixed with the lignite before they were conveyed to the burner.

Tab 5.3. Test program

	term	mass ratio, %		thermal ratio, %	
		lignite	PS	lignite	PS
Test 1	Lig2-100	(Lig 2) 100	0	100	0
Test 2	Lig2/PS-95/5	(Lig 2) 95	5	98.73	1.27
Test 3	Lig2/PS-90/10	(Lig 2) 90	10	97.55	2.45
Test 4	Lig1/PS-80/20	(Lig 1) 80	20	94.6	5.4
		lignite	CP	lignite	CP
Test 5	Lig1/CP-92/8	(Lig 1) 92	8	97.08	2.92

Following measurements and ash samplings were carried out during combustion test:

- Profile measurements of flue gas temperature and composition.
- Deposit ash samplings:
  - from two temperature-controlled Corrosion/Deposition probes, which simulated superheater and waterwall tube temperature condition. The probes were positioned at 0.99 metre and 2.16 metre below the burner;
  - from two non-cooled ceramic probes exposed at 1.5 metre and 2.67 metre below the burner.
- fly ashes sampling from furnace and different positions in the flue gas pass.

5.1.2 Test results

Flue gas temperature and composition

The flue gas temperature profile along the centre line of furnace height is illustrated in Fig.5.1. During the co-combustion of lignite fuels with paper sludge, flue gas temperature near the burner is higher than that of pure lignite combustion. This implies that intensive ignition of the paper sludge took place. However, all the flue gas temperatures in the co-firing flame fell down more quickly than that in the pure lignite flame. Co-firing compost with Lig I resulted in overall high flue gas temperature. This is probably caused by the high heating value of the fuel blend “Lig 1/CP-92/8”.

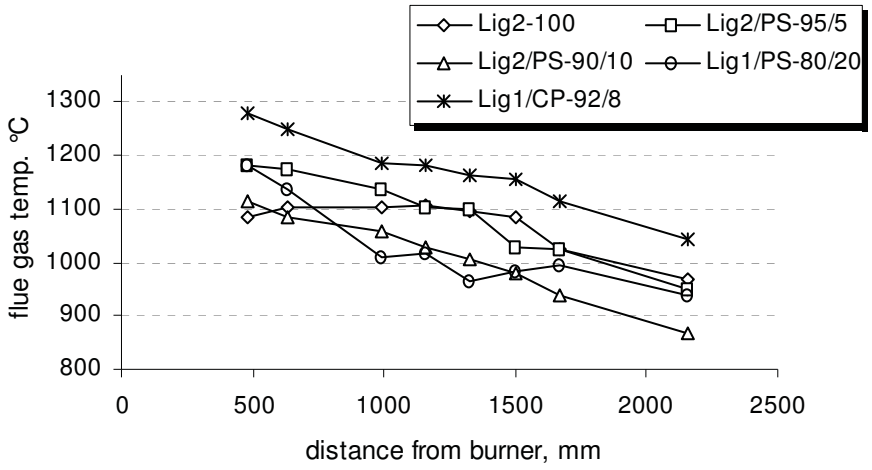

Fig. 5.1. Flue gas temperature profile along furnace height

The concentration of SO_2 in flue gas is an important parameter for chlorine corrosion, since SO_2 in flue gas is effective to convert alkali chlorides to alkali sulphates, so that the deposition of alkali chlorides can be reduced. The SO_2 concentrations along the centre line of the furnace height are shown in Fig.5.2. SO_2 concentration in pure lignite flame was higher than that in co-firing flames. During the paper sludge co-combustion, SO_2 concentrations were generally so low that they were almost not detectable. In the case of co-firing compost with lignite, although the SO_2 concentration at the initial stage was comparable with that in the pure lignite combustion, it fell quickly down after that. Since the total sulphur amount in some fuel blends are higher than that in pure lignite, the low SO_2-concentration in all the fuel blend flames indicate that SO_2-concentration in flue gas is not only related with the fuel sulphur content, but also related with combustion conditions and other mineral matters. There is a high level of calcium in the fuel blends of lignite and paper sludge, which is originated

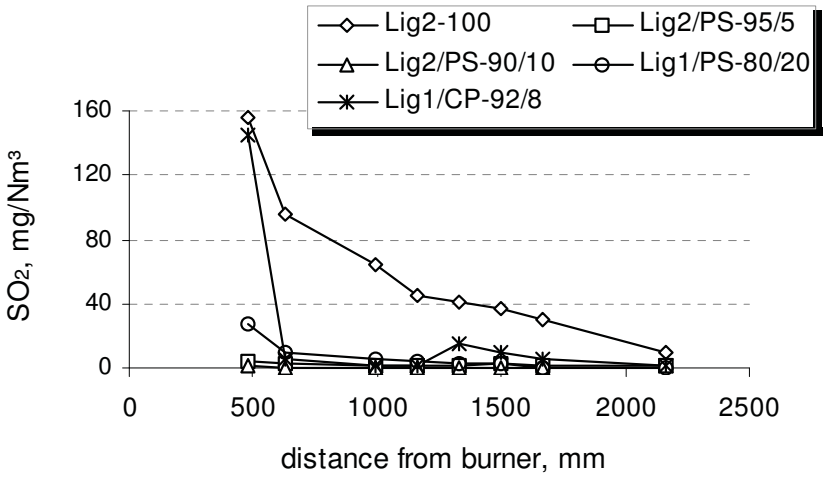

Fig. 5.2. SO_2 profile along furnace height

from the waste paper sludge. Calcium oxide is an effective SO_2 absorber. This can lead to a low SO_2 concentration in the flue gas. The fate of sulphur during combustion and ash formation process can be proved in the following investigations of ash and deposit.

During all the tests, O_2 was depleted in the flame zone at about 0.6 metre below the burner due to the intensive oxygen consumption. Afterwards, the oxygen concentrations recovered slightly (Fig. 5.3). This could be a result of flue gas homogenization between the O_2-depleted zone in the flame centre and the O_2-enriched zone near the furnace wall. There was no clear influence of the waste fuel on the O_2 distribution.

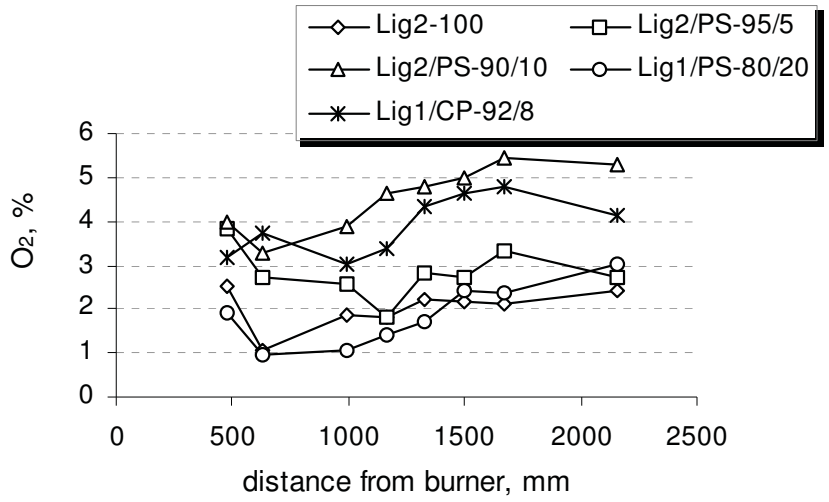

Fig. 5.3. O_2 concentration profile along furnace height

Ash and deposits

The ash and deposit features are presented from three representative tests: pure lignite test (Test I: Lig2-100), the co-firing test of Lig 1 with 20% paper sludge (Test 4: Lig1/PS-80/20), and the co-firing test of Lig 1 with 8% compost (Test 5: Lig1/CP-92/8).

- **Test 1 (Lig2-100)**

The composition of fly ashes along flue gas pass and the deposit ashes are shown in Fig. 5.4. Following ash characteristics are especially notable:

- The total percentage of each ash lies more or less below 100%. The missing fraction in the ashes is unburned combustibles. Fly ash in the lower part of the furnace and in the furnace bottom contained the highest fraction of unburned combustibles. Among deposit ashes, the deposit formed on the non-cooled probe near the burner area (Depo-Ceramic 1.5) had the poorest burnout.

- The ash composition is very different between coarse fly ash particles and fine fly ash particles: coarse fly ashes, mainly accumulated in furnace bottom, air preheater and cyclone, contained more iron and earth alkalis, but less aluminium, silicon and alkali metals (Na, K); the fine ashes, such ash filter ash, were enriched in Si, Al, alkalis and sulphur.

- In comparison with fly ashes, deposit ashes showed following characteristics:

    - high sulphur and alkalis. Alkali metals were enriched in the deposit ashes of the temperature controlled corrosion probe. The highest alkali content was found in the cooled deposit at the lower flue gas temperature area;
    - low silicates and alumina;
    - chlorine could not be detected in all ashes;
    - calcium and iron compounds constituted the major part of deposit ashes.

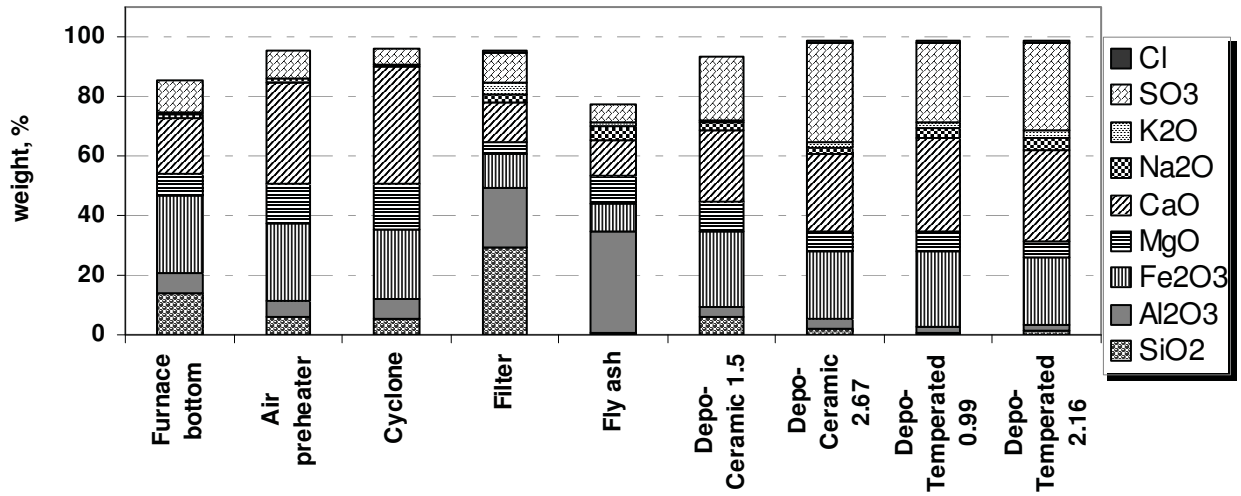

Fig. 5.4. Ash composition in Test 1 (100% Lig 2)

- **Test 4 (Lig 1/PS-80/20) (Fig. 5.5)**

Influenced by paper sludge, the burnout of fly ashes in the co-firing test was improved. The minerals in paper sludge delivered their features to fly ashes during combustion: in comparison with the Test I (Lig2-100), all the ashes generated in Test 4 (Lig1/PS-80/20) contained higher Al, Si, Ca and lower Fe, Mg, S. Despite of the differences in absolute values, the trends of mineral distribution in fly ashes and in deposit ashes were similar to that in Test I: deposit ashes from the temperature-controlled probe were enriched in sulphur, alkalis, calcium and iron. The highest alkali fraction was presented in the cooled deposit at the lower gas temperature region. Furthermore, chlorine was detected in the deposit ash on the cooled corrosion probe at the lower gas temperature.

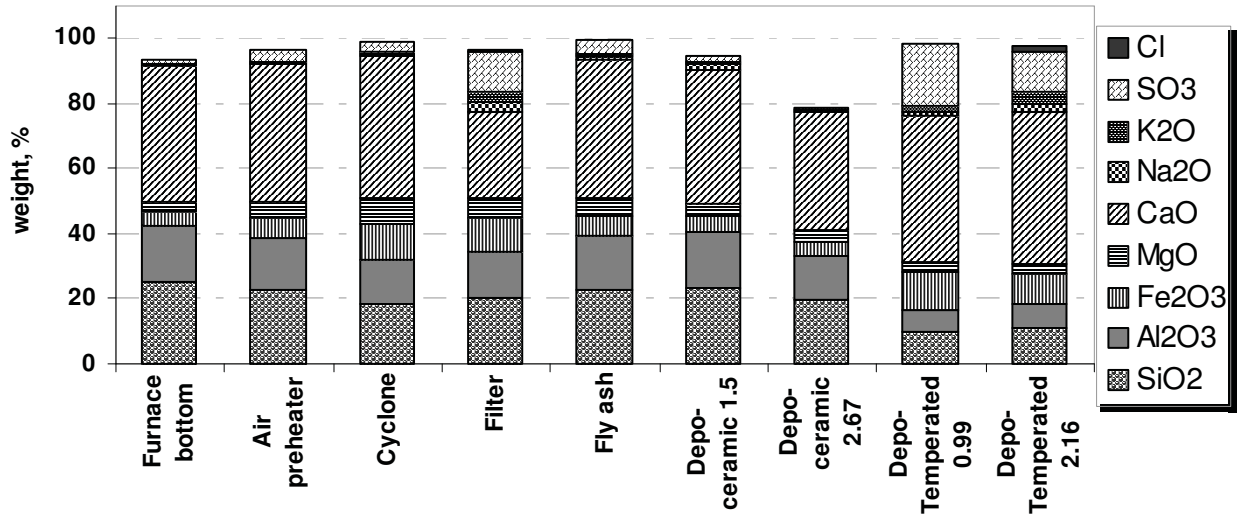

Fig. 5.5. Ash compositions in Test 4 (Lig1/PS-80/20)

- **Test 5 (Lig1/CP-92/8)**

The ash compositions of Test 5 are illustrated in Fig.5.6. The influence of the straw-like compost on the fly ash composition was apparent: in comparison with Test I (Lig2-100), the ashes from co-firing with compost contained higher sulphur, alkalis, silicon and calcium. Calcium remained as the most abundant element in the deposit ashes. In the deposit ash on the cooled corrosion/deposition probe (Depo-temperated 0.99), which is the most critical deposit in the corrosion point of view, considerable high concentration of chlorine, sulphur, alkali were detected.

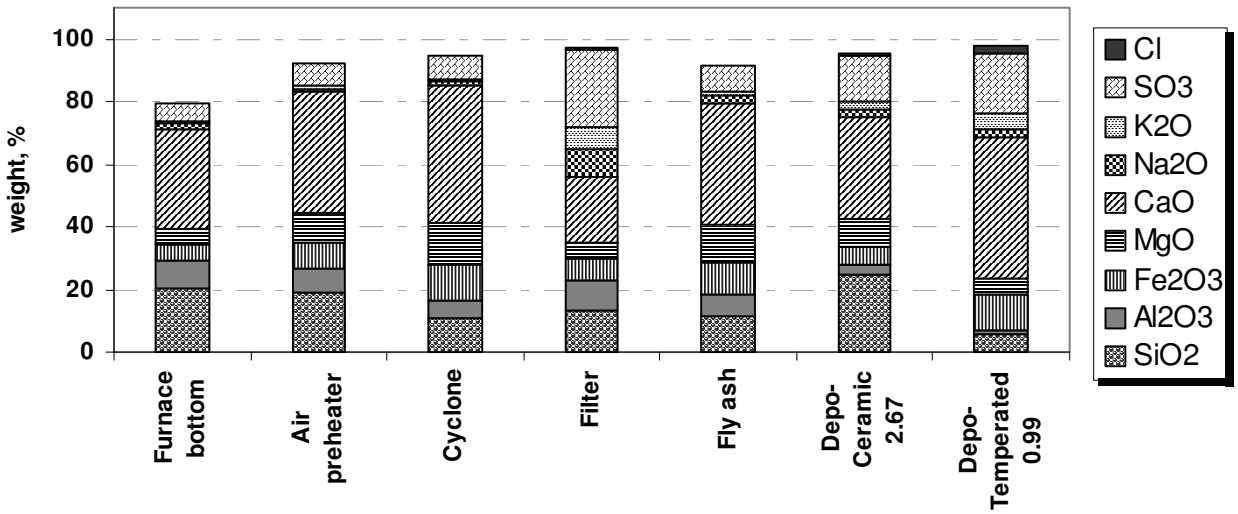

Fig.5.6. Ash composition in Test 5 (Lig1/CP-92/8)

SEM-EDX mappings were carried out on the deposited boiler steel X20 from the temperature-controlled probe in Test 3 (Lig2/PS-90/10) and Test 5(Lig1/CP-92/8). Fig. 5.7 shows the mapping of the wind-side deposit from the test of Lig2/PS-90/10. Fine particles and coarse particles coexisted in the wind-side deposit ash. The fine particles were mainly composed of S and Ca, suggesting that $CaSO_4$ was the main compound in the fine particles. $CaSO_4$ was also enriched on the surfaces of big particles. The core of the big particles was composed of Ca-Mg-Al-Si mineral complexes. Potassium was favoured in association with Al-Mg mineral complexes in middle size particles. Chlorine could not be detected. Besides the deposit structure, the detached scale of X20 showed a two-layer structure: the thick outer layer of the scale is mainly composed of iron oxides, whereas the inner layer of the scale was enriched in chromium.

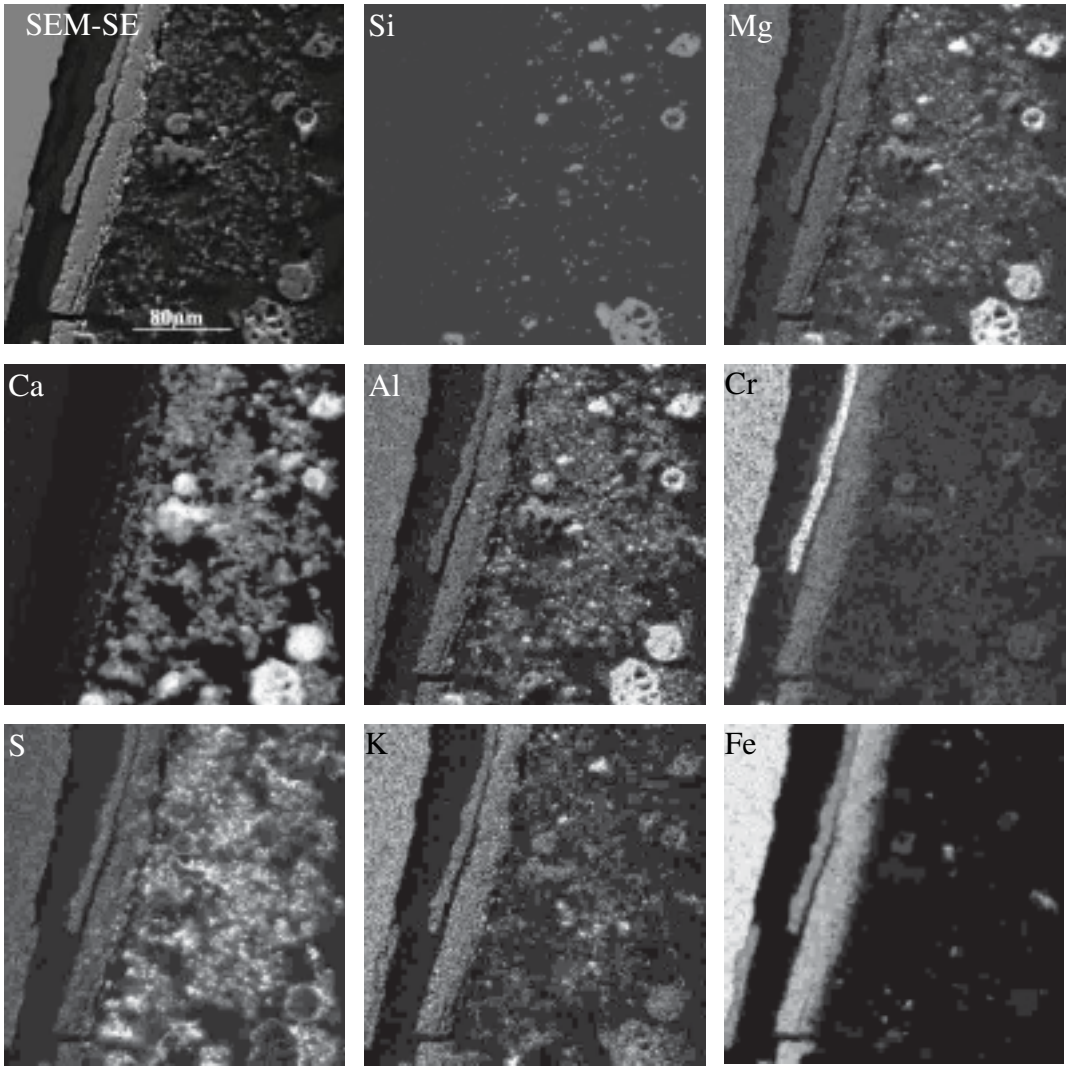

Fig. 5.7. SEM-Mapping of deposit at 0.99m of Test 3 (Lig2/PS-90/10)

The mapping of the lee side deposit from Test 5 (Lig1/CP-92/8) is shown in Fig. 5.8. The deposit was mainly composed of fine particles of $CaSO_4$. A little Mg could also be observed. Other elements, such as K and Cl could not be clearly detected. Since a relatively high concentration of potassium and chlorine were detected in the ash analysis (Fig. 5.6), the missing potassium and chlorine in the mapping could be a result of the dissolution of potassium chloride during the grinding process of the mounting specimen.

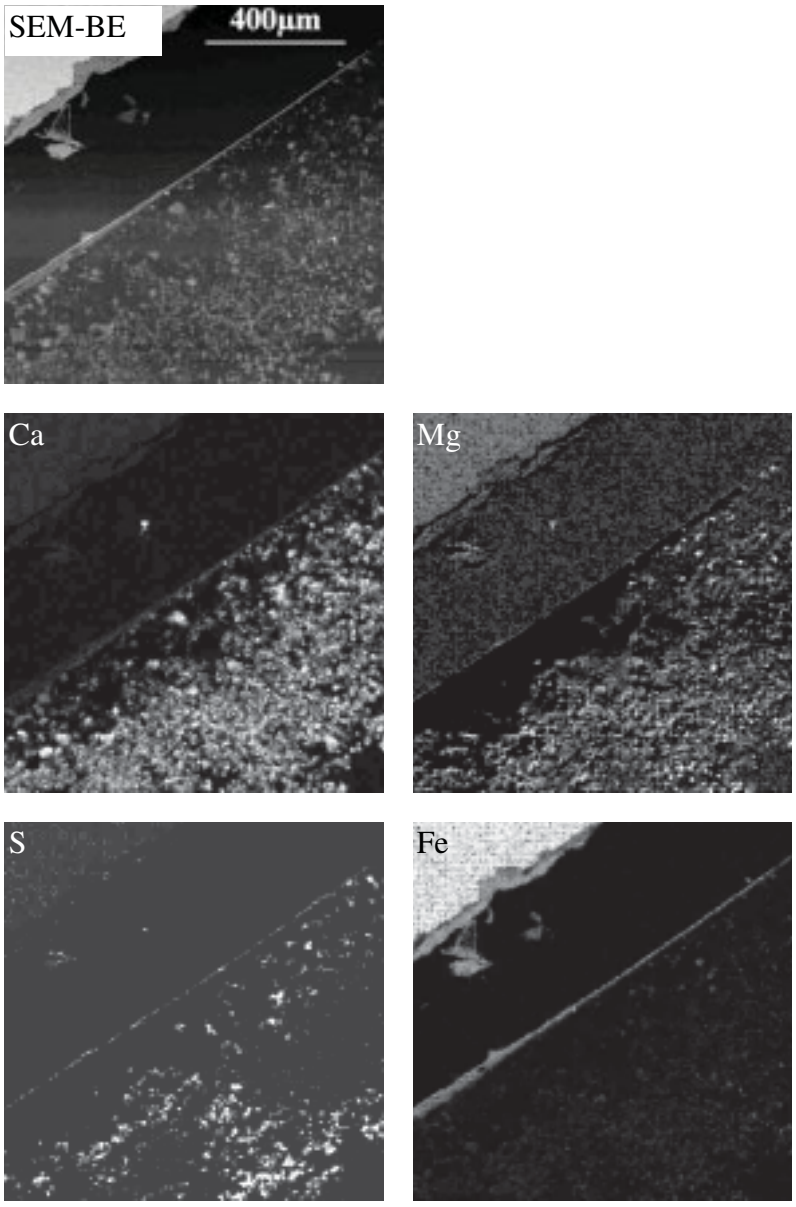

Figure 5.8. SEM-Mapping of deposit ash of Test 5 (Lig1/CP-92/8) below the burner (lee side)

- **General analysis**

In corrosion point of view, attention is mainly given on the concentration of chlorine, sulphur and alkali metals in the deposit ashes formed on the temperature-controlled probe. The ash

analyses in Test 1, Test 4 and Test 5 show that, both co-firing lignite with paper sludge and co-firing lignite with compost create more corrosive deposit ashes.

In order to identify the influence of other ash components on chlorine deposition, four mineral groups of fuel ash and laboratory ash are selected for comparison: i) sulphates in the form of SO_3, ii) chlorine, iii) alkali compounds and iv) aluminosilicates. Tab. 5.4 lists the concentration of the four mineral groups in laboratory fuel ash and in ash deposits.

Tab. 5.4. Concentration of the mineral groups in fuel ashes and in deposit ashes

		SO_3 %	Cl %	K_2O+Na_2O %	$SiO_2+Al_2O_3$ %
Laboratory fuel ash	Test 1: Lig2-100	13.8	0.652	1.5	18.6
	Test 4: Lig1/PS- 80/20	2.69	0.465	1.2	38.5
	Test 5: Lig1/CP-92/8	15.28	3.308	4	23.4
Deposit ash at 2.16m	Test 1: Lig2-100	29.81	0.23	6.29	3.38
	Test 4: Lig1/PS- 80/20	12.17	2.14	6.51	18.15
	Test 5: Lig1/CP-92/8	29.17	1.66	12.81	6.62

The first attention is given to sulphur content, since fuel sulphur compounds are believed to suppress the deposition of alkali chlorides effectively /82, 147/. This general trend is proved by the test results in this study. The least sulphur content in fuel ash in Test 4 (fuel blends of Lig1/PS-80/20) corresponded with the highest concentration of chlorine in the deposit ash, although chlorine content in the fuel blends of Lig1/PS-80/20 was lowest among those in the three fuels.

However, when this test results are studied in detail, it is found that the effectiveness of fuel sulphur to prevent chlorine deposition may be limited. In the Test 5 (Lig1/CP-92/8), the S/Cl molar ratio in fuel is approx. 3 to 1, the chlorine concentration in the deposit ash is still considerably high (1.66%). Bearing in mind that chlorine in the ash deposit was continuously sulphated during test period, the chlorine concentration could be even higher at the initial exposure period. The SO_2 concentration in flue gas shown in Fig. 5.2 implies that although high SO_2 was generated at the beginning of the combustion, SO_2 concentration reduced dramatically afterwards, as result, there was still not sufficient SO_2 in flue gas to convert alkali chlorides. Many evidences were found that fuel sulphur was captured during combustion. In the deposit ash of Test 4, sulphur content was over proportional high in comparison with its sulphur content in fuel ash (Tab. 5.4). In Test 5, a high concentration of $CaSO_4$ was found in the deposit ashes (Fig. 5.6 and Fig.5.8). Therefore, it is reasonable to

suggest that the calcium from paper sludge was effective to capture SO_2 in flue gas. The sulphur capture function of Ca is well known, its general chemical reaction in PF combustion can be described as /148/:

$$CaO + SO_2 + ½\, O_2 \rightarrow CaSO_4 \qquad (5.1)$$

$CaSO_4$ can be formed homogenously as fine particles, or on the surface of large particles by the gas/solid reaction of SO_2 with Ca containing particles.

The influence of aluminosilicates on the deposition of alkali chlorides could be implied by the SEM-EDX mapping of Test 4 (Fig. 5.7). When aluminium oxides are abundant in fuel, potassium can be bound with such minerals. In such way, the formation of KCl can be somewhat prevented. However, the high concentration of chlorine in deposit ash indicates that the amount of aluminium in the fuel blend of Test 4 was still not enough to exert decisive influence on the prevention of KCl deposition.

Another attention is given to the influence of ash content on the deposition composition. A large ash amount in fuel can dilute sulphur and chlorine concentration in the deposit ash. An example is given in Tab. 5.5. Although the fuel sulphur content in lignite (Lig2-100) is comparable with that in the fuel blend Lig2/PS-80/20, the sulphur content in the laboratory fuel ash of fuel blends Lig2/PS-80/20 is considerably lower than that in Lig.2. Corresponding to the sulphur in fuel ash, the sulphur concentration in deposit is lower than that in the deposit of Lig2-100.

Tab. 5.5. Sulphur concentration in fuel, laboratory fuel ash and deposit ash

	S_{fuel} %	$S_{fuel\ ash}$ %	**SO_3 % Deposit (2.16m)**
Lig2-100	0.11	5.52	29.81
Lig2/PS- 80/20	0.118	1.08	12.17
Lig1/CP-92/8	0.313	6.11	29.17

Therefore, it should be noted that the prediction of the corrosion tendency should be based on the sulphur, chlorine and alkali concentration in fuel ash instead of in fuel. This is especially important when fuel blends are fired, which are composed of fuels with very different ash content and ash composition.

Conclusions

Co-firing both lignite with paper sludge and lignite with compost can create more corrosive

deposit ash than pure lignite firing. In case of paper sludge co-firing, the high chlorine concentration in deposit is traced back to the low sulphur and high calcium content in fuel. In case of compost co-firing, besides the low SO_2 concentration in flue gas due the formation of $CaSO_4$, the high chlorine concentration is also a result of the high chlorine and potassium content in compost. Although aluminium compounds can absorb potassium in flue gas, this effect is not essential to reduce the formation of KCl during the co-firing of lignite with paper sludge.

Deposit ash on cooled tube surfaces is more corrosive than normal fly ashes, since compounds of chlorine, sulphur and alkalis tend to depose on cooler tube surface. The major fine deposit particles are $CaSO_4$, whereas coarse ash particles are mainly composed of Ca or Ca-Al-Mg mix phases.

The composition of deposit ashes is more relevant to the mineral contents in laboratory-generated fuel ash than that in fuel itself. This point should be given especial attention when two fuels with great ash content difference are co-fired. Since the high concentration of corrosive elements, such as sulphur and chlorine, in one fuel with little ash could be diluted by the large amount of minerals from the other fuel.

5.2 Co-combustion of South Africa coal with olive husk

5.2.1 Fuel characteristics and test program

Fuel and ash characteristics

The fuel features and fuel ash composition of South Africa Coal (SAC) and olive husk (OL) are listed in Tab. 5.6 and Tab. 5.7 respectively. South Africa Coal is a kind of bituminous coal with about 10% ash and 0.63 % sulphur. Its coal ash is mainly composed of Si and Al. The contents of Fe, alkalis and earth alkalis in South Africa Coal are low. Olive husk is characterised with high volatiles, low ash, and moderate water. The fuel ash of olive husk shows somewhat the common feature of biomass: high Si and K, moderate Cl, P and low Al and S. The heating value of olive husk is relatively high in biomass fuels.

Olive husk was sieved with 3 mm sieve before burning. The particle size distributions of SAC and OL are listed in Tab. 5.8. Of the whole distribution spectrum, olive husk particles are about 3 times as large as SAC particles. The large particles of olive husk led to poor burnout of fly ash and deposit ash.

Tab. 5.6. Fuel characteristics of South Africa Coal (SAC) and olive husk (OL)

		SAC	*OL*			*SAC*	*OL*
calorific values				elem. analy.			
HHV raw	MJ/kg raw	29.00	17.83	N	% raw	1.50	1.16
LHV raw	MJ/kg raw	28.18	16.08	C	% raw	74.89	44.69
				S	% raw	0.62	0.10
water content	% raw	2.24	9.48	H	% raw	3.55	7.10
volatiles	% raw	24.50	61.10	Cl	% raw	0.01	0.14
ash (815 °C)	% raw	10.65	5.0	O, diff.	% raw	6.55	32.47
volatiles	% wf	25.01	67.50	N	% wf	1.53	1.28
ash	% wf	10.90	5.50	C	% wf	76.61	49.37
total carbon	% wf	76.61	49.38	S	% wf	0.63	0.11
				H	% wf	3.63	7.84
				Cl	% wf	0.01	0.15
				O	% wf	6.70	35.87

Tab. 5.7. laboratory fuel ash composition of SAC and OL

Lab. ash		*SAC*	*OL*	*Lab. ash*		*SAC*	*OL*
SiO_2	%	46.06	32.79	Na_2O	%	0.20	1.37
Al_2O_3	%	31.01	2.38	K_2O	%	0.43	21.54
Fe_2O_3	%	4.35	16.36	TiO_2	%	1.49	0.00
MgO	%	2.11	1.76	P_2O_5	%	1.87	4.02
CaO	%	7.91	15.13	SO_3	%	14.45	4.57

Fig.5.8 partical size distribution of SAC and OL

	d 10 %, um	*d 50%, um*	*d 90%, um*
SAC	14	88	331
OL	40	230	900

Test program

A 100 % SAC test and a co-firing test of SAC with OL were carried out in the pulverized fuel test rig at IVD. The mass share and the thermal share of the fuels are listed in Tab. 5.9. The

thermal load of both tests was 350 KW. For the co-firing test, OL was premixed with coal before conveyed to the burner. Each test period took 8 hours.

Tab. 5.9. The thermal and mass share of the fuels

Test		*mass share*		*thermal share*	
		SAC	OL	SAC	OL
SAC	%	100	0	100	0
SAC/OL	%	76	24	85	15

The flue gas temperature and composition along the centre line of furnace height were measured. Due to combustion disturbances during the measuring period in SAC test, the profile data from 0.6 to 1.33m below the burner were unfortunately not available.

During each test, two temperature-controlled corrosion probes were inserted in the furnace at Level 8 (1.33 metre below the burner) and Level 11 (2.16 metre below the burner) respectively. The surface temperatures of the both probes were automatically controlled at 650°C. Deposit ashes on the temperature-controlled probe were sampled separately from the wind side and lee side, and from the outer deposit layer and the inner deposit layer. Fig. 5.9 shows the positions of the ash sampling.

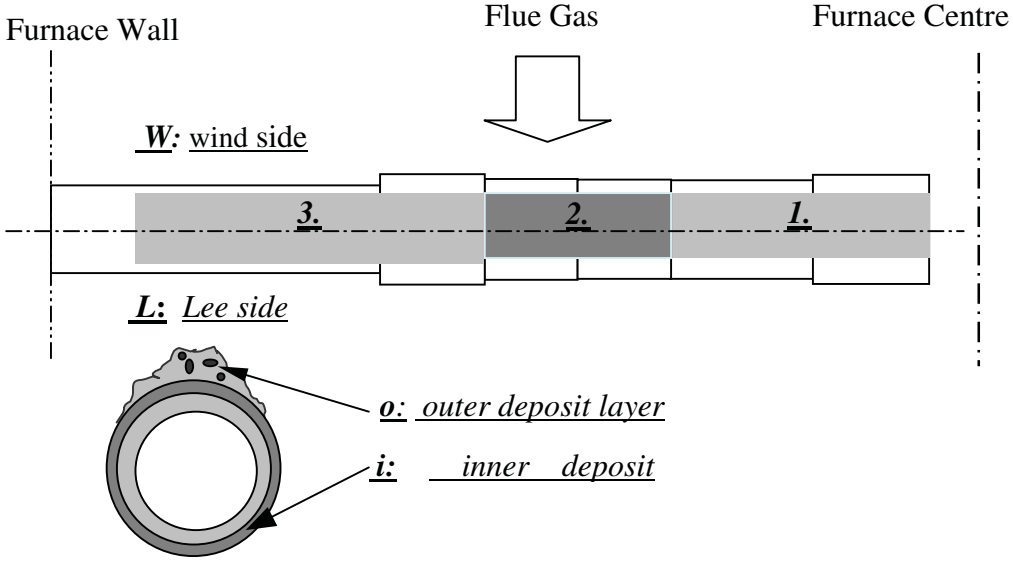

Fig. 5.9. Positions of deposit ash collection on the temperature-controlled probe

The terms of deposit ash are described in following, for example:

L8-1-W- o: *L8*: Level 8 of the furnace (1.33 m below the burner),
1: Position 1 (front part of the probe)

W: wind side
o: outer deposit layer

L11-2-L : *L11*: Level 11 of the furnace (2.16 m blow the burner)
2: Position 2 (middle part of the probe)
L: Lee side

In addition, a non-cooled ceramic probe was exposed at Level 8. Besides the deposit ashes, fly ash from the lower part of the furnace and ashes from furnace bottom, air preheater, cyclone and filter bag were collected.

5.2.2 Test results

Flue gas temperature and composition

The flue gas temperature, O_2 concentration and SO_2 concentration along furnace height of the two tests are shown in Fig. 5.10.

- The flue gas temperature of both tests were similar, both reached 1340°C at the flame centre. The flue gas temperature at the positions of corrosion probes was between

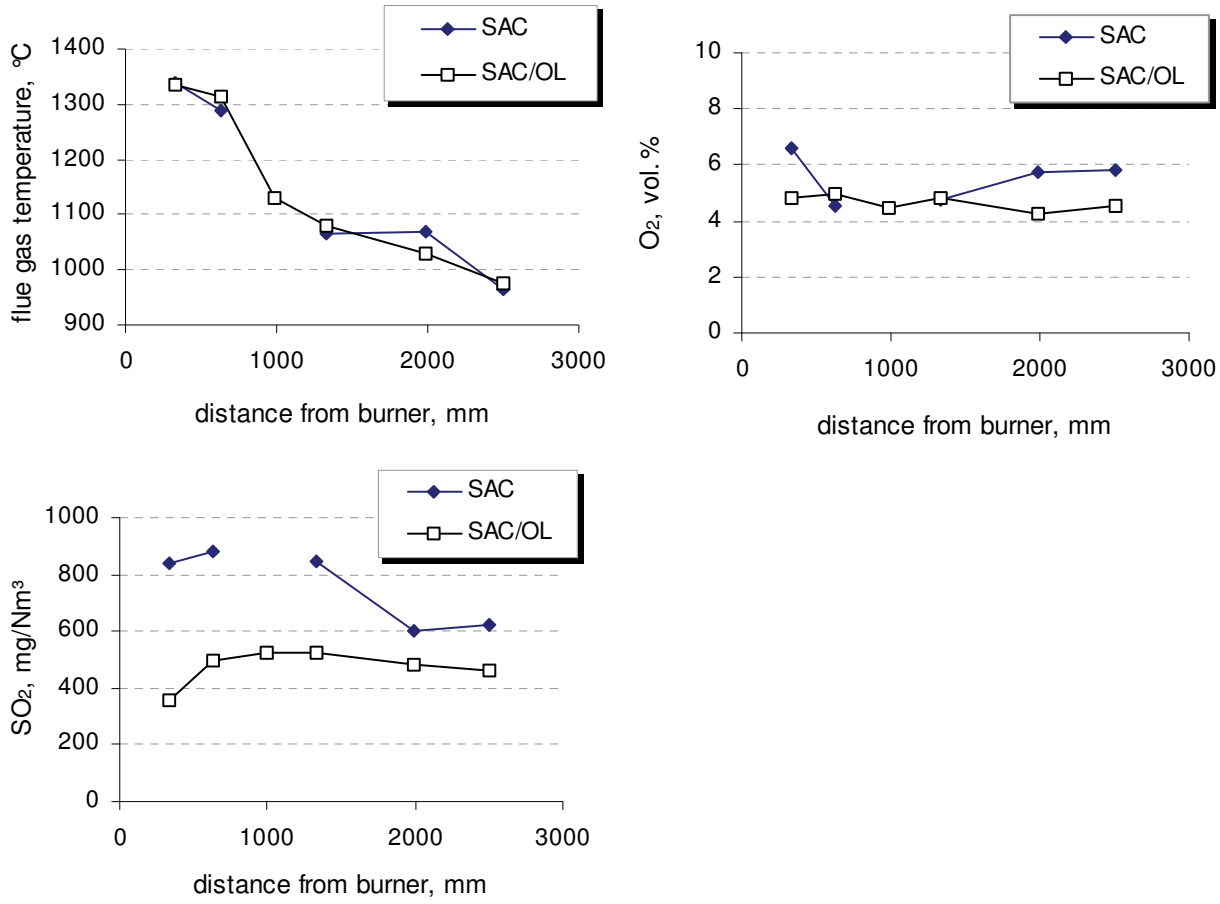

Fig. 5.10. Profiles of gas temperature, O_2 concentration and SO_2 concentration along furnace height

1100°C and 1000°C.

- The oxygen concentration in SAC/OL test remained relatively constant along the furnace height. This could be a result of postponed ignition and burnout of olive husk. The SAC flame, in contrary, showed the typical feature of coal combustion: oxygen was enriched just near the burner, but depleted in the flame zone due to the intensive combustion.
- Considerable lower SO_2 concentration was measured in the flame of SAC/OL test than that of SAC test. Besides the fact that olive husk has only one-fifth sulphur in the fuel than that of SAC, the sulphur-bonding-elements in olive husk, such as calcium and potassium, could contribute to the low SO_2 in the SAL/OL co-firing flame.

Fly ashes

The burnout of olive husk was very poor. Large amount of olive particles fell down to the furnace bottom and continued to burn out there. As consequence, the temperature of the bottom ash was very high. Fig.5.11 shows the fraction of unburned matters in the combustion ashes of the both tests. The poor burnout of olive husk also explains the constant oxygen consumption along the furnace height in Fig. 5.10. The burnout of middle-size ash particles from the SAC/OL test was a little better than that from the SAC test.

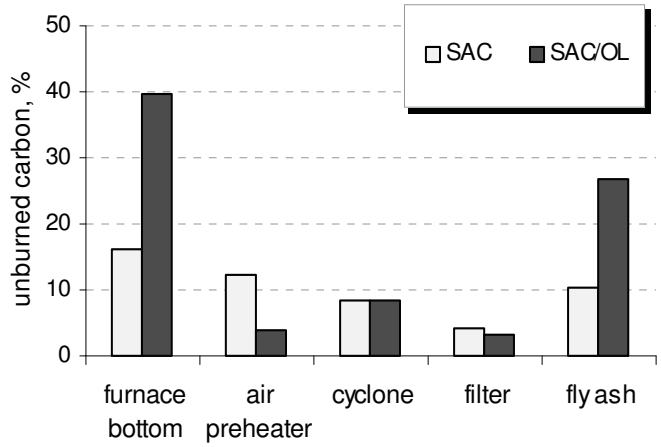

Fig. 5.11. Burnout of fly ashes from furnace and convective pass

It is interesting to note that although sulphur content in olive husk was only one fifth of that in SAC, the coarse ash particles from SAC/OL test contained higher sulphur than their counterparts in SAC test (Fig. 5.12). The enrichment of sulphur species in fly ash in the SAC/OL test could be the reason of the low SO_2 concentration in the flame. Besides, high

chlorine concentration was detected in the bottom ash and in the air preheater ash of the SAC/OL test. This is probably a result of the poor burnout of olive husk. Due to the low temperatures at these positions, chlorine in the unburned olive husk remained inactive.

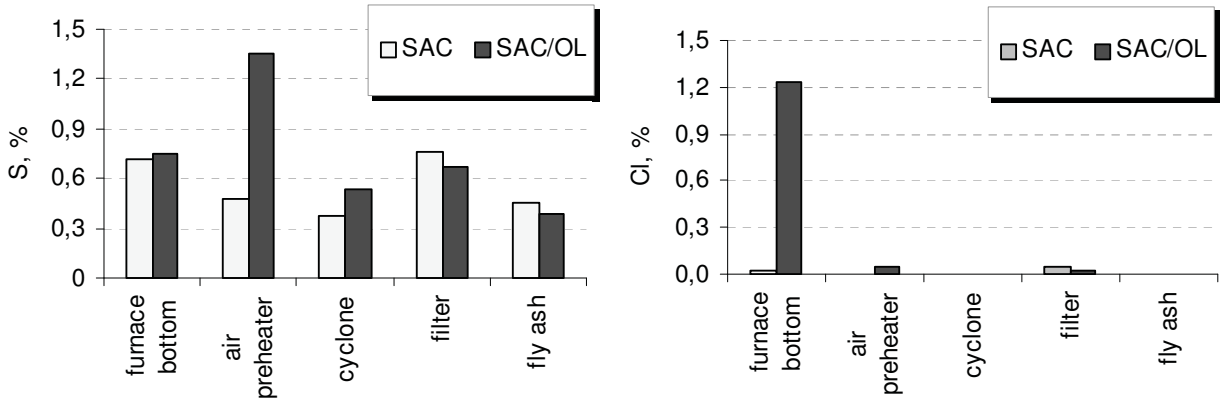

Fig. 5.12. Sulphur and chlorine concentration in fly ashes from furnace and convective pass

Ash deposit

Significantly more deposit ash was built up in SAC test than that in SAC/OL test both on the non-cooled ceramic probes and on the cooled corrosion/deposition probes. The deposit ash on the wind side in SAC test was partially sintered. Fig. 5.13 shows the deposit structure on the non-cooled ceramic probes from the two tests. The morphology of the deposit on the cooled probe surface was similar to that on the non-cooled deposits. Although olive husk contained less ash than SAC, but the total ash amount in SAC/OL test should be similar to that in SAC test, since more olive husk was burned to maintain the same thermal load. One reason of the low deposition tendency in SAC/OL test could be the favourable formation of large particles during combustion, which is mainly composed of Ca and Fe. Due to the high inertia of large

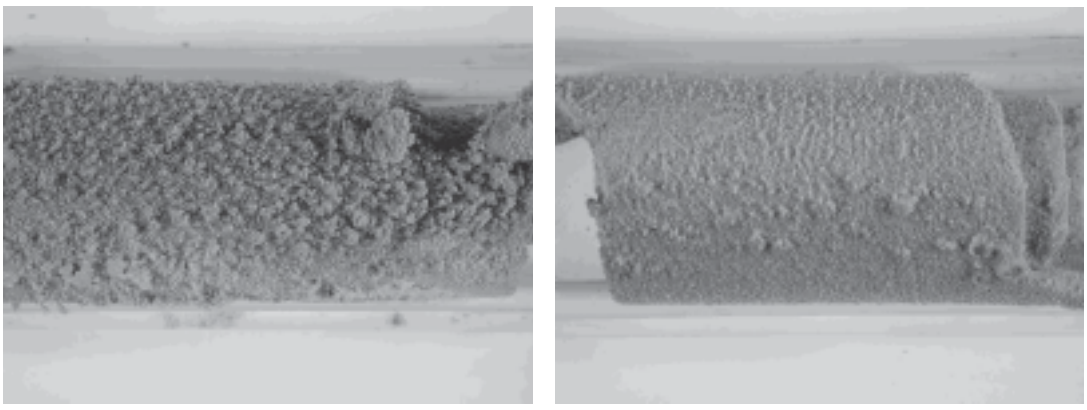

Fig. 5.13. Non-cooled deposition probe at Level 8: left: SAC test, right: SAC/OL test

fly ash particles, they are difficult to deposit on the tube surface, furthermore, they can also destroy the already deposited fine ash layer on tube surface. This effect can be verified by the following ash analyses.

- **Ash deposit microstructure**

The deposits on the cooled metal rings of NF709 from both tests were examined with SEM-EDX. Fig. 5.14 presents the morphology and elemental mapping of the deposit from SAC/OL test. For the SAC test, only point analyses of ash deposit were carried out, as shown in Fig. 5.15.

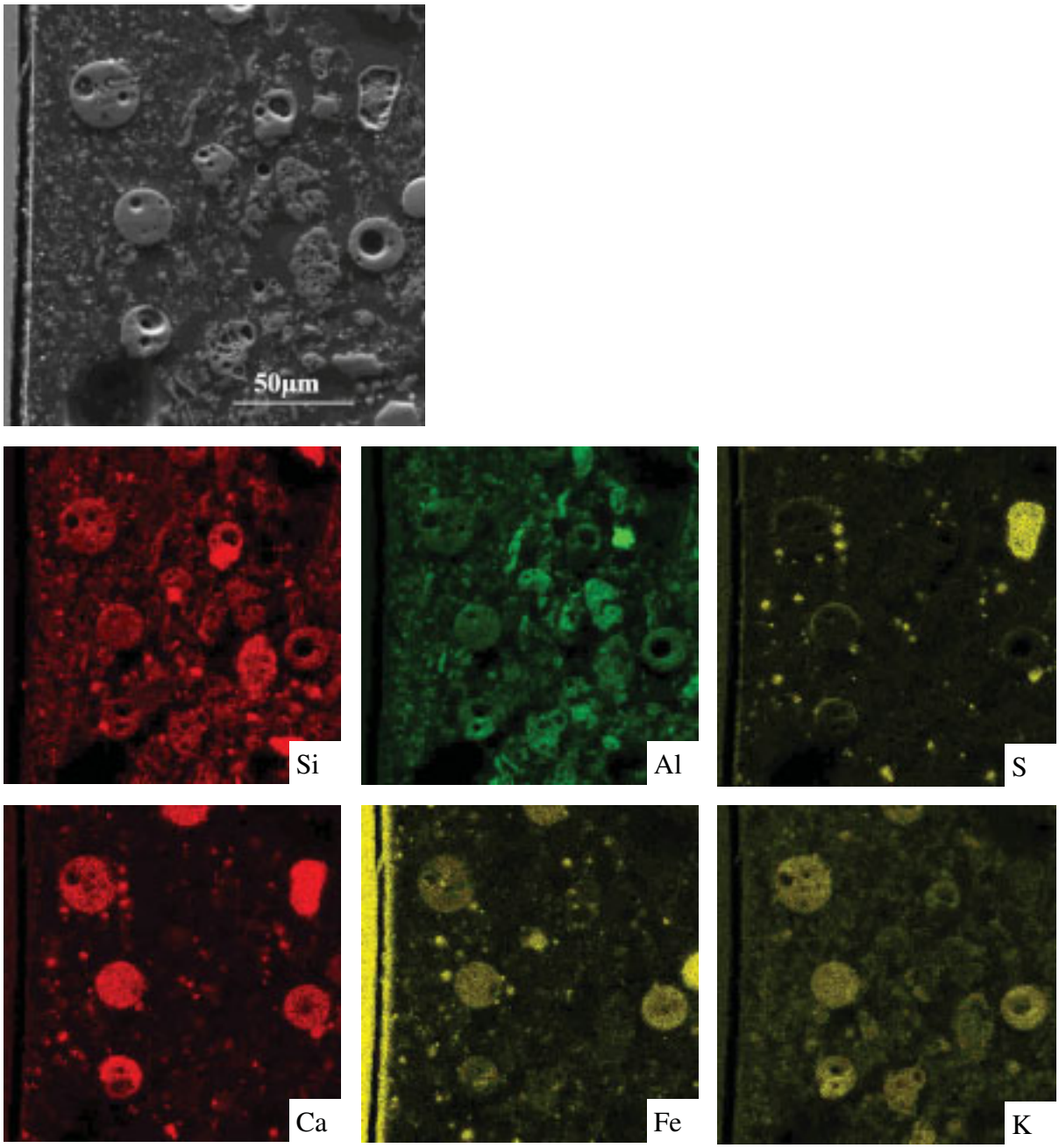

Figure 5.14. SEM-EDX mapping of deposit on 1.33m below the burner of SAC/OL test

SAC/OL test: fine particles and coarse particles coexisted in the wind-side deposit. Ultra-fine particles were mostly composed of aluminosilicates. $CaSO_4$ is the main form of sulphur species in ash deposit. $CaSO_4$ formed either homogenous fine ash particles or on the surface of coarse particles enriched with Ca. The enrichment of $CaSO_4$ in ash deposits explains also the reason of the low SO_2-concentration in flue gas (Fig.5.10).

Potassium was partially associated with aluminosilicates in fine particles, and partially bound in Ca-Fe-Al-Si complexes in large particles. No K_2SO_4 was detected. The preferential bonding between potassium and aluminosilicates were also observed by other researchers during co-combustion of bituminous coal and biomass /30/, /87/, /156/.

Besides forming $CaSO_4$, calcium was also the main element in large ash particles. The spherical form of the Ca-Fe-Al-Si mix phases in Fig. 5.13 is an evidence that they were soften or molten in the flue gas temperature. This phenomenon was also reported by Manton /149/ that a fuel or a fuel blends containing high iron and CaO reduce the melting temperature of the whole ash. He suggested that within the compositional limits of Fe_2O_3 between 10-50 wt.% or CaO between 5-40 wt.%, the ash system contains sufficient fluxing oxides to reduce its viscosity to a value at which viscous flow sintering can occur. The melting temperature of ashes enriched in Ca and Fe was calculated by Kondratiev /64/, who proved that the general viscosities of the slag system decrease with the increase of CaO/SiO_2 ratios from 0 to 1.2 and with the decrease of the SiO_2/Fe ratios from 5.0 to 1.0. More in detail, Zygarlicke suggested that the large particles of amorphous and crystalline Ca-silicate or Ca-aluminosilicate phases are generated from the intensive reaction of quartz and clay minerals with organically-bound Ca /61/.

SAC test: different to the SAC/OL test, the deposit formed in the SAC test was mainly composed of fine particles. The Ca- and Fe-rich large particles were not often observed (Fig. 5.15). This could be traced back to the low Ca and Fe content in the SAC. Again, $CaSO_4$ was the only form of sulphur compound in the ash deposit (Point 6). The particles can be composed of compounds of (Fe-Si-Al) (point 1), Si-Al-Ca (point 3), or be dominated by one compound, e.g., SiO_2 (Point 2), iron oxide (Point 5) or $CaSO_4$ (point 6). The SEM-EDX analysis gave a general picture of the possible compounds in the inner layer of deposits.

To obtain more detailed information about deposit ashes, especially regarding the composition differences between wind side and leeside deposit, and between outer deposit layer and inner deposit layer, quantitative elemental distribution of ashes were analysed, which is illustrated in Fig.5.16.

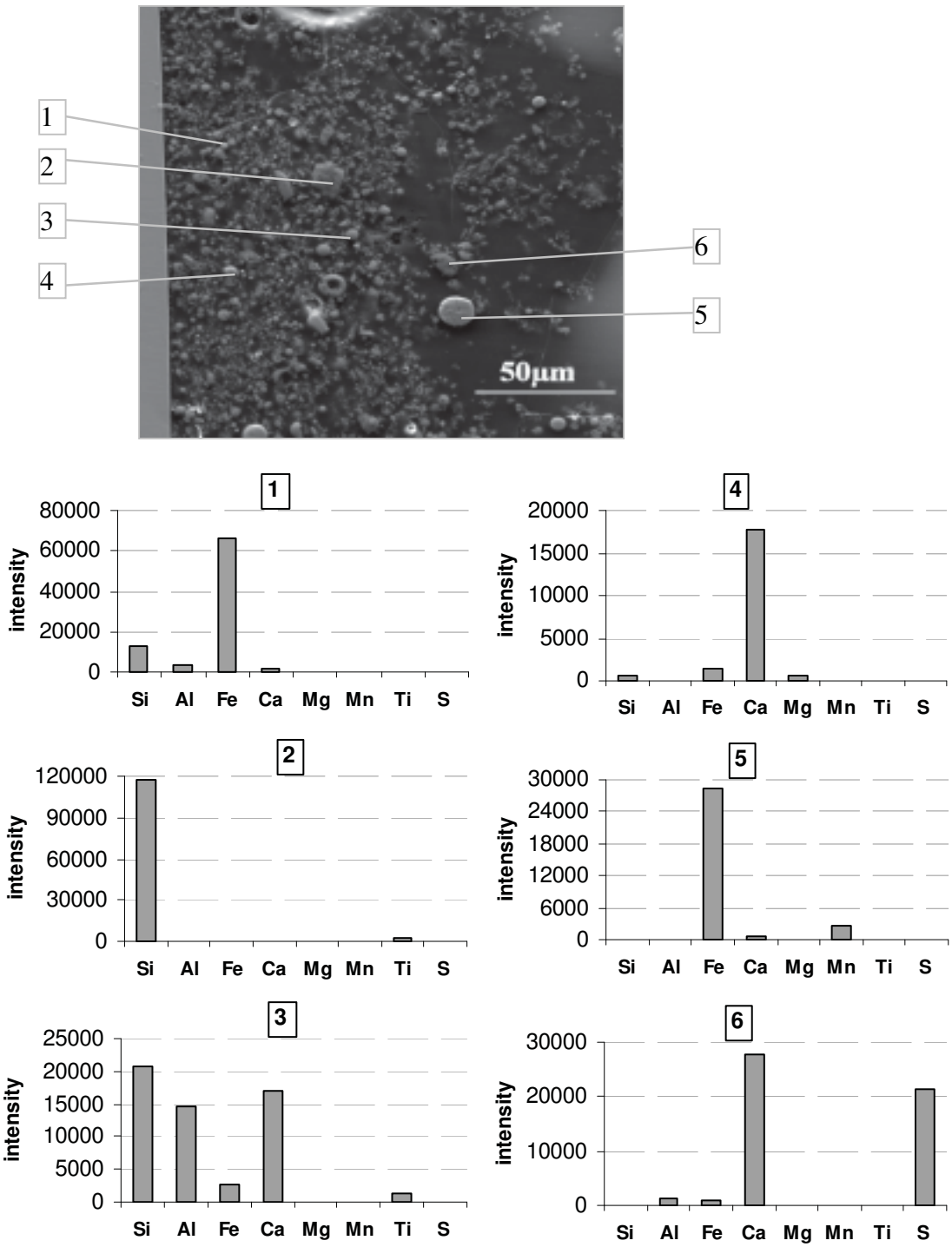

Fig. 5.15. SEM and point analysis of deposit ash at E8 of burning SAC

- **Quantitative elemental distribution in ashes**

Fig. 5.16. shows the ash elemental distribution of the wind side and the leeside deposit, in the outer deposit layer and the inner deposit layer, and the distributions in deposit from different flue gas temperature regions. The selective deposition of ash elements is caused by different deposition mechanisms. Fine ashes tend to depose adjacent to tube surface and on the leeside of a tube, which are transported by vapour diffusion and condensation, or thermophoresis;

large particles prefer to depose on the outer layer of the deposit and on the wind side of the tube due to their large inertia. In addition, different flue gas temperature along furnace height may influence the extension and completeness of a reaction. This can postpone the deposition

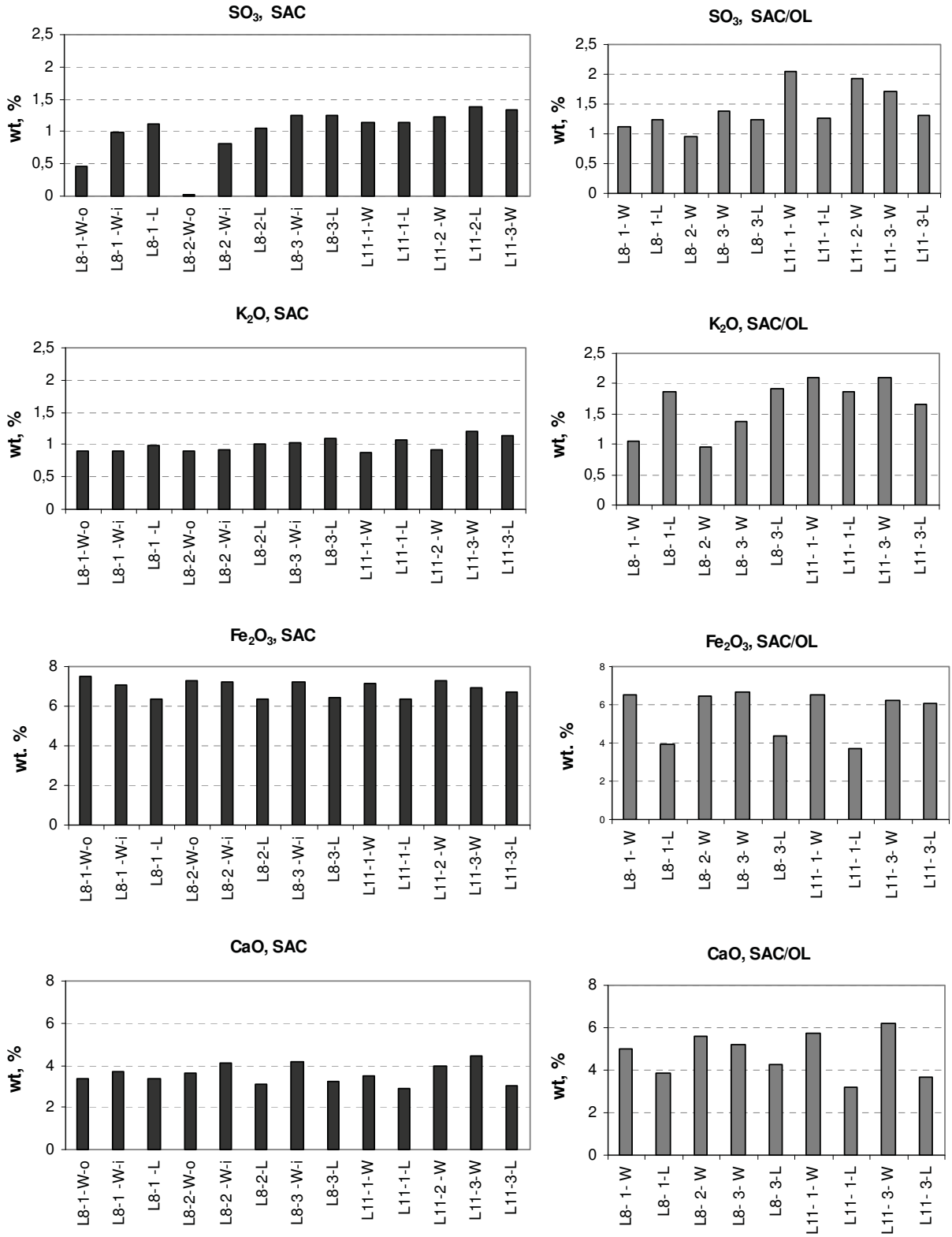

Fig. 5.16. Composition of deposits at different positions on cooled probe surface

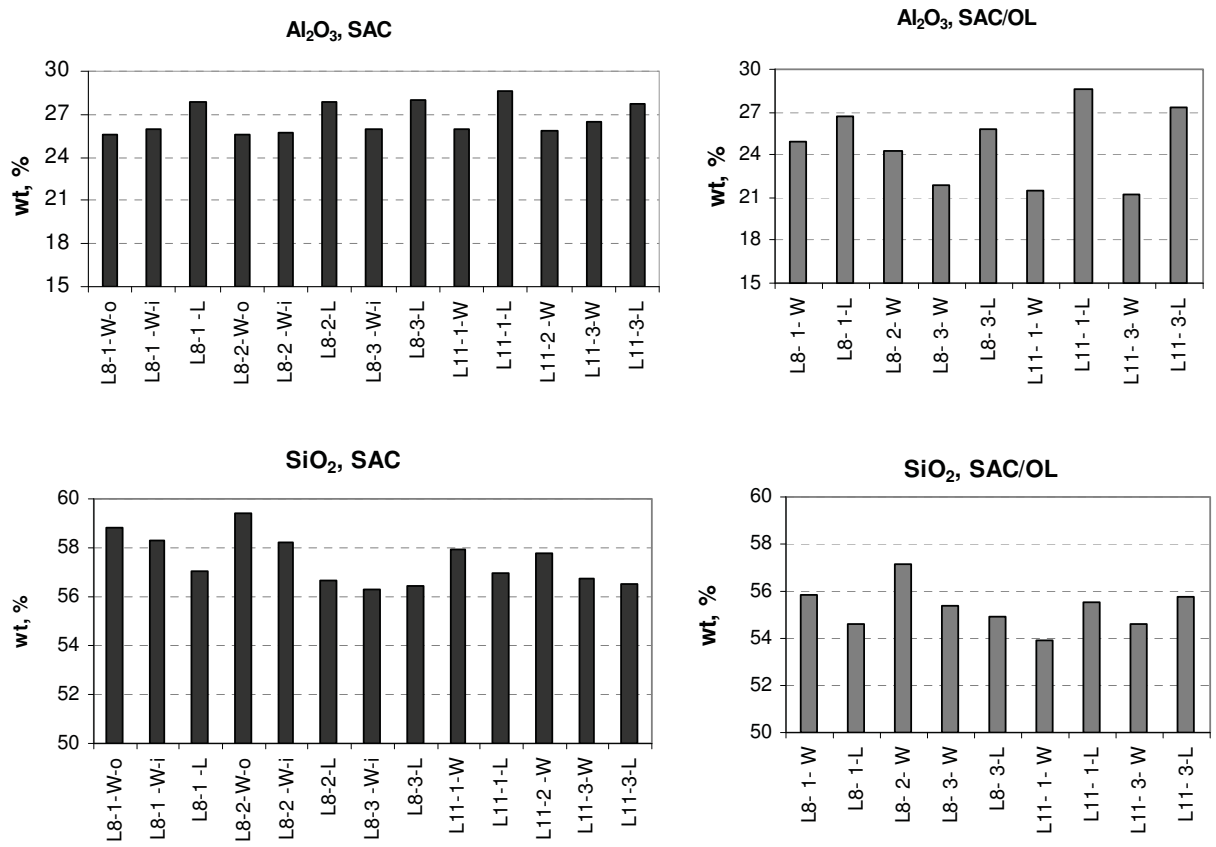

Fig. 5.16. Continued

of such large particles to low temperature region. The distribution features of each element are discussed in following:

<u>Sulphur</u>: Sulphur content in fly ashes and in the deposits in SAC/OL test was higher than that in SAC test, although the sulphur content in the fuel blends was lower than that in SAC. This explains again the reason of low SO_2 concentration in flue gas of the SAC/OL flame. In both tests, sulphur was enriched on the temperature-controlled probes in lower flue gas temperature (Level 11 of the furnace height in the tests). The selective deposition of sulphur implies that the formation of $CaSO_4$ is benefited below 1000°C of flue gas temperature.

<u>Potassium</u>: due to the high potassium content in olive husk, the potassium concentration in SAC/OL deposit ash was correspondingly higher than that in SAC test. Similar to the behaviour of sulphur, more potassium was deposited in area of lower flue gas temperature. The difference of potassium concentration in the deposit ashes in SAC test was relatively small. Whereas in the SAC/OL test, the high potassium concentrations in the leeside deposit at Level 8 and at the wind side of level 11 are notable. A possible explanation is that the formation of large potassium-containing particles took place in lower flue gas temperature

zone. As a consequence, at Level 8 only fine particles containing potassium was deposited, mainly on the leeside, whereas at the Level 11, coarse particles containing potassium tended to accumulate on the wind side.

Iron: although iron content in olive husk is high, less Fe_2O_3 was deposited on the cooled surface in SAC/OL test. From the SEM mapping in Fig. 5.14, it is observed that iron was mainly enriched in large round particles. Inertia impaction should be the main mechanism of iron deposition. This is proved by the apparent higher iron concentration on the wind side deposits than in the leeside deposit in the SAC/OL test. Nevertheless, the low deposit amount in SAC/OL test also implies that deposition of large particles on the cooled tube surface was not severe.

Calcium: Calcium concentration in SAC/OL ash deposits was slightly higher than that in SAC deposits. Although calcium existed both in fine particles (mainly of $CaSO_4$) and in coarse particles, it seems that the calcium enriched in coarse particles counted more in mass. Similar to iron species, calcium compounds were more enriched in the wind side deposit than in the leeside ones.

Aluminium: Al_2O_3-rich minerals took about a quarter of the deposit mass for both tests. Since aluminium existed mostly in ultra fine and fine particles (Fig.5.14), which deposited on the tube surface per thermophoresis or eddies on the lee side, the inner deposit layer and the leeside deposit were correspondingly enriched with aluminium. Besides, since the deposition of coarse particles was preferential on the wind-side of tube, the share of aluminium in wind side deposit was comparatively lower than that in leeside deposit.

Silicon: SiO_2 was the dominant mineral compound in ash deposits in both tests, which accounted for more than 50% of the deposit mass. SiO_2 content in SAC test was higher than that in SAC/OL test. A little higher SiO_2 was observed in the wind side deposits and outer deposit layers. This implies that the deposition mechanism of SiO_2 is not vapour diffusion or vapour condensation of low melting point minerals, but thermophoresis, which only depends on particle size.

Chlorine could not be clearly detected.

Considering the deposits on the non-cooled probes, a general view is given in Fig. 5.17, which shows the deposit compositions at Level 8 in SAC and SAC/OL test. There is a clear contrast of the deposit character: in SAC test, the deposit ash is constituted mainly of fine aluminosilicates, whereas in SAC/OL test, the large particles enriched in Ca and Fe took a

considerable part in the deposit. Comparing the Fe deposition on the non-cooled probe with that on the cooled probe in SAC/OL test (Fig. 5.16), it is found that the iron-rich spherical particles are more likely deposited on non-cooled deposits.

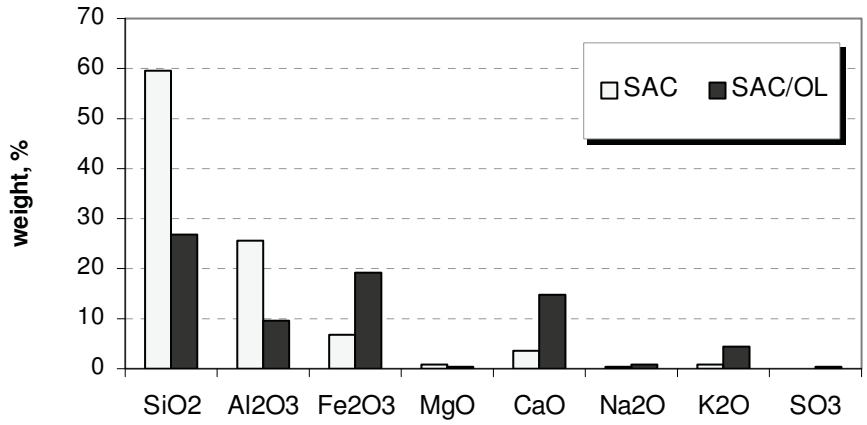

Fig. 5.17. Composition of deposits formed on the non-cooled probe at Level 8 (1.33m form the burner)

Conclusions

1. No chlorine corrosion took place during co-firing of bituminous coal with olive rest.
2. Co-firing a high-sulphur, low-calcium coal with another fuel with higher calcium content lead to the favoured formation of $CaSO_4$. As result, the SO_2 concentration in flue gas is decreased.
3. Bituminous coal, which is usually rich in aluminosilicates, tends to form a thick deposit ash layer on tube surface. This kind of deposit layer consists mainly of fine aluminosilicates particles. In contrary, co-firing bituminous coal with a fuel enriched in Ca and Fe leads to the dominant formation of coarse particles, which are difficult to be accumulated on heat transfer surface.
4. Potassium is partially bound in fine aluminosilicates, partially in Ca-Fe-rich large particles. At high flue gas temperature, potassium is probably bound in fine Al-Si particles, whereas at low flue gas temperature (below1000°C), potassium is favoured to be bound in Al-Si-Ca complexes. From the view of chlorine corrosion, the co-combustion of SAC and OL can provide a benefit effect that potassium from olive husk is inactivated by Al-Si or Ca-Fe complexes, this means, the potential of formation and deposition of alkali chlorides and alkali sulphates are reduced.

5. The different deposition mechanisms to form outer/inner deposit layer and wind side/leeside deposits are based on particle size and particle melting temperature. Fine particles approach cooler heat transfer surfaces per thermophoresis or vapour diffusion /condensation, they constitute the inner deposit layer and are enriched in the lee side. Large particles are transported to the tube surface due to their large inertia, which are accumulated on the wind side of tube surface. In comparison with bulk fly ashes, more fine particles are deposited on the cooled probe surface.

6. Thermodynamic Calculation of Combustion Products of Coal-Straw Fuel Blends

This chapter focuses on the potential of chlorine corrosion when a chlorine-rich fuel is co-fired with a kind of coal. The concern is: which kind of fuel is the best candidate to be co-fired with chlorine-rich fuel? Straw is taken as example for such chlorine-rich fuel in this study. Straw contains usually high chlorine and potassium. This can lead to the formation of potassium chlorides during combustion. During cooling process, potassium chloride either deposes on heat transfer surfaces or is collected in flue gas pass. It is known that heat transfer material beneath chlorine-enriched ash deposits suffers more serious corrosion than a bare tube exposed in gas environment /138/. The suitable fuel for the co-firing with straw should suppress the formation or the deposition of potassium chlorides, and promote the formation of relative harmless gaseous HCl.

In this chapter, based on the behaviour of corrosion-related fuel elements during combustion and cooling, the suitability of bituminous coal/straw co-firing and lignite/straw co-firing was predicted. Furthermore, the acceptable share of straw for the co-firing was evaluated. Comparison was also given between the calculation results and the results from combustion tests.

6.1 Calculation method and fuel data

The thermodynamic calculation was carried out with the program “FACTSage”. The commercial program FACTSage and its sister program ChemSage are widely applied in thermodynamic equilibrium calculations of combustion, slagging and corrosion process in power plants or in metallurgy facilities /150-154/. The calculation principle is based on minimizing total Gibbs free energy in a system. When the total Gibbs energy of a system is in its minimum, the system is in a thermodynamic equilibrium state where all possible reactions reach equilibrium. In general, an equilibrium state will be approached with increasing temperature and extending reaction time.

The thermodynamic calculation is a proper tool to predict fast chemical and physical processes. During pulverized fuel combustion and cooling process, most gas phase reactions can be treated as quasi equilibrium process. Some physical and chemical processes, such as condensation, solid-state transformation of mineral complex, SO_2/SO_3 conversion, and reactions among coarse particles in flue gas and in ash deposition, could be difficult to approach equilibrium.

Co-firing bituminous coal with straw and co-firing lignite with straw were studied in this study. The cases with straw thermal shares of 0%, 12.5%, 25%, 50% and 100% were calculated. In each calculation, the air ratio "λ" was defined at 1.2. The thermal input was based on the lower heating value of fuel blends. In the calculation, most important elements from fuel and combustion air were considered, they were N, C, S, H, O, Cl, Si, Al, Fe, Mn, Mg, Ca, Na, K, Ti, P. Global equilibrium analysis was performed to predict thermodynamically stable chemical and physical forms of mineral species. About 700 species of possible combustion products in the temperature range from 1200°C to 400°C were selected as output data. Special attention was given to the products that could arise or suppress serious fouling and corrosion problem. They are compounds or mineral complexes of chlorine, sulphur, alkali metals, silicon and aluminium.

Fuel data of a bituminous coal from the Saarland and a lignite fuel from the Rheinish area in Germany were applied. The lignite was already dried before delivery. The applied lignite is a high quality lignite and it is used for briquet production. It has low ash content and extraneous minerals such as silicon and aluminium. The quality of this lignite deviates from the lignite applied to power plants, which contains generally more ash and extraneous minerals. Straw came from Denmark. The fuel characteristics are listed in Table 6.1. In the following text and

Tab. 6.1. Fuel and ash characteristics

Fuel		***Bit***	***Lig***	***S***	***Fuel ash***		***Bit***	***Lig***	***S***
Ultimate analysis					SiO_2	%	40.09	6.99	68.59
N	% wf	1.48	0.75	1.09	Al_2O_3	%	23.57	4.29	0.36
C	% wf	73.52	65.24	41.43	Fe_2O_3	%	13.27	14.52	0.26
S	% wf	0.88	0.37	0.10	MnO_2	%	-		-
H	% wf	4.26	4.69	4.18	MgO	%	2.92	15.51	0.87
Cl	% wf	0.22	0.02	0.53	CaO	%	5.48	37.95	4.34
O (as difference)	% wf	9.98	24.82	38.94	Na_2O	%	1.51	2.73	0.35
Heat values					K_2O	%	2.91	0.63	14.79
HHV	MJ/kg wf	31.82	25.54	16.92	TiO_2	%	0.95	0.23	0.02
LHV	MJ/kg wf	30.89	24.51	16.01	P_2O_5	%	0.19	0.03	1.93
Proximate analy.					SO_3	%	7.4	15 .28	1.93
water content	% raw	2.03	10.48	11.71					
volatiles	% raw	32.93	47.88	62.96					
ash (815°C)	% raw	9.23	3.83	11.86					
fixed carbon	% raw	55.83	37.80	13.48					

tables, short terms of “Bit”, “Lig” and “S” are used to express bituminous coal, lignite and straw, respectively.

Bituminous coal contains more chlorine and sulphur than lignite does. But the large ash content in bituminous coal can dilute the concentration of chlorine, sulphur and alkalis in fly ashes and in deposit ashes. The low sulphate content (in the form of SO_3) in the fuel ash of bituminous coal is an evidence of this phenomenon. Regarding the mineral distributions in fuel ash, aluminates and silicates are the main mineral groups in the bituminous coal, whereas earth alkalis are the main mineral components in lignite. In straw, silicates are dominant, which constitute about 70% of the fuel ash; potassium and chlorine are the next two major elements in the straw ash; the contents of aluminium, earth alkalis and sulphur are very low.

6.2 Calculation results

Percentage distribution of chlorine compounds (Fig. 6.1)

The calculation result reveals different trends of chlorine distribution between bituminous coal-straw co-firing and lignite-straw co-firing. Gaseous HCl is the dominant chlorine compound during the bituminous coal combustion and the co-combustion of bituminous coal-straw with straw share up to 25 %. Further increase in straw share reduces the HCl-dominated temperature zone, instead, gaseous alkali chlorides become the main chlorine compound above 1000°C and solid alkali chlorides are the dominant chlorine species below 500°C. Opposite trend is revealed in the case of firing lignite with straw: during lignite combustion, gaseous and solid alkali chlorides are dominant chlorine species; the HCl percentage increases with the increasing share of straw. At the straw share of 25%, HCl is the main chlorine species between 900°C and 500°C. Further increase in straw share leads to overwhelming formation of potassium chloride, which condenses or solidifies below 650°C.

Although the calculation results of especially lignite-straw co-firing show that gaseous alkali chlorides at high temperature undergo a transition to HCl before they convert to solid alkali chlorides, this equilibrium transition could possibly not be fully reached in the real combustion facilities near heat transfer surface, since gaseous alkali chlorides can condense or solidify quickly on the cooler tube surface.

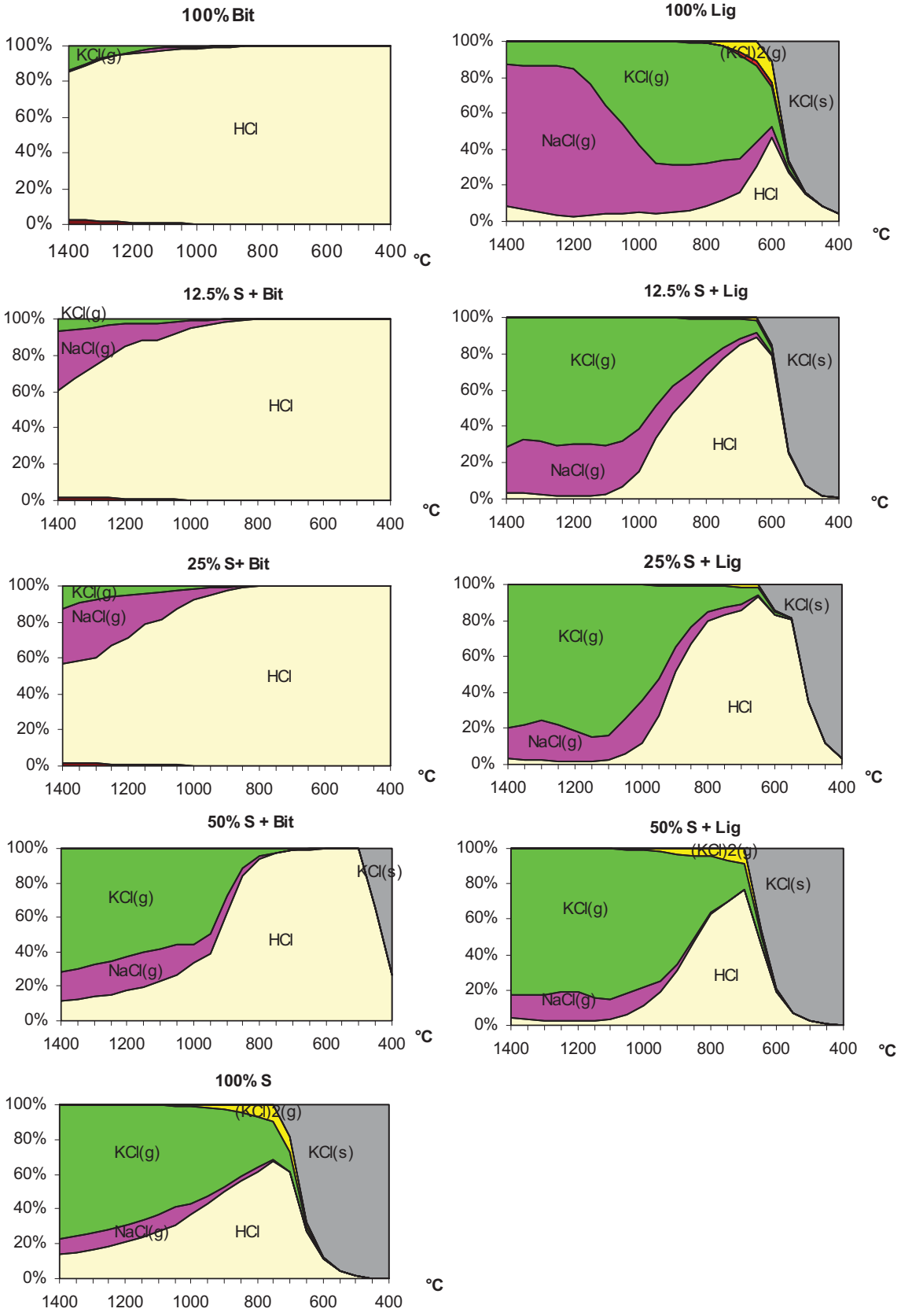

Fig. 6.1. Chlorine distribution of co-firing straw with bituminous coal and with lignite

Quantitative distribution of Cl compounds (Fig. 6.2)

Although the percentage distribution of chlorine compounds can elucidate the fate of chlorine during combustion and cooling process, it can not predict corrosion potential. A realistic prediction of the corrosivity of fly ashes should be based on the quantitative concentration of chlorine compounds in flue gas and in fly ashes. The quantitative chlorine concentration is not only determined by chlorine compound distribution during combustion, but also by absolute chlorine and ash contents in fuel. For example, when a fuel contains very little chlorine but

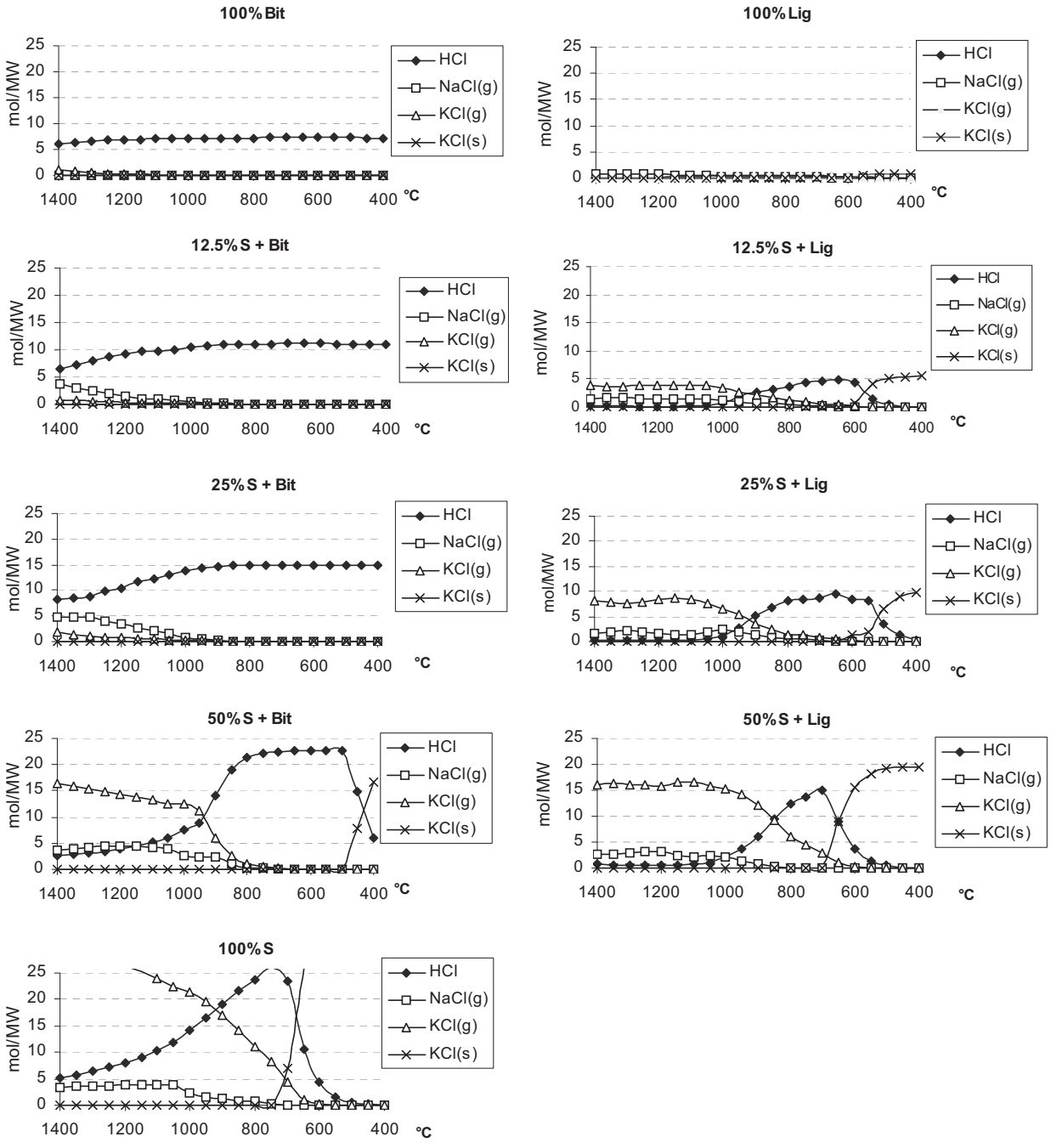

Fig. 6.2. molar concentration of chlorine compounds of co-firing straw with bituminous coal and lignite

large amount of inert minerals, even all the chlorine is bound with alkali metals and deposits on tube surface, it could still not be critical due to the absolute low concentration of alkali chlorides in the deposits.

The molar distribution of chlorine products, which is based on fuel thermal input, is illustrated in Fig.6.2. Comparing chlorine molar distribution during bituminous coal combustion and lignite combustion, it is found that although chlorine content in bituminous coal is high, most of chlorine forms less critical HCl gas; lignite contains little chlorine and alkali, but most of them form alkali chlorides during combustion. As consequence, both bituminous coal combustion and lignite combustion have low potential to form chlorine-rich fly ashes. With the increase of straw share, alkali chlorides increase their concentration in both cases, but with different increasing rate. When an acceptable limit of the total alkali chloride concentration is set at 3 mole/MW in flue gas, and the flue gas temperature in the superheater/reheater area is below 1000°C, then up to 25% thermal share of straw is allowed to be co-fired with bituminous coal, whereas straw is not suitable to be co-fired with lignite at all.

In addition, it is noted that not all potassium is bound in KCl (g), even though theoretically the total potassium is in surplus for the formation of KCl. When there were sufficient free potassium cations in flue gas, the formation of KCl (g) from HCl would occur at the burnout region. The low KCl (g) concentration between 1000°C-500°C during the bituminous-straw co-firing implies that potassium must be bound in compounds which are more stable than KCl (Fig. 6.2).

The fate of potassium during combustion is explained in Fig. 6.3. It is obvious that Al-Si minerals in bituminous coal act as effective potassium absorbents, with which potassium forms solid or liquid K-Al-Si-O mineral complexes. In the case of lignite, due to the absent of aluminosilicates, the major part of potassium is bound in KOH (g), K_2SO_4 (g) and KCl (g) at high temperature, and in K_2SO_4(s) at low temperature. This indicates the advantage of co-firing bituminous coal with straw: the abundant aluminosilicates in bituminous coal can deactivate potassium by forming stable K-Si-Al-O mineral complexes. As consequence, due to the lack of free potassium cation in flue gas, most chlorine from straw forms HCl gas in flue gas, instead of KCl (g,s).

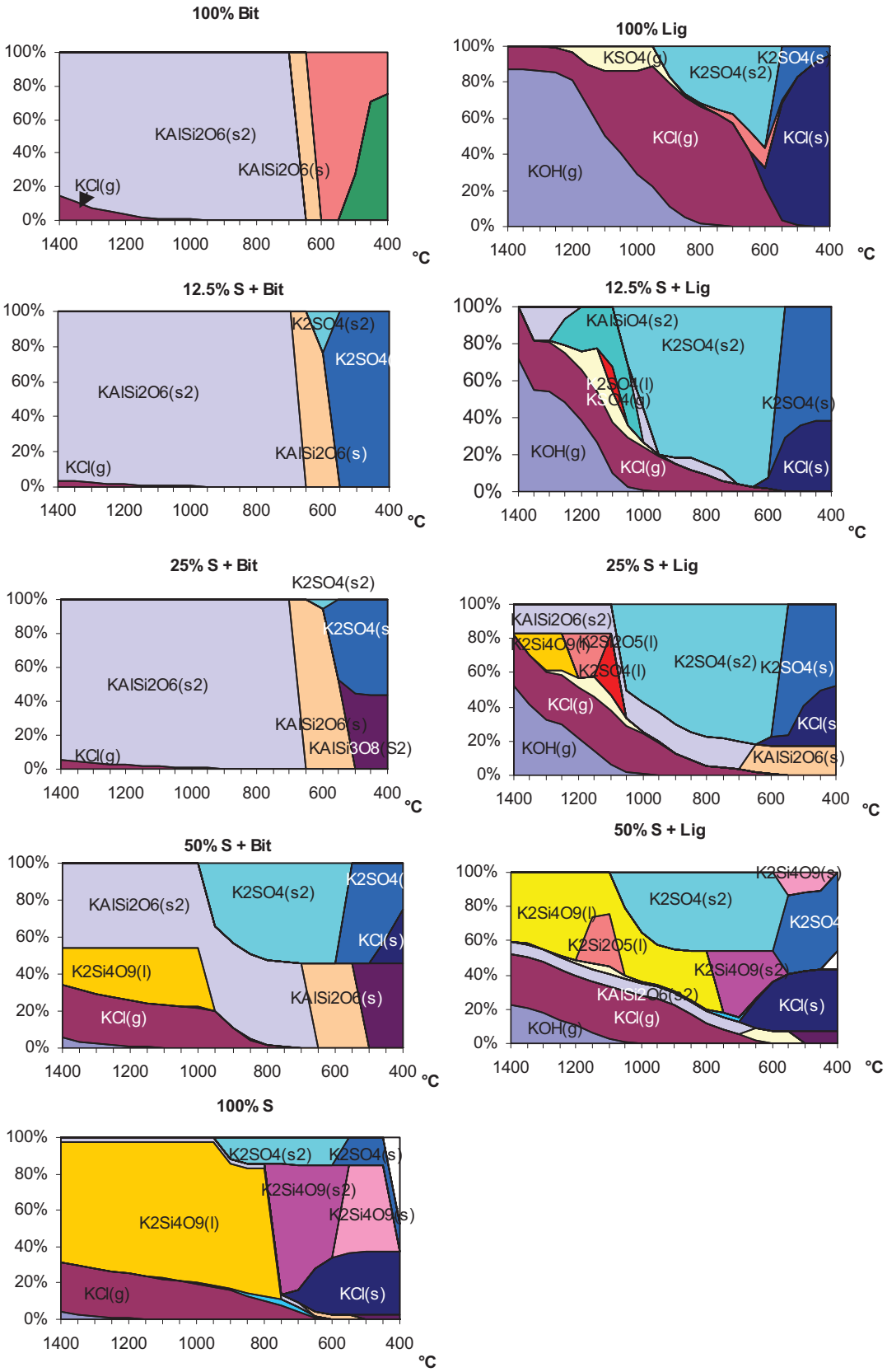

Fig. 6.3. Potassium distribution during co-firing of bit. coal/straw and lignite/straw

Distribution of sulphur

Sulphur is also considered as alkali absorbent in many studies, and the molar rate of S/Cl or S/Ca in fuel is given for suppressing the formation of alkali chlorides /156, 155/. Such simple

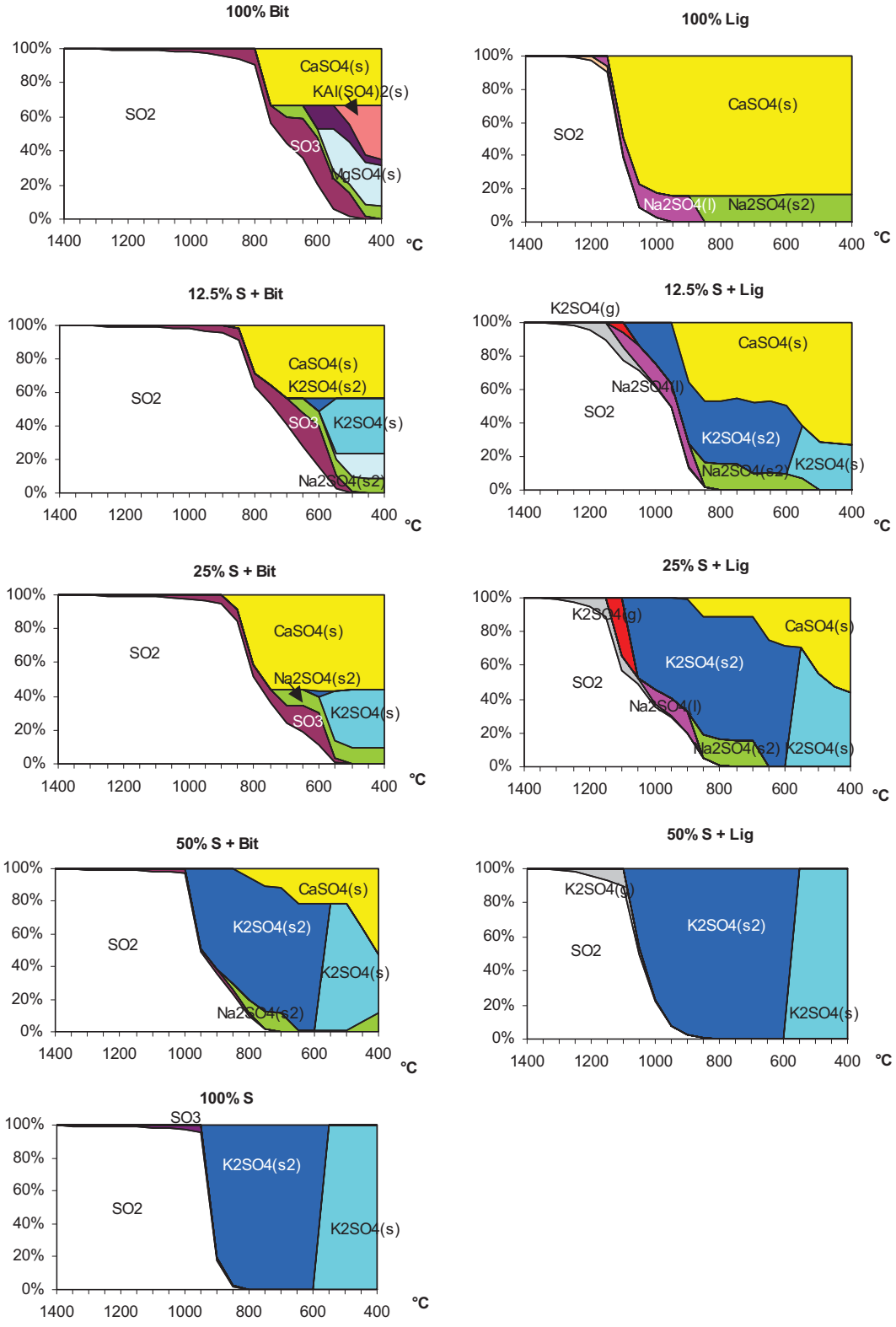

Fig. 6.4. Sulphur distribution of co-firing straw with bituminous coal and lignite

criteria, however, should be applied with caution. Since other mineral groups, such as aluminosilicates in fuel or in fuel blend, could exert greater influence on the fate of alkali. As shown in this study, although the concentration of sulphur is higher in bituminous coal than that in lignite, less K_2SO_4 is formed in the bituminous coal flame than in the lignite flame.

The sulphur distributions in flue gas and in fly ash are shown in Fig. 6.4. It reveals that during co-firing of bituminous coal with up to 25% straw, most sulphur exists in SO_2 above 800°C and in $CaSO_4$ below 800°C. The KCl concentration is low. The fate of sulphur can also be traced back to the lack of free potassium cation in flue gas: due to the effective potassium absorption by Al-Si minerals, there is no dramatic increase of K_2SO_4(s) until the straw share is higher than 25%. In the case of firing 50% straw with bituminous coal, the large amount of potassium from straw can not be completely bound by Al-Si complexes, as result, the surplus of potassium forms K_2SO_4.

Sulphur distribution in lignite flame is significantly different. $CaSO_4$ and K_2SO_4 are the dominant sulphur species below 1000°C. And the solid sulphates increase their share at high temperature zone with increasing straw mixture rate. Above 25% of straw share, K_2SO_4 is the dominant species below 1100°C.

The different sulphur distribution between 1100°C and 800°C implies that, during co-firing bituminous coal with straw, the deposits on superheater and reheater area contain less sulphates, and such sulphates are likely $CaSO_4$; whereas the deposit in co-firing lignite with straw contains more sulphates, and most sulphates is bound in K_2SO_4.

Following points can be generalized from calculation results:

1. If a kind of coal contains dominant acid mineral groups, such as bituminous coal with large amount of aluminosilicates, it is more suitable to be co-fired with straw than the coal which contains dominant base mineral groups, such as lignite with high content of earth alkalis. The beneficial effect of co-firing bituminous coal with straw due to the aluminosilicates in the coal, which can deactivate potassium from straw by forming solid and liquid K-Al-Si-O mineral complexes, so that potassium is not available to form KCl and K_2SO_4. This leads to the low concentration of alkali chlorides and alkali sulphates in superheater deposits during co-firing of bituminous coal and straw.

2. In lignite, high calcium content is effective to capture sulphur below 850°C. This results in low SO_2 concentration in flue gas. As consequence, a large proportion of

potassium is present as KCl, which leads to the enrichment of KCl in deposit ashes. Similar conclusion was reported by Seifert /156/, who calculated the distribution of Cl, K and S during bituminous coal combustion and lignite combustion.

3. Sulphur has the similar fate as chlorine in the bituminous coal flame. Due to the lack of free potassium in flue gas, fuel sulphur can only form SO_2 at high temperature and $CaSO_4$ at low temperature. In contrary, the aluminium and silicon content in the lignite under investigation is very low, this leads to the overwhelming formation of gaseous KCl and KOH at high flue gas temperature and solid K_2SO_4 at low flue gas temperature.

4. For the bituminous coal-straw co-firing, the acceptable limit of the thermal share of straw is in the range of 25%, whereas lignite is not suitable to be co-fired with any share of straw.

6.3 Experimental results

Four combustion tests were carried out in the pulverized fuel test rig of IVD. The testing fuels are the same with that in the thermodynamic calculations. Four tests with following fuel mixture rates were investigated:

- 100% bituminous coal
- 25 thermal. % straw + bituminous coal
- 100% lignite
- 25 thermal. % straw + lignite

The aim of the combustion tests is to examine the behaviour of chlorine, sulphur, and alkali metals during combustion and cooling process: whether they tend to form critical ash components, such as alkali chlorides or alkali sulphates, or rather form less critical HCl or SO_2. During each test, SO_2 concentration in flue gas at the lower part of the furnace was measured. Fly ashes collected from furnace bottom, air preheater, cyclone and filter were analysed.

Qualitative comparisons regarding the enrichment of alkali chlorides and alkali sulphates in fly ashes between calculation results and test results are possible. But quantitative comparisons are difficult, since the fly ashes collected at different positions in the flue gas pass have very different ash composition. Therefore, there is no simple comparison basis between tests results and calculation results. Sampling of deposit ash on a temperature-controlled probe was not possible at the time of test. However, sampling from cold tube

surface has similar character to that of filter ash regarding the concentration of chlorine, sulphur and alkalis. Based on above fact, emphasis was given to filter ashes, which should approximately reflect the ash characters on superheater surfaces.

Chlorine distribution in ash

Chlorine concentrations of the laboratory fuel ash (ashed at 815°C) and of the ashes from the combustion process are illustrated in Fig. 6.5. Chlorine concentration of the ashes is obviously different between lignite/straw tests and bituminous coal/straw tests: a) although lignite contains less chlorine, more chlorine was detected in the fine combustion ashes in pure lignite combustion than that in pure bituminous coal combustion; b) increasing straw share leads to significantly higher selective deposition of chlorine in the combustion ash in lignite/straw flame than that in bituminous coal/straw flame, e.g. the chlorine content in the filter ash of the Lig/S-75/25 is 13 times higher than their counterpart of Bit/S-75/25 test; and c) the highest chlorine concentration was in the finest fly ash, filter ashes. The high concentration of chlorine in fine fly ash implies that chlorine comes from the condensation and agglomeration of gaseous alkali chlorides.

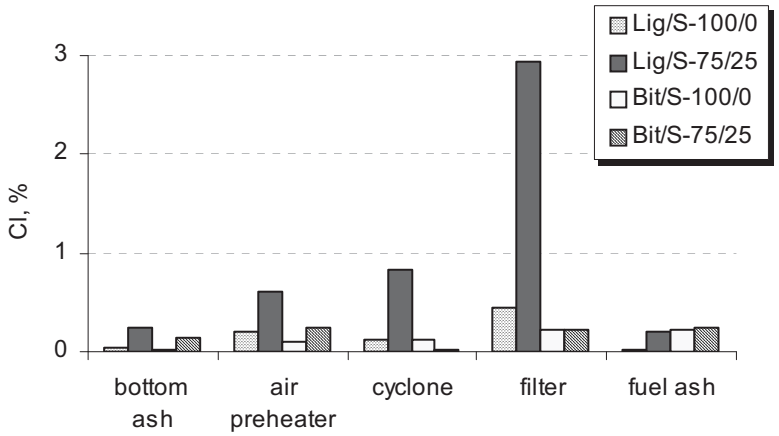

Fig. 6.5. Chlorine concentration in ashes from combustion and in laboratory fuel ash

The test results of chlorine concentration correspond well to the calculation results. It proves that chlorine tends to form alkali chlorides in lignite flame, whereas in the bituminous coal flame, the main part of chlorine forms gaseous HCl instead of alkali chlorides.

Alkali distribution in deposit ash

The presence of alkalis in deposit ash from above tests was reported by Heinzel /25/. He showed that potassium exists dominantly in aluminosilicate complexes in the deposit ashes from bituminous coal/straw co-firing (25% thermal share of straw). Other researchers got

similar results that potassium tends to be bound with Al-Si minerals during PF combustion /30, 157/. The ash deposits from temperature-cooled probe were investigated by Anderson /158/, who carried out the co-firing trials of bituminous coal and 20% straw in a 150MW PF-boiler. He found that potassium is both bound in fine Si-Al particles and in K_2SO_4 melt. This observation is in good agreement with the calculation results: the potassium distribution in Fig. 6.3 shows that below 25% straw share, most potassium is bound with aluminosilicates above 600°C, below this temperature, part of potassium is present as alkali sulphates.

However, it needs to be noted that the complete absorption of potassium by aluminosilicates at high temperature and the transition of potassium from aluminosilicates to potassium sulphate with decreasing temperature could be difficult in practice. Potassium favours to be bound in aluminosilicates at high temperature, however, such reactions are difficult to fully reach their equilibrium in the flue gas conditions of a PF boiler. A share of potassium can remain in flue gas in form of gaseous KOH and KCl at high temperature, which convert to solid K_2SO_4 at low flue gas temperature.

The absorbent effect of aluminosilicates to alkali chlorides is well known /159, 160, 161/. Wang et al proposed that alkali chlorides react with aluminosilicates according to the reaction in (6.1) /162/:

$$2MeCl(g) + Al_2O_3 \cdot 6SiO_2(s) + H_2O\,(g) \rightarrow Me_2O \cdot Al_2O_3 \cdot 6SiO_2(s) + 2HCl(g) \qquad (6.1)$$

Where Me is alkali metal. This reaction is thermodynamically favoured over reactions with silica alone. In addition, alkali sulphates both in vapour phase and in condensed phase can also react with aluminosilicates, for example, according to the following reaction. Since alkali sulphates are less volatile than alkali chlorides, the reaction should proceed at temperatures above 1000K. The best effect an be achieved at above 1300K.

$$K_2SO_4(c) + Al_2O_3 \cdot SiO_2(s) + 5SiO_2(s) \rightarrow 2KAlSi_3O_8(s) + SO_2\,(g) + \tfrac{1}{2}\,O_2\,(g) \qquad (6.2)$$

The particle size of getter material is very important for the absorbent efficiency. Finer particles could achieve higher absorbent efficiency. Kauppinen reported that during combustion of pulverized fuel, the absorbent efficiency of aluminosilicates could be beneficial since fine particles of silica and aluminates are formed from the volatilization and condensation of such minerals, the original size of which is less than 10 nm /163/.

Sulphur distribution in combustion ash

The test results of sulphur concentration in ashes from combustion process and in laboratory

fuel ash (ashed at 815°C) are shown in Fig. 6.6. Although different sulphur distribution between firing bituminous coal and firing lignite is observed, the difference is not so obvious as in the case of chlorine distribution. In order to obtain a clear view of the sulphur distribution in ashes, a "SO_3 /$SO_{3\ \text{fuel ash}}$" ratio is defined. When the ratio is greater than 1, sulphur is enriched in the combustion ash; when the ratio is less than 1, sulphur is depleted in the combustion ash. Fig.6.7 shows the ratio of "$SO_3/SO_{3\ \textit{fuel ash}}$" of combustion ashes. In this diagram, similar trends with that of chlorine are revealed: fine ash particles contain higher sulphur than coarse particles, and more sulphur exits in the filter ash from firing lignite than that from firing bituminous coal.

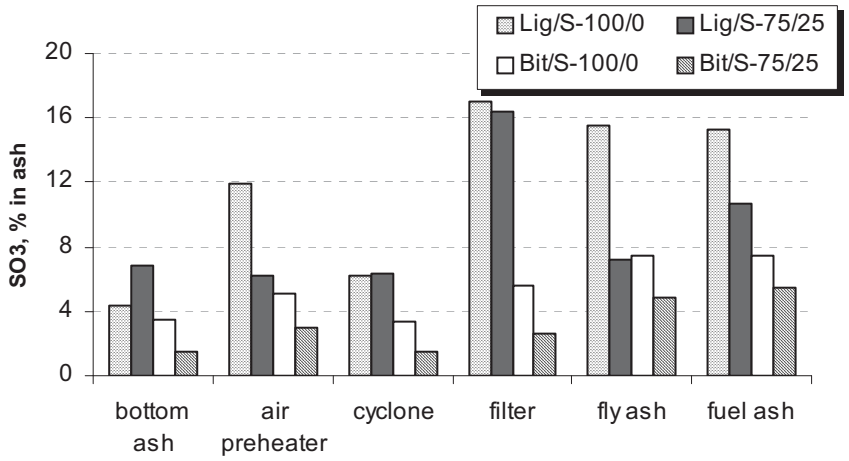

Fig. 6.6. Sulphur concentration in fly ashes and in fuel ashes

The SO_2 concentration measured at about 700-800°C in combustion tests further confirmed the trends of sulphur deposition, as shown in Fig.6.8. Significant high SO_2 concentration was measured in the flue gas of co-firing bituminous coal with straw. At the straw thermal share of 25%, SO_2 concentration in the bituminous coal/straw flame was about 5 times higher than that in the lignite/straw flame.

Since all the fly ashes were collected at the positions where the flue gas temperature was below 600°C, the fly ash composition should be compared with the calculation results of sulphur distribution below 600°C. The calculation diagram in Fig. 6.4 shows that, at low temperature, most sulphur is bound either with alkalis or earth alkalis both in bituminous coal flame and in lignite flame. The moderate sulphur content in the ashes of the bituminous coal-straw test in Fig. 6.7 is in agreement with the calculation result at the corresponding flue gas temperature.

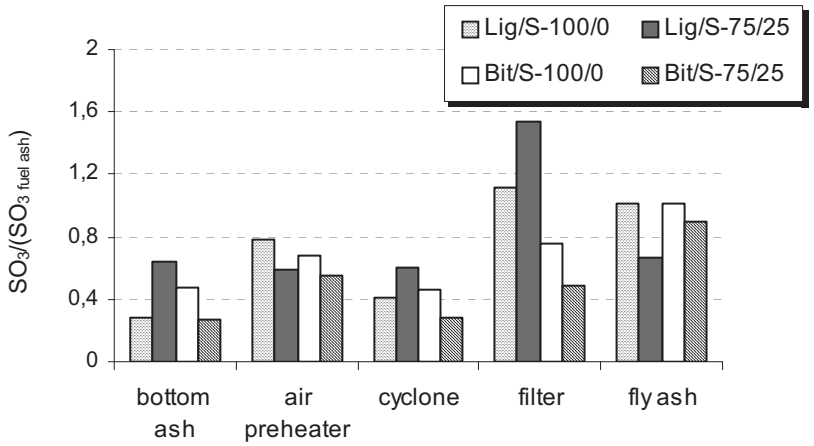

Fig. 6.7. Selective deposition of sulphur in ashes from combustion process (calculated as SO_3)

The relatively high sulphur content in coarse particles shown in Fig.6.7 implies that coarse particles contain also a non-negligible fraction of sulphur. This is different to the chlorine distribution in ashes. According to the analysis in Chapter 5, $CaSO_4$ not only exists in homogenous fine particles, but also sticks on the surface of big particles, and in no seldom cases, non-compact big ash particles of $CaSO_4$ can be formed by the agglomeration of fine $CaSO_4$ particles. Therefore, sulphur is not only bound with fine ash particles, but also exists in coarse ash particles.

6.4 Conclusion

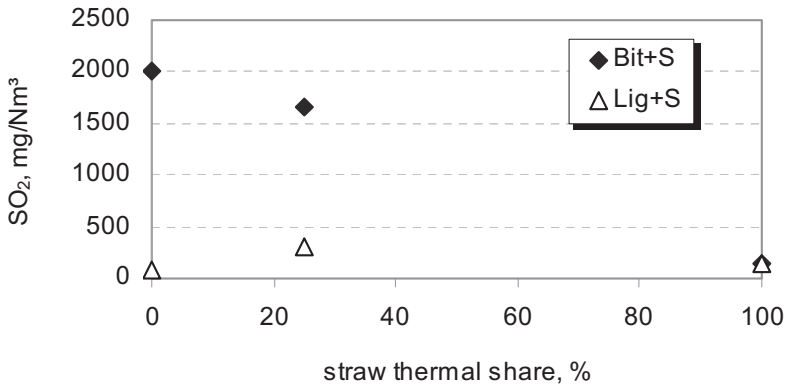

Fig. 6.8. SO_2 concentration in bituminous coal-straw co-firing flame and in lignite-straw flame

In the view of chlorine corrosion and deposition, co-firing straw with a fuel enriched in acid-rich minerals, such as bituminous coal, is more suitable than the fuel enriched in base-rich minerals, such as lignite. During co-firing bituminous coal with straw, most of potassium from straw can be bound with acid Si-Al minerals. In such way, chlorine forms uncritical

gaseous HCl instead of potassium chlorides. Due to the same reason, fuel sulphur is mainly present as SO_2 in higher temperature region. However, sulphur tends to convert to $CaSO_4$ or K_2SO_4 when flue gas cools down. In lignite, the contents of Al and Si are very low, but Ca is abundant. Therefore, K from straw and CaO from lignite tend to form KCl, K_2SO_4 and $CaSO_4$ during co-firing straw with lignite. Consequently, KCl, K_2SO_4 and $CaSO_4$ are enriched in fly ashes and in deposits in superheater areas.

The maximum thermal straw share for the bituminous coal-straw co-firing is 25%, whereas straw is not suitable to be co-fired with lignite.

7. Conclusion of the Present Study and Outlook of the Further Research

7.1 Conclusion

When chlorine-rich biomass or waste is burned in a combustion facility, chlorine in fuel is regarded as a very corrosive element for the materials of high temperature heat transfer equipments such as superheater and waterwall. Due to the deposition of chloride salts on tube surface, fast oxidation of tube materials is often observed. The corrosion process in oxidizing flue gas atmosphere is described as “active oxidation”, in which a high metal loss rate is resulted by a chain of reactions: the chlorination of metal; the evaporation of solid metal chlorides and the release of chlorine gas (Cl_2) by the oxidation of vapour metal chlorides. Although the general process of the chlorine-induced corrosion in oxidizing atmosphere is well known, the detailed knowledge about corrosion morphology and corrosion rate, depending on materials and exposing temperatures, are still not deeply investigated. Nevertheless, the corrosion mechanisms in reducing atmosphere are poorly understood, although a number of reports revealed severe corrosion beneath chlorine-rich deposits in reducing regions.

Based on the above open questions, this work concentrated on the following topics. Each topic is followed with a brief description of the own contribution.

a). Chlorine corrosion in reducing atmosphere

In reducing atmosphere with chlorine-containing gases, such as HCl, the growth of oxide scale is slow in all cases of three investigated metal groups: 1-2.5%-Cr ferritic steels, 9-12%-Cr ferritic/martensitic steels and austenitic alloys (Cr>14%). At the initial stage, metal oxidation, metal chlorination and evaporation of metal chlorides occur simultaneously; with time prolongation, a kind of honeycomb-like scale is formed. It is caused by the vacancies in the scale, which is generated by the evaporation of solid metal chlorides, and it can not be occupied again due to the low oxygen potential in the atmosphere. The vacancies in the oxide scale provide shortcuts for gas diffusion between flue gas and metal front. As result, there is no concentration gradient of reactants and products through the scale. The “active oxidation”, characterized with the circulation of chlorine gas (Cl_2) beneath the scale, can therefore not take place.

The reported high corrosion rate under chlorine-rich deposits in reducing atmosphere from other researchers is more likely attributed by alternating reducing/oxidizing atmosphere, resulted either by low-NOx furnace combustion technologies or by flame maladjustments. In such cases, non-oxidized chloride salts in the flue gas are firstly transported to the tube surface, and then, they are subsequently oxidized in the following alternated oxidizing atmosphere and release corrosive chlorine gases near the tube surface. As consequence, a high corrosion rate occurs.

b). Features of chlorine corrosion in oxidizing atmosphere

In contrast to the corrosion process under reducing conditions, in oxidizing atmosphere the vacancies created by the evaporation of metal chlorides can be occupied by the metal oxides from the oxidation of vapour metal chlorides. Once such scale forms, the "active oxidation" caused by chlorine attack is active underneath the scale. However, the morphology of the "active oxidation" is very different depending on exposing temperature and material.

At low temperatures (<450°C), the main corrosion topography is the fast-growing metal chloride buds scattered on slowly-growing oxide scale; at high temperatures (>600°C), the thick and porous oxide scale builds up so quickly, that it becomes corrugated and tends to spall. Solid metal chlorides can only build up beneath such thick oxide scale. The difference in the corrosion morphology is a result of the temperature-dependent vapour pressure of metal chlorides. The significantly higher vapour pressure of metal chlorides at high temperature leads to overwhelming evaporation of solid metal chlorides and oxidation of the vaporized metal chlorides.

Low ferritic steels build up thick oxide scale, which is not easily broken down by the growth of metal chlorides underneath the scale; in contrary, the oxide film formed on austenitic steels is thinner and more fragile.

c). The kinetics of chlorine corrosion at the initial stage

This study pointed out that, due to the simultaneous weight gain and weight loss character of the chlorine corrosion process, the metal loss of a specimen is a more precise indicator for the corrosion rate than the weight change. The metal loss defined in this study is the amount of metal, which is consumed to form corrosion products. A correlation between the weight change and the metal loss was also given with "R"-value:

$$R = \textit{(weight of corrosion products) / metal loss}$$

The “R”-value can provide very important information about the dominant reaction in a whole corrosion process, since the “R”-value of each single reaction in the process can be calculated. For example:

- The “R” of the oxidation of Fe to Fe_2O_3 is 1.429 ;
- The “R” of the chlorination of Fe to $FeCl_2$ is 1.607 ;
- The “R” of the formation of gaseous $FeCl_2$, which diffuses outwards to the gas phase, is –1.607 .

Both the weight change and the metal loss of 1-2.5%-Cr ferritic steels and 9-12%-Cr ferritic/martensitic steels were experimentally investigated. And the “R”-values of these materials were determined based on these experimental data. The “R”-values interestingly imply different dominant reactions at the initial stage for various materials, this dominant reaction can be one of the following reactions: the oxidation of metal, the chlorination of metal or the evaporation of metal. However, after about 60 hours of exposure time, the “R”-values of all test materials tend to approach 1.429, indicating the net effect of the active oxidation: from Fe to Fe_2O_3. This implies that the chlorine-induced “active oxidation” dominates the corrosion process after the initial stage.

d). The combined influence of flue gas and ash deposit on the chlorine-induced corrosion

Under a deposit ash layer, different mechanisms of chlorine corrosion were identified in reducing environment and in oxidizing environment. In reducing environment, due to the depletion of oxygen in flue gas, chloride salts in the deposit can not be easily oxidized and set chlorine gas (Cl_2) free. However, when sulphates are also present in the deposit, the corrosion rate can be slightly enhanced, since the sulphates in the deposit are not stable in a very reducing atmosphere and can be decomposed. In this way, oxidants (e.g. O_2 and SO_2) for the oxidation of the chloride salts are available. The corrosion rate of chlorine corrosion depends directly on the decomposition rate of sulphates, but not so much on the chlorine concentration in the deposit. In general, the corrosion rate is low in reducing atmosphere.

In oxidizing atmosphere, oxygen pressure in the flue gas is high enough to oxidize alkali chlorides in deposit. Sulphates in deposit are stabilized by oxygen and do not play an essential role on chlorine corrosion as they do in reducing atmosphere. Metal loss is correlated more with chlorine content in deposit ash than with the availability of O_2 and SO_2. SO_2 in flue gas can enhance the chlorine corrosion dramatically when alkali chlorides exist in deposit ash.

e). Corrosion resistance of materials under straw ash deposit and under coal ash deposit

***Metal loss*:** All the three groups of test materials: 1-2.5%-Cr ferritic steels, 9-12%-Cr ferritic/martensitic steels and austenitic alloys (Cr>14%) suffer more severe corrosion under straw ash than under coal ash. Although the austenitic alloys show less metal loss than the 9-12%-Cr steels under coal ash deposit, they have no clear advantage against chlorine attack under straw ash deposit.

Under straw ash, SO_2 enhances the corrosion rate of all steels significantly. Under coal ash, however, SO_2 exerts only negative influence on the corrosion rate when the coal ash is enriched in acid minerals, such as aluminosilicates from bituminous coals. When basic minerals are enriched in a coal, such as limestone in lignites, fuel sulphur is expected to be bound with such basic minerals during combustion. As consequence, the influence of SO_2 on chlorine corrosion is decreased. Austenitic steels are expected to be more sensitive to SO_2 attack than other materials both under straw ash and under coal ash.

Internal corrosion: The chlorine-induced internal corrosion results from the preferential attack of chlorine gas to chromium carbides in an alloy. This study found out that, although both 9-12%-Cr steels and austenitic steels are vulnerable to chlorine-induced internal corrosion, their corrosion morphologies are very different:

- The morphology of the internal corrosion of 9-12%-Cr steels is the selective attack of carbide and ferrite particles that distribute evenly in grain matrix. No apparent grain boundary corrosion takes place.
- In contrary, the internal corrosion of 14-20%-Cr austenitic steels is characterized with a deep front of grain boundary attack, followed by evenly distributed vacancies within the grain matrix near the metal surface.
- Austenitic steels with Cr>20% have also shown certain depth of chlorine penetration. However, the cavity in metal matrix resulted by chlorine attack is lower than that of the 9-12%-Cr steels and the austenitic steels with Cr<20%. In general, austenitic steels suffer more severe internal corrosion than 9-12%-Cr ferritic/martensitic steels.

Following suggestions are given for the material selection for the combustion facilities, in which chlorine-enriched fuels are applied:

- Applying higher grade of materials than usual for the parts of the heat transfer equipment, which are particularly endangered by the chlorine corrosion. E.g.:

1. For the material temperature between 400°C and 550°C, instead of 15Mo3, 13CrMo44 (Cr-content < 2.5%), 9-12%-Cr steels such as T91, X20 or HCM12A should be selected;
2. For the material temperature between 550°C and 600°C, instead of T91 or X20, high-alloyed austenitic steels with Cr > 20%, such as NF709, should be selected;
3. For the material temperature up to 600°C, Inconel alloys or coating alloys should be selected.

- The boiler and the heat transfer facilities should be designed and constructed in such a way, that later revision and replacement of the critical parts of the heat exchanger are made possible.

f). The influence of fuel minerals on the deposition behaviour of chlorine ash components

Since a high concentration of alkali chlorides in deposit could cause severe chlorine corrosion, the formation or deposition of chlorine chlorides should be prevented as much as possible during the combustion process. Through the combustion tests, this study proved the positive effect of SO_2 in flue gas and the aluminosilicates in fuel to reduce the deposition of chlorine salts:

- SO_2 in flue gas can convert gaseous alkali chlorides to alkali sulphates. In such way, the deposition of alkali chlorides is reduced. However, if there is a high concentration of basic ash components in flue gas, e.g. CaO, SO_2 tends to be bound with such minerals below 900°C and forms sulphate salts. This process leads to maintained chloride concentration in flue gas;
- Aluminosilicates in fuel is capable to bond potassium-ion at high flue gas temperature region and form K-Al-Si mineral complexes. Due to the depletion of potassium-ion, chlorine prefers to be bound in the relatively non-critical form of HCl.

The above results imply two effective ways to reduce the formation or the deposition of alkali chlorides:

- Mixing the chlorine-rich fuel with a sulphur-rich fuel or with a fuel abound of aluminosilicates;
- Putting alkali-absorbent additives, which mainly consist of sulphur compounds or aluminosilicates, to the chlorine-rich fuel.

In addition, this work pointed out that the chlorine concentration in deposit ash is also correlated with the mineral amount in the fuel. For example, high fuel sulphur and chlorine could still not be critical in the corrosion point of view, when they are diluted by a large amount of inert minerals in the deposit ash.

g). The distribution of ash components in deposit layers and around tube surface

The distribution of ash components in deposit layers and around tube circumference is important for the understanding of chlorine corrosion at certain tube positions, since an enrichment of alkali chlorides near such positions can possibly lead to a high corrosion rate. Through the systematic analysis of ash composition from the outer, middle and inner deposit layer on the wind site and the ash composition on the leeside, following results are concluded:

- Chlorine compounds locate mainly in the inner deposit layer and on the cooler leeside of tube surface.
- The main part of K_2SO_4 and $CaSO_4$ show similar behaviour as chlorine compounds, which build up homogenous fine particles and accumulate in the inner deposit layer. However, it can not be excluded that a part of the fine K_2SO_4 particles is the result of KCl conversion in the deposit. A little part of sulphates is also bound with big ash particles, which are responsible for the fast build up of bulk ash deposit on the wind side.
- Al-Si-minerals are mainly found in ultra-fine particles, which distribute evenly around the tube surface. A little part of Al-Si-mix phase is bound in large molten particles. They are accumulated in the middle and outer deposit layers on the wind side.
- Calcium and iron compounds tend to build up large molten particles, which compose the main part of bulk ash on the wind side.

Above results imply that, for the same general ash composition, the heterogeneous ash deposit formed in real combustion condition can be more corrosive than the homogeneous one, which is usually applied for laboratory exposure tests.

h). Fuel selection for the co-combustion with chlorine-rich fuels

In the corrosion point of view, a primary fuel for co-combustion with a chlorine-rich secondary fuel consists of minerals which can reduce the chloride formation or deposition during the combustion process. A bituminous coal and a lignite were selected in this study to be co-fired with straw. Both thermodynamic calculations and combustion tests showed that,

co-firing straw with a fuel, which contains rich acid mineral matters such as Al and Si, results in less deposition of alkali chlorides and sulphates. As explained above in point f), the aluminosilicates in bituminous coal can capture potassium effectively during combustion process, this leads to the formation of HCl and SO_2 rather than KCl and K_2SO_4. In contrary, the dominant basic mineral amount in a fuel, such as calcium compounds in lignite, can lead to SO_2 reduction in flue gas. At the same time, the acid compounds of Al and Si in such fuel are also not sufficient. As result, the abundant potassium from the straw is available for the formation of KCl or K_2SO_4 in flue gas. In the corrosion point of view, the maximum thermal share of straw for the co-firing with bituminous coal is 25%, whereas lignite is not suitable to be co-fired with straw.

Inadequacies in this study

Although this study has obtained a number of theoretical and practical contributions, many points need to be improved, or to be further investigated, which have not been involved in this study due to time and equipment limitations.

- Exposure time of the laboratory test: the most laboratory tests were exposed for 100-300 hours. This time is too short for the corrosion rate prediction in the standard unit of nm/h. Longer exposure periods could provide more regular corrosion rate trends.
- During this research period it was not possible to analyse the quantitative elemental distribution of ash deposits around a tube surface. This task could be accomplished by modern SEM equipments. Quantitative elemental distribution can provide a guide of ash composition for the laboratory tests, and thus help to setup a corrosion model between ash deposition and metal corrosion rate.

7.2 Outlook of further research activities

Based on this study and bearing the purpose to provide solutions for practical application, some main points are listed below for the possible further research activities:

Testing coating, extruding alloys and Ni-based alloys

Many coating and extruding tube materials with an inner core layer of ferrite/martensite und an outer layer of high Cr or Inconel alloy are drawing more attention for practical applications. The consideration of such structure is to provide both high temperature strength by the inner steel layer and high corrosion resistance by the outer high-Cr alloy layer. The manufacture methods are very different. There are enormous requirements to test the chemical and mechanical reliabilities of such materials under certain operational conditions or by firing

problematic fuels. Concerning the topic of chlorine corrosion, the materials should be tested in different kinds of lab-scale and semi-technical scale combustors, and by firing different kinds of fuel or fuel mixtures.

A close combination between combustion test and laboratory test

To give more convincible prediction, short-term combustion tests could be closely combined with laboratory tests. One point is that metal specimens with original ash deposits from combustion test should be further exposed in the laboratory furnace for a long time. This consideration is based on the heterogeneous ash deposition structure created in combustion tests, which is more corrosive than homogenous ones, since the most corrosive compounds, chlorides and sulphates, are usually deposited closely on the tube surfaces.

Another improvement of laboratory test could be a cooled probe, which carries testing specimens in the laboratory furnace. This will create more realistic test condition, since the temperature difference between flue gas and heat transfer tubes in a combustion facility is one of the driving force of the selective deposition of alkali chlorides and alkali sulphates on tube surface.

Based on above improvement, a corrosion prediction model can be developed, which gives corrosion rate prediction according to the ash deposit composition and gas environment.

Setup a complete prediction model from fuel input to corrosion rate

The simulation work of co-combustion straw with coal in this thesis proves to be valuable to predict corrosion tendency during combustion and cooling process. More work could be done on the standardization of the data processing, e.g. the evaluation, selection and interpretation of output data. Based on this, the behaviour of firing other fuel or fuel blends can be calculated, and a deposition model to predict deposition behaviour of firing different fuels can be set up.

The thermodynamic calculation should be verified by combustion tests. Mineralogical analysis of typical fly ash particles could further help to explain the details of mineral complexes.

Based on the deposition model from fuel to deposit composition with FACTSage, and on the corrosion prediction model from deposit composition to corrosion rate, as mentioned above, a complete model from fuel input to corrosion rate prediction can be established. Such a combined modelling tool will be useful for the prediction of corrosion rates and tube life times.

Literature

1. J. Neumann, H.R. Kautz: Auswertung der internationalen Literatur zur Hochtemperaturkorrosion in Kohle- und Müllkraftwerken; VGB Conf. Corrosion and Corrosion Protection in Power plant technology 95, pp. 329-334

2. M. Kehr, M, Wagner: Auswirkungen aktueller Entwicklungen im Energiemarkt auf Kraftwerksprojekte, XXXIII Kraftwerkstechnisches Kolloquium, 2001, Dresden, pp. 65

3. European Commission, Clean coal technology, Newsletter: The role of conventional coal-fired plant, Feb., 1999

4. W.A. Benesch: Kohlekraftwerktechnik für den liberalisierten Markt. XXXIII, Kraftwerkstechnisches Kolloquium, 8, 2001, Dresden, pp. 129

5. J. Franke, R. Kral, E. Wittchow, Dampferzeuger für die nächste Kraftwerksgeneration, VGB KraftwerkTechnik, 9/99, pp. 40

6. P. Voigtländer, M. Gottinger, U. Lenk: Wettbewerb der Technologien zur Stromerzeugung, XXXIII. Kraftwerkstechnisches Kolloquium, October, Dresden, pp. 49

7. K. Maile, W. Bernstein: Forschungen zur Bauteillebensdauer unter den Betriebsbedingungen des liberalisierten Strommarktes, XXXIII. Kraftwerkstechnisches Kolloquium, October 2002, Dresden, pp. 153

8. D. Hourfar, H. Koll, D. Kübler: Neue Dampfparameter für fortschrittliche Steinkohlekraftwerke, VGB Kraftwerkstechnik 77(1997), Heft 6, pp. 45-48

9. K. Godlewski: Review on high temperature corrosion of PCF boilers in Poland, Werkstoffe und Korrosion 39, 1988, pp. 67-69

10. S. Kihara, A. Ohtomo et al.: Recent plant experience and research into fireside corrosion in Japan, Werkstoffe und Korrosion 39, 1988, pp. 69-83

11. St. Inselmann: Danish experience with fireside corrosion, Werkstoffe und Korrosion 39 , 1988. pp. 64-66

12. Alstom Power Company Information CD

13. G. Scheffknecht, R. Blum, Q, Chen, A. Vanderschaeghe: Ein Vorhaben zur Ermittlung der Hochtemperaturkorrosionseigenschaften verschiedener Dampfererzeugerwerkstoffe unter Betriebsbedingungen und Dampftemperaturen bis 620°C, VGB Kraftwerkstechnik 76 (1996), Heft 10, pp. 856-862

14. Bund Position of Biomass: www.bund.net/themen/energiepolitik/biomasse.shtm

15. S. Kliniski: Vergünstigungen für die Verstromung von Biomasse, BWK Bd. 53, 2001, Special Biomasse pp. S1-S9

16. Bundesministerium, Referat Öffentlichkeitsarbeit, Art. Nr. 6404: Waste management policy in Germany

17. R. Romey: Rauchgasreinigungsanlagen für Biomassefeuerungen, BWK Bd. 53, 2001, Special Biomasse pp. S11-S16

18. H. Wefing, F. Vollmer: Biomassgefeuerte Heiz- und Heizkraftwerke, BWK Bd. 53, Nr. 10, pp. 53-58

19. N. Henriksen, M. Montgomery, O.H. Larsen: High temperature corrosion in biomass-fired boilers, VDI-W VGB Tagung, Korrosion in energieerzeugende Anlagen, Sep. 2002, Würzberg, pp. 111-131

20. U Schirmer: Korrelation zwischen Korrosionsproblematik und Dampfparametern bei Müllverbrennung, VDI-W VGB Tagung, Korrosion in energieerzeugende Anlagen, Sep. 2002, Würzberg, pp. 27

21. M. Spiegel, R. Warnecke: Korrosion hochlegierter Stähle und nichtmetallischer Werkstoffe unter Müllverbrennungsbedingungen, VDI-W VGB Tagung, Korrosion in energieerzeugende Anlagen, Sep. 2002, Würzberg, pp. 134-145

22. M. Montgomery, A. Karlsson: In-situ corrosion investigation at MasnedØ CHP plant – a straw-fired power plant, Materials and Corrosion 50, (1999), pp. 579-584

23. A. Mory, J. Tauschnitz: Co-combustion of biomass in coal-fired power plants in Austria, VGB PowerTech, 1/99. pp. 50-55

24. I. Rasmussen, P. Overgaard: General overview over recent s and plans concerning co-combustion of biomass and coal, Proc. of the 9th European Bioenergy Conf. Biomass for energy and the environment, Vol. 1. 1996, pp. 158-163

25. T. Heinzel; J. Maier, S. Unterberger, K.R.G. Hein: Fuel, ash and deposit analysis of biomass and fuel blends from pilot-scale combustion tests. Proceedings: Conf. Biomass for Energy & Industry, 1, 2000, pp. 229-234

26. R. Cenni, PhD. Thesis: Heavy metals behavior in co-combustion of coal and sewage sludge
Fortschritt-Berichte VDI, Reihe 6, Energietechnik, Düsseldorf 2001, ISBN 3-18-3460006-8

27. M. Sorensen, P. Jespersen: General overall over results and plans for large biomass boilers in Denmark. Proc. of the 9th European Bioenergy Conf. Biomass for energy and the environment, Vol. 1. 1996, pp. 186-191

28. H.P. Nielsen, F.J. Frandsen, K. Dam-Johansen, L.L. Baxter: The implications of chlorine-associated corrosion on the operation of biomass-fired boilers; Progress in Energy and Combustion Science 26 (2000), pp. 283-298

29. M. Born: Rahmenbedingungen für den Einsatz von Ersatzbrennstoffen (EBS) in Kohlefeuerungen, VGB-Konf. „Thermische Abfallverwaltung 2000“, Nov. 2000, Essen

30. M. Montgomery, OH Larsen: Field investigation into the effect of co-firing of straw and coal on high temperature corrosion, EuroCorr 2000

31. D.B. Meadowcroft: An introduction to fireside corrosion experience in the Central Electricity Generating Board, Materials und Corrosion 39, 1988, pp. 45-48

32. Rahmel, Wood, Kopstad, Douglass, International Workshop on "Critical Issues Concerning the mechanisms of High-temperature corrosion, Oxidation of Metals, Vol. 23, Nos. 5/6, 1995, pp. 253

33. D. Bramhoff: PhD thesis: Untersuchung des Einflusses von HCl(g) und N_2 auf die Hochtemperaturkorrosion von Eisenbasislegierung, Universität Dortmund, Abteilung Chemie, 1988

34. M. Spiegel: Hochtemperaturkorrosion niedrig- und hochlegierter Stähle unten simulierten Müllverbrennungsbedingungen, VDI-Berichte: Reihe 5, Nr. 371

35. Wood, Stott: Directions for future research in high-temperature corrosion, Oxidation of Metals, Vol. 44, ½, 1995, pp. 375

36. G.C. Wood and J. Stringer: The adhesion of growing oxide scales to the substrate; Journal de Physique IV, Colloque C9, Journal de Physique III, Volume 3, Dec. 1993, pp. 65-75

37. P. Kofstad, A. Rahmel, R.A. Rapp, D.L. Douglass: International Workshop on "New Fundamentals of Scale Growth", Oxidation of Metal, Vol. 32, Nos.1/2, 1989 pp. 154

38. B. Pieraggi, Robert A. Rapp, J. P. Hirth: Role of interfacial defects in oxide scale growth, Oxidation of Metals, Vol. 44, Nos. ½, 1995, pp. 63

39. Y. Zhang W. Wu: Summary of studies on hot corrosion of iron-based alloys by sodium sulfate in $O_2/SO_2/SO_3$ environment, Journal de Physique IV, Colloque C9, pp. 319

40. P. Atkins, Physical chemistry, ISBN 0-7167-2871-0, Oxford University Press, pp. 216

41. H. Kirsch und H. Reichel, Zur Rolle der Oxidschichten bei rauchgasseitigen Hochtemperaturkorrosionen, VGB Kraftwerktechnik 57, 1977, pp. 567-571

42. M. Schulte, A. Rahmel, M. Schütze: The sulfidation behavior of several commercial ferrtic and austenitic steels, Oxidation of metals, Vol. 49, Nos. ½, 1998, pp. 33-70

43. N.J. Harb, E.E. Smith: Fireside corrosion in PC-fired boilers, Prog. Energ. Combust. Sci. 1990, Vol. 16, pp. 169-190

44. Douglass, Kopstad, Rahmel, Wood: International Workshop on High temperature corrosion, Oxidation of Metals, Vol. 45, Nos. 5/6, 1996, pp. 529

45. L. A. Hansen, PhD Thesis: Melting and sintering of ashes, 1998, ISBN 87-90142-31-4

46. H.P. Nielsen: PhD Thesis: Deposition and high-temperature corrosion in biomass-fired boilers, 1998, TU Denmark, ISBN 87-90142-47-0

47. Dayton, D.C., French, R.J. et al. "Direct observation of alkali vapor release during biomass combustion and Gasification" Energy & Fuels 9, 1995, pp. 855

48. K.A Christensen,, M. Stenholm, et al.: The formation of submicron aerosol particles, HCl and SO_2 in straw-fired boilers, J. Aerosol Sci., 29, 1998, pp. 421

49. N. Bolt, J.T.W. Pastoors: Fireside corrosion in boilers of the Dutch electricity undertakings, Werkstoffe und Korrosion 39, 1988, pp. 48-54

50. G.A. Osborn: Review of sulphur and chlorine retention in coal-fired coiler deposits, Fuel, Vol. 71, Feb. 1992, pp. 131-142 Keywords: sulfur, chlorine retention, boiler deposits.

51. B. Meyer, O. Willmes und B. Röper: Mechanismen der chlorinduzierten Korrosion von Wirbelschicht-Heizflächen, VGB Kraftwerkstechnik 75, 1995, pp. 1043

52. P. H. Effertz, D.Wiume: Mechanismen und Schadenformen der Hochtemperaturkorrosion an Überhitzerrohren steinkohlengefeuerter Großkessel, VGB Kraftwerkstechnik 59, 1979, pp. 595-608

53. H. Stringer: Current limitations of high temperature alloys in practical applications, Oxidation of Metals, Vol. 44, 1995, pp. 265.

54. S.A. Benson, E.A. Sondreal, ash-related issues during combustion and gasification, 97 Conf. "The impact of Mineral Impurities in Solid Fuel Combustion, Hawaii, 1997

55. Xiaoyang Liu, Fireside High Temperature Corrosion at Advanced Power Plant Boilers, Diplom arbeit, Universität Stuttgart, 2000

56. W. T. Reid, External Corrosion and Deposits, ISBN: 0-444-00081-x, 1971

57. T. Flatley, E.P. Latham, C.W. Morris: Mechanistic features of molten salt corrosion in coal fired boilers, Werkstoffe und Korrosion 39, 1998, pp. 84-89

58. A.B. Anderson, N.C. Debnath: Reaction of NaCl(s) with SO_2(g) and O_2(g) to form Na_2SO_4(s). A charge-transfer reaction, The Journal of physical Chemistry, Vol. 87, No.11, 1983, pp. 1938-1941

59. A.L. Plumpy, W.R. Roczniak: Coal ash corrosion field testing of advanced boiler tube materials-II, the second int. Conf. on improved coal-fired power plants. Nov. 1988, Palo Alto, USA

60. L. Yan, R.P. Gupta: The implication of mineral coalescence behavior on ash formation and ash deposition during pulverized coal combustion, Fuel 80, 2002, pp. 1333-1340

61. C.J. Zygarlicke, E.N. Steadman, S.A. Benson: Studies of transformations of inorganic constituents in a Texas lignite during combustion, Prog. Energ. Combust. Sci. Vol. 16, 1990, pp. 195-204

62. Steam 40, Fuel ash effects on boiler design and operation, Babcock & Wilcox, pp. 20-5-20-7

63. X. Liu, T. Heinzel, J. Maier, K.R.G. Hein: Fireside Slagging and Corrosion on the Superheater by Firing Lignite Coals and Coal Blends in a PF Boiler, 6th Inter. Conf. of Clean air, Porto, Portugal, 2002

64. Kondratiev, E. Jak: Viscosity model in the Al2O3-CaO-FeO-SiO2 system, Minprex 2000

65. O. Bozic, R. Leithner, A Kinetic model for iron based mineral matter transformations in coal combustion environment, , 9th International Conference on coal science, (Proceedings ICCS, 97), DGMK Tagungsberichte 9703, pp. 1167-1170

66. G.P. Huffman, F.E. Huggins, Behavior of basic elements during coal combustion, Prog. Energ. Combustion. Sci, 1990, Vol. 16, pp. 243-251

67. J. F. Norton, M. Maier, W.T. Bakker, Corrosion of heat exchanger alloys exposed to a non-equilibrated CO-based sulfidizing environment at 550°C, Materials and Corrosion 51, 2000 pp. 424-433

68. J. Gilewicz-Wolter: High-temperature corrosion of iron in sulfur dioxide at low pressure, Oxidation of metals, Vol. 45, 5/6, 1996, pp. 129-145

69. J. Colannino: Prevent boiler tube failures, Part 1. Fire-side mechanisms, Chemical Engineering Process, October 1993, pp. 33-36

70. K. Nakagawa, M. Kitagawa, Y. Tumita, S. Ooki: High temperature corrosion of water wall tube in coal-fired combustion gases, Journal de Physique IV, Colloque C9, Vol. 3, December, 1993, pp. 787-806

71. J. Mayrhuber, H. Cerjak: The role of materials in maximizing the energy utilization from solid waste fuels-recent developments in material optimization and process design, 6th Liege Conference

72. L A Hansen, H P Nielsen, et al.: Influence of deposit formation on corrosion at a straw-fired boiler, Fuel Processing Technology 64 (2000) pp. 189-209

73. S. Kihara, K. Nakagawa, W. Wolowodiuk, L.J. Bluogh, W.T. Bakker: Corrosion resistance of advanced tube materials in coal-fired boilers, High temperature corrosion of advanced materials and protective coatings , Editors: Y. Saito, B. Onay, T. Maruyama, Elsevier Science Publishers B.V. 1992, pp. 197

74. R. Prescott, F.H. Stott, P. Elliott, Investigations of the degradation of high-temperature alloys in a potentially oxidizing-chloridizing gas mixture, oxidation of metals, vol. 31, Nos. ½, 1989. pp. 145-151

75. D. Bramhoff, H.J. Grabke, H.P. Schmidt, Werkst. Korrosion, 41, pp. 303-307

76. PA Alexsander, Laboratory studies of the effects of Sulphates and chlorides on the oxidation of superheater alloys, in: Johnson R, Littler DJ, editors, The mechanism of corrosion by fuel impurities, London: Butterworths, 1963, pp. 571

77. L.H. Toft, R. A. Marsden: Metallurgical aspects of the fireside corrosion of superheater tube materials; The Mechanism of corrosion, by fuel impurities, Proceedings of the inter. Conference, 1963, pp. 591-603

78. H.T. Shirley: Sulphate-chloride attack on alloy steels and nickel-base alloys, The Mechanism of corrosion by fuel impurities, Proceedings of the inter. Conference, 1963, pp. 617-628.

79. E.P. Doane, M.F. Abbott: Low corrosivity of coal chlorine, Conf. "The impact of Mineral Impurities in Solid Fuel Combustion, Hawaii, 1997

80. Skrifvars: The role of alkali sulfates and chlorides in post cyclone deposits from circulating fluidized bed boilers, Conf. "The impact of Mineral Impurities in Solid Fuel Combustion, Hawaii, 1997

81. R. Blum, O.H. Larsen, N. Henriksen, Superheater failures in ultra supercritical boilers-cases studies, Power Plant Chemistry 1999 1(6), pp21-27

82. Rene Kull, Diplomarbeit, Institut für Verfahrenstechnik und Dampfkesselwesen, Unviersität Stuttgart

83. K. Salmenoja, K.P. Oy, Laboratory studies on the influence of gaseous HCl on superheater corrosion, 97 Conf. “The impact of mineral impurities in solid fuel combustion.

84. Wei Xie, Wei-Ping Pan, J.T. Riley, Behavior of chloride during coal combustion in an AFBC system, Energy &Fuels 1999, pp585.

85. K. Liu, W. Pan, J.T. Riley, I.G. Wright, The effects of ash deposits on high-temperature corrosion of alloys in a fluidized Bed combustion system, Corrosion, Vol. 57, No. 3, pp. 253-264.

86. M Montgomery, A Karlsson, OH Larson, In-situ corrosion experiments at various straw-fired power plants in Denmark, EuroCorr 2000

87. Xiaoyang Liu, Diplomarbeit, Fireside High Temperature Corrosion at Advanced Power Plant Boilers, 2000, University of Stuttgart

88. T. Heinzel, C. López, J. Maier, H. Spliethoff, K.R.G Hein : Ash, deposit and corrosion characteristics of coal-biomass blends in a 0.5MW pulverised fuel test facility. Proceedings: Conf. UEFC, 2000

89. G. E. Moores and Bernard M. Gibbs: The Effects of Trace Metals on Fireside Corrosion in Coal and Waste Fired Plant, Keywords: trace metals, fireside corrosion, coal, waste, austenitic steel, Inconel; The Impact of Mineral Impurities in Solid Fuel Combustion‘, Kona, Hawaii, USA, 1997

90. R.U. Husemann: Korrosionserscheinungen und deren Reduzierung an Verdampfern und Überhitzerbauteilen in Kommunalen Müllverbrennungsanlagen, VGB Kraftwerkstechnik 72 1992, Heft 10, pp. 918-927

91. P. A. Alexander; Laboratory Studies of the Effects of Sulphates and Chlorides on the Oxidation of Superheater Alloys; Salt Coating in Thermal Balance, pp. 571-581

92. N. Otsuka and T. Kuno: Hot Corrosion of Commercial Tube Steel Materials in a Japanese Waste Incinerator Environment; High Temperature Corrosion of Advanced Materials and Protective Coatings; Proceeding of the Workshop on High Temperature Corrosion of Advanced Materials and Protective Coating, Tokyo, Japan,. 1990, pp. 205-211

93. H.P. Nielsen, L.L. Baxter, G. Sclippab, C. Morey, F.J. Frandsen, K. Dam-Johansen: Deposition of potassium salts on heat transfer surfaces in straw-fired boilers: a pilot-scale study; Fuel 79, 2000, pp. 131-139

94. P.A. Jensen, M. Stenholm, P. Hald: Deposition investigation in straw-fired boilers, Energy Fuels 1997, 11, pp. 1048-1055

95. L. Boonsongsup, K. Iisa, W.J. Frederick, Jr: Kinetics of the sulfation of NaCl at combustion conditions, Int. Eng. Chem. Res. 1997, 36, pp. 4212-4216

96. H.J. Grabke, E. Reese, M. Spiegel: The effects of chlorides, hydrogen chloride, and sulfur dioxide in the oxidation of steels below deposits. Corrosion science 1995, 37,7, pp. 1023-1043

97. E. Reese, E.M. Müller, H.J. Grabke: Investigation of the transient state of oxidation-chlorination, Joural de Phsique, IV, Colloque C9, Vol. 3, December 1993 pp. 133-141.

98. H. Tallermo, L. Klevtsov: Hochtemperaturkorrosion der Stähle 12 Ch 1 MF, 13CrMo44, 10CrMo9 10 im SF-Kessel bei der Temperatur des Metalls bis zu 540°C, VGB Kraftwerkstechnik 8/98, pp. 105-111

99. H-H. Reichel: Fireside corrosion in German fossil-fuel fired power plants. Appearance, mechanism and causes, Werkstoffe und Korrosion 39, 1988, pp. 54-63

100. R.A. Rapp: Chemistry and electrochemistry of hot corrosion of metals, Materials Science and Engineering, 1987, pp. 319-327

101. K. Natesan, A. Purohit, D.L.Pink: Fireside corrosion of alloys for combustion power plants, Power Plant Chemistry, 2002, 4(9), pp. 549-555

102. Krause: Corrosion by chlorine in waste-fuelled boilers, international Engineering Conference, Florida, 1989

103. Balting, Katerbau, Kautz and Woitscheck: Fireside Corrosion and ferritic/austenitic steels and high-alloy materials for superheaters, especially reheaters of coal-fired generators, Werkstoffe und Korrosion 39, 1988, pp. 90-97

104. G. F. Vander: Applied metallolography: ISBN: 0-442-28836-0

105. M. Voorde: Environmental Effect o the damage of high temperature materials, Material science and Engineering, 1987, pp. 341-346

106. P.J.Ennis, W.J. Quadakkers: High chromium martensitic steels – Microtructure, properties and potential for further development, VGB PowerTech 8/2001, pp. 87-90

107. R. Viswanathan, W.T. Bakker: Materials for ultra supercritical coal power plants, Part 1, Boiler Materials, Power Plant Chemistry, 2001, 3, pp. 383-397

108. R.U. Husemann, Werkstoffseitige Maßnahmen zur Reduzierung der Hochtemperatur-korrosion in Kohlebefeuerten Dampferzeugern, VGB Kraftwerkstechnik 69, Januar 1989, pp. 105-114

109. K. Zabelt, B. Melzer, A. Reuter, P. Seliger: Results of recent investigations for boiler application on austenitic steels to ensure long-term service integrity at high steam temperature, VGB PowerTech 2/2001, pp. 85-91

110. European Commission, Clean coal technology newsletter No. 14: Breaking the steel barrier, September 2000

111. R. Blum, J.Hald, W.Bendick, A. Rosselet, J.C. Vaillant: Neuentwicklungen hochwarmfester ferritisch-martensitischer Stähle aus den USA, Japan und Europa, VGB Kraftwerkstechnik 74, 1994, Helt 8, pp. 641-652

112. P.J. Ennis, O. Wachter: Die Eigenschaften des 9%- Chromstahles vom Typ 9 Cr-0,5Mo-1,8W-V-Nb im Hinblick auf seine Verwendung als Rohrleitungs- und Kesselbaustahl, VGB KraftwerksTechnik 1/98, pp. 95-105

113. X. Liu, T. Heinzel, H. Spliethoff, K.R.G. Hein, China International Corrosion Control Conference´99 (CICCC´99) Fireside high temperature Corrosion by firing high chlorine fuels, Beijing, October, 1999,

114. G. Scheffknect, A. Kather: Neue Werkstoffe im Dampferzeugerbau, BKW, Bd 49, Nr 11/12, 1997, pp. 62-67

115. W. Bendick, K. Haarmann, M. Ring, M.Zschau: Stand der Entwicklung neuer Rohrwerkstoffe für den Kraftwerksbau in Deutschland und Europa, VGB Kraftwerkstechnik 77, 1997, Heft 5, pp. 62-67

116. B. Schaffernak, H. Cerjak, P. Hofer: Neues Konzept zur Optimierung moderner 9- bis 12%-Cr- Stähle, VGB Kraftwerkstechnik 3/2000, pp. 80-84

117. G. Waltenberger, P. Mattern: Einsatz austenitischer Werkstoffe in Dampfkessel, Betriebliche Erfahrung mit der ersten 600°C-Hochtemperatur-Dampfkesselanlage, VGB Kraftwerkstechnik 1/1990, pp. 68-70

118. K.H. Mayer, W. Bendick, R.U. Husemann, K.Kern, R.B. Scarlin: Neue Werkstoffe zur Verbesserung des Wirkungsgrades von fossilbefeuerten Dampfkraftwerken, VGB Kraftwerkstechnik 1/98, pp. 27-32

119. R.U. Husemann, O. Wachter, K. Zabelt, Verarbeitung und Betriebseinsatz von neuen Werkstoffen im Kraftwerksbau, VGB Kraftwerkstechnik 75, 1995, Heft 3, pp. 265-279

120. B. Walser: Material developments for advanced coal-fired power plants in the COST-Program, 97 Conf. “The Impact of mineral impurities in solid fuel combustion” Hawaii, 1997

121. A.H. Rudd, J.M. Tanzosh: Developments applicable to improved coal fired power plants, the first International Conf. on Improved coal-fired power plants, Nov. 1986, USA

122. M. Spiegel, R. Warnecke: Korrosion thermisch gespritzter Schichten unter simulierten Müllverbrennungsbedingungen, VGB-Konf. „Thermische Abfallverwertung 2000“, Essen

123. Y. Saito, et al , The reactive element effect (REE) in oxidation of alloys, Journal de Physique IV, C9, Vol. 3, Dec. 1993, pp. 217-230

124. B. Pieraggi, R.A. Rapp: A novel explanation of the “Reactive element effect” in alloy oxidation, Journal de Physique IV, C9, Vol. 3, Dec. 1993, pp. 275-280

125. R. Guillamet, et. al.: Oxidation of stainless steels(AISI 304 and 316) at high temperature. Influence on the metallic substratum, Journal de Physique IV, C9, Vol. 3, Dec. 1993, pp. 349-356

126. R. Boldt, W.M. Cox: Kontinuierliche Korrosionsmessung, VGB Kraftwerkstechnik 90 1990, pp. 949-955

127. European Federation of Corrosion Publication, Nr 4: Guidelines on electrochemical corrosion measurements, the institute of metals, 1990.

128. www.integritisolutions.com/technology/corrosion.htm: Corrosion Management Technology from Integration Solutions

129. D.M. Farrell, B. Robbins: On-line monitoring of furnace wall and superheater corrosion in power generation boilers; VTER TECHNICAL PAPER, CSS 98, 39th Corrosion Science Symposium, 8th Sept.98, Newcastle, U.K

130. A. J. Bard Larry R. Faulkne: Electrochemical Methods – Fundamentals and Applications chapter 7 Controlled Current Microelectrode Techniques; John Wiley & Sons, pp. 249-573

131. G. Voort: Metallography: principles and practice, 1984, ISBN 0-07-066970-8

132. M.J. Graham and R.J. Hussey: Analytical Techniques in High Temperature Corrosion; Oxidation of Metals, Nos. ½, 1995, pp. 339-341

133. R.E. Reed-Hill, Physical Metallurgy Principles, C-6864-997-X, published by VAN NOSTRAND REINHOLD COMPANY, 1964, pp. 1-3

134. Schumann, Metallographie, VEB Deutsche Verlag für Grundstoffindustrie, VLN: 152-915/78/83, LSV: 3015, 1997, pp. 24-25

135. Structure and properties of alloys, McGraw-Hill Book Company, 1965, pp. 225

136. G. Petzow: Metallographisches Keramographisches Platographisches Ätzen, Gebrüder Borntraeger Berlin, Stuttgart 1994

137. T. Heinzel, PhD Thesis: Ascheseitige Probleme bei der Mitverbrennung von Biomasse in Kohlenstaubfeuerungen, Berichte aus der Energietechnik, Shaker Verlag Aachen, 2004. ISBN 3-8322-2632-X, ISSN 0945-0762

138. H. Maier: PhD Thesis: Experimentelle Untersuchungen der Kohlenstaubverbrennung unter Berücksichtigung der Brennstoffaufbereitung, Shaker Verlag, Aachen 1998, Berichte aus der Energietechnik, ISBN 3-8265-3295-3

139. Volker Siegle, PhD Thesis: Biogene Brennstoffe in Aufbereitung und Verbrennung Shaker Verlag, Aachen 2000, Berichte aus der Energietechnik, ISBN 3-8265-7711-6

140. T. Heinzel, W. Scheurer, J. Baum, J. Maier, H. Spliethoff, K.R.G Hein: A comparison of dry ash removal PF and slag-tap furnace regarding biomass and sewage sludge co-combustion on the basis of pilot-scale tests. Proceedings: DGMK-Fachtagung Velen IV, 4, 2000

141. Zahs, M. Spiegel, H.G. Grabke: The influence of alloying elements on the chlorine-induced high temperature corrosion of Fe-Cr alloys in oxidizing atmosphere, Materials and Corrosion 50, 1999, pp. 561-578

142. T. Valente: Fireside Corrosion of superheater materials in chlorine containing flue gas, Journal of Materials Engineering and Performance, 2001, 10, pp. 608-614

143. M. Spiegel, H.J. Grabke: Hochtemperaturkorrosion hochlegierter Stähle unter simulierten Müllverbrennungsbedingungen, Materials and Corrosion 47, 1996, pp. 179-189

144. A.J. B. Cutler, W.D. Halstead, J.W. Laxton, C. G. Stevens: The role of chloride in the corrosion caused by flue gases and their deposits, Journal of Engineering for Power, July, 1971, pp. 307-312

145. E. Reese H.J. Grabke: Einfluß von Natriumchlorid auf die Oxidation von hochlegierten Chrom- und Chrom-Nickel-Stählen, Werkstoffe und Korrosion 44, 1993, pp. 41-47

146. H.J. Grabke, E. Reese, M. Spiegel: The effects of chlorides, hydrogen chlorine, and sulfur dioxide in the oxidation of steels below deposits, Corrosion science, Vol. 37, No. 7, 1997, pp. 1023-1043

147. Y. Shinata, F. Takahashi, K. Hashiura, NaCl-induced hot corrosion of stainless steels, Materials science and engineering, 87 (1987) pp. 399-405

148. K. Tjokro, D.J. Young, R.E. Johansson, B.G. Ivarsson: High temperature sulfidation-oxidation of stainless steels. Journal de Physique IV, Colloque C9, Vol. 3, December, 1993. pp. 357-363

149. Ralf Bürgel: Handbuch Hochtemperatur-Werkstofftechnik, Vieweg Technik, ISBN 3-528-03107-7, 1998

150. F. Umland: Einfluß von Brennstoffverunreinigungen und die Hochtemperaturkorrosion metallischer Werkstoffe, VGB Kraftwerkstechnik, Heft 3, 1979, pp. 206-211

151. H.J. Grabke, R. Krajak, E.M. Müller: Metal dusting of high temperature alloys, Werkstoffe und Korrosion 44, 1993, pp. 89-97

152. M.J. McNallen, S. Thongtem, J.C. Liu, et al: Corrosion of chromium containing alloys in non-steady state environments containing oxygen, carbon, and chlorine, Journal de Physique, IV, Colloque C9, Vol. 3, December 1993 . pp. 143-150

153. PJ Henderson, P Ljung, P Kallner, J Tollin: Fireside corrosion of superheater materials in a wood-fired circulating fluidized bed boiler, EuroCorr 2000

154. N. Alekhnovich, V.V. Bobomolov, et al.: An investigation of the slagging behavior of blended coals, Thermal Engineering, Vol. 47, No. 8, 2000, pp. 705-711

155. N.J. Manton, J. Williamson: Changes in slagging behavior with composition for blended fuels, Conf. The impact of Mineral Impurities in Solid Fuel Combustion, Hawaii, 1997

156. E. Jak, P. C. Hayes: Application of the new database for predicting the high temperatures behaviour of coal mineral matter, CRC Newsletter, Number 14, January 2000

157. Starke, W. Horlbeck, T .Bause, B. Meyer, O. Willmes, W. Glaser: Thermodynamische Modellierung von Kohleschlacke-System, BWK, Bd, 52 (2000), Nr. 9, pp. 45-48

158. B. Meyer, O. Willms, W. Glaser u. B. Röper: Vergleichende thermodynamische Untersuchungen zur Verbrennung von Braunkohle in Dampferzeugern mit Staubfeuerung und Wirbelschichtfeuerung, VGB-Tagung, 1998, TU Bergbauakademie, Freiburg

159. X. Wei, C. Lopez, et. al : Assessment of chlorine-alkali-minerals interactions during co-combustion of coal and straw, Energy & Fuels Vol. 17, 2003, pp. 1392 – 1398

160. X. Wei, Christian Lopez, T. Puttkamer, U. Schnell, K.R. G. Hein: Release of chlorine and its retention in ash during co-combustion of biomass and coal in a pulverized fuel combustor, 6th Inter. Conf. of Clean air, Porto, Portugal, 2002, pp. 541-550

161. K. Salmenoja, K. Mäkelä: Chlorine-induced superheater corrosion in boilers fired with biofuels, Conf. “The impact of mineral impurities in solid fuel combustion, 1997

162. P. Seifert, M- Born: Einfluß der Brennstoffzusammensetzung auf die Chlorkorrosion in Feuerung, TU Bergakademie Freiberg

163. F. J. Frandsen, Hanne P. Nielsen, P. A. Jesen, L. A. Hansen, H. Livbjerg, Kim Dam-Johansen, P. F.B. Hansen K. H. Andersen, H. S.S ørensen, O. H.Larsen, B. Sander N. Henriksen and P. Simonsen: Deposition and Corrosion in Straw- and Coal-Straw Co-Fired Utility Boilers; Eng. Found. Conf. ‘The Impact of Mineral Impurities in Solid Fuel Combustion, Hawaii, 1997

164. K.H. Andersen, F.J. Frandsen, P.F.B. Hansen et al, Full scale deposition trials at 150Mwe pf-boiler co-firing coal and straw: Summary of results, Conf. "The impact of Mineral Impurities in Solid Fuel Combustion, Hawaii, 1997

165. L.A. Scandrett, R. Clift: The thermodynamics of alkali removal from coal derived gases, Journal of the Institute of Energy, December, 1984, pp. 391-397

166. T. Reichelt, Ph.D. Thesis: Freisetzung gasförmiger Alkaliverbindungen bei atmosphärischer und druckaufgeladener Verbrennung, Fortschritt-Berichte VDI, Düsseldorf 2001, Reihe 3, Verfahrenstechnik, ISBN 3-18-368703-8

167. M. Uberoi, W.A. Punjak, F. Shadman: The kinetics and mechanism of alkali removal from flue gas gases by solid sorbents, Prog. Energy. Combust. Sci, 1990, Vol. 16, pp. 205-211

168. H. Wang, J. N. Harb: Modelling of ash deposition in large-scale combustion facilities burning pulverized coal, Prog. Energy Combustion Sci, Vol. 23, 1997, pp. 267-282

169. E. I. Kauppinen, T. M.Lind, et.al.: Ash particle formation mechanisms during pulverized and fluidized bed combustion of solid fuels; Ashes and Particulate emissions from biomass combustion, Ingwald obernberger (ed.), dbv-Verlag, Verlag für die Technische Universität Graz, pp. 141-153

170. M. Breuers: Siliziumkarbid und sein Verhalten in der thermischen Abfallbehandlung, VGB-Konf: Thermische Abfallverwaltung 2000, November, Essen

171. M. Bugajski, B. Wilhelmi: Neue Entwicklungen von feuerfesten Massen für die Anwendung in der thermischen Entsorgung, Thermische Abfallverwaltung 2000, November, Essen

172. St. Mulch, L. Elstner, D. Grimm, H. Kinne: Korrosionsvorgänge an feuerfesten Werkstoffe in kommunalen Müllverbrennungsanlagen, VGB KraftwerksTechnik, 3/98, pp. 70-74